

UCSF

UC San Francisco Electronic Theses and Dissertations

Title

Re-Replication Induced Gene Amplification: Phenomenon, Mechanism, and Significance

Permalink

<https://escholarship.org/uc/item/85w067p6>

Author

Finn, Kenneth John

Publication Date

2013

Peer reviewed|Thesis/dissertation

Re-Replication Induced Gene Amplification:
Phenomenon, Mechanism, and Significance

by

Kenneth John Finn

DISSERTATION

Submitted in partial satisfaction of the requirements for the degree of

DOCTOR OF PHILOSOPHY

in

Biochemistry and Molecular Biology

in the

GRADUATE DIVISION

of the

UNIVERSITY OF CALIFORNIA, SAN FRANCISCO

Copyright 2013
by
Kenneth John Finn

Acknowledgments

This dissertation and the completion of my pre-doctoral training would not have been possible without the support, advice, and assistance of many people along the way.

I would like to thank my advisor, Joachim Li, for the many years of support and direction he has provided. He has helped to sharpen my skills as an experimentalist, as a writer, and as a presenter. Whenever I've wanted to discuss science, both of the practical day to day nature and in the abstract, his door has always been open. He allowed me a great deal of autonomy, permitting me the freedom to determine the direction of my research, for which I am most grateful.

My thesis committee members, Bruce Alberts, David Toczyski, and Thea Tlsty, have been a wonderful source of support and advice over the years. Their perspectives on my work and the related fields have been invaluable.

I would also like to thank my lab mates, Chris Richardson and Stacey Hanlon, for the many years of helpful discussions and feedback.

My development as a scientist began before arriving at UCSF. I am deeply thankful for the incredible foundational training I received from my mentors Trudy Kohout and Amy Pasquinelli at Neurocrine Biosciences and UCSD, respectively. Both of their labs were amazing places work and learn, and I am fortunate to have had such opportunities.

Graduate school has often been stressful and frequently taxing. Throughout the years, and especially at those trying times, I have been blessed to have my friends and family to support me. My classmates and dear friends Ian Foe and Scott Foster have been a great source of support and diversion, each knowing first-hand what the pre-doctoral training process here at UCSF is like. Anthony Austin, my closest friend, has also supported me greatly, believing unwaveringly in my ability to succeed.

I am deeply grateful for the support and love of my family, especially my parents,

throughout my training and my life in general. Despite not understanding a word of what I tell them regarding my research, they always ask about what I'm working on and offer encouraging remarks. They believe in me and what I can do, and knowing that has been so important. Much of what has made me a great experimentalist and scientist comes from my family. My parents instilled a strong work ethic in me from an early age, along with a sense of taking pride in one's work. My upbringing helped shape me into the person, and scientist, I now am.

Above all, I am grateful for my loving and incredibly supportive wife, Gia DiNicola, to whom I dedicate this Thesis. I cannot imagine my life without her, and consider myself truly blessed to share each day with her. She has enriched my life so deeply, and has made getting through this training period possible. We've shared so many wonderful experiences together over the years, and many trying ones as well, and have grown together through them all. She makes me laugh (pretty much constantly), helps me cry, and loves me unconditionally. I love her more and more each day.

The work described in Chapter 2 is a reprint of the material as it appears in “Loss of DNA Replication Control is a Potent Inducer of Gene Amplification” Brian M. Green, Kenneth J. Finn, and Joachim J. Li (2010) *Science*, **329**: (943-946); doi:10.1126/science.1190966. The American Association for the Advancement of *Science*, the non-profit publisher of *Science*, reserves the right for authors to reproduce their contributions in whole or in part in a thesis or dissertation without acquiring specific permission. Brian Green and Kenneth Finn performed the experiments and analyzed the data. All authors contributed to the study design, writing of the manuscript, and editing of the manuscript.

The work described in Chapter 3 is a reprint of the material as it appears in “Single-Stranded Annealing Induced by Re-Initiation of Replication Origins Provides a Novel and Efficient Mechanism for Generating Copy Number Expansion via Non-Allelic Homologous Recombination” Kenneth J. Finn and Joachim J. Li (2013) *PLoS Genet.* 9(1): e1003192; doi:10.1371/journal.pgen.1003192. The Public Library of Science (PLOS), the non-profit publisher of *PLoS Genetics*, permits unrestricted reuse of published material by the authors without acquiring specific permission. Kenneth J. Finn performed the experiments and analyzed the data. Kenneth J. Finn and Joachim J. Li contributed to the study design, writing of the manuscript, and editing of the manuscript.

The work described in Chapter 4 is not yet published, but will be submitted for publication in the near future. Kenneth J. Finn performed the experiments and analyzed the data. Kenneth J. Finn, Liam J. Holt, and Joachim J. Li contributed to the study design. Kenneth J. Finn wrote and edited the manuscript.

Abstract

Re-Replication Induced Gene Amplification: Mechanism, Phenomenon, and Significance

Kenneth John Finn

Eukaryotic cells employ a battery of overlapping control mechanisms to ensure that each segment of their genome is replicated once, and only once, per cell cycle. While the long standing view of the field is that this tight block to re-replication is necessary for the preservation of genome integrity, there is no direct experimental evidence supporting this belief. The work presented in Chapter 2 critically evaluates this idea and demonstrates that experimental induction of low, sub-lethal levels of re-replication in *Saccharomyces cerevisiae* can indeed cause at least one form of genomic instability, namely gene amplification. The mechanism of such Re-Replication Induced Gene Amplification (RRIGA) is explored in Chapter 3. There, I show that re-replication forks are prone to frequent breakage, which instigates a repair response. Non-allelic repetitive sequence elements positioned to either side of the re-initiating origin undergo homologous recombination through a single-stranded annealing mechanism, ultimately generating a head-to-tail duplication *in loco*. These duplications have repetitive sequence elements at the amplicon boundaries and a hybrid repetitive element at the inter-amplicon junction. The details of the mechanism provide insight into why re-replication is so efficient at producing segmental amplifications. Finally, in Chapter 4 I address the relevance of RRIGA. There I present evidence that RRIGA is a likely driver of spontaneous segmental amplifications in cells with intact replication controls. Furthermore, I show that very slight disruption of replication control greatly increases the rate of such amplifications. These findings strongly suggest a role for RRIGA in both evolution and oncogenesis.

Table of Contents

Acknowledgments	iii
Abstract	vi
List of Tables	viii
List of Figures	x
Chapter 1:	
General Introduction.....	1
Chapter 2:	
Loss of DNA Replication Control Is a Potent Inducer of Gene Amplification.....	23
Chapter 3:	
Single-Stranded Annealing Induced by Re-Initiation of Replication Origins Provides a Novel and Efficient Mechanism for Generating Copy Number Expansion via Non-Allelic Homologous Recombination.....	79
Chapter 4:	
Re-Replication Underlies Spontaneous Segmental Amplification in Normal <i>S. cerevisiae</i> Cells	181
Chapter 5:	
Conclusions.....	240

List of Tables

Chapter 2:

Table S1. Frequency of 1/2, 1/4, and 1/8 red sectored colonies observed in this work.....	44
Table S2. Analysis of sectored colonies generated by re-replicating strain containing reporter cassette at Chr IV _{567kb} (YJL6558).....	47
Table S3. CGH analysis of sectored colonies generated by re-replicating strain containing reporter cassette at Chr IV _{1089kb} (YJL6561).....	48
Table S4. CGH analysis of sectored colony isolates generated by non-re-replicating strain containing reporter cassette at ChrIV _{567kb} (YJL6974).....	49
Table S5. CGH analysis of sectored colonies generated by DNA damage from 20 µg/ml phleomycin in diploid strain containing reporter cassette at 567kb on one homolog of ChrIV (YJL7007).....	50
Table S6. CGH analysis of sectored colonies generated in <i>rad52Δ</i> (YJL7452) and <i>dnl4Δ</i> (YJL7443) re-replicating strains containing reporter cassette at ChrIV _{567kb}	51
Table S7. Oligonucleotides used in this study.....	53
Table S8. Plasmids used in this study.....	54
Table S9. Yeast strains used in this study.....	55

Chapter 3:

Table S1. Frequency of 1/2, 1/4, and 1/8 red sectored colonies observed in this work.....	130
--	-----

Table S2. aCGH analysis of red-sectoring colony isolates.....	132
Table S3. Frequency of uracil prototrophs from the selection assay observed in this work.....	142
Table S4. aCGH analysis of uracil prototroph isolates.....	144
Table S5. Yeast strains used in this study.....	149
Table S6. Plasmids used in this study.....	158
Table S7. Oligonucleotides used in this study.....	159

Chapter 4:

Table 1. Amplification rates for deregulated strains.....	228
Table 2. Amplification rates for replication stress strains.....	228
Table 3. Amplification rates for recombination mutants in the wild-type context.....	229
Table 4. Amplification rates for recombination mutants in the <i>orc2-cdk6A orc6-cdk4A</i> context.....	229
Table 5. Amplification rates for <i>CLB</i> deletions.....	230
Table S1. Oligonucleotides used in this study.....	231
Table S2. Plasmids used in this study.....	234
Table S3. Yeast strains used in this study.....	236

List of Figures

Chapter 1:

Figure 1. Replication initiation In <i>S. cerevisiae</i>	18
Figure 2. Breakage-Fusion-Bridge model.....	20
Figure 3. Unequal Exchange model.....	21
Figure 4. 1980s model for over-replication mediated gene amplification.....	22

Chapter 2:

Figure 1. Re-replication greatly stimulates gene amplification.....	32
Figure 2. Structure of gene amplifications induced by re-replication.....	33
Figure 3. Role of nonallelic homologous recombination in RRIGA.....	34
Figure S1. Screening for re-replication induced gene amplification using colony sectoring.....	35
Figure S2. Re-replication from Chr IV _{1089kb} induces primary gene amplification.....	37
Figure S3. Specificity of primary gene amplifications induced by re-replication.....	39
Figure S4. Sequence of hybrid Ty elements at interamplicon junctions.....	41
Figure S5. Breakage-fusion-bridge model.....	43

Chapter 3:

Figure 1. Homologous sequences are necessary and sufficient in <i>cis</i> to support RRIGA.....	116
Figure 2. A selection based assay for detecting RRIGA events.....	117
Figure 3. RRIGA is primarily mediated by single-stranded annealing (SSA).....	119

Figure 4. Re-replication induces double stranded DNA breaks distal to flanking repetitive elements.....	120
Figure 5. Flanking repetitive elements must be re-replicated in order for RRIGA to occur.....	121
Figure 6. RRIGA proceeds most efficiently when the re-initiating origin lies within the amplicon.....	122
Figure S1. Detailed schematics of <i>YDRCTy1-1</i> , <i>YDRCTy2-1</i> , and <i>URA3</i> gene fragment replacements.....	123
Figure S2. RRIGA requires homology in <i>cis</i> and is not enhanced by the presence of inverted LTR repeats or tRNA genes.....	124
Figure S3. aCGH analysis of selected isolates from the sectoring assay.....	125
Figure S4. RRIGA is primarily mediated by single-stranded annealing (SSA).....	126
Figure S5. Re-replication induces double stranded DNA breaks distal to flanking repetitive elements on both sides of the origin.....	127
Figure S6. Decreased frequency of amplification observed for relocation of the amplicon boundaries is not caused by fitness defects.....	128
Figure S7. RRIGA proceeds most efficiently when the re-initiating origin lies within the amplicon.....	129

Chapter 4:

Figure 1. A recurrent spontaneous amplification is structurally consistent with RRIGA.....	224
Figure 2. Split <i>natR</i> reconstitution fluctuation analysis.....	226
Figure 3. Replication stress levels in deregulated strains are comparable to the levels in the replication stress strains.....	228

Chapter 1

General Introduction

Duplication of the genome is arguably the most important task a cell is faced with. Cell proliferation hinges upon the successful execution of this process; failure precludes the distribution of copies of the parental genome to the two daughter cells. It is therefore unsurprising that numerous control systems, safeguards, and surveillance mechanisms are employed to ensure that complete, exact copies of the genome are produced. Indeed, the fact that evolutionary forces have selected for such extremely high fidelity in the DNA replication process is evidence in itself for the importance of accuracy of DNA replication for the cell.

The exact duplication of the parental genome requires more than extreme accuracy at the level of nucleotide incorporation and subsequent proofreading, however. In addition to ensuring precision in the actual sequence of each segment of the genome, the cell must also ensure that each segment is replicated exactly once during each cell cycle. To guarantee this once and only once replication, eukaryotic cells employ multiple overlapping mechanisms to prevent re-initiation of replication from any of the hundreds to thousands of origins within a given cell cycle [1–3]. While the details of individual mechanisms preventing re-initiation are not well conserved across evolution the general theme is: re-licensing of replication origins is blocked through inhibition of components of the pre-replicative complex (pre-RC).

Replication Control in *Saccharomyces cerevisiae*

All known strategies to restrict replication to once and only once per cell cycle employed in *S. cerevisiae*, and in all eukaryotes for that matter, act at the stage of replication initiation. The initiation process is divided into two separate phases, origin licensing and firing, which each occur during distinct phases of the cell cycle (Figure 1). During the licensing phase, which occurs from the end of M phase and through G₁, pre-RCs are assembled at potential origins of replication. In budding yeast the Origin Recognition Complex (ORC), a heterohexameric complex composed of Orc1-6, is bound

throughout the cell cycle to specific DNA sequences, called Autonomously Replicating Sequences (ARS) [1,4,5], which define the locations of potential origins. To form a pre-RC, ORC first recruits Cdc6, an AAA+ ATPase, followed by two complexes consisting of Cdt1 and the core replicative helicase, the Mcm2-7 heterohexamer [6,7]. Loading of the pair of core helicases is completed through ATP hydrolysis by Cdc6, resulting in a head to head double hexamer of Mcm2-7 bound at origin DNA, along with dissociation of Cdt1 from the pre-RC [8]. At the end of this licensing process the loaded helicases are still inactive.

After licensing and following passage through START, DNA replication can then be triggered during the firing phase. Triggering of initiation requires conversion of the inactive core helicases into an active state. This requires the action of two critical kinases, Cyclin-Dependent Kinase (CDK) and Dbf4-Dependent Kinase (DDK). CDK phosphorylates two principal targets, Sld2 and Sld3, which has the net effect of forming a transient complex known as the pre-Loading Complex (pre-LC) composed of Sld2, Dpb11, the GINS complex, and Pol ϵ [9], and recruiting this pre-LC to the existing pre-RC through an interaction between Dpb11 and phosphorylated Sld3 [10,11], which associates with pre-RCs along with Cdc45 [12]. The recruitment of the pre-LC to the pre-RC generates the pre-Initiation Complex (pre-IC). The pre-IC is in turn converted into an active replisome upon activation, during which Cdc45 and GINS associate with Mcm2-7 to form the CMG complex, the active form of the replicative helicase. The other components of the pre-LC dissociate upon activation. The action of DDK is also required for conversion of the pre-RC into an active replisome, though its precise function is less clear [13]. DDK phosphorylates components of the Mcm2-7 complex, which likely causes a conformational change in the complex. This conformational change may in turn modulate the interaction of the complex with other components of the replisome, or its interaction with the DNA.

The key to blocking re-initiation of replication lies in the separation of the

initiation reaction into its two separate stages. In addition to triggering initiation from existing pre-RCs, CDK activity prevents the formation of new pre-RCs. This is accomplished through CDK phosphorylation of multiple components of the pre-RC: Cdc6, Mcm2-7, and ORC. CDK phosphorylation inhibits the activity of each of these components in different ways. Cdc6 is targeted for ubiquitination and proteolytic degradation [14], is directly inhibited through binding by mitotic CDK Clb2/Cdc28 [15], and is transcriptionally down-regulated [16]. Cdt1/Mcm2-7 is exported out of the nucleus [17–20] and is thereby segregated from the DNA owing to a closed mitosis in budding yeast. Phosphorylation of ORC blocks one of its Cdt1 binding sites, thereby preventing helicase loading [3,21]. Thus, when the level of CDK activity rises upon passage through START and entry into S-phase, replication is initiated from existing pre-RCs, but re-licensing is prevented. As cells exit the M phase and CDK activity drops pre-RCs can once again be assembled, but cannot be fired until CDK activity rises again.

The various mechanisms blocking re-initiation in budding yeast are not redundant, but rather work in an overlapping manner [22,23]. That is, each individual mechanism contributes in a quantitative fashion to the block to re-initiation. Disruption of increasing numbers of these control mechanisms causes increasing amounts of re-replication. Inactivation of a sufficient number of these controls results in extensive DNA damage and cell death, demonstrating the importance of preventing high levels re-replication [24,25].

But why is the block to re-replication so stringent? While it is clear that high levels of re-replication are lethal, what are the effects of low levels? The answer submitted by the field has long been that re-replication threatens genome stability. That is, re-replication can result in heritable genomic alterations. However, while this argument seems reasonable, there was no direct evidence to support it prior to the work described as part of this dissertation [26].

Critical evaluation of the consequences of re-replication on genome stability requires the ability to induce low, sub-lethal levels of re-replication, as well as techniques

capable of measuring that re-replication. Previous work in our laboratory identified a combination of disruptions to replication control that causes re-initiation from primarily a single origin, *ARS317* [22]. This re-initiation is undetectable using conventional assays such as flow cytometry, but can be measured using a more sensitive array Comparative Genomic Hybridization (aCGH) method. Importantly, significant cell viability can be retained if re-initiation is only transiently induced in this setting, affording us the first opportunity to critically evaluate the long standing belief that re-replication can cause genomic instability. Of the various kinds of genomic alterations that might be caused by re-replication, we first examined the effect of re-initiation on the induction of gene amplification, a process by which the copy number of a given gene or segment of the genome is increased.

Gene Amplification

The emergence of new genes with novel functions has long been regarded as a major driving force in evolution [27–29]. The duplication or amplification of existing genes, or in many cases large stretches of the genome containing multiple genes, is thought to play a major role in the creation of these new genes by providing a substrate for adaptive molecular innovation. One proposed model for such innovation, known as neofunctionalization, posits that the presence of duplicate, redundant copies of a given gene relaxes the selective pressures acting upon one copy. The ancestral function of the original gene is retained in one copy of the gene while the duplicate copy is free to acquire random mutations. These mutations will generally be deleterious and lead to pseudogenization, but in some cases may result in the genesis of a gene with novel, advantageous functions. Alternatively, duplication of a gene with multiple activities can lead to a division of those activities between the duplicate copies, a process known as subfunctionalization. The mere presence of multiple, identical copies of a gene can have phenotypic consequences as well. Examples of each of these outcomes of gene

duplication/amplification are evident in the genomes of organisms from all three domains of life [28]. Moreover, the importance of gene amplification/amplification in evolution is underscored by the large percentage of duplicated genes in many sequenced genomes (for example, 30% in *S.cerevisiae* and 38% in *H. sapiens*).

Gene amplification also plays a major role in human cancer [30–32].

Amplification of oncogenes can drive tumor initiation and/or progression, and acquired resistance to chemotherapeutic agents is frequently achieved through amplification of resistance genes, leading to their over-expression [32,33]. Multiple examples of this latter phenomenon have been documented, including amplification of the *DHFR* and *CAD* genes, conferring resistance to the drugs methotrexate and PALA, respectively [33 and references therein]. Furthermore, amplification is of clinical importance in that amplification of particular genes or clusters of genes has diagnostic and/or prognostic utility for certain cancers, and can serve as an indicator for particular treatments. Thus, understanding the origins of these amplifications has the potential to improve both our understanding of tumor biology, as well as advance our clinical treatments. For example, if the pathways that promote amplification of drug resistance genes could be identified perhaps they could be inhibited to prevent such amplification and thereby improve the efficacy of existing chemotherapeutic interventions.

Direct molecular analysis of primary gene amplification events is often precluded, owing to the rarity of such events. Thus, their mechanisms have been inferred primarily from structural studies of the resulting amplifications. Amplifications can be either extrachromosomal or intrachromosomally arrayed [32–36]. Extrachromosomal amplifications are generally unstable and are maintained due to the selective advantage they provide to a cell. Intrachromosomal amplifications consist of tandemly arrayed amplicons, oriented either in inverted repeat (head-to-head) or direct repeat (head-to-tail), or more complicated combinations thereof, and can be positioned at their endogenous locus or at ectopic loci.

A veritable surfeit of mechanisms has been proposed over the years to explain the source of gene amplifications. Some of these models remain purely theoretical, with no clear experimental evidence to support them, while others at the opposite extreme are well validated. A discussion of a subset of these mechanisms is warranted here.

The most popular model for intrachromosomal gene amplification in tumor cells is the breakage-fusion-bridge model (BFB). In this model the initiating event consists of a double stranded break (DSB), or telomere erosion [32,37]. As shown in Figure 2, multiple cycles of chromosome breakage, fusion, and mitotic “bridging” can lead to increasing levels of amplification until the broken ends are healed by the addition or capture of telomeres. This model is supported by experimental observation of the intermediate events (ie. mitotic bridges) [38–40], by examination of some amplification structures in cell lines and in tumor cells [41–43], and through direct induction of the process in budding yeast [44,45]. Importantly, the BFB model can account for amplicons arrayed in inverted repeat, but not those arrayed in direct repeat, like the *HER2/ERBB2* amplifications frequently observed in human breast cancer [46–52]. Furthermore, BFB results in a loss of all of the sequences distal to the amplicon out to the telomere. This massive genomic collateral damage makes BFB a less attractive mechanism to explain amplifications in the context of organismal evolution. Hence, it is clear that a full understanding of gene amplification requires alternative models to complement the BFB model.

Perhaps the most favored model for generating head-to-tail, direct repeat amplifications is the so-called unequal exchange model, which is essentially a variation on normal allelic homologous recombination (Figure 3) [53–55]. The proposed initiating event is a simple double stranded break in or near a repetitive sequence element. An imperfect homology search results in the selection of a homologous, but non-identical sequence element on a sister chromatid or homolog as the repair template. Resolution of the double Holliday junction formed between the misaligned sisters or homologs can

result in a crossover event, generating a reciprocal sequence gain and loss on the two recombining molecules. Evidence for this model is, however, limited. The expected reciprocal gain and loss events predicted by this model have only been observed in the context of large arrays of tandem sequences in rDNA [56,57], *CUP1* gene repeats [58], and subtelomeric repeats [59], as well as in a few human genetic disorders [60]. Another model more recently proposed posits that duplications can be generated using a form of break-induced replication (BIR) [61,62]. Again, a double stranded break serves as the initiating event. Following a homology search, the broken end can invade a non-identical homologous sequence on a sister chromatid or homolog and establish a replication fork at the site of invasion. This fork can then replicate all of the sequences to the end of the telomere, resulting in a tandem, head-to-tail duplication. Unlike the unequal exchange model, this model does not necessitate reciprocal expansion and contraction events. As with the unequal exchange model, though, evidence for this mechanism is limited.

An alternative model, first published in 1981, proposed that gene amplification could be initiated by re-replication within a single cell cycle of the amplified region [33,35,63–67]. This model was partly inspired by observations of multiple rounds of replication from viral DNA integrated in the human genome and by the final “onion-skin” re-replication structures observed for the amplification of the chorion gene cluster in terminally differentiated *Drosophila* follicle cells [68–71]. According to this model, multiple rounds of re-initiation could give rise to a nested series of replication bubbles which could subsequently be resolved by some form of recombination into a variety of different gene amplification structures (Figure 4). At the time this model was proposed no methods were available to reliably detect re-replication, and too little was understood regarding replication control to induce it experimentally. Thus, no experimental support for the model could be obtained, leading to its general dismissal by the field.

Work in our laboratory and others’ during the past several decades has advanced

our knowledge of replication control considerably and provided us with new tools for detecting re-replication. As mentioned above, we now have the ability to induce re-replication in a temporally and spatially controlled fashion, providing us the opportunity to re-evaluate the long abandoned re-replication model for gene amplification. In Chapter 2 I will present evidence that re-replication can indeed potently induce the formation of intrachromosomal gene amplifications arrayed as head-to-tail repeats. This represents the first experimental evidence demonstrating that re-replication is a source of heritable genomic alterations, validating the longstanding belief that re-replication threatens genome stability. Following this initial phenomenological observation, I investigated the molecular details of the mechanism of Re-Replication Induced Gene Amplification (RRIGA), which is presented in Chapter 3. Finally, Chapter 4 provides evidence suggesting that spontaneous re-initiation of replication may in fact be a driver of gene amplification in the context of evolution. It also demonstrates that disruption of individual replication control mechanisms dramatically increases the rate of gene amplification, raising the possibility that the kind of dysregulation of replication control proteins observed in human tumors causes genomic instability.

References

1. Arias EE, Walter JC (2007) Strength in numbers: preventing rereplication via multiple mechanisms in eukaryotic cells. *Genes Dev* 21: 497–518. doi:10.1101/gad.1508907.
2. Diffley JFX (2011) Quality control in the initiation of eukaryotic DNA replication. *Philos Trans R Soc Lond, B, Biol Sci* 366: 3545–3553. doi:10.1098/rstb.2011.0073.
3. Nguyen VQ, Co C, Li JJ (2001) Cyclin-dependent kinases prevent DNA re-replication through multiple mechanisms. *Nature* 411: 1068–1073. doi:10.1038/35082600.

4. Bell SP, Dutta A (2002) DNA replication in eukaryotic cells. *Annu Rev Biochem* 71: 333–374. doi:10.1146/annurev.biochem.71.110601.135425.
5. Symeonidou I-E, Taraviras S, Lygerou Z (2012) Control over DNA replication in time and space. *FEBS Lett* 586: 2803–2812. doi:10.1016/j.febslet.2012.07.042.
6. Remus D, Beuron F, Tolun G, Griffith JD, Morris EP, et al. (2009) Concerted loading of Mcm2-7 double hexamers around DNA during DNA replication origin licensing. *Cell* 139: 719–730. doi:10.1016/j.cell.2009.10.015.
7. Takara TJ, Bell SP (2011) Multiple Cdt1 molecules act at each origin to load replication-competent Mcm2-7 helicases. *EMBO J* 30: 4885–4896. doi:10.1038/emboj.2011.394.
8. Randell JCW, Bowers JL, Rodríguez HK, Bell SP (2006) Sequential ATP hydrolysis by Cdc6 and ORC directs loading of the Mcm2-7 helicase. *Mol Cell* 21: 29–39. doi:10.1016/j.molcel.2005.11.023.
9. Muramatsu S, Hirai K, Tak Y-S, Kamimura Y, Araki H (2010) CDK-dependent complex formation between replication proteins Dpb11, Sld2, Pol (epsilon), and GINS in budding yeast. *Genes Dev* 24: 602–612. doi:10.1101/gad.1883410.
10. Zegerman P, Diffley JFX (2007) Phosphorylation of Sld2 and Sld3 by cyclin-dependent kinases promotes DNA replication in budding yeast. *Nature* 445: 281–285. doi:10.1038/nature05432.
11. Tanaka S, Umemori T, Hirai K, Muramatsu S, Kamimura Y, et al. (2007) CDK-dependent phosphorylation of Sld2 and Sld3 initiates DNA replication in budding yeast. *Nature* 445: 328–332. doi:10.1038/nature05465.
12. Kamimura Y, Tak YS, Sugino A, Araki H (2001) Sld3, which interacts with Cdc45 (Sld4), functions for chromosomal DNA replication in *Saccharomyces cerevisiae*. *EMBO J* 20: 2097–2107. doi:10.1093/emboj/20.8.2097.

13. Labib K (2010) How do Cdc7 and cyclin-dependent kinases trigger the initiation of chromosome replication in eukaryotic cells? *Genes Dev* 24: 1208–1219. doi:10.1101/gad.1933010.
14. Drury LS, Perkins G, Diffley JF (1997) The Cdc4/34/53 pathway targets Cdc6p for proteolysis in budding yeast. *EMBO J* 16: 5966–5976. doi:10.1093/emboj/16.19.5966.
15. Mimura S, Seki T, Tanaka S, Diffley JFX (2004) Phosphorylation-dependent binding of mitotic cyclins to Cdc6 contributes to DNA replication control. *Nature* 431: 1118–1123. doi:10.1038/nature03024.
16. Moll T, Tebb G, Surana U, Robitsch H, Nasmyth K (1991) The role of phosphorylation and the CDC28 protein kinase in cell cycle-regulated nuclear import of the *S. cerevisiae* transcription factor SWI5. *Cell* 66: 743–758.
17. Labib K, Diffley JF, Kearsley SE (1999) G1-phase and B-type cyclins exclude the DNA-replication factor Mcm4 from the nucleus. *Nat Cell Biol* 1: 415–422. doi:10.1038/15649.
18. Nguyen VQ, Co C, Irie K, Li JJ (2000) Clb/Cdc28 kinases promote nuclear export of the replication initiator proteins Mcm2-7. *Curr Biol* 10: 195–205.
19. Liku ME, Nguyen VQ, Rosales AW, Irie K, Li JJ (2005) CDK phosphorylation of a novel NLS-NES module distributed between two subunits of the Mcm2-7 complex prevents chromosomal rereplication. *Mol Biol Cell* 16: 5026–5039. doi:10.1091/mbc.E05-05-0412.
20. Tanaka S, Diffley JFX (2002) Interdependent nuclear accumulation of budding yeast Cdt1 and Mcm2-7 during G1 phase. *Nat Cell Biol* 4: 198–207. doi:10.1038/ncb757.
21. Chen S, Bell SP (2011) CDK prevents Mcm2-7 helicase loading by inhibiting Cdt1 interaction with Orc6. *Genes Dev* 25: 363–372. doi:10.1101/gad.2011511.

22. Green BM, Morreale RJ, Ozaydin B, Derisi JL, Li JJ (2006) Genome-wide mapping of DNA synthesis in *Saccharomyces cerevisiae* reveals that mechanisms preventing reinitiation of DNA replication are not redundant. *Mol Biol Cell* 17: 2401–2414. doi:10.1091/mbc.E05-11-1043.
23. Wilmes GM, Archambault V, Austin RJ, Jacobson MD, Bell SP, et al. (2004) Interaction of the S-phase cyclin Clb5 with an “RXL” docking sequence in the initiator protein Orc6 provides an origin-localized replication control switch. *Genes Dev* 18: 981–991. doi:10.1101/gad.1202304.
24. Green BM, Li JJ (2005) Loss of rereplication control in *Saccharomyces cerevisiae* results in extensive DNA damage. *Mol Biol Cell* 16: 421–432. doi:10.1091/mbc.E04-09-0833.
25. Archambault V, Ikui AE, Drapkin BJ, Cross FR (2005) Disruption of mechanisms that prevent rereplication triggers a DNA damage response. *Mol Cell Biol* 25: 6707–6721. doi:10.1128/MCB.25.15.6707-6721.2005.
26. Green BM, Finn KJ, Li JJ (2010) Loss of DNA replication control is a potent inducer of gene amplification. *Science* 329: 943–946. doi:10.1126/science.1190966.
27. Ohno S (1970) *Evolution by gene duplication*. Springer-Verlag. 184 p.
28. Zhang J (2003) Evolution by gene duplication: an update. *Trends in Ecology & Evolution* 18: 292–298. doi:10.1016/S0169-5347(03)00033-8.
29. Kaessmann H (2010) Origins, evolution, and phenotypic impact of new genes. *Genome Res* 20: 1313–1326. doi:10.1101/gr.101386.109.
30. Beroukhi R, Mermel CH, Porter D, Wei G, Raychaudhuri S, et al. (2010) The landscape of somatic copy-number alteration across human cancers. *Nature* 463: 899–905. doi:10.1038/nature08822.
31. Santarius T, Shipley J, Brewer D, Stratton MR, Cooper CS (2010) A census of amplified and overexpressed human cancer genes. *Nat Rev Cancer* 10: 59–64. doi:10.1038/nrc2771.

32. Albertson DG (2006) Gene amplification in cancer. *Trends Genet* 22: 447–455. doi:10.1016/j.tig.2006.06.007.
33. Stark GR, Wahl GM (1984) Gene amplification. *Annu Rev Biochem* 53: 447–491. doi:10.1146/annurev.bi.53.070184.002311.
34. Albertson DG, Collins C, McCormick F, Gray JW (2003) Chromosome aberrations in solid tumors. *Nat Genet* 34: 369–376. doi:10.1038/ng1215.
35. Schimke RT (1984) Gene amplification in cultured animal cells. *Cell* 37: 705–713.
36. Hahn PJ (1993) Molecular biology of double-minute chromosomes. *Bioessays* 15: 477–484. doi:10.1002/bies.950150707.
37. Debatisse M, Malfoy B (2005) Gene amplification mechanisms. *Adv Exp Med Biol* 570: 343–361. doi:10.1007/1-4020-3764-3_12.
38. Toledo F, Buttin G, Debatisse M (1993) The origin of chromosome rearrangements at early stages of AMPD2 gene amplification in Chinese hamster cells. *Curr Biol* 3: 255–264.
39. Ma C, Martin S, Trask B, Hamlin JL (1993) Sister chromatid fusion initiates amplification of the dihydrofolate reductase gene in Chinese hamster cells. *Genes Dev* 7: 605–620.
40. Reshmi SC, Roychoudhury S, Yu Z, Feingold E, Potter D, et al. (2007) Inverted duplication pattern in anaphase bridges confirms the breakage-fusion-bridge (BFB) cycle model for 11q13 amplification. *Cytogenet Genome Res* 116: 46–52. doi:10.1159/000097425.
41. Hellman A, Zlotorynski E, Scherer SW, Cheung J, Vincent JB, et al. (2002) A role for common fragile site induction in amplification of human oncogenes. *Cancer Cell* 1: 89–97.

42. Toledo F, Le Roscouet D, Buttin G, Debatisse M (1992) Co-amplified markers alternate in megabase long chromosomal inverted repeats and cluster independently in interphase nuclei at early steps of mammalian gene amplification. *EMBO J* 11: 2665–2673.
43. Poupon MF, Smith KA, Chernova OB, Gilbert C, Stark GR (1996) Inefficient growth arrest in response to dNTP starvation stimulates gene amplification through bridge-breakage-fusion cycles. *Mol Biol Cell* 7: 345–354.
44. Narayanan V, Mieczkowski PA, Kim H-M, Petes TD, Lobachev KS (2006) The pattern of gene amplification is determined by the chromosomal location of hairpin-capped breaks. *Cell* 125: 1283–1296. doi:10.1016/j.cell.2006.04.042.
45. Narayanan V, Lobachev KS (2007) Intrachromosomal gene amplification triggered by hairpin-capped breaks requires homologous recombination and is independent of nonhomologous end-joining. *Cell Cycle* 6: 1814–1818.
46. Kuwahara Y, Tanabe C, Ikeuchi T, Aoyagi K, Nishigaki M, et al. (2004) Alternative mechanisms of gene amplification in human cancers. *Genes Chromosomes Cancer* 41: 125–132. doi:10.1002/gcc.20075.
47. Akiyama K, Nishi Y (1991) Cloning and physical mapping of DNA sequences encompassing a region in N-myc amplicons of a human neuroblastoma cell line. *Nucleic Acids Res* 19: 6887–6894.
48. Amler LC, Schwab M (1989) Amplified N-myc in human neuroblastoma cells is often arranged as clustered tandem repeats of differently recombined DNA. *Mol Cell Biol* 9: 4903–4913.
49. Herrick J, Conti C, Teissier S, Thierry F, Couturier J, et al. (2005) Genomic organization of amplified MYC genes suggests distinct mechanisms of amplification in tumorigenesis. *Cancer Res* 65: 1174–1179. doi:10.1158/0008-5472.CAN-04-2802.

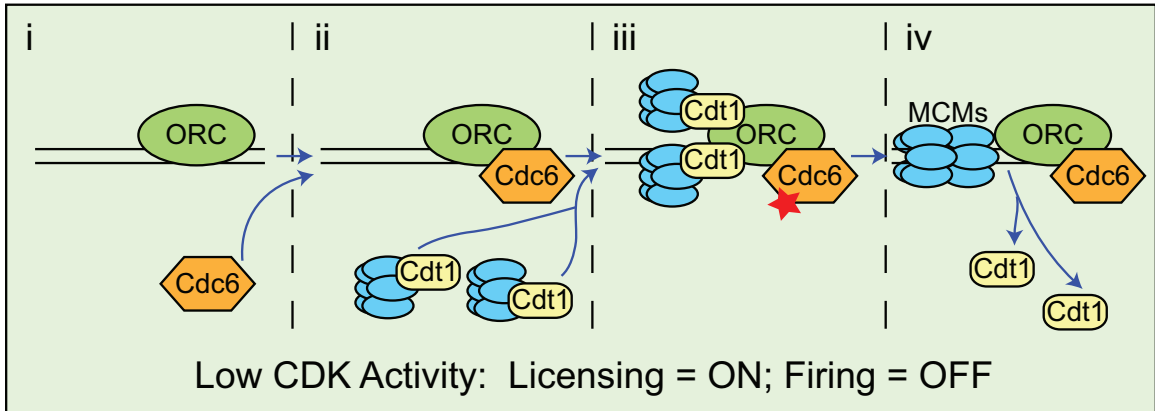
50. Lahortiga I, De Keersmaecker K, Van Vlierberghe P, Graux C, Cauwelier B, et al. (2007) Duplication of the MYB oncogene in T cell acute lymphoblastic leukemia. *Nat Genet* 39: 593–595. doi:10.1038/ng2025.
51. O’Neil J, Tchinda J, Gutierrez A, Moreau L, Maser RS, et al. (2007) Alu elements mediate MYB gene tandem duplication in human T-ALL. *J Exp Med* 204: 3059–3066. doi:10.1084/jem.20071637.
52. Strout MP, Marcucci G, Bloomfield CD, Caligiuri MA (1998) The partial tandem duplication of ALL1 (MLL) is consistently generated by Alu-mediated homologous recombination in acute myeloid leukemia. *Proc Natl Acad Sci USA* 95: 2390–2395.
53. Chen J-M, Cooper DN, Férec C, Kehrer-Sawatzki H, Patrinos GP (2010) Genomic rearrangements in inherited disease and cancer. *Semin Cancer Biol* 20: 222–233. doi:10.1016/j.semcancer.2010.05.007.
54. Hoang ML, Tan FJ, Lai DC, Celniker SE, Hoskins RA, et al. (2010) Competitive repair by naturally dispersed repetitive DNA during non-allelic homologous recombination. *PLoS Genet* 6: e1001228. doi:10.1371/journal.pgen.1001228.
55. Hastings PJ, Lupski JR, Rosenberg SM, Ira G (2009) Mechanisms of change in gene copy number. *Nat Rev Genet* 10: 551–564. doi:10.1038/nrg2593.
56. Szostak JW, Wu R (1980) Unequal crossing over in the ribosomal DNA of *Saccharomyces cerevisiae*. *Nature* 284: 426–430.
57. Petes TD (1980) Unequal meiotic recombination within tandem arrays of yeast ribosomal DNA genes. *Cell* 19: 765–774.
58. Welch JW, Maloney DH, Fogel S (1990) Unequal crossing-over and gene conversion at the amplified CUP1 locus of yeast. *Mol Gen Genet* 222: 304–310.
59. Louis EJ, Haber JE (1990) Mitotic recombination among subtelomeric Y’ repeats in *Saccharomyces cerevisiae*. *Genetics* 124: 547–559.

60. Liu P, Carvalho CM, Hastings P, Lupski JR (2012) Mechanisms for recurrent and complex human genomic rearrangements. *Current Opinion in Genetics & Development* 22: 211–220. doi:10.1016/j.gde.2012.02.012.
61. Simmons AD, Carvalho CMB, Lupski JR (2012) What have studies of genomic disorders taught us about our genome? *Methods Mol Biol* 838: 1–27. doi:10.1007/978-1-61779-507-7_1.
62. Payen C, Koszul R, Dujon B, Fischer G (2008) Segmental duplications arise from Pol32-dependent repair of broken forks through two alternative replication-based mechanisms. *PLoS Genet* 4: e1000175. doi:10.1371/journal.pgen.1000175.
63. Roberts JM, Axel R (1982) Gene amplification and gene correction in somatic cells. *Cell* 29: 109–119.
64. Roberts JM, Buck LB, Axel R (1983) A structure for amplified DNA. *Cell* 33: 53–63.
65. Schimke RT, Sherwood SW, Hill AB, Johnston RN (1986) Overreplication and recombination of DNA in higher eukaryotes: potential consequences and biological implications. *Proc Natl Acad Sci USA* 83: 2157–2161.
66. Varshavsky A (1981) On the possibility of metabolic control of replicon “misfiring”: relationship to emergence of malignant phenotypes in mammalian cell lineages. *Proc Natl Acad Sci USA* 78: 3673–3677.
67. Stark GR, Debatisse M, Giulotto E, Wahl GM (1989) Recent progress in understanding mechanisms of mammalian DNA amplification. *Cell* 57: 901–908.
68. Botchan M, Topp W, Sambrook J (1979) Studies on simian virus 40 excision from cellular chromosomes. *Cold Spring Harb Symp Quant Biol* 43 Pt 2: 709–719.
69. Osheim YN, Miller OL, Beyer AL (1988) Visualization of *Drosophila melanogaster* chorion genes undergoing amplification. *Mol Cell Biol* 8: 2811–2821.
70. Spradling AC (1981) The organization and amplification of two chromosomal domains containing *Drosophila* chorion genes. *Cell* 27: 193–201.

71. Spradling AC, Mahowald AP (1981) A chromosome inversion alters the pattern of specific DNA replication in *Drosophila* follicle cells. *Cell* 27: 203–209.

Figure 1

A



B

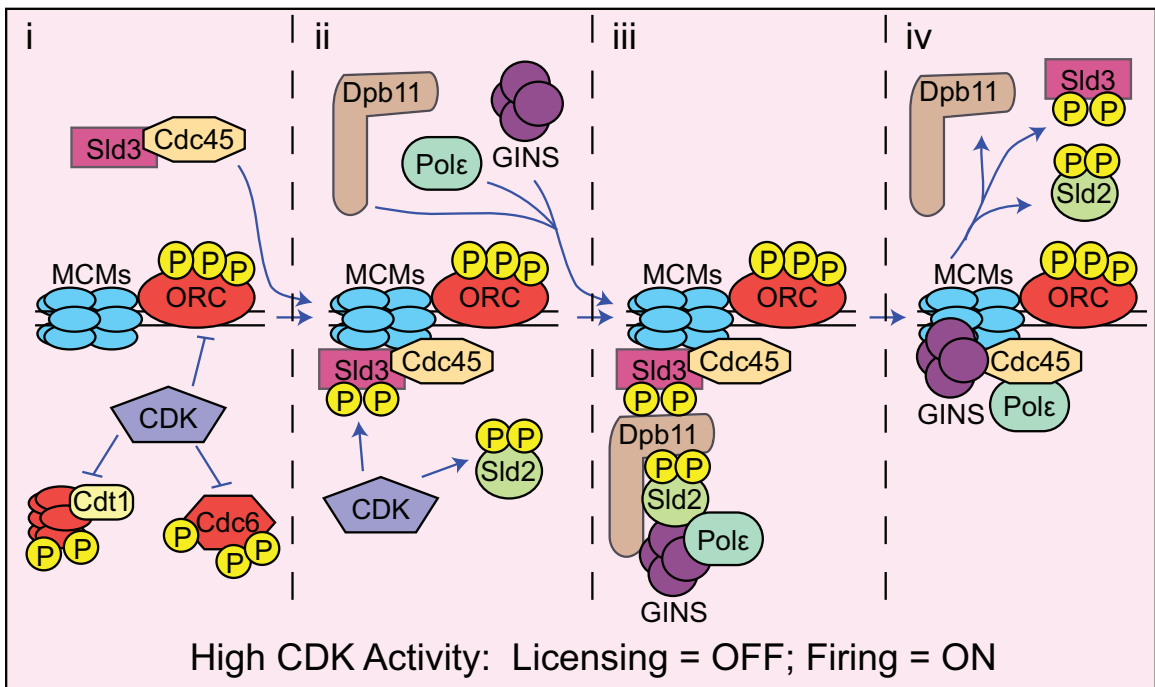


Figure 1. Replication initiation in *S. cerevisiae*. A) Origin licensing phase. (i) Origin bound ORC recruits Cdc6, (ii) followed by two complexes of Cdt1/Mcm2-7. (iii) ATP hydrolysis by Cdc6 (red star) results in (iv) loading of a head-to-head double hexamer of Mcm2-7 onto the DNA and dissociation of Cdt1. Low CDK activity during the licensing phase permits pre-RC assembly but not firing. B) Origin firing phase. Upon passage through START and entry into S-phase, CDK activity rises. (i) CDK phosphorylation (indicated by yellow balls labeled with a 'P') of ORC, Cdc6, and MCMs inhibits their functions (see text for details). (ii) CDK also phosphorylates Sld3, which associates with the pre-RC along

with Cdc45, and Sld2. (iii) Phosphorylation of Sld2 promotes its association with Dpb11 and formation of the pre-LC, composed of Dpb11, Sld2, the GINS complex, and Pol ϵ . The pre-LC is then recruited to the pre-RC through an interaction between Dpb11 and phosphorylated Sld3, forming the pre-IC. (iv) Cdc45 and the GINS complex associate with the MCMs to form the CMG complex, which is the active form of the replicative helicase. Pol ϵ will be incorporated into the replisome along with the CMG, while Dpb11, Sld2, and Sld3 will dissociate. For simplicity recruitment of only one pre-LC complex is shown. Two such complexes will be recruited by two separate Sld3/Cdc45 complexes to yield two CMGs.

Figure 2

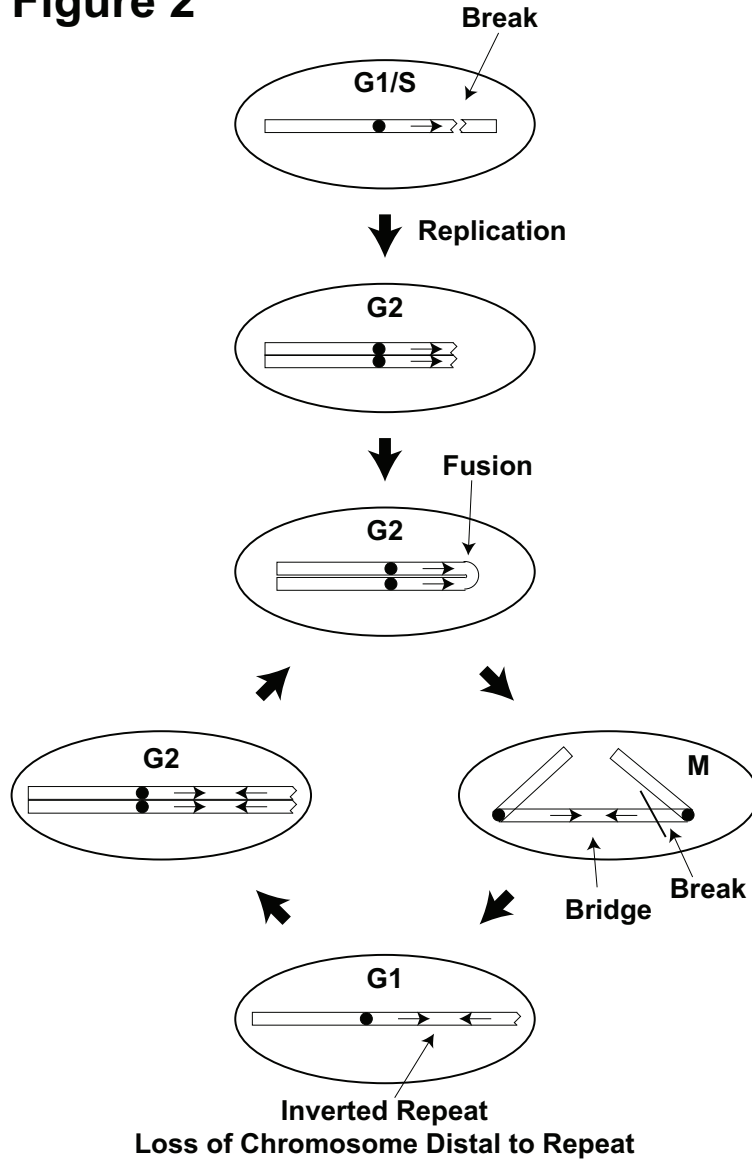


Figure 2. Breakage-Fusion-Bridge model. The initiating event in BFB is a simple DSB. Replication of the broken chromatid will result in a pair of sister chromatids, each with a broken end, which can then be joined together by non-homologous end-joining, resulting in a dicentric chromosome. This can result in an attempt to pull each centromere toward opposing poles during mitosis, forming a ‘bridge.’ This will cause in a new break, resulting in an inverted duplication of the end of one portion of the chromosome, along with deletion of all repeat distal sequences. The new broken end can re-initiate the cycle.

Figure 3

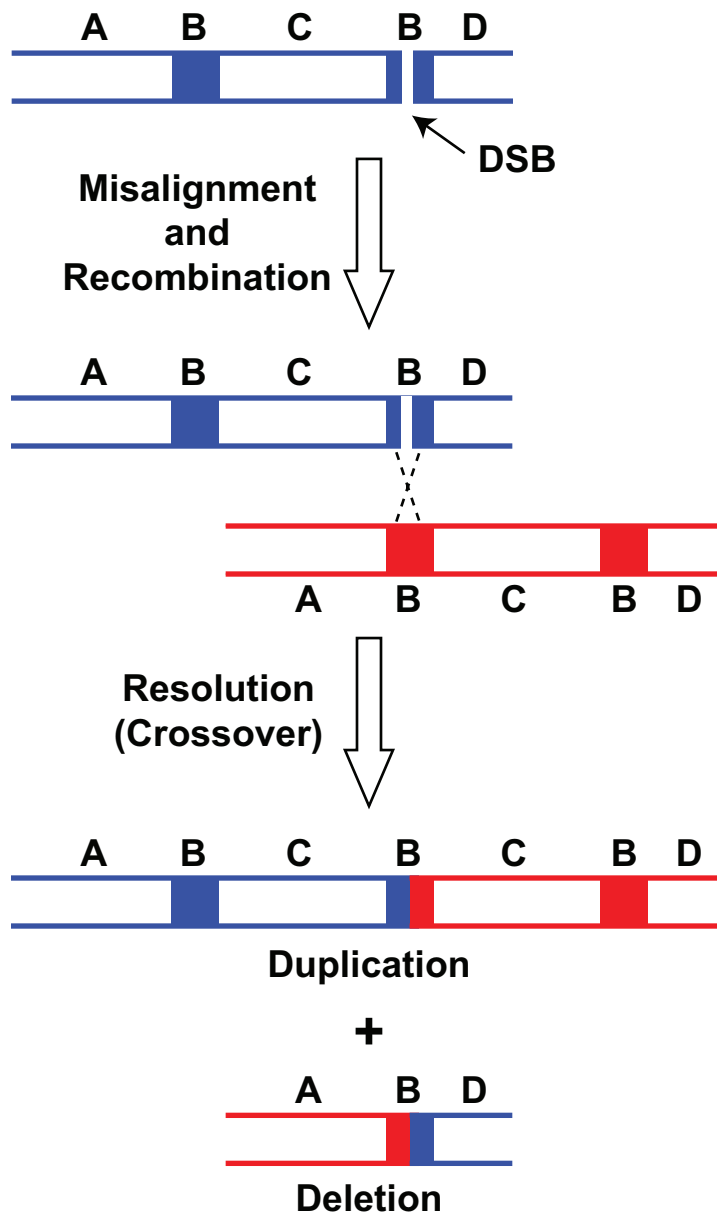


Figure 3. Unequal Exchange model. A DSB in or near a repetitive sequence (sequence 'B' in this diagram) provokes a search for a homologous sequence to use as a repair template. Misalignment with a sister chromatid or homolog results in the use of a homologous, but non-identical sequence as the repair template. Resolution of the resultant double Holliday junction as a crossover generates a reciprocal duplication and deletion of sequences for the two products.

Figure 4

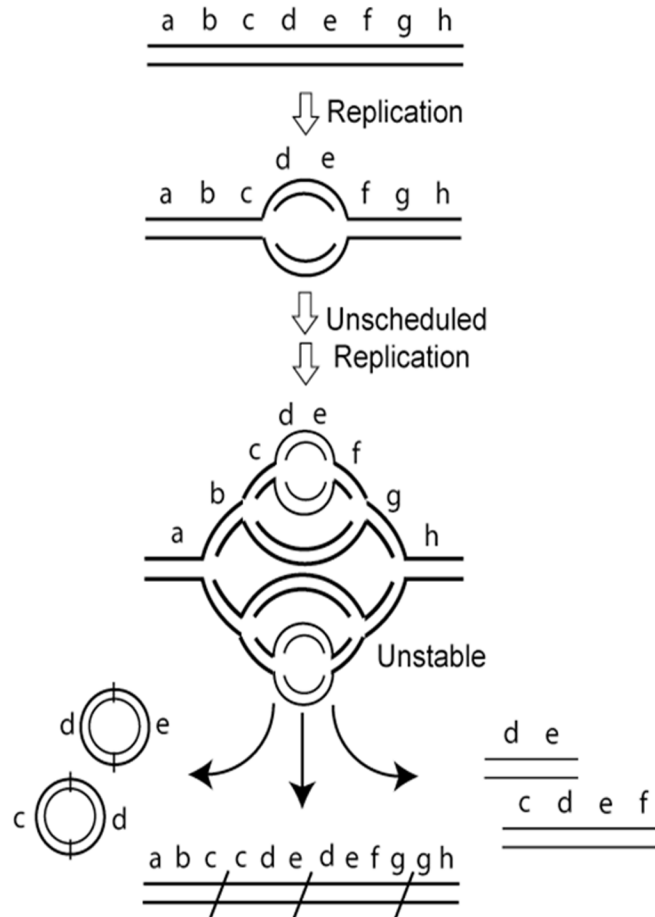


Figure 4. 1980s model for over-replication mediated gene amplification. Multiple rounds of unscheduled replication could generate a nested series of replication bubbles (the so-called “onion-skin” structure). This structure was proposed to be mitotically unstable. Some form of recombination was invoked to explain the resolution of this structure. Such resolution could generate circular or linear extrachromosomal amplifications, as well as linear intrachromosomal arrays of amplicons. Adapted from Stark and Wahl (1984).

Chapter 2

Loss of DNA Replication Control Is a Potent Inducer of Gene Amplification

Abstract

Eukaryotic cells use numerous mechanisms to ensure that no segment of their DNA is inappropriately re-replicated, but the importance of this stringent control on genome stability has not been tested. Here we show that re-replication in *Saccharomyces cerevisiae* can strongly induce the initial step of gene amplification, increasing gene copy number from one to two or more. The resulting amplicons consist of large internal chromosomal segments that are bounded by Ty repetitive elements and are intrachromosomally arrayed at their endogenous locus in direct head-to-tail orientation. These re-replication–induced gene amplifications are mediated by non-allelic homologous recombination between the repetitive elements. We suggest that re-replication may be a contributor to gene copy number changes, which are important in fields such as cancer biology, evolution, and human genetics.

Main Text

A central tenet of eukaryotic cell biology is that cells replicate their DNA only once every cell cycle. Although it has become an article of faith that this regulation is important because re-replication would threaten genome stability (1), that faith has never been experimentally tested. Preventing re-replication in eukaryotic cells requires blocking re-initiation at thousands of origins scattered throughout the genome, and eukaryotic cells use numerous overlapping mechanisms to do this (2, 3). By disrupting these mechanisms in a controlled manner, we are now able to examine re-replicated cells for possible genomic alterations. The alterations we first looked for were heritable increases in gene copy number. Such increases are observed in the gene amplifications commonly associated with cancers (4, 5), the gene duplications important for molecular evolution (6), and the copy number variations prevalent in human genomes (7). Although re-replication was once a leading model for copy number increases, specifically during gene amplification (8, 9), the model has long been abandoned for lack of experimental support for it (10). Hence, re-replication is not seriously considered as a possible source of heritable copy number changes (4, 11, 12). Here, we demonstrate that re-replication can readily induce copy number changes, provoking reconsideration of re-replication as a potential source of such changes in cancer and evolution (8).

We have developed a system to detect and quantify early amplification events arising from a transient and limited pulse of re-replication at a defined genomic locus in the budding yeast *Saccharomyces cerevisiae* (Fig. 1A and Figs. S1 and S2A). We took advantage of our ability to induce re-replication predominantly from a single origin (*ARS317*) by conditionally deregulating the replication initiation proteins Mcm2-7 and Cdc6 (MC_{2A} genetic background) (13). We also adapted a copy number assay in which cells with a single copy of the *ade3-2p* allele turn pink, and cells with two or more copies turn red (14).

ARS317 and *ade3-2p* were combined in a re-replicating reporter cassette (Fig.

S1A) that was integrated at either of two loci on Chromosome IV (Chr IV_{567kb} and Chr IV_{1089kb}) in a haploid MC_{2A} background from which the endogenous *ARS317* was deleted. After arresting cells at the G2/M phase [time (t) = 0 hours], we transiently induced re-replication until half of the *ARS317* origins re-initiated (t = 3 hours), then plated for isolated colonies at both time points. The mostly pink colonies were screened for heritable amplification of *ade3-2p* by looking for colonies with red sectors (Fig. S1B). Colonies with one-half, one-quarter, or one-eighth red sectors were scored to focus on amplifications arising within three generations of the re-replication pulse (Table S1).

Inducing re-replication for 3 hours from the *ade3-2p-ARS317* cassette integrated at Chr IV_{567kb} (strain YJL6558) caused a 42-fold increase in red sectors to 3.3% of all colonies (Fig. 1B). Suppressing this re-replication by removing deregulated Cdc6 from the MC_{2A} background (YJL6974) or *ARS317* from the cassette (YJL6555) resulted, respectively, in only 4- and 12-fold increases in red sectors (Fig. 1B), most of which had not amplified the *ade3-2p* cassette. Re-replication also induced colony sectoring by 38-fold when the *ade3-2p-ARS317* cassette was relocated to Chr IV_{1089kb} (Fig. S2B and Table S1).

Array comparative genomic hybridization (aCGH) on 35 red sectors derived from YJL6558 (Table S2) confirmed that most [31 of 35 (31/35)] had at least two copies of an internal chromosomal segment encompassing the *ade3-2p-ARS317* cassette. Amplicons ranged in size from 135 to 470 kb (Fig. 1C) with boundaries mapping within a few kilobases of Ty elements or, rarely, long terminal repeats (LTRs) oriented in direct repeat. Similar aCGH results were obtained for red sectors arising from re-replication of the *ade3-2p* cassette integrated at Chr IV_{1089kb} (Fig. S2C and Table S3). In contrast, few amplifications were observed among the less frequent red sectors isolated from the control strains YJL6974 (3/32) (Table S4) and YJL6555 (1/6).

Using the aCGH data to convert sectoring to amplification frequency (10), we estimated relative amplification frequencies of 1:8:230 for YJL6974:YJL6555:YJL6558,

respectively, and an absolute frequency of 3×10^{-2} for YJL6558 (Fig. 1B and Table S2). This frequency roughly translates into an order of magnitude rate of 10^{-2} per generation (10), which is significantly higher than spontaneous rates of segmental duplications (10^{-7} to 10^{-6} per generation) or higher-order amplifications (10^{-10}) reported for budding yeast (15, 16).

Re-replication generates slowed or stalled forks and DNA damage (17–20), perturbations that have been implicated in genomic alterations (21). Nonetheless, neither disruption of DNA replication by means of hydroxyurea or temperature sensitive replication mutations (Fig. S3, A and B) nor treatment of cells with the DNA-damaging agent phleomycin (Fig. S3, C to E, and Table S5) induced substantial *ade3-2p* amplification comparable to re-replication. Thus, re-replication appears to be particularly effective at inducing gene amplification (10), and we refer to these events as re-replication-induced gene amplification (RRIGA).

To investigate the mechanism of RRIGA, we determined the position, orientation, and boundaries of 20 segmental amplifications arising from re-replication of the *ade3-2p* cassette integrated at Chr IV₅₆₇. All 20 were located to Chr IV, because this chromosome increased in size by an amount consistent with the length and copy number of the additional amplicon(s) (Fig. 2A and Table S1). No other chromosomes increased in size, and probing for the *ADE3* sequences on the *ade3-2p* cassette confirmed that the amplicons resided only on Chr IV (Fig. 2A).

We then tested the hypothesis that the amplicons were tandemly arrayed at their endogenous locus. The three possible arrangements for such tandem duplications (head to tail, head to head, or tail to tail) each generate a particular set of junctions and boundaries that are distinguishable by polymerase chain reaction (PCR) (Fig. 2B). Moreover, we could confirm the presence of Ty or LTR elements at these boundaries by using primers that flank these elements. Of the 20 amplifications examined, PCR products from 19 of them established that RRIGA amplicons are indeed tandemly arrayed at their endogenous

locus in head-to-tail orientation and are bounded by Ty or LTR elements in direct repeat (Fig. 2B) (10).

Such structures could arise from non-allelic homologous recombination (NAHR). To examine this possibility, we sequenced the PCR products for inter-amplicon junctions from four independent amplifications spanning kilobases 515 to 650 on Chr IV. The sequences revealed hybrid Ty elements generated by precise crossovers between Ty2-1 at 515 kb and Ty1-1 at 650 kb (Fig. 3A and Fig. S4). In addition, RRIGA was greatly reduced by deletion of *RAD52*, which is essential for homologous recombination (Fig. 3, B and C, and Tables S1 and S6), but was not affected by deletion of *DNL4*, which is required for nonhomologous end-joining (NHEJ). Thus, RRIGA in budding yeast is mediated by NAHR between repetitive elements flanking a re-replicated chromosomal segment.

How re-replication might stimulate NAHR with such high efficiency is illustrated in Fig. 3D. First, re-replication increases the copy number of a chromosome segment. Second, re-replication forks, which display compromised progression, may stall, collapse, and break with high frequency. Third, in contrast to stalled replication forks in S phase, isolated re-replication forks are unlikely to be rescued by converging forks from neighboring origins. Fourth, the re-replication bubble structure can facilitate recombinational repair between re-replicated segments in a variety of ways, such as by pairing double-stranded breaks that might occur at both forks in trans.

In short, re-replication appears capable of promoting several key events in an optimal temporal order and spatial context to stimulate gene amplifications. The critical events occur before repair pathways are recruited, leaving room for alternative ways to resolve broken re-replication bubbles (10). Hence, although RRIGA is preferentially mediated by NAHR in budding yeast, additional repair pathways, such as NHEJ, might be used by other species. In fact, repair of broken re-replication bubbles may well stimulate other genomic alterations besides RRIGA.

Our results demonstrate that loss of eukaryotic DNA replication control can indeed induce genome instability, and in the case of RRIGA does so with extraordinary efficiency. Such efficiency suggests that even lower levels of re-replication, below the sensitivity of current assays (<5 to 10%), may cause substantial induction of RRIGA (10). Thus, although some consider the multiple mechanisms used to control replication as redundant, because disrupting them individually does not lead to detectable re-replication (2), we view each as essential for the stringent control needed to safeguard genome stability (2, 3, 13). Establishing that re-replication can induce copy number changes raises the question of whether re-replication actually does induce such changes in cancer and evolution (10). Several recent observations hint that RRIGA might indeed play a role in oncogenesis or tumor progression. For example, segmental duplications found in two tumor genomes bear striking similarity to RRIGA structures observed in budding yeast: Oncogenes are duplicated in a head-to-tail arrangement *in loco*, with repetitive Alu elements at the outer amplicon boundaries and a hybrid recombinant Alu element at the inter-amplicon junction (22, 23). Additionally, replication initiation proteins are overexpressed in a number of human cancers (1, 24), and modest overexpression of the replication proteins Cdt1 and Cdc6 can potentiate oncogenesis in mouse cells (25–27). We thus hope that our study provokes further investigation into the possible role of RRIGA in cancer and evolution.

References and Notes

1. J. J. Blow, P. J. Gillespie, *Nat. Rev. Cancer* 8, 799 (2008).
2. E. E. Arias, J. C. Walter, *Genes Dev.* 21, 497 (2007).
3. V. Q. Nguyen, C. Co, J. J. Li, *Nature* 411, 1068 (2001).
4. D. G. Albertson, *Trends Genet.* 22, 447 (2006).
5. W. W. Lockwood et al., *Oncogene* 27, 4615 (2008).
6. H. Innan, F. Kondrashov, *Nat. Rev. Genet.* 11, 97 (2010).

7. F. Zhang, W. Gu, M. E. Hurles, J. R. Lupski, *Annu. Rev. Genomics Hum. Genet.* 10, 451 (2009).
8. R. T. Schimke, S. W. Sherwood, A. B. Hill, R. N. Johnston, *Proc. Natl. Acad. Sci. U.S.A.* 83, 2157 (1986).
9. G. R. Stark, M. Debatisse, E. Giulotto, G. M. Wahl, *Cell* 57, 901 (1989).
10. See supporting material below.
11. P. J. Hastings, J. R. Lupski, S. M. Rosenberg, G. Ira, *Nat. Rev. Genet.* 10, 551 (2009).
12. R. Koszul, G. Fischer, *C. R. Biol.* 332, 254 (2009).
13. B. M. Green, R. J. Morreale, B. Ozaydin, J. L. Derisi, J. J. Li, *Mol. Biol. Cell* 17, 2401 (2006).
14. D. Koshland, J. C. Kent, L. H. Hartwell, *Cell* 40, 393 (1985).
15. C. Payen, R. Koszul, B. Dujon, G. Fischer, *PLoS Genet.* 4, e1000175 (2008).
16. M. J. Dorsey, P. Hoeh, C. E. Paquin, *Curr. Genet.* 23, 392 (1993).
17. V. Archambault, A. E. Ikui, B. J. Drapkin, F. R. Cross, *Mol. Cell. Biol.* 25, 6707 (2005).
18. B. M. Green, J. J. Li, *Mol. Biol. Cell* 16, 421 (2005).
19. M. Melixetian et al., *J. Cell Biol.* 165, 473 (2004).
20. C. Vaziri et al., *Mol. Cell* 11, 997 (2003).
21. A. Aguilera, B. Gómez-González, *Nat. Rev. Genet.* 9, 204 (2008).
22. J. O'Neil et al., *J. Exp. Med.* 204, 3059 (2007).
23. M. P. Strout, G. Marcucci, C. D. Bloomfield, M. A. Caligiuri, *Proc. Natl. Acad. Sci. U.S.A.* 95, 2390 (1998).
24. M. A. Gonzalez, K. E. Tachibana, R. A. Laskey, N. Coleman, *Nat. Rev. Cancer* 5, 135 (2005).
25. E. Arentson et al., *Oncogene* 21, 1150 (2002).
26. M. Liontos et al., *Cancer Res.* 67, 10899 (2007).

27. J. Seo et al., *Oncogene* 24, 8176 (2005).
28. We thank R. Bainton for the use of his microscope; A. Johnson for the use of his pulsed-field gel electrophoresis system and microscope; and A. Sil, D. Morgan, A. Johnson, D. Toczyski, E. Blackburn, P. O'Farrell, T. Tlsty, J. Haber, S. Elledge, and F. Winston for helpful discussions. This work was supported by grants to J.J.L. from the Sandler Program in Basic Sciences, the Stewart Trust Fund, UCSF Research Evaluation and Allocation Committee, UCSF Academic Senate, UC Cancer Research Coordinating Committee, and NIH (grant R01 GM59704). B.M.G. was supported by an NSF Predoctoral Fellowship and a Department of Defense Breast Cancer Predoctoral Fellowship (W81XWH-04-1-0409). K.J.F. was supported by an NSF Predoctoral Fellowship. Microarray data are deposited with the Gene Expression Omnibus (accession number GSE22018).

Figure 1

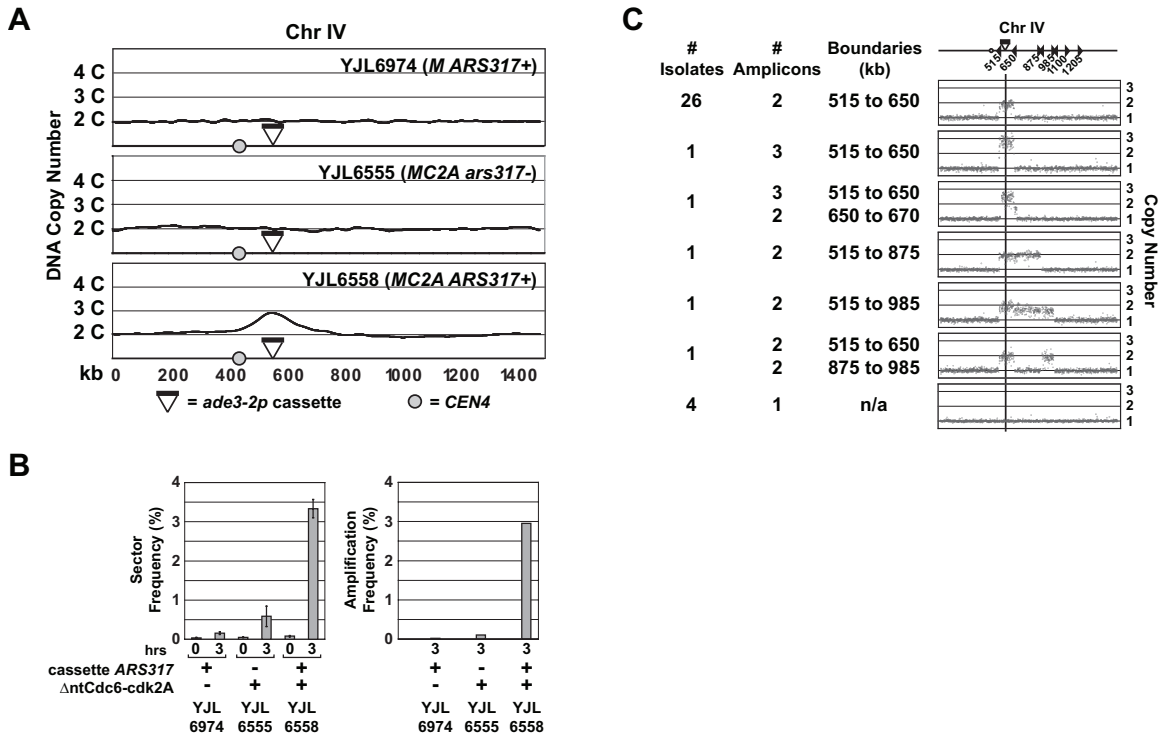


Figure 1. Re-replication greatly stimulates gene amplification. A) Induction of re-replication from *ARS317*. Strains containing an *ade3-2p* copy number reporter cassette integrated at Chr IV_{567kb} were arrested in G2/M phase and treated with galactose to trigger re-initiation of *ARS317*. aCGH analysis of re-replication (>2C) is shown for Chr IV. All other chromosomes maintained a 2C copy number (data not shown). Top panel: YJL6974, non-re-replicating strain with *ARS317* in cassette. Middle panel: YJL6555, re-replicating strain with no *ARS317* in cassette. Bottom panel: YJL6558, re-replicating strain with *ARS317* in cassette. B) *ARS317* re-replication stimulates gene amplification. Left Panel: frequency of 1/2 - 1/8 red sector colonies (mean \pm SEM, N = 2 to 7 induction replicates; see Table S1) after 0 or 3 hr galactose induction of YJL6974, YJL6555, and YJL6558. Right Panel: amplification frequency estimated by multiplying sector frequency by fraction of sector colonies displaying reporter cassette amplification (see text and Tables S2 and S4). C) Red sectors induced by re-replication display gene amplifications. 35 red sectors derived from YJL6558 were analyzed by aCGH and classified based on the copy number profile of Chr IV. Schematic of Chr IV shows positions of Ty elements (triangles), centromere (circle), and *ade3-2p* cassette (black bar).

Figure 2

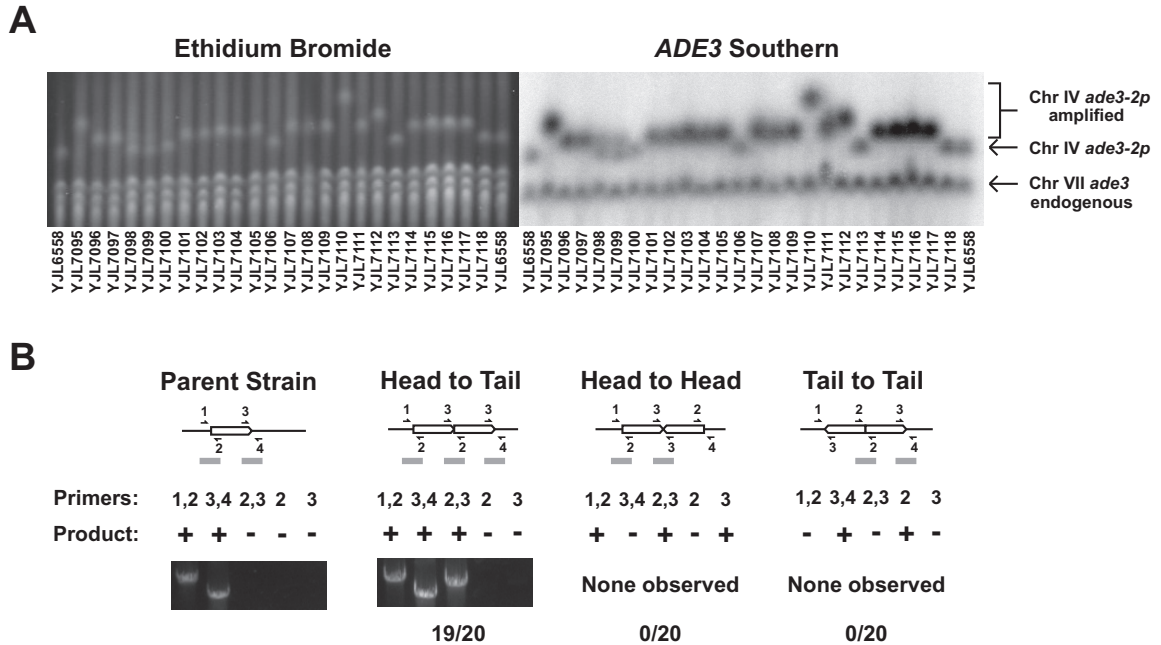


Figure 2. Structure of gene amplifications induced by re-replication. A) Amplicons remain on the endogenous chromosome. PFGE separated chromosomes from 24 sectors analyzed in Fig. 1C (Table S2) were visualized by ethidium bromide staining (left panel) then probed for *ADE3*, which detects both *ade3* on Chr VII and *ade3-2p* in the reporter cassette (right panel). YJL6558, the parental strain, YJL7100, YJL7106, YJL7113, and YJL7118 did not contain amplifications. The Chr IV doublet pattern for YJL7098 and YJL7099 is consistent with partial loss of amplification from population. B) Amplicons are tandemly arrayed *in loco* in direct head-to-tail orientation. Schematics of an unamplified amplicon and three possible orientations for amplicons tandemly duplicated *in loco* are shown. Predicted PCR junction fragments (10) are shown for five sets of primers that flank amplicon boundaries (+, PCR product expected; -, no PCR product expected). Representative PCR products are shown for parental strain YJL6558 and 19 of the 20 amplified strains displayed in A).

Figure 3

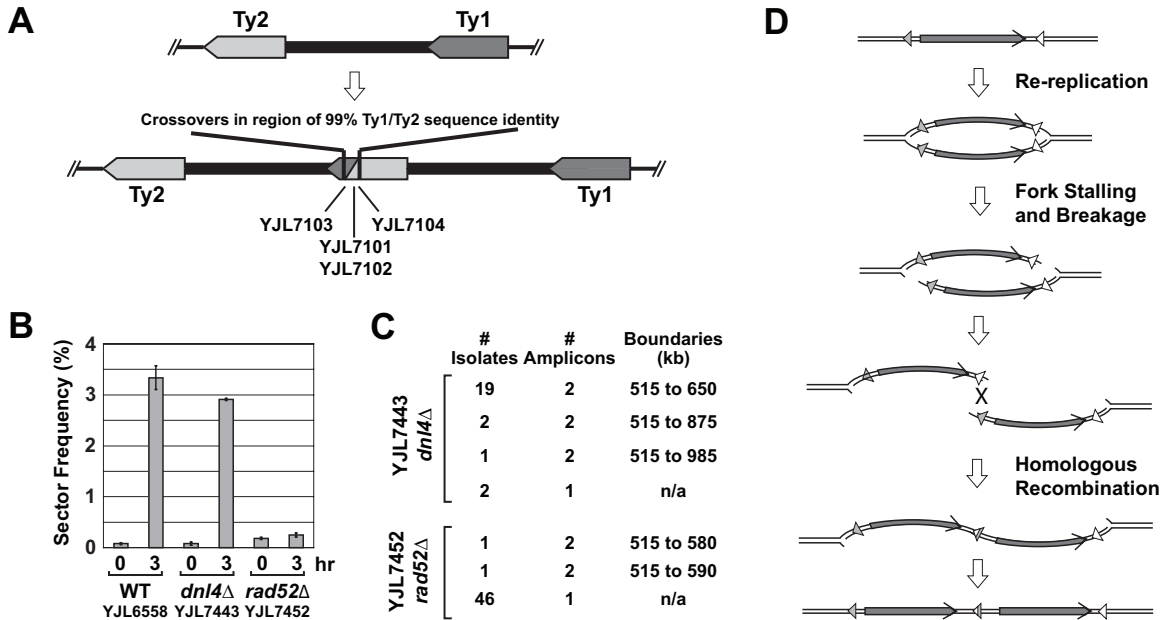


Figure 3. Role of nonallelic homologous recombination in RRIGA. A) Schematic of hybrid recombinant Ty elements (Fig. S4) found at the inter-amplicon junction of four isolates with segmental amplifications on Chr IV from 515-650 kb. B) Re-replication induced sectoring is dependent on HR and not NHEJ. YJL7443 (*dnl4*Δ) and YJL7452 (*rad52*Δ) are otherwise isogenic with re-replicating strain YJL6558. Re-replication induced sectoring frequency (mean ± SEM, n = 2 to 7 induction replicates; see Table S1) was analyzed as described for Fig. 1B. C) Re-replication induced gene amplification is dependent on HR and not NHEJ. Representative aCGH analysis of Chr IV for 24 red sectors derived from YJL7443 (*dnl4*Δ) and 48 derived from YJL7452 (*rad52*Δ) (Table S6). D) How re-replication might stimulate NAHR. See text for details. Arrowheads, non-allelic or hybrid recombinant repetitive element. Arrows, amplified segments.

Figure S1

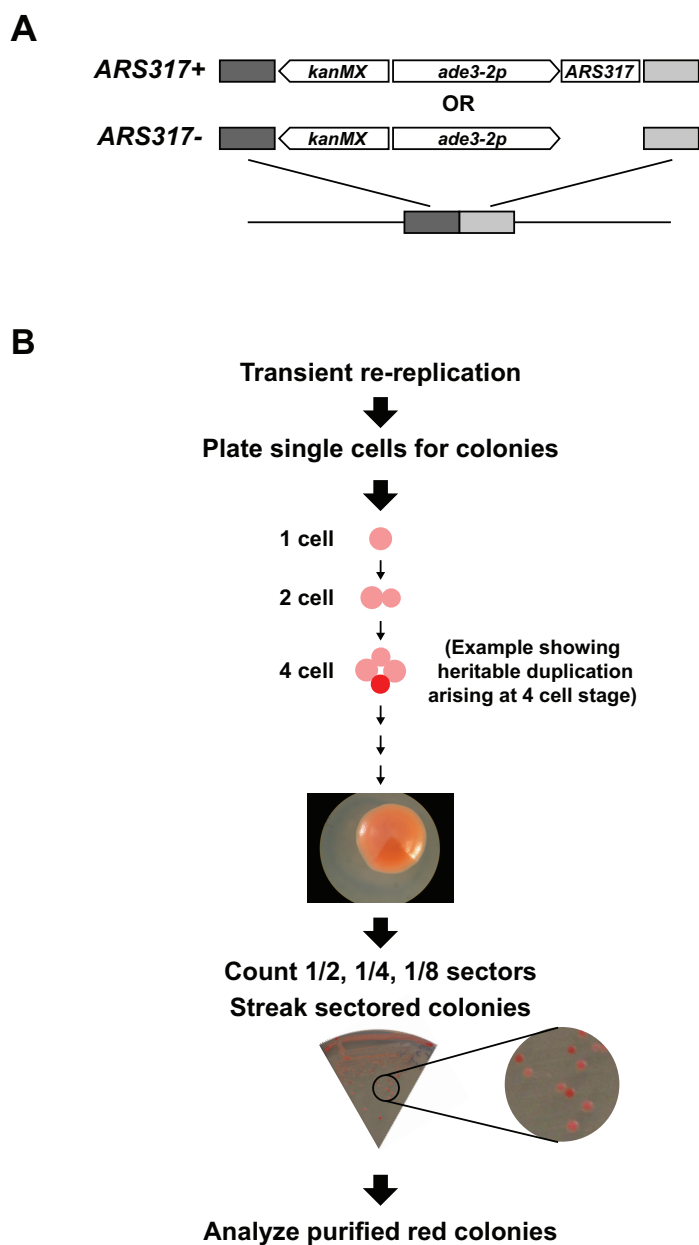


Figure S1. Screening for re-replication induced gene amplification using colony sectoring.

A) Integrated copy number reporter cassette consists of the *kanMX* marker, *ade3-2p* copy number reporter gene, and several hundred base pairs of homology to the left (dark grey box) and right (light grey box) of the desired integration site (see Supplementary Methods). Two versions of the cassette were used: (top) one containing an *ARS317* fragment that preferentially re-initiates in the MC_{2A} re-replicating strain background, and (bottom) one lacking the ARS. B) Schematic of gene amplification screen. Cells were induced to re-replicate for 3 hr at a G2/M phase arrest then plated for single colonies on plates that remove

the induction for rereplication and allow colony color development. Parental cells with a single copy of the *ade3-2p* cassette are pink. Cells in a colony lineage that acquire a stable heritable amplification of the *ade3-2p* reporter gene will generate a red sector, whose size reflects when the amplification occurred. Shown is an example of a colony where the *ade3-2p* cassette was stably amplified by one cell at the four-cell stage, resulting in a pink colony with a red quarter sector. Pink colonies with 1/2, 1/4, and 1/8 red sectors were streaked to colony purify red cells. Red sectors that successfully restreaked were quantified and their genomic DNA analyzed by aCGH to determine if they indeed had amplified their reporter cassette. Sectoring was a good indicator of cassette amplification in cells that re-initiated *ARS317* on the *ade3-2p* cassette (Fig. 1C, Fig. S2B, Table S2 and S3). However, color development is affected by other factors besides *ade3-2p* copy number. In other settings, such as in non-rereplicating strains (Table S4), strains perturbed by DNA damage (Fig. S3C and Table S5), or re-replicating strains with a *RAD52* deletion (Fig. 3C and Table S6), red sectors usually did not contain amplification of the *ade3-2p* cassette and presumably arose from other genetic alterations.

Figure S2

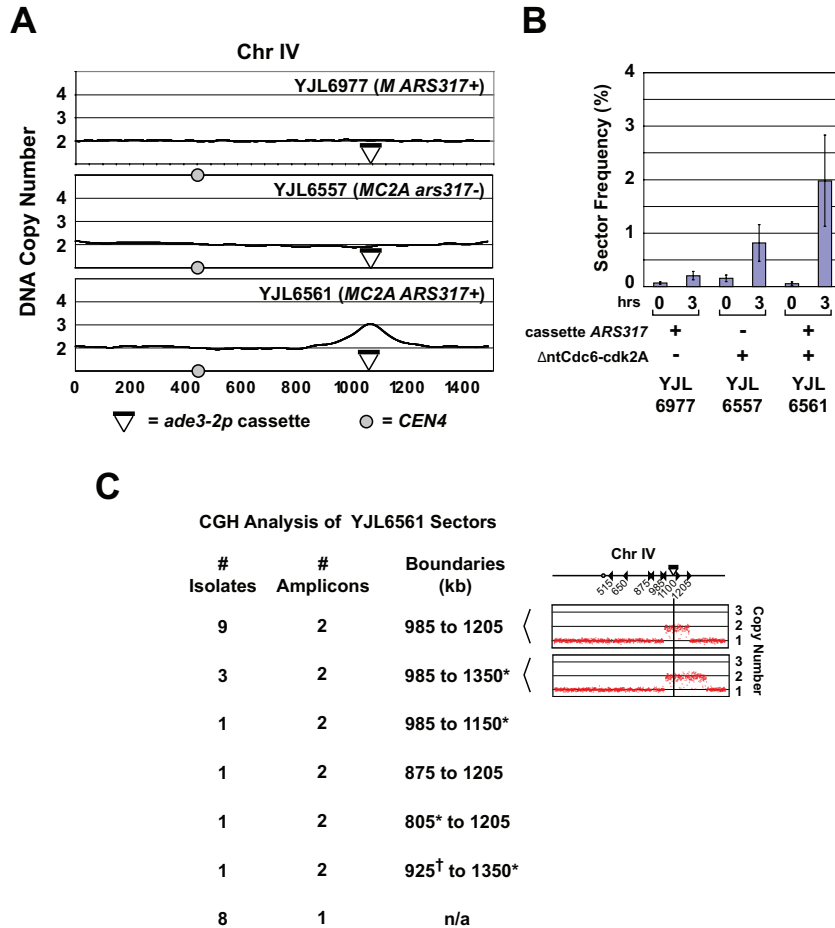


Figure S2. Re-replication from Chr IV_{1089kb} induces primary gene amplification. A) Induction of re-replication at Chr IV_{1089kb}. Strains containing an *ade3-2p* copy number reporter cassette integrated at Chr IV_{1089kb} were arrested in G2/M phase and treated with galactose for 3 hr to trigger re-initiation of *ARS317*. Copy number analysis of re-replication (>2C) by aCGH is shown for Chr IV. All other chromosomes maintained a copy number at or close to 2C (data not shown). Top panel: YJL6977, non-re-replicating strain with *ARS317* in *ade3-2p* cassette (*MATa MCM7-2NLS orc6-cdk1A₁₁₆ ura3-52::pGAL, URA3*) *Chr IV_{1089kb}::{ade3-2p, ARS317, kanMX}* *ade2 ade3 ars317Δ::natMX*). Middle panel: YJL6557, re-replicating strain with no *ARS317* in *ade3-2p* cassette (*MATa MCM7-2NLS orc6-cdk1A₁₁₆ ura3-52::pGAL-ΔntCDC6-cdk2A, URA3*) *Chr IV_{1089kb}::{ade3-2p, kanMX}* *ade2 ade3 ars317Δ::natMX*). Bottom panel: YJL6561, re-replicating strain with *ARS317* in *ade3-2p* cassette (*MATa MCM7-2NLS orc6-cdk1A₁₁₆ ura3-52::pGAL-ΔntCDC6-cdk2A, URA3*) *Chr IV_{1089kb}::{ade3-2p, ARS317, kanMX}* *ade2 ade3 ars317Δ::natMX*). B) Re-replication of the *ade3-2p* reporter cassette stimulates colony sectoring at Chr IV_{1089kb}. YJL6977, YJL6557, and YJL6977 were treated as described in A. After 0 or 3 hr galactose

induction, isolated cells were plated for single colonies on media containing dextrose to block further re-replication and limiting adenine to promote color development (see Fig. S1B). The frequency of pink colonies with 1/2, 1/4, or 1/8 red sectors were then quantified (mean \pm SEM, n = 2 to 3 induction replicates; see Table S1). C) Red sectors induced by re-replication at Chr IV_{1089kb} display primary gene amplifications. 24 red sectors derived from YJL6561 were analyzed by aCGH and distributed into seven classes based on the copy number profile of Chr IV (see Table S3). Chr IV profiles of the two largest classes are shown. Schematic of Chr IV shows positions of Ty elements (triangles), centromere (circle), and *ade3-2p* cassette (black bar). * boundary maps to Ty LTR element and not full Ty element in genome sequence of *S. cerevisiae*, S288c (S50). † boundary does not map to any full Ty or LTR element present in the genome sequence of *S. cerevisiae*, S288c (S50); whether the boundary coincides with an unmapped Ty or LTR element in YJL6561, which has a different strain background derived from A364a and W303, was not determined.

Figure S3

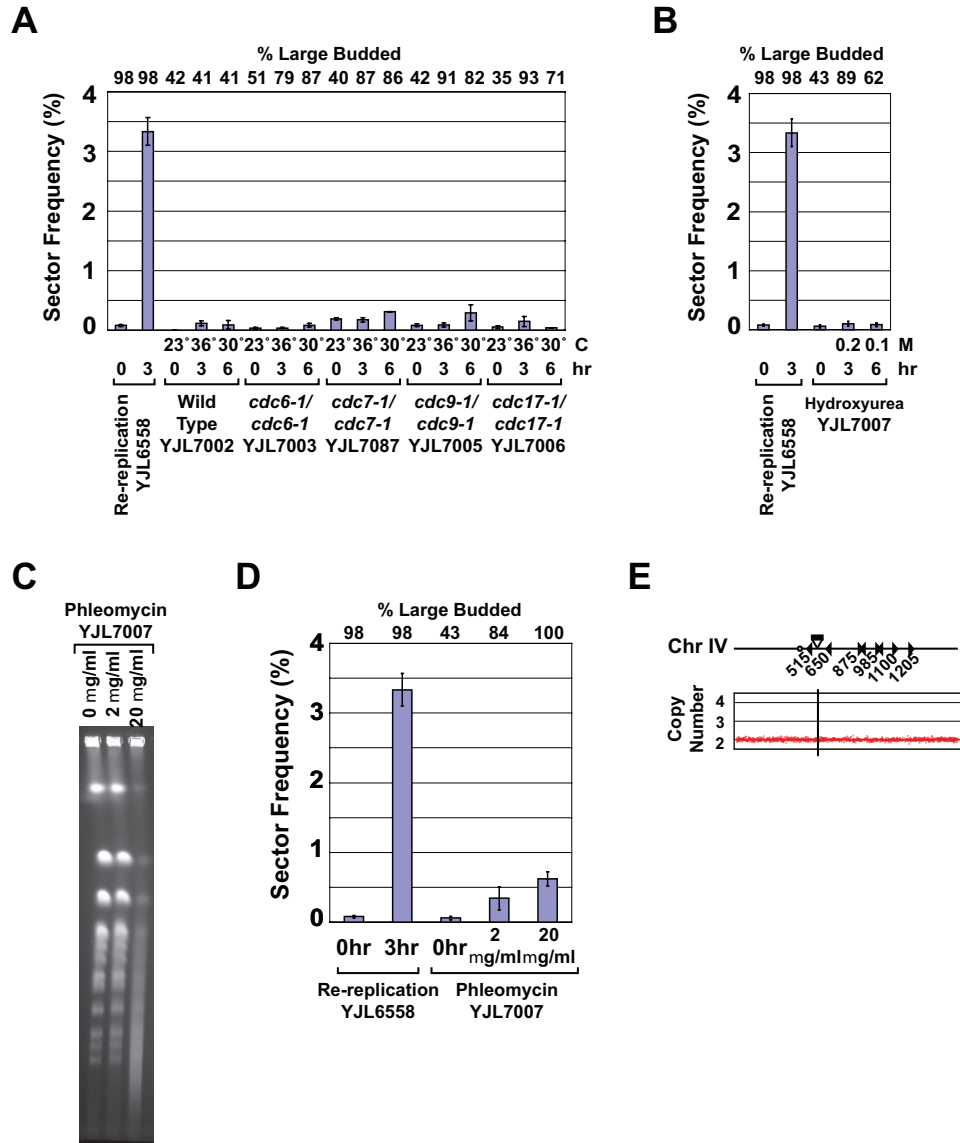


Figure S3. Specificity of primary gene amplifications induced by re-replication. A) Replication mutants did not generate frequent red sectors. Diploid strains YJL7002 (WT), YJL7003 (*cdc6-1/cdc6-1*), YJL7087 (*cdc7-1/cdc7-1*), YJL7005 (*cdc9-1/cdc9-1*), and YJL7006 (*cdc17-1/cdc17-1*), all containing *Chr IV*_{567kb}::{*ade3-2p*, *ARS317*, *kanMX*} on one homolog were grown exponentially at 23°C then shifted to restrictive temperatures (36°C) for 3 hr or semipermissive temperatures (30°C) for 6 hr to perturb DNA replication. Cells were plated and red sectors quantified (mean ± SEM, n = 2 induction replicates; see Table S1) as described in Fig. 1B with results for YJL6558 shown for comparison. % large budded cells were quantified right before plating to monitor the effectiveness of the *cdc* perturbation. B) HU induced replication stress did not generate frequent red sectors. Exponentially growing WT diploid YJL7007 were

treated with 0.1 M or 0.2 M HU for the indicated times then plated and red sectors quantified (mean \pm SEM, n = 2 to 3 treatment replicates; see Table S1) as described in Fig. 1B with results for YJL6558 shown for comparison. % large budded cells were quantified right before plating to monitor the effectiveness of the HU treatment. C) DNA damage induced chromosomal fragmentation. Exponentially growing WT diploid cells (*YJL7007*, *MATa/MATa MCM7/MCM7 ORC2/ORC2 ORC6/ORC6 ChrIV/Chr IV_{567kb}*::*{ade3-2p, ARS317, kanMX}*) were treated with indicated concentrations of phleomycin for 3 hr before chromosomes were analyzed by PFGE and ethidium bromide staining. D) DNA damage induced red sectoring. *YJL7007* (WT) cells treated as described in C were plated for red sectoring colonies and quantified (mean \pm SEM, n = 2 to 3 treatment replicates; see Table S1) as described in Fig. 1B with results for YJL6558 shown for comparison. % large budded cells were quantified right before plating to confirm induction of the DNA damage response. E) Red sectors induced by DNA damage did not display gene amplification. Representative aCGH profile of Chr IV displayed by 24/24 red sectors obtained from treatment of *YJL7007* with 20 μ g/ml phleomycin as described in D (see Table S5).

proximal) segment of approximately 1.4 kb, which spans the region where YDRCTy2-1 and YDRCTy1-1 share 99% identity (unboxed sequence). Crossover events were detected as transitions from sequence specific to YDRCTy1-1 (grey box) to sequence specific to YDRCTy2-1 (white box). Additional sequence obtained to the left and right of the displayed sequence are consistent with crossovers in these isolates only occurring in this region (data not shown). To the left of all four isolates, we sequenced at least 170 bp that proved to be identical to genomic sequences centromere proximal to the endogenous YDRCTy1-1. Similarly, in all four isolates we sequenced at least 560 bp to the right that turned out to be identical to YDRCTy2-1. For two of the isolates, YJL7103 and YJL7104, the rightward sequence continued all the way past the end of the hybrid Ty element and this sequence was shown to be identical to YDRCTy2-1 and the centromere distal genomic sequence flanking this Ty element at its endogenous location. * marks the position of every tenth nucleotide.

Figure S5

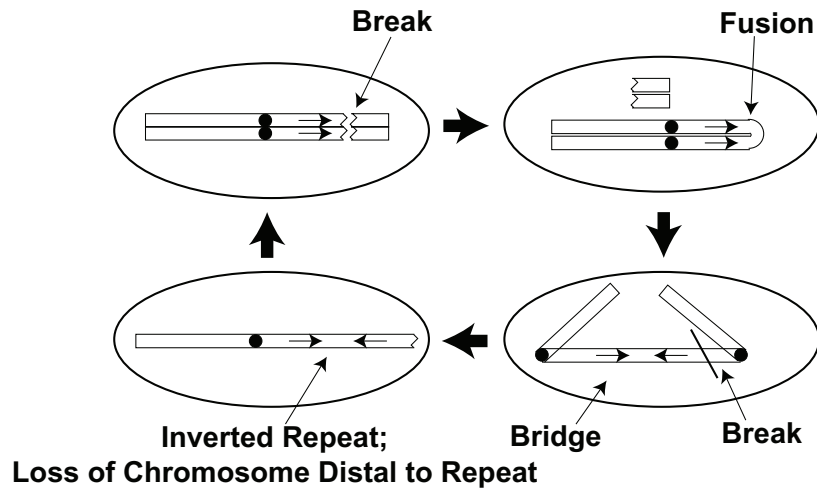


Figure S5. Breakage-fusion-bridge model. A schematic of a breakage fusion bridge cycle is shown. Breakage through both sister chromatids, or a break in G1 phase of the cell cycle followed by chromatid replication, (upper left) can result in fusion of the two sisters in inverted orientation (upper right). Such a fusion, which can also be initiated by telomere erosion, results in a dicentric chromosome. Attempts to segregate the two centromeres generate a mitotic bridge (lower right) and often results in breakage between the centromeres. The larger chromosome fragment contains an inverted duplication of part of the region centromeric to the original break and is missing the region telomeric to that break (lower left). Replication of this DNA results in two sister chromatids each with a break, allowing the cycle to be repeated multiple times (upper left) until a telomere is finally captured by one of the broken ends.

Table S1

Frequency of 1/2, 1/4, and 1/8 red sectored colonies observed in this work

Parent Strain	Genotype	Cassette	Conditions	# Trials	Total Colonies Screened	Mean Sector Frequency	Standard Error of the Mean
YJL6974	MCM7-2NLS pGAL	ChrIV:567kb ade3-2p ARS317	Nocodazole Arrest + 0 hr Galactose	4	15243	0.04%	0.008%
YJL6974	MCM7-2NLS pGAL	ChrIV:567kb ade3-2p ARS317	Nocodazole Arrest + 3 hr Galactose	4	30453	0.14%	0.030%
YJL6555	MCM7-2NLS pGAL- Δ ntCDC6-cdk2A	ChrIV:567kb ade3-2p	Nocodazole Arrest + 0 hr Galactose	2	8612	0.05%	0.005%
YJL6555	MCM7-2NLS pGAL- Δ ntCDC6-cdk2A	ChrIV:567kb ade3-2p	Nocodazole Arrest + 3 hr Galactose	2	17076	0.58%	0.258%
YJL6558	MCM7-2NLS pGAL- Δ ntCDC6-cdk2A	ChrIV:567kb ade3-2p ARS317	Nocodazole Arrest + 0 hr Galactose	7	22922	0.08%	0.017%
YJL6558	MCM7-2NLS pGAL- Δ ntCDC6-cdk2A	ChrIV:567kb ade3-2p ARS317	Nocodazole Arrest + 3 hr Galactose	7	21754	3.34%	0.232%
YJL6977	MCM7-2NLS pGAL	ChrIV:1089kb ade3-2p ARS317	Nocodazole Arrest + 0 hr Galactose	2	14176	0.07%	0.021%
YJL6977	MCM7-2NLS pGAL	ChrIV:1089kb ade3-2p ARS317	Nocodazole Arrest + 3 hr Galactose	2	13488	0.20%	0.075%
YJL6557	MCM7-2NLS pGAL- Δ ntCDC6-cdk2A	ChrIV:1089kb ade3-2p	Nocodazole Arrest + 0 hr Galactose	3	14728	0.15%	0.059%
YJL6557	MCM7-2NLS pGAL- Δ ntCDC6-cdk2A	ChrIV:1089kb ade3-2p	Nocodazole Arrest + 3 hr Galactose	3	20762	0.82%	0.345%
YJL6561	MCM7-2NLS pGAL- Δ ntCDC6-cdk2A	ChrIV:1089kb ade3-2p ARS317	Nocodazole Arrest + 0 hr Galactose	3	11544	0.05%	0.034%
YJL6561	MCM7-2NLS pGAL- Δ ntCDC6-cdk2A	ChrIV:1089kb ade3-2p ARS317	Nocodazole Arrest + 3 hr Galactose	3	13450	1.98%	0.855%
YJL7007	WT/WT	ChrIV:567kb ade3-2p ARS317	Asynchronous*	3	15788	0.06%	0.022%
YJL7007	WT/WT	ChrIV:567kb ade3-2p ARS317	Asynchronous + 3 h 2 μ g/ml Phleomycin	2	10454	0.34%	0.167%
YJL7007	WT/WT	ChrIV:567kb ade3-2p ARS317	Asynchronous + 3 h 20 μ g/ml Phleomycin	2	9088	0.62%	0.100%

Table S1 (continued)

Frequency of 1/2, 1/4, and 1/8 red sectored colonies observed in this work

Parent Strain	Genotype	Cassette	Conditions	# Trials	Total Colonies Screened	Mean Sector Frequency	Standard Error of the Mean
YJL7002	WT/WT	ChrIV:567kb ade3-2p ARS317	Asynchronous (22° C)	2	4451	0.00%	0.000%
YJL7002	WT/WT	ChrIV:567kb ade3-2p ARS317	Asynchronous (22° C) + 3 h 36° C	2	5419	0.11%	0.040%
YJL7002	WT/WT	ChrIV:567kb ade3-2p ARS317	Asynchronous (22° C) + 6 h 30° C	2	8240	0.09%	0.071%
YJL7003	cdc6-1/cdc6-1	ChrIV:567kb ade3-2p ARS317	Asynchronous (22° C)	2	10416	0.03%	0.014%
YJL7003	cdc6-1/cdc6-1	ChrIV:567kb ade3-2p ARS317	Asynchronous (22° C) + 3 h 36° C	2	8208	0.04%	0.010%
YJL7003	cdc6-1/cdc6-1	ChrIV:567kb ade3-2p ARS317	Asynchronous (22° C) + 6 h 30° C	2	11168	0.08%	0.030%
YJL7087	cdc7-1/cdc7-1	ChrIV:567kb ade3-2p ARS317	Asynchronous (22° C)	2	5840	0.19%	0.022%
YJL7087	cdc7-1/cdc7-1	ChrIV:567kb ade3-2p ARS317	Asynchronous (22° C) + 3 h 36° C	2	7952	0.17%	0.039%
YJL7087	cdc7-1/cdc7-1	ChrIV:567kb ade3-2p ARS317	Asynchronous (22° C) + 6 h 30° C	2	7144	0.31%	0.004%
YJL7005	cdc9-1/cdc9-1	ChrIV:567kb ade3-2p ARS317	Asynchronous (22° C)	2	5136	0.08%	0.022%
YJL7005	cdc9-1/cdc9-1	ChrIV:567kb ade3-2p ARS317	Asynchronous (22° C) + 3 h 36° C	2	10224	0.09%	0.036%
YJL7005	cdc9-1/cdc9-1	ChrIV:567kb ade3-2p ARS317	Asynchronous (22° C) + 6 h 30° C	2	8448	0.29%	0.134%
YJL7006	cdc17-1/cdc17-1	ChrIV:567kb ade3-2p ARS317	Asynchronous (22° C)	2	7520	0.05%	0.024%
YJL7006	cdc17-1/cdc17-1	ChrIV:567kb ade3-2p ARS317	Asynchronous (22° C) + 3 h 36° C	2	6576	0.15%	0.084%
YJL7006	cdc17-1/cdc17-1	ChrIV:567kb ade3-2p ARS317	Asynchronous (22° C) + 6 h 30° C	2	4816	0.04%	0.001%

Table S1 (continued)

Frequency of 1/2, 1/4, and 1/8 red sectored colonies observed in this work

Parent Strain	Genotype	Cassette	Conditions	# Trials	Total Colonies Screened	Mean Sector Frequency	Standard Error of the Mean
YJL7007	WT/WT	<i>ChrIV::567kb ade3-2p ARS317</i>	Asynchronous*	3	15788	0.06%	0.022%
YJL7007	WT/WT	<i>ChrIV::567kb ade3-2p ARS317</i>	Asynchronous + 3 h 0.2M Hydroxyurea	2	7384	0.10%	0.040%
YJL7007	WT/WT	<i>ChrIV::567kb ade3-2p ARS317</i>	Asynchronous + 6 h 0.05M Hydroxyurea	2	7952	0.08%	0.028%
YJL7443	<i>dnl4Δ MCM7-2NLS pGAL-ΔntCDC6-cdk2A</i>	<i>ChrIV::567kb ade3-2p ARS317</i>	Nocodazole Arrest + 0 hr Galactose	2	6593	0.08%	0.030%
YJL7443	<i>dnl4Δ MCM7-2NLS pGAL-ΔntCDC6-cdk2A</i>	<i>ChrIV::567kb ade3-2p ARS317</i>	Nocodazole Arrest + 3 hr Galactose	2	8569	2.91%	0.020%
YJL7452	<i>rad52Δ MCM7-2NLS pGAL-ΔntCDC6-cdk2A</i>	<i>ChrIV::567kb ade3-2p ARS317</i>	Nocodazole Arrest + 0 hr Galactose	2	7244	0.18%	0.020%
YJL7452	<i>rad52Δ MCM7-2NLS pGAL-ΔntCDC6-cdk2A</i>	<i>ChrIV::567kb ade3-2p ARS317</i>	Nocodazole Arrest + 3 hr Galactose	2	31883	0.25%	0.040%

* Same set of experiments used as asynchronous untreated control for both Phleomycin and Hydroxyurea experiments

Table S2

Analysis of sectored colonies generated by re-replicating strain containing reporter cassette at Chr IV_{567kb} (YJL6558).

Sectored Colony	Copy Number (CGH)	Amplicon Boundaries (CGH)	Chr IV Size Status (PFGE)	Chr IV Expected kb Increase	Direct Repeat (Jxn PCR)	Other CGH Changes
YJL7095	3	515 to 650	Increased	290	-	None
YJL7096	2	650 to 670	Increased	135	+	None
YJL7097	2	515 to 650	Increased	135	+	None
YJL7098	2	515 to 650	Increased	135	+	None
YJL7099	2	515 to 650	Increased	135	+	None
YJL7100	1	n/a	No change	0	ND	Chr V disomy
YJL7101	2	515 to 650	Increased	135	+	None
YJL7102	2	515 to 650	Increased	135	+	None
YJL7103	2	515 to 650	Increased	135	+	None
YJL7104	2	515 to 650	Increased	135	+	None
YJL7105	2	515 to 650	Increased	135	+	None
YJL7106	1	n/a	No change	0	ND	None
YJL7107	2	515 to 650	Increased	135	+	None
YJL7108	2	515 to 650	Increased	135	+	None
YJL7109	2	515 to 650	Increased	135	+	None
YJL7110	2	515 to 985	Increased	470	+	None
YJL7111	2	515 to 650	Increased	135	+	None
YJL7112	2	515 to 650	Increased	245	+	None
YJL7113	1	n/a	No change	0	ND	None
YJL7114	2	515 to 650	Increased	135	+	None
YJL7115	2	515 to 650	Increased	135	+	None
YJL7116	2	515 to 650	Increased	135	+	None
YJL7117	2	515 to 650	Increased	135	+	Chr III disomy
YJL7118	1	n/a	No change	0	ND	None
YJL7556	2	515 to 650	ND	ND	ND	None
YJL7557	2	515 to 650	ND	ND	ND	None
YJL7558	2	515 to 650	ND	ND	ND	None
YJL7559	2	515 to 650	ND	ND	ND	None
YJL7584	2	515 to 875	ND	ND	ND	None
YJL7585	2	515 to 650	ND	ND	ND	None
YJL7586	2	515 to 650	ND	ND	ND	None
YJL7587	2	515 to 650	ND	ND	ND	None
YJL7689	2	515 to 650	ND	ND	ND	None
YJL7690	2	515 to 650	ND	ND	ND	None
YJL7691	3	515 to 650	ND	ND	ND	None

Copy Number and Amplicon Boundaries refer to locus encompassing reporter cassette. Boundaries are reported as kilobases (kb) from the left telomere of ChrIV. Boundaries correspond to the position of Ty elements (515=Ty2; 650=Ty1; 875=Ty1; 985=Ty1) or LTRs (670=6) mapped for S288c on the Saccharomyces Genome Database. Boundary numbers were used to calculate the expected size increase in ChrIV after all amplifications screened by PFGE were shown to be intrachromosomal. Direct Repeat refers to whether junction PCR (see Fig. 2) confirmed the presence of a head-to-tail amplicon junction. The one negative (YJL7095) may have failed because we used PCR primers to detect a junction between 515 kb and 650 kb and not a junction between 515 kb and 670 kb. n/a- not applicable; ND - not done.

Table S3

CGH analysis of sectored colonies generated by re-replicating strain containing reporter cassette at Chr IV_{1089kb} (YJL6561).

Sectored Colony	Copy Number	Amplicon Boundaries	Other CGH Changes
YJL7119	2	805 to 1205	None
YJL7120	2	985 to 1205	None
YJL7121	2	875 to 1205	None
YJL7122	2	985 to 1205	None
YJL7123	2	985 to 1205	None
YJL7124	1	n/a	Chr X segmental duplication, 200kb to 355kb
YJL7125	1	n/a	Chr V disomy
YJL7126	2	985 to 1350	None
YJL7127	2	985 to 1205	None
YJL7128	2	985 to 1205	Chr V partial disomy, left TEL to 285kb Chr XVI partial disomy, left TEL to 100kb
YJL7129	2	985 to 1205	None
YJL7130	1	n/a	Chr II disomy
YJL7131	2	985 to 1205	None
YJL7132	1	n/a	None
YJL7133	2	985 to 1205	None
YJL7134	1	n/a	Chr V disomy
YJL7135	2	985 to 1350	None
YJL7136	2	985 to 1350	None
YJL7137	2	925 to 1350	None
YJL7138	1	n/a	None
YJL7139	2	985 to 1205	None
YJL7140	1	n/a	None
YJL7141	1	n/a	Chr II disomy
YJL7142	2	985 to 1150	None

Copy Number and Amplicon Boundaries refer to locus encompassing the reporter cassette. n/a - not applicable. Boundaries are reported as kilobases (kb) from the left telomere of ChrIV and correspond to the position of Ty elements (875=Ty2; 985=Ty2; 1205=Ty1) or LTRs (805=δ; 1150=δ; 1350=δ) mapped for S288c on the Saccharomyces Genome Database, except for 925kb. TEL is yeast telomere sequences.

Table S4

CGH analysis of sectored colony isolates generated by non-re-replicating strain containing reporter cassette at ChrIV_{567kb} (YJL6974).

Sectored Colony	Copy Number	Amplicon Boundaries	Other CGH Changes
YJL7548	1	n/a	Chr V disomy
YJL7549	1	n/a	Chr II partial disomy, left TEL to 260kb Chr III partial disomy, 170 kb to right TEL
YJL7550	1	n/a	Chr V disomy
YJL7551	2	515 to 875	None
YJL7552	1	n/a	Chr V disomy
YJL7553	1	n/a	Chr XIII disomy
YJL7554	1	n/a	None
YJL7555	1	n/a	Chr V disomy
YJL7560	1	n/a	Chr II disomy
YJL7561	1	n/a	Chr II disomy
YJL7562	1	n/a	Chr XIII disomy
YJL7563	1	n/a	Chr XIII disomy
YJL7564	1	n/a	Chr II disomy Chr III disomy
YJL7565	1	n/a	Diploid Chr I monosomy Chr III trisomy
YJL7566	1	n/a	Chr II disomy Chr XVI disomy
YJL7567	1	n/a	Chr II disomy
YJL7568	1	n/a	Chr III disomy
YJL7569	1	n/a	Chr V disomy
YJL7570	1	n/a	Chr IV disomy
YJL7571	1	n/a	Chr V disomy
YJL7572	2	515 to 985	None
YJL7573	1	n/a	Chr V disomy Chr XIII disomy Chr XVI disomy
YJL7574	1	n/a	Chr V disomy
YJL7575	1	n/a	Chr XIII disomy
YJL7576	1	n/a	None
YJL7577	1	n/a	Chr II disomy
YJL7578	1	n/a	Chr II disomy
YJL7579	1	n/a	None
YJL7580	1	n/a	Chr II disomy
YJL7581	1	n/a	Chr II disomy
YJL7582	2	515 to 650	None
YJL7583	1	n/a	Chr II disomy Chr V disomy

Copy Number and Amplicon Boundaries refer to locus encompassing the reporter cassette. Boundaries are reported as kilobases (kb) from the left telomere of ChrIV and correspond to the position of Ty elements (515=Ty2; 650=Ty1; 875=Ty1; 985=Ty1) identified for S288c in the Saccharomyces Genome Database. n/a - not applicable. TEL - telomere.

Table S5

CGH analysis of sectored colonies generated by DNA damage from 20 µg/ml phleomycin in diploid strain containing reporter cassette at 567kb on one homolog of ChrIV (YJL7007).

Sectored Colony	Diploid Copy Number	Amplicon Boundaries	Other CGH Changes
YJL7143	2	n/a	Chr VI partial monosomy, left arm Chr III partial trisomy, left arm
YJL7144	2	n/a	None
YJL7145	2	n/a	None
YJL7146	2	n/a	Chr V partial monosomy, right arm Chr V partial trisomy, left arm
YJL7147	2	n/a	Chr V trisomy
YJL7148	2	n/a	None
YJL7149	2	n/a	None
YJL7150	2	n/a	None
YJL7151	2	n/a	None
YJL7152	2	n/a	Chr VIII monosomy
YJL7153	2	n/a	Chr V partial monosomy, right arm Chr XIII partial trisomy, right arm
YJL7154	2	n/a	Chr IV partial trisomy, right arm Chr XVI partial monosomy, left arm
YJL7155	2	n/a	None
YJL7156	2	n/a	Chr V partial trisomy, left arm Chr V segmental duplication Chr VII segmental deletion Chr XV partial monosomy, right arm
YJL7157	2	n/a	None
YJL7158	2	n/a	None
YJL7159	2	n/a	Chr I monosomy
YJL7160	2	n/a	None
YJL7161	2	n/a	None
YJL7162	2	n/a	Chr I monosomy
YJL7163	2	n/a	Chr III partial trisomy, left arm Chr III partial monosomy, right arm
YJL7164	2	n/a	None
YJL7165	2	n/a	None
YJL7166	2	n/a	Chr I partial trisomy, right arm Chr III partial monosomy, left arm Chr VIII monosomy

Diploid Copy Number and Amplicon Boundaries refer to locus encompassing the reporter cassette. Unamplified diploid copy number is 2. No boundaries are reported because no amplification of the reporter cassette was observed. n/a is not applicable.

Table S6

CGH analysis of sectored colonies generated in *rad52Δ* (YJL7452) and *dnl4Δ* (YJL7443) re-replicating strains containing reporter cassette at ChrIV_{567kb}.

Colony Isolate	Parent Strain	Copy Number	Amplicon Boundaries	Other CGH Changes
YJL7609	YJL7452	1	n/a	None
YJL7610	YJL7452	1	n/a	None
YJL7611	YJL7452	1	n/a	Chr II disomy
YJL7612	YJL7452	1	n/a	None
YJL7613	YJL7452	1	n/a	None
YJL7614	YJL7452	1	n/a	None
YJL7615	YJL7452	1	n/a	None
YJL7616	YJL7452	1	n/a	None
YJL7617	YJL7452	1	n/a	None
YJL7618	YJL7452	1	n/a	Chr XIII disomy
YJL7619	YJL7452	1	n/a	None
YJL7620	YJL7452	1	n/a	None
YJL7621	YJL7452	1	n/a	None
YJL7622	YJL7452	1	n/a	None
YJL7623	YJL7452	1	n/a	None
YJL7624	YJL7452	1	n/a	None
YJL7625	YJL7452	1	n/a	None
YJL7626	YJL7452	1	n/a	None
YJL7627	YJL7452	1	n/a	Chr XIII disomy
YJL7628	YJL7452	1	n/a	None
YJL7629	YJL7452	1	n/a	None
YJL7630	YJL7452	1	n/a	None
YJL7631	YJL7452	1	n/a	Chr XIII disomy
YJL7632	YJL7452	1	n/a	None
YJL7633	YJL7452	1	n/a	None
YJL7634	YJL7452	1	n/a	None
YJL7635	YJL7452	1	n/a	None
YJL7636	YJL7452	1	n/a	None
YJL7637	YJL7452	1	n/a	None
YJL7638	YJL7452	1	n/a	None
YJL7639	YJL7452	1	n/a	None
YJL7640	YJL7452	1	n/a	None
YJL7641	YJL7452	1	n/a	None
YJL7642	YJL7452	2	515 to 590	None
YJL7643	YJL7452	1	n/a	None
YJL7644	YJL7452	1	n/a	Diploid Chr I monosomy
YJL7645	YJL7452	1	n/a	None
YJL7646	YJL7452	1	n/a	None
YJL7647	YJL7452	1	n/a	None
YJL7648	YJL7452	1	n/a	None
YJL7649	YJL7452	1	n/a	None
YJL7650	YJL7452	1	n/a	None

Table S6 (continued)

CGH analysis of sectored colonies generated in *rad52Δ* (YJL7452) and *dnl4Δ* (YJL7443) re-replicating strains containing reporter cassette at ChrIV_{567kb}.

Colony Isolate	Parent Strain	Copy Number	Amplicon Boundaries	Other CGH Changes
YJL7651	YJL7452	2	515 to 580	None
YJL7652	YJL7452	1	n/a	None
YJL7653	YJL7452	1	n/a	None
YJL7654	YJL7452	1	n/a	None
YJL7655	YJL7452	1	n/a	None
YJL7656	YJL7452	1	n/a	None
YJL7657	YJL7443	2	515 to 650	None
YJL7658	YJL7443	2	515 to 650	None
YJL7659	YJL7443	2	515 to 650	None
YJL7660	YJL7443	2	515 to 650	None
YJL7661	YJL7443	2	515 to 650	None
YJL7662	YJL7443	1	n/a	Chr V segmental duplication, 60kb to 110kb
YJL7663	YJL7443	2	515 to 650	None
YJL7664	YJL7443	2	515 to 650	None
YJL7665	YJL7443	2	515 to 650	None
YJL7666	YJL7443	2	515 to 650	None
YJL7667	YJL7443	2	515 to 985	None
YJL7668	YJL7443	2	515 to 650	None
YJL7669	YJL7443	2	515 to 650	None
YJL7670	YJL7443	2	515 to 650	None
YJL7671	YJL7443	2	515 to 650	None
YJL7672	YJL7443	2	515 to 650	None
YJL7673	YJL7443	2	515 to 650	None
YJL7674	YJL7443	2	515 to 650	None
YJL7675	YJL7443	2	515 to 650	None
YJL7677	YJL7443	2	515 to 875	Chr V segmental duplication, 290kb to 445kb
YJL7685	YJL7443	2	515 to 875	None
YJL7686	YJL7443	1	n/a	None
YJL7687	YJL7443	2	515 to 650	None
YJL7688	YJL7443	2	515 to 650	None

Copy Number and Amplicon Boundaries refer to locus encompassing the reporter cassette. Boundaries are reported as kilobases (kb) from the left telomere of ChrIV. Boundaries correspond to the position of Ty elements (515=Ty2; 650=Ty1; 875=Ty1; 985=Ty1) mapped for S288c on the Saccharomyces Genome Database, except for 580kb and 590kb. n/a - not applicable

Table S7

Oligonucleotides used in this study. Listed 5' to 3', left to right. Uppercase letters indicate sequence that anneals to the template during PCR or sequencing. Lowercase letters indicate sequence added by PCR, either to provide homology for genomic integration or to provide restriction sites for cloning. Subscript numbers are nucleotide coordinates provided by the Saccharomyces Genome Database (Nov 2009)

Name	Sequence	Purpose
O.U.L.1639	atlaaacatattgatttttaaatcgcacatttaaacccggatccccggggttaatttaa	ars317::NamMX
O.U.L.1640	attttatggaaagataagcctataactctggcggggatcctcgatgaaattcgagctcg	ars317::NamMX
O.U.L.1684	gatcagaccgcccggggttagctctgcaaaaggtgtg	ChrII ₂₄₆₃₃₄₋₂₄₆₃₅₆ for pB.JL2876
O.U.L.1685	gatglltaaacaggcctcaagagtgcatgtaatttt	ChrII ₂₄₆₃₃₄₋₂₄₆₃₅₆ for pB.JL2876
O.U.L.1686	gatccaccggcctcagggagtgagctgagctgcatcataat	ChrII ₂₄₆₃₅₆₋₂₄₇₄₁₀ for pB.JL2876
O.U.L.1687	gatcggcagccggccgctatttggaaaagggttactttgg	ChrII ₂₄₆₃₅₆₋₂₄₇₄₁₀ for pB.JL2876
O.U.L.1757	CAAAAGCATTCAAAGGTCACG	ADE3 probe
O.U.L.1758	TCAAATTCGCAATGTTGGTGT	ADE3 probe
O.U.L.1794	gctcaaatgggttaaacctagctacttAAAAAACCTG	ARS317 for cloning
O.U.L.1795	gctcaaatgggttaaacctcagagatcctcgcttat	ARS317 for cloning
O.U.L.1796	gctcaaatggaaagctggccctgittgggtcctggtaagaaaa	ChrIV ₆₆₇₁₀₈₋₆₆₇₈₆₅ for pB.JL2889 and pB.JL2890
O.U.L.1797	gctcaaatggaaagctgctacaaaattggggatcatgg	ChrIV ₆₆₇₁₀₈₋₆₆₇₈₆₅ for pB.JL2889 and pB.JL2890
O.U.L.1798	gctcaaatggcggcggcgaatgccccttgagagttagcc	ChrIV ₆₆₇₂₆₅₋₆₆₈₁₃₃ for pB.JL2889 and pB.JL2890
O.U.L.1799	gctcaaatggaaagctctcaagaggctgagcctcaaaacata	ChrIV ₆₆₇₂₆₅₋₆₆₈₁₃₃ for pB.JL2889 and pB.JL2890
O.U.L.1804	gctcaaatggaaagctggcctgaataaacacagacacttccctg	ChrIV ₆₆₈₂₀₀₋₁₀₈₆₀₈ for pB.JL2891 and pB.JL2892
O.U.L.1805	gctcaaatggaaagctgatgggaaccctaaagccttc	ChrIV ₆₆₈₂₀₀₋₁₀₈₆₀₈ for pB.JL2891 and pB.JL2892
O.U.L.1806	gctcaaatggcggcggcagggagatcacttctgccc	ChrIV ₆₆₈₂₀₀₋₁₀₈₆₀₈ for pB.JL2891 and pB.JL2892
O.U.L.1807	gctcaaatggaaagctctcaatagctgagggaaacacctca	ChrIV ₆₆₈₂₀₀₋₁₀₈₆₀₈ for pB.JL2891 and pB.JL2892
O.U.L.1852	AAAGGATGCTGATGTTGG	Hybrid Ty Junction Sequencing
O.U.L.1853	GTTCAACAGAAAGCCACAG	Hybrid Ty Junction Sequencing
O.U.L.1955	TCATGCTTTTGATGACGGGTATGACATACATAGTAGC	Primer 1 for junction PCR
O.U.L.1956	CTCTCTTTACAGAAATACAAAAGGATGCTGATTTGG	Primer 2 for junction PCR. Hybrid Ty Junction Sequencing
O.U.L.1957	ACTGATGTTTCAACAGAGACCACAGTTAAAAGGTTCC	Primer 3 for junction PCR (amplicons 515-650kb). Hybrid Ty Junction Sequencing
O.U.L.1958	TAGAAAACGTACTGTGATTTGAATACACTGGAATAGG	Primer 4 for junction PCR (amplicons 515-650kb)
O.U.L.1983	TTACGATCCAAGCACTATTGGCATTITTTGGCCCTTC	Primer 3 for junction PCR (amplicons 515-985kb)
O.U.L.1984	GGGAGGACGACCTAGCTCTAAACCCTTCATATGATC	Primer 4 for junction PCR (amplicons 515-985kb)
O.U.L.2059	CAACAAGACTATGGCCCTC	Hybrid Ty Junction Sequencing
O.U.L.2081	GTATAAATTATACCTGATAC	Hybrid Ty Junction Sequencing
O.U.L.2082	CAAGAATAGTGGATAATACGGTAATCGTATG	Hybrid Ty Junction Sequencing
O.U.L.2083	CTGGATTAACGGCAGTGTCTTGACAAATC	Hybrid Ty Junction Sequencing
O.U.L.2087	GACTGAGGTTTCAATAGCGGAATAGCTTC	Hybrid Ty Junction Sequencing
O.U.L.2091	CAATGTTAGCGACAGATTGGCCCTGTC	Hybrid Ty Junction Sequencing
O.U.L.2092	GATCGGATGGTACAGTACTAGCTC	Hybrid Ty Junction Sequencing
O.U.L.2093	GATCTAGAGCCACGGTGTGCGTGAAC	Hybrid Ty Junction Sequencing
O.U.L.2094	GAAATGATGCCACATATCTGAATAC	Hybrid Ty Junction Sequencing
O.U.L.2095	GAGAACTGGAACCAACCAAGATCGAAG	Hybrid Ty Junction Sequencing
O.U.L.2096	GCACATCGAAAGATTGCGGATGGTC	Hybrid Ty Junction Sequencing
O.U.L.2097	gaacagaggaataagtaacgattattatggagcagcattgactgagagtg	dn14::TRP1, Step 1
O.U.L.2098	caaaaattaaacctcccaaaaacccaccacgcactctgctgggtatttcac	dn14::TRP1, Step 1
O.U.L.2099	gtggaaataataactaataaataaactagactgaaaggaatagtaaccgg	dn14::TRP1, Step 2
O.U.L.2100	taacatagtagtagtaataaactcaaaaatttaagcctccgc	dn14::TRP1, Step 2
O.U.L.2117	gaaggtcttggtgcttgggtggtgagcagattgactgagagtg	rad52::TRP1, Step 1
O.U.L.2118	aalgtaccaaatattttttggtccaggagccttgcactctgtgcccgtatttcac	rad52::TRP1, Step 1
O.U.L.2119	atgcaaacaggagggtgccaagaactgctgaaaggttctggtggcctttgg	rad52::TRP1, Step 2
O.U.L.2120	aactagaggattggagtaataaataatgatgcaaaattttttattttggttcggc	rad52::TRP1, Step 2
O.U.L.2144	CTGTGTTAAAGTGTGGTGG	Hybrid Ty Junction Sequencing
O.U.L.2145	CATGAAGATTGGTGAATTTGAG	Hybrid Ty Junction Sequencing
O.U.L.2146	GCAAGTGAATTTACGGAGG	Hybrid Ty Junction Sequencing
O.U.L.2147	CTGATAGTAGATCAACGATCAG	Hybrid Ty Junction Sequencing

Table S8

Plasmids used in this study.

Name	Description	Source
pAG25	<i>natMX</i>	Goldstein, A.L. et al. <i>Yeast</i> 15 , 1541-1553 (1999)
pBJL2889	<i>ChrIV</i> ₅₆₇₁₀₈₋₅₆₇₆₅₅ , <i>ade3-2p</i> , <i>kanMX</i> , <i>ChrIV</i> ₅₆₇₆₅₆₋₅₆₈₁₃₃	This study
pBJL2890	<i>ChrIV</i> ₅₆₇₁₀₈₋₅₆₇₆₅₅ , <i>ade3-2p</i> , <i>ARS317</i> , <i>kanMX</i> , <i>ChrIV</i> ₅₆₇₆₅₆₋₅₆₈₁₃₃	This study
pBJL2891	<i>ChrIV</i> ₁₀₈₉₅₀₀₋₁₀₈₉₀₃₉ , <i>ade3-2p</i> , <i>kanMX</i> , <i>ChrIV</i> ₁₀₈₉₀₄₀₋₁₀₈₉₆₃₃	This study
pBJL2892	<i>ChrIV</i> ₁₀₈₉₅₀₀₋₁₀₈₉₀₃₉ , <i>ade3-2p</i> , <i>ARS317</i> , <i>kanMX</i> , <i>ChrIV</i> ₁₀₈₉₀₄₀₋₁₀₈₉₆₃₃	This study
pDK243	<i>ade3-2p</i> , <i>LEU2</i>	Koshland, D., et. al. <i>Cell</i> 40 , 393-403 (1985)
pFA6a-pGAL1-3HA	<i>kanMX</i>	Longtine, M.S. et al. <i>Yeast</i> 14 , 953-961 (1998)
pJL737	<i>ORC6</i> , <i>URA3</i>	Nguyen, V.Q. et al. <i>Nature</i> 411 , 1068-1073 (2001)
pJL806	<i>pGAL1</i> , <i>URA3</i>	Nguyen, V.Q. et al. <i>Nature</i> 411 , 1068-1073 (2001)
pJL1033	<i>MCM7</i> , <i>URA3</i>	Nguyen, V.Q. et al. <i>Curr Biol</i> 10 , 195-205 (2000)
pJL1206	<i>MCM7-2NLS</i> , <i>URA3</i>	Nguyen, V.Q. et al. <i>Nature</i> 411 , 1068-1073 (2001)
pJL1488	<i>pGAL1-antCDK6-cdk2A</i> , <i>URA3</i>	Green, B.M. et al. <i>Mol Biol Cell</i> 17 , 2401-2414 (2005)
pMP933	<i>ORC2</i> -(NotI-SgrAI), <i>URA3</i>	Nguyen, V.Q. et al. <i>Nature</i> 411 , 1068-1073 (2001)
pRSS56	<i>Amp^r</i>	Sikorski, R.S. et al. <i>Genetics</i> 122 , 19-27 (1989)
pSB283	<i>pGAL-HO</i> , <i>LEU2</i> , <i>URA3</i> , <i>CEN7</i>	Berlin, V. et al. <i>Meth Enzymol</i> 194 , 774-792 (1991)

Table S9

Yeast strains used in this study.

Strain	Genotype	Source
4524-1-3	MATa <i>cdc7-1 leu2 ade2 ade3 his7 sap3 gal1 ura1 can1</i>	Palmer et al. ¹
4525-061	MATa <i>cdc6-1 leu2 ade2 ade3 his7 sap3 gal1 ura1 can1</i>	Palmer et al. ¹
4528-091	MATa <i>cdc9-1 leu2 ade2 ade3 his7 sap3 gal1 ura1 can1</i>	Palmer et al. ¹
4532-171	MATa <i>cdc17-1 leu2 ade2 ade3 his7 sap3 gal1 ura1 can1</i>	Palmer et al. ¹
4541-8-5	MATa <i>leu2 ade2 ade3 his7 sap3 gal1 ura1 can1</i>	Palmer et al. ¹
YJL1737	MATa <i>orc2-cdk6A orc6-cdk4A ura3-52 leu2 trp1-289 ade2 ade3 bar1::LEU2</i>	Nguyen et al. ²
YJL2067	MATa MCM7-2NLS <i>orc2-cdk6A orc6-cdk4A ura3-52 leu2 trp1-289 ade2 ade3 bar1::LEU2</i>	This study
YJL3151	MATa MCM7-2NLS <i>orc2 orc6-cdk4A ura3-52 leu2 trp1-289 ade2 ade3 bar1::LEU2</i>	This study
YJL3155	MATa MCM7-2NLS <i>orc2 orc6 ura3-52 leu2 trp1-289 ade2 ade3 bar1::LEU2</i>	This study
YJL3165	MATα MCM7-2NLS <i>orc2 orc6 ura3-52 leu2 trp1-289 ade2 ade3 bar1::LEU2</i>	This study
YJL3516	MATa MCM7 <i>orc2 orc6 ura3-52 leu2 trp1-289 ade2 ade3 bar1::LEU2</i>	This study
YJL3519	MATα MCM7 <i>orc2 orc6 ura3-52 leu2 trp1-289 ade2 ade3 bar1::LEU2</i>	This study
YJL3756	MATa MCM7-2NLS <i>ura3-52:::pGAL, URA3} orc2 orc6 leu2 trp1-289 ade2 ade3 bar1::LEU2</i>	This study
YJL3758	MATa MCM7-2NLS <i>ura3-52:::pGAL-ΔntCDC6-cdk2A, URA3} orc2 orc6 leu2 trp1-289 ade2 ade3 bar1::LEU2</i>	This study
YJL4486	MATa MCM7-2NLS <i>ura3-52:::pGAL, URA3} orc2 orc6 leu2 trp1-289 ade2 ade3 bar1::LEU2</i> <i>cdc20:::pMET3-HA3-CDC20, TRP1}</i>	Green et al. ³
YJL6032	MATa MCM7-2NLS <i>ura3-52:::pGAL-ΔntCDC6-cdk2A, URA3} orc2 orc6 leu2 trp1-289 ade2 ade3 bar1::LEU2</i> <i>ChrIII_{297kb}:::ade3-2p, kanMX}</i>	This study
YJL6555	MATa MCM7-2NLS <i>ura3-52:::pGAL-ΔntCDC6-cdk2A, URA3} orc2 orc6 leu2 trp1-289 ade2 ade3 bar1::LEU2</i> <i>ChrIV_{567kb}:::ade3-2p, kanMX} ars317::natMX</i>	This study
YJL6557	MATa MCM7-2NLS <i>ura3-52:::pGAL-ΔntCDC6-cdk2A, URA3} orc2 orc6 leu2 trp1-289 ade2 ade3 bar1::LEU2</i> <i>ChrIV_{1089kb}:::ade3-2p, kanMX} ars317::natMX</i>	This study
YJL6558	MATa MCM7-2NLS <i>ura3-52:::pGAL-ΔntCDC6-cdk2A, URA3} orc2 orc6 leu2 trp1-289 ade2 ade3 bar1::LEU2</i> <i>ChrIV_{567kb}:::ade3-2p, ARS317, kanMX} ars317::natMX</i>	This study
YJL6561	MATa MCM7-2NLS <i>ura3-52:::pGAL-ΔntCDC6-cdk2A, URA3} orc2 orc6 leu2 trp1-289 ade2 ade3 bar1::LEU2</i> <i>ChrIV_{1089kb}:::ade3-2p, ARS317, kanMX} ars317::natMX</i>	This study
YJL6974	MATa MCM7-2NLS <i>ura3-52:::pGAL, URA3} orc2 orc6 leu2 trp1-289 ade2 ade3 bar1::LEU2</i> <i>ChrIV_{567kb}:::ade3-2p, ARS317, kanMX} ars317::natMX</i>	This study

Table S9 (continued)

Yeast strains used in this study.

Strain	Genotype	Source
YJL6977	MATa MCM7-2NLS ura3-52::[pGAL, URA3] ORC2 ORC6 leu2 trp1-289 ade2 ade3 bar1::LEU2 ChrIV _{1089kb} ::[ade3-2p, ARS317, kanMX] ars317::natMX	This study
YJL6993	MATa MCM7 ORC2 ORC6 ura3-52 leu2 trp1-289 ade2 ade3 bar1::LEU2 ChrIV _{567kb} ::[ade3-2p, ARS317, kanMX]	This study
YJL7002	MATa/MATa leu2/leu2 ade2/ade2 ade3/ade3 his7/his7 sap3/sap3 gal1/gal1 ura1/ura1 can1/can1 ChrIV/ChrIV _{567kb} ::[ade3-2p, ARS317, kanMX]	This study
YJL7003	MATa/MATa cdc6-1/cdc6-1 leu2/leu2 ade2/ade2 ade3/ade3 his7/his7 sap3/sap3 gal1/gal1 can1/can1 ChrIV/ChrIV _{567kb} ::[ade3-2p, ARS317, kanMX]	This study
YJL7005	MATa/MATa cdc9-1/cdc9-1 leu2/leu2 ade2/ade2 ade3/ade3 his7/his7 sap3/sap3 gal1/gal1 ura1/ura1 can1/can1 ChrIV/ChrIV _{567kb} ::[ade3-2p, ARS317, kanMX]	This study
YJL7006	MATa/MATa cdc17-1/cdc17-1 leu2/leu2 ade2/ade2 ade3/ade3 his7/his7 sap3/sap3 gal1/gal1 ura1/ura1 can1/can1 ChrIV/ChrIV _{567kb} ::[ade3-2p, ARS317, kanMX]	This study
YJL7007	MATa/MATa leu2/leu2 ura3-52/ura3-52 trp1-289/trp1-289 ade2/ade2 ade3/ade3 bar1::LEU2/bar1::LEU2 ChrIV/ChrIV _{567kb} ::[ade3-2p, ARS317, kanMX]	This study
YJL7087	MATa/MATa cdc7-1/cdc7-1 leu2/leu2 ade2/ade2 ade3/ade3 his7/his7 sap3/sap3 gal1/gal1 can1/can1 ChrIV/ChrIV _{567kb} ::[ade3-2p, ARS317, kanMX]	This study
YJL7443	MATa dnl4::TRP1 MCM7-2NLS ura3-52::[pGAL-AnfCDC6-cdk2A, URA3] ORC2 ORC6 leu2 trp1-289 ade2 ade3 bar1::LEU2 ChrIV _{567kb} ::[ade3-2p, ARS317, kanMX] ars317::natMX	This study
YJL7452	MATa rad52::TRP1 MCM7-2NLS ura3-52::[pGAL-AnfCDC6-cdk2A, URA3] ORC2 ORC6 leu2 trp1-289 ade2 ade3 bar1::LEU2 ChrIV _{567kb} ::[ade3-2p, ARS317, kanMX] ars317::natMX	This study
YJL7695	MATa MCM7 ura3-52 ORC2 ORC6 leu2 trp1-289 ade2 ade3 bar1::LEU2 ChrIV _{567kb} ::[ade3-2p, ARS317, kanMX] ars317::natMX	This study

¹ Palmer, R. E. et al. *Genetics* **125**, 763-774 (1990)

² Nguyen, V.Q. et al. *Nature* **411**, 1068-1073 (2001)

³ Green, B.M. et al. *Mol Biol Cell* **17**, 2401-2414 (2006)

Supplementary Discussion

Our studies in budding yeast have shown that re-replication is very efficient at inducing the critical first step of gene amplification, the increase in gene copy number from one to two or more. In principal, re-replication in subsequent generations can expand copy number beyond the duplications and triplications we observed. However, once tandem copies of a large chromosomal segment are generated, other routes for expansion are available, such as non-allelic homologous recombination between sister chromatids. Hence, just inducing this first step of amplification may greatly stimulate higher order amplifications as well.

Structural analysis of the resulting amplicons as well as aCGH analysis of re-replication hint at a mechanism involving fork collapse, DNA breakage, and some type of recombinational repair at re-replication bubbles (Fig. 3D). In principle, DNA fragments with broken ends can also be generated during multiple rounds of re-replication when a re-replication fork from one round catches up to a fork from the preceding round (*SI*). However, given that only half the population of *ade3-2p* reporter cassettes re-replicated in our experimental strains and an even smaller fraction may re-replicate in more biologically relevant settings (see below), we have focused on scenarios where at most one round of re-replication occurs on any molecule. Ultimately, elucidating the precise mechanism of RRIGA will require further molecular and genetic analysis of the event.

We note that, in principle, the combination of fork collapse, breakage, and repair implicated in RRIGA can also occur at replication bubbles during S phase replication. Nonetheless, re-replication appears to mobilize and coordinate these steps particularly well. Simply disrupting DNA replication with hydroxyurea or temperature sensitive replication mutations (*cdc6-1*, *cdc7-1*, *cdc9-1*, or *cdc17-1*) or inducing DNA breaks with the DNA damaging agent phleomycin did not result in the high levels of amplification generated by rereplication (Fig. S3).

This striking efficiency of RRIGA may be due to both the nature of re-replication

forks and the context in which they appear. The limited size of re-replication bubbles (apparent in Fig. 1A and Fig. S2A (S2)) and the extensive DNA damage induced by re-replication (S3-6) raise the possibility that re-replication forks are more susceptible to irreversibly stalling, collapse, and breakage than replication forks. Although more detailed structural and functional studies of re-replication forks will be needed to determine if they do indeed lack the integrity of replication forks (S7), such a possibility could help explain why re-replication is particularly efficient at inducing the recombination events leading to gene amplifications. What is clear is that serious and highly recombinogenic fork problems can be much better tolerated during limited re-replication than they can during replication.

More sporadic problems with replication forks can occur during S phase replication, and if unresolved are thought to lead to low levels of genomic rearrangements (S8-10), possibly even gene amplification (S11-13). However, the redundancy of origins available for firing during replication provides opportunities to rescue stalled forks by converging forks originating from neighboring origins. Moreover, should these converging forks also run into problems, dormant origins may become activated in between the stalled forks to rescue both (S14). Hence, by protecting themselves with multiple safeguards, cells have reduced their vulnerability to genomic rearrangements from S phase accidents. In contrast, the lack of such extensive fork backup in the context of limited re-replication, when only isolated origins re-initiate, may enhance the efficiency with which RRIGA occurs.

In essence, the loss of replication control may create a highly defective extraneous round of re-replication, providing a fertile setting for genomic rearrangement of duplicated chromosome segments, without compromising the essential first round of replication. In such a setting, it would not be surprising if other genetic alterations were also induced, such as extrachromosomal amplifications, loss of heterozygosity, aneuploidy, and translocations.

Our studies on RRIGA resurrect a model proposed nearly three decades ago for gene amplification. This re-replication model was inspired by observations of nested “onionskin” re-replication bubbles during activation of an integrated DNA tumor virus (S15) and during the developmentally regulated amplification of *Drosophila* chorion genes (S16). However, with limited ability to detect re-replication and no ability to induce it, direct support for the model could not be obtained, contributing to its abandonment (S17-19).

Also contributing to this abandonment was the rise of the breakage-fusion-bridge (BFB) model for gene amplification (Fig. S5). The BFB model has since become the predominant model for intrachromosomal amplifications because various aspects of its structural signature (e.g. amplicons oriented in inverted repeat, telomeric deletions, and dicentric chromosomes) have been observed in amplifications in drug-resistant cells selected in culture, in some mouse cancer models, and in a number of human tumors (S20). Nonetheless, among the few tumor amplifications whose structures have been extensively characterized, there are notable examples of amplified oncogenes arranged in direct repeat (S21-24), which are incompatible with BFB. More recently, sequencing of breast cancer genomes has revealed hundreds of tandem duplications in direct repeat (S25), suggesting that duplications and higher order amplifications in direct repeat may be prevalent in cancers.

The ability of re-replication to induce amplification structures that cannot be explained by BFB suggests that RRIGA could provide a complementary gene amplification model for human tumors. Nonetheless, there are several challenges to determining whether and how much RRIGA contributes to such amplifications. First, amplicon orientation and location have not been established for most tumor-associated amplifications, so it is not yet possible to assess how many exhibit the structural signature for RRIGA versus that for BFB. Second, the minimal structural signature for RRIGA, segmental amplicons *in loco* in direct tandem repeat, is not specific to RRIGA. Even the

more specific version of this signature that we observed in budding yeast, which includes repetitive elements at amplicon junctions, could arise from a non-allelic homologous recombination event that is not associated with re-replication. Hence, corroborating evidence of re-replication may be required to implicate RRIGA in tumors.

Detecting such re-replication will likely require the development of more sensitive replication assays. Standard assays in current use, such as flow cytometry and density shift, have difficulty detecting re-replication that increases DNA content by less than 5-10%. Compounding this detection problem is the likelihood that only extremely low or sporadic levels of re-replication will contribute to genomic instability. Currently detectable levels of re-replication cause widespread cell death or apoptosis (*S3-6, 26-28*), presumably because of the extensive DNA damage it causes (*S3-6*). In fact, the very limited re-replication occurring in our MC_{2A} strains (Fig. 1A and Fig. S2A) was both undetectable by flow cytometry (although detectable by our more sensitive aCGH assay) and too lethal for sustained induction. We had to transiently induce re-replication in order to see the massive stimulation of gene amplification that is possible in these strains.

We thus suspect that the most likely pathological context for RRIGA to occur will involve mutations that constitutively disrupt replication control just enough to take advantage of the extreme efficiency of RRIGA but not enough to significantly compromise viability. In effect, currently undetectable levels of re-replication could provide an oncogenic “mutator” phenotype (*S29*). The difficulty of detecting re-replication in this context could account for why re-replication has not been widely reported in tumor cells or cell lines susceptible to gene amplification. It may also explain why modest overexpression of the replication proteins Cdt1 or Cdc6 can potentiate oncogenesis in mice without causing overt re-replication (*S30-32*). Interestingly, if more sensitive replication assays do eventually demonstrate that some tumors are associated with low levels of re-replication, one can imagine that these tumor cells might be especially vulnerable to therapeutic agents that incrementally deregulate replication

control further, thereby increasing re-replication in these cells to highly lethal levels.

Finally, given that gene copy number increases are important in the diversification and evolution of species (S33, 34), it is tempting to revive speculation that sporadic re-replication might contribute to evolutionary changes as well (S35). Recent studies suggest that the fidelity of wild type DNA polymerases are less than maximal, possibly to ensure sufficient genetic plasticity for evolutionary change (S36). It is conceivable that replication controls in eukaryotic cells are similarly tuned below maximal stringency to facilitate adaptive genomic alterations on an evolutionary time scale.

Supplementary Materials and Methods

Oligonucleotides

Oligonucleotides used in the plasmid and yeast strain constructions described below as well as the PCR analysis of amplicon boundaries and junctions are listed in Table S7.

Plasmids

All plasmids used for strain construction are listed in Table S8. The plasmids containing the *ade3-2p* copy number reporter cassette (schematized in Fig. S1A) are described below.

Plasmids pBJL2890 and pBJL2892 effectively consist of the following fragments of DNA: Homology Left (SacI to StuI of PCR product from YJL4489 (S2) genomic DNA using OJL1796 and OJL1797 for pBJL2890 and OJL1804 and OJL1805 for pBJL2892), a StuI-PmeI linker sequence (5'-AGGCCTGTTTAAAC-3'), kanMX6 (PmeI to XmaI of pFA6a-pGAL1-3HA (S37)), *ade3-2p* (XmaI to SgrAI of pDK243 (S38)), an SgrAI-XbaI linker sequence (5'-CACCGGCGTCTAGA-3'), *ARS317* (SpeI to XbaI of PCR product from S288c genomic DNA using OJL1794 and OJL1795 cloned into pCR2.1 TA TOPO, which picks up part of the polylinker including the XbaI site

5'-GTTTAAACCCATTTGAGCAAGGGCGAATTCTGCAGATATCCATCACAC TGGCGGCCG CTCGAGCATGCATCTAGA-3'), Homology Right (XbaI to NotI of PCR product from YJL4489 (*S2*) genomic DNA using OJL1798 and OJL1799 for pBJL2890 and OJL1806 and OJL1807 for pBJL2892), a NotI-SalI linker sequence (5'-GCGGCCGCGTCGAC-3') and vector backbone (SalI to SacI of pRSS56 (*S39*)).

Plasmids pBJL2889 and pBJL2891 consist of the same fragments as pBJL2890 and pBJL2892, respectively, except they lack the *ARS317* fragment. Plasmid pBJL2876 has the same cassette lacking *ARS317* but the Homology Left fragment was amplified from yeast genomic DNA using OJL1684 and OJL1685 and the Homology Right fragment was amplified using OJL1686 and OJL1687.

For all plasmids, a SacI to SalI fragment spanning the inserted sequences from Homology Left to Homology Right was used in the strain constructions described below.

Strains

All strains used in this study have their genotypes listed in Table S9. Re-replicating strains were derived from YJL3758 (*MATa MCM7-2NLS ura3-52::pGAL-ΔntCDC6-cdk2A, URA3; ORC2 ORC6 leu2 trp1-289 ade2 ade3 bar1::LEU2*). YJL3758 was in turn derived as follows from YJL1737 (*MATa orc2-cdk6A orc6-cdk4A ura3-52 leu2 trp1-289 ade2 ade3 bar1::LEU2*) (*S40*). YJL2067 was generated from YJL1737 by loop-in/loop-out gene replacement of *MCM7* with *MCM7-2NLS* using AspI-linearized pJL1206 (*S40*). YJL3151 was generated from YJL2067 by loop-in/loop-out gene replacement of *orc2-6A* with *ORC2- (NotI, SgrAI)* using EcoNI-linearized pMP933 (*S40*); *ORC2-(NotI, SgrAI)* is a phenotypically wild-type version of *ORC2* containing 5'-ATGGCACCGGTGGGCGGCCGC-3' inserted just upstream of the ORF ATG and is referred to simply as *ORC2* in strain genotypes. YJL3155 was generated from YJL3151 by loop-in/loop-out gene replacement of *orc6-4A* with *ORC6* using SphI-linearized pJL737 (*S40*). YJL3758 was generated from YJL3155 by loop-in integration of StuI-

linearized pJL1488 (S2) (*pGAL1-ΔntCDC6-cdk2A*) at *ura3-52*.

*(Correction added in proofs. YJL3155, YJL3758 and all re-replicating strains derived from YJL3758 were discovered to have one Orc6 CDK consensus site still mutated (codon ACG for Serine 116 mutated to codon GCG for Alanine 116). Although CDK consensus mutations N- and C-terminal to this site were converted back to wild-type during loop-in/loop-out with pJL737, this site in the middle somehow was not. Genotypes in Table S9 have been corrected where appropriate by including the allele *orc6-cdk1A₁₁₆*. When we reconstructed a true *MC_{2A}* strain with fully wild-type *ORC6*, we found that it still preferentially re-initiates *ARS317* but the level of re-initiation is 3-fold lower than the *MC_{2A} orc6-cdk1A₁₁₆* background used in the experiments published here.)*

YJL6558 and YJL6561, re-replicating strains with an *ade3-2p* reporter cassette containing *ARS317*, were generated from YJL3758 by the integration of the SacI to Sall fragment from pBJL2890 or pBJL2892, respectively, into Chromosome IV followed by disruption of the endogenous *ARS317* with a PCR product of *natMX* derived from pAG25 (*S41*) using OJL1639 and OJL1640. Chromosome IV, the largest chromosome in *Saccharomyces cerevisiae*, was chosen as the integration site for the reporter cassettes because *ade3-2p* duplication is least likely to arise from re-replication of the entire chromosome initiated at the cassette. The endogenous *ARS317* on Chromosome III was deleted to minimize additional gross chromosomal alterations that could be stimulated by re-replication at this site.

YJL6555 and YJL6557, re-replicating strains with an *ade3-2p* reporter cassette lacking *ARS317*, were generated from YJL3758 by the integration of the SacI to Sall fragment from pBJL2889 or pBJL2891, respectively, followed by disruption of the endogenous *ARS317* with the PCR product of *natMX* described above.

The non-re-replicating strains, YJL6974 and YJL6977, were derived from YJL3756 (*MATa MCM7-2NLS ORC2 orc6-cdk1A₁₁₆ ura3-52:: {pGAL, URA3} leu2 trp1-289 ade2 ade3 bar1::LEU2*), by the integration of the SacI to Sall fragment

from pBJL2890 or pBJL2892, respectively, followed by disruption of the endogenous *ARS317* with the PCR product of *natMX* described above. YJL3756 was generated from YJL3155 by loop-in integration of *StuI* linearized pJL806 (*S40*) (*pGALI*) at the *ura3-52* locus.

YJL6032, a strain used as a source of reference DNA for some of the aCGH analysis, was derived from YJL3758 by integration of the *SacI* to *Sall* fragment from pBJL2876. This introduces a *ade3-2p* reporter cassette without *ARS317* about 5 kb centromere distal to the endogenous *ARS317*. YJL7695, another strain used as a source of reference DNA for some of the aCGH analysis, was derived from YJL6974 by loop-out removal of pJL806, followed by loop-in/loop-out replacement of *MCM7-2NLS* with *MCM7* using *BamHI*-linearized pJL1033 (*S42*).

YJL7007, a wild-type diploid used to analyze the effect of hydroxyurea and phleomycin on gene amplification, was generated as follows. The mating type of YJL3155 (*MAT α* *MCM7-2NLS* *ORC2* *orc6-cdk1A₁₁₆* *ura3-52* *leu2* *trp1-289* *ade2* *ade3* *bar1::LEU2*) was switched using *pGAL-HO* in pSB283 (*S43*) to form YJL3165. In both YJL3155 and YJL3165, *MCM7-2NLS* was converted back to *MCM7* by loop-in/loop-out gene replacement using *BamHI*-linearized pJL1033 to generate YJL3516 and YJL3519, respectively. An *ade3-2p* *ARS317* reporter cassette was introduced into YJL3516 by integration of the *SacI* to *Sall* fragment from pBJL2890 to generate YJL6993. YJL3519 and YJL6993 were mated to generate YJL7007.

Strains used to study the effects of *cdc* mutants on gene amplification were generated as follows. For the wild-type *CDC* control, an *ade3-2p* *ARS317* reporter cassette (*SacI* to *Sall* fragment of pBJL2980) was integrated into 4541-8-1 (*S44*) (*MAT α* *leu2* *ade2* *ade3* *his7* *sap3* *gal1* *ura1* *can1*). In parallel, a *MAT α* version of 4541-8-1 was generated by mating type switching using *pGAL-HO* in pSB283 (*S43*). Mating of the two strains generated YJL7002. YJL7003, YJL7005, YJL7006, and YJL7087 were similarly generated using different starting strains described in Palmer et al. (*S44*): YJL7003 was

derived from 4525-061 (*MAT α cdc6-1 leu2 ade2 ade3 his7 sap3 gal1 can1*); YJL7005 was derived from 4528-091 (*MAT α cdc9-1 leu2 ade2 ade3 his7 sap3 gal1 ura1 can1*); YJL7006 was derived from 4532-171 (*MAT α cdc17-1 leu2 ade2 ade3 his7 sap3 gal1 ura1 can1*); and YJL7087 was derived from 4524-1-3 (*MAT α cdc7-1 leu2 ade2 ade3 his7 sap3 gal1 ura1 can1*).

YJL7443 and YJL7452 were generated from YJL6558 by the integration of a *TRP1* disruption fragment to replace *DNL4* or *RAD52*, respectively. *TRP1* disruption fragments were generated using PCR in two steps. Step 1 primers (see table S7) were used to amplify *TRP1* from pRS304 (*S39*) and add short regions of homology flanking either *DNL4* or *RAD52*. Step 2 primers extended the region of homology, using the PCR product obtained in Step 1 as a template.

Strain Growth and Induction of Re-Replication, DNA Damage, or Replication Stress

Cells were grown in or on YEP or synthetic complete (SC) medium supplemented with 2% wt/vol dextrose (to form YEPD or SDC) or 3% wt/vol raffinose + 0.05% wt/vol dextrose (to form YEPRaf or SRAfC). For synthetic medium, 1x amino acid concentrations were as described by Sherman (*S45*) except the amount of leucine was doubled to 60 μ g/ml and the amount of serine was halved to 200 μ g/ml. With the exception of plates for red/pink colony color development, all synthetic medium contained 2x amino acids. Color development plates contained 1x amino acids except 0.5x adenine (10 μ g/ml). All cell growth was performed at 30°C except where otherwise noted.

To obtain reproducible induction of re-replication, cells were diluted from a fresh unsaturated culture grown in YEPD into YEPRaf and allowed to grow exponentially for 12–15 h overnight till they reached an OD₆₀₀ of 0.2-0.8. At this cell density, 15 μ g/ml nocodazole (Sigma M1404 or US Biological N3000) was added for 120-150 min to arrest cells in G2/M phase. The *GAL1* promoter (*pGAL1*) was then induced by addition

of 2-3% galactose for 3 hr. Tight maintenance of the arrest was confirmed by quantifying the percent of large budded cells (buds with diameters $> 0.5x$ mother cell diameter) and analyzing the distribution of total DNA content by flow cytometry as previously described (S46).

To perturb S phase replication, the indicated *cdc* mutant strains were grown exponentially overnight in YEPD at 23°C to an OD₆₀₀ of 0.2-0.8, then shifted to 36°C or 30°C for 3 or 6 hr, respectively. Alternatively, a wild type *CDC* strain was grown exponentially overnight in YEPD at 30°C to an OD₆₀₀ of 0.2-0.8, then 0.2M or 0.1M hydroxyurea (US Biological H9120) was added for 3 or 6 hr, respectively. To induce DNA damage, cells were grown exponentially in YEPD at 30°C overnight to an OD₆₀₀ of 0.2-0.8, then 2 µg/ml or 20 µg/ml phleomycin (Invivogen ant-ph-1) was added for 3 hr. The effect of these treatments on cell cycle progression was monitored by quantifying the percent of large budded cells and analyzing the distribution of total DNA content by flow cytometry as previously described (S46).

Colony Sectoring Assay

To score the frequency of red sectors, ~200 colonies were plated per SDC plate containing limiting (0.5x) adenine. Temperature sensitive strains were grown for 7-10 days at 23°C and other strains were grown at 30°C for 5 days. Then cells were shifted to 23°C for 2-6 days till colony color development was optimal. Plates were randomized and scored blind. Red sectors were counted if: 1) the sectors were greater than 1/8 of the colony, 2) darker red than the neighboring colonies (i.e., not a pink sector in a nearly white colony) and 3) the junctions between the red sector and pink colony were largely straight, to minimize sectors due to poor growth. The frequency of sectoring colonies was determined by dividing the total sector counts by the total number of viable colonies. This frequency was measured in at least two independent induction experiments, and the mean and standard error of the mean are reported (see Table S1).

We cannot be sure whether red sectors between 1/8 and 1/2 of the colony arose because persistence of $\Delta ntCdc6-cdk2A$ allowed residual re-replication to occur after release from the nocodazole arrest or because re-replication bubbles generated during the nocodazole arrest can somehow be propagated for a few generations before being converted to a stable gene amplification. Nonetheless, it is clear that re-replication induced an increase in the number of all red sectors 1/8 and larger (Fig. 1B), and that most of these displayed segmental amplifications.

Amplification Frequency and Rate

The amplification frequencies arising from re-replication of the *ade3-2p* cassette at ChrIV_{567kb} for YJL6974, YJL6555, and YJL6558 were calculated by multiplying their sector frequencies (Table S1) by the fraction of red sectors containing *ade3-2p* amplifications, as determined by aCGH. These fractions were 3/32, 1/6, and 31/35, yielding amplification frequencies of 1.3×10^{-4} , 9.7×10^{-4} , and 3.0×10^{-2} , for YJL6974, YJL6555, and YJL6558, respectively.

Frequencies of genomic instability reported in the literature have often been converted to rates by using Lea and Coulson's method of the median (S47), an approximation of Luria-Delbruck fluctuation analysis. Fluctuation analysis, however, applies to constitutive rates of mutations, which generate fluctuations in the frequency of accumulated mutations because mutations that appear earlier during population growth contribute more mutants to the population than mutations acquired later. Fluctuation analysis does not apply and is not needed for mutations induced by transient genetic perturbations. In the simplest case of a perturbation that is experienced within a single generation and causes mutations in just that generation, the rate of mutation (per generation) would equal the observed frequency of mutation. For our RRIGA analysis, re-replication was induced within a single cell cycle, and amplifications acquired over the three immediately following generations were scored, so the observed amplifications

could be attributed to a specific pulse of re-replication. Thus, we divided the observed frequency of 3.0×10^{-2} for YJL6558 by three generations to obtain an order of magnitude RRIGA rate of 10^{-2} per generation.

Pulsed Field Gel Electrophoresis

Cells were prepared for pulsed field gel electrophoresis as described (S4). Plugs were cut in half and loaded on a 1% SeaKem LE agarose (wt/vol) gel in 1x TAE (40 mM Tris, 40 mM acetate, and 2 mM EDTA, pH 8.0). Electrophoresis was carried out at 14°C in 1x TAE on a CHEF DR-III system with a switch time of 500 s, run time of 48 hr, voltage of 3 V, and angle of 106°. The DNA was transferred as described (S4) and probed with an *ADE3* probe generated by PCR of pBJL2889 with oligonucleotides OJL1757 and OJL1758.

Genomic DNA Preparation for aCGH Analysis

Method 1: ~10 OD₆₀₀ units of yeast were collected for DNA preparation. With the exception of samples for YJL7452 sector isolates, cultures were grown in YEPD and were either arrested with α -factor (40-50 ng/ml) or nocodazole (10-15 μ g/ml), or were grown to saturation in YEP + 7-8% dextrose. YJL7452 isolates arrested poorly under all conditions, so samples were collected from asynchronous populations. In all cases DNA was prepared using the MasterPure Yeast DNA Purification Kit (Epicentre, Madison, WI), according to the manufacturer's instructions. aCGH performed with this DNA generates data points with greater scatter than DNA prepared by Method 2, but is still reliable for mapping quantal copy number changes.

Method 2: 250 ml of culture (arrested with either α -factor or nocodazole as described above) was mixed with 1.2 ml of 20% sodium azide and added to 25 ml of frozen, -80°C, 0.2 M EDTA, 0.1% sodium azide. Cells were pelleted, washed with 50 ml 4°C TE (10 mM Tris-Cl, 1 mM EDTA pH 7.5) and stored frozen at -80°C. Pellets were resuspended

in 4 ml Lysis buffer (2% Triton X-100, 1% SDS, 100 mM NaCl, 10 mM Tris-Cl, 1 mM EDTA pH 8.0) and mixed with 4 ml of phenol:CHCl₃:isoamyl alcohol (25:24:1) and 8 ml 0.5 mm glass beads (BioSpec Products, Inc., Bartlesville, OK). The suspension was vortexed seven times for 2-3 min separated by 2-3 min intervals at RT to get at least 95% of the cells lysed. The lysate was diluted with 8 ml phenol:CHCl₃:isoamyl alcohol (25:24:1) and 8 ml TE, vortexed once more, and then centrifuged at 18,500 x g for 15 min at RT. After collecting the aqueous phase, the interphase was re-extracted with 8 ml TE, and the second aqueous phase from this re-extraction pooled with the first. The combined aqueous phases were extracted with an equal volume of CHCl₃. The bulk of the RNA in the extract was selectively precipitated by addition of 0.01 volume 5 M NaCl (to a final concentration of 50 mM) and 0.4 volumes isopropanol followed by centrifugation at 9,000 x g for 15 min at RT. The RNA pellet was discarded and an additional 0.4 volumes of isopropanol was added to the supernatant to precipitate the DNA. Following centrifugation at 9,000 x g for 15 min at RT, the pellet was washed with 70% ethanol, dried, and resuspended with 3.5 ml of 10 mM Tris-Cl (pH 8), 1 mM EDTA. RNase A (Qiagen, Valencia, CA) was added to 340 µg/ml and the sample incubated at 37°C for 30 min. Then Proteinase K was added to 555 µg/ml followed by another incubation at 55°C for 30 min. Finally, 0.5 ml of 10% (w/v) Cetyltrimethylammonium Bromide (CTAB, Sigma H6269), 0.9 M NaCl (prewarmed to 65°C) and 0.9 ml of 5 M NaCl was added. The sample was incubated for 20 min at 65°C before being extracted with 8 ml CHCl₃:isoamyl alcohol (24:1) and centrifuged at 6000 x g for 15 min at RT. The DNA in the aqueous phase was precipitated with 0.8 volumes isopropanol at RT, washed with 70% ethanol, dried, and resuspended in 6 ml of 25 mM Tris-Cl (pH 7), 1 mM EDTA. RNase A (Qiagen, Valencia, CA) was added to 33 µg/ml and the sample incubated at 37°C for 15 min. Then the following were added to the sample in the order listed: 1) 1.5 ml of 5 M NaCl; 2) 0.5 ml of 1M MOPS (pH 7); 3) 0.5 ml of Triton X-100 (3% vol/vol); 4) 1.5 ml of isopropanol. The sample was then mixed by vortexing, then purified

on a Qiagen Genomic-tip 100/G column as per the manufacturer's instructions (Qiagen, Valencia, CA). The eluted DNA was precipitated with 0.8 volumes isopropanol at 4°C, washed with 70% ethanol, dried, and resuspended in 275 µl of 2 mM Tris-Cl pH 7.8. Genomic DNA was then sheared by sonication with a Branson Sonifier 450 to an average fragment size of 500 bp. This method of DNA preparation was used for all aCGH profiles shown in the figures.

aCGH Analysis of Gene Amplification

For DNA purified by Method 1, 80-100% of each DNA sample was labeled with Cy3 and 1.5-2 µg of purified reference DNA from YJL6032 or YJL6558 was labeled with Cy5 essentially as described (S2). The labeled DNA was isolated using one of two previously described methods (low-throughput (S2) or high-throughput (S48)). For DNA prepared by Method 2, 2-2.5µg of each DNA sample was labeled with Cy5 and 1.5-2µg of purified reference DNA from YJL6032, YJL6974, or YJL7695 was labeled with Cy3 essentially as described (S2), and labeled DNA was isolated as previously described (S2). All samples were hybridized and analyzed as described (S2). All microarray data is deposited with the Gene Expression Omnibus (<http://www.ncbi.nlm.nih.gov/geo/>) with accession number GSE22018.

aCGH Analysis of Re-replication

Re-replication profiles were performed by aCGH as described above, using Method 2 for DNA preparation. Because aCGH reports on a population average of DNA copy number, re-replication of a locus in a small percentage of cells (we estimate < 5-10%) would probably not register as a significant copy number increase above the 2C baseline of M phase arrested cells. Hence, although *ARS317* is the predominant origin reinitiating in MC_{2A} strains, the lethality that persists when *ARS317* is absent from the genome (data not shown), suggests that other origins throughout the genome may be

firing below the sensitivity of detection for aCGH. All microarray data is deposited with the Gene Expression Omnibus (<http://www.ncbi.nlm.nih.gov/geo/>) with accession number GSE22018.

Junction PCR

PCR amplification of the amplicon junctions required special care because of the large repetitive Ty element(s) at each junction. DNA was prepared from 5 ml of saturated culture using a modified Winston-Hoffman DNA prep (S49). Cells were pelleted in a screw cap tube and resuspended in 200 μ l of Winston-Hoffman Lysis buffer (2% Triton X-100, 1% SDS, 100mM NaCl, 10mM Tris-Cl pH8.0, 1mM EDTA pH8.0). 200 μ l of glass beads and 200 μ l of phenol:CHCl₃:isoamyl alcohol (25:24:1) were added and the tubes were vortexed in a Tomy multi mixer (setting of 7) for 10 min at room temperature. 450 μ l 1x TE was added to each tube, which were then mixed well and microfuged at 20,000 x g for 3 min. 500 μ l of the aqueous layer was transferred to new screw cap tube containing 10 μ l of RNase A (10 mg/ml) and incubated at 23°C for 2 hours. 300 μ l of phenol:CHCl₃:isoamyl alcohol (25:24:1) was added to each tube, which were then vortexed in the Tomy mixer for 5 min and microfuged at 20,000 x g for 3 min. 400 μ l of the aqueous layer was transferred to new Eppendorf tubes containing 300 μ l chloroform, vortexed, and microfuged at 20,000 x g for 3 min. 300 μ l of the aqueous layer was transferred to new Eppendorf tubes containing 3 μ l 10N ammonium acetate pH 7.0 and 750 μ l 100% ethanol. Tubes were vortexed, then microfuged at 20,000 x g for 7 min. The DNA pellet was washed with 300 μ l of 70% ethanol, dried, and resuspended in 50 μ l of 1x TE. 0.5 μ l of DNA was subjected to PCR with 2.5 μ l Roche Long Template Buffer, 1.25 μ l 10 μ M of each oligo, 2.5 μ l 5mM dNTPs, 1.25 U Roche Expand polymerase and H₂O to a final volume of 25 μ l. The PCR conditions were 94°C for 3 min, then 30 cycles of 94°C for 30 sec, 60°C for 1 min, 68°C for 15 min, and finally 68°C for 10 min.

The oligonucleotide primers used for these PCR reactions are listed in Table S7.

As schematized in Figure 2B, these primers hybridize to unique sequences close to either side of the Ty elements that array CGH data suggested would be at or near the boundaries of the amplicons. Primers 1₅₁₅ and 2₅₁₅ flank YDRCTy2-1 at Chr IV_{515kb}, which mapped close to the left boundary of all amplicons. Primers 3₆₅₀ and 4₆₅₀ flank YDRCTy1-1 at Chr IV_{650kb}, which mapped close to the right boundary of all but one amplicon analyzed by PCR (YJL7110). Primers 3₉₈₅ and 4₉₈₅ flank the inverted Ty pair of YDRWTy2-3 and YDRCTy1-3 at Chr IV_{985kb}, which mapped close to the right-most boundary of the amplicon in YJL7110.

For all strains analyzed by PCR except YJL7110, if the amplicons were in direct repeat due to non-allelic homologous recombination between YDRCTy2-1 and YDRCTy1-1, the prediction is that they would successfully yield PCR products for primer sets 1₅₁₅ and 2₅₁₅ (8016 bp), 3₆₅₀ and 4₆₅₀ (6494 bp), and 2₅₁₅ and 3₆₅₀ (7564 bp) and no PCR product for primers 2₅₁₅ alone or 3₆₅₀ alone. In all cases except one the presence and size of the products from these five PCR reactions matched this prediction, and a representative set of these products from one strain is shown in Fig. 2B. For the one exception, YJL7095, no product was obtained for the inter-amplicon junction PCR involving primers 2₅₁₅ and 3₆₅₀. We note that the aCGH data indicate that the amplification is complex, with some regions triplicated and others duplicated, and thus cannot be unequivocally defined using this PCR approach.

For YJL7110, the structural premise that best fits the data is a direct repeat of amplicons formed by non-allelic homologous recombination between YDRWdelta7 at Chr IV_{520kb} and YDRWdelta20 near Chr IV_{985kb} (which is part of the inverted Ty elements YDRWTy2-3 and YDRCTy1-3 at Chr IV_{985kb}). Such a premise predicts PCR products for primer sets 1₅₁₅ and 2₅₁₅ (8016 bp), 3₉₈₅ and 4₉₈₅ (12110 bp), and 2₅₁₅ and 3₉₈₅ (6339 bp) and no PCR product for primers 2₅₁₅ alone or 3₉₈₅ alone. The presence and size of the PCR products matched these predictions, and sequencing of the inter-amplicon junction PCR product (as described below) from primers 2₅₁₅ and 3₉₈₅ confirmed a crossover

between the two delta elements as proposed (data not shown).

Inter-amplicon Junction Sequencing

Genomic DNA was prepared from YJL7101, YJL7102, YJL7103, and YJL7104 (see Table S9) using a modified Winston-Hoffman DNA prep (S49), as described above for Junction PCR using oligonucleotide primers 2₅₁₅ and 3₆₅₀. PCR reactions were cleaned up using a Qiagen PCR Clean-up kit, according to the manufacturer's instructions (Qiagen, Valencia, CA). Cleaned up PCR products were sequenced by MCLabs (South San Francisco, CA) using oligonucleotides described in Table S7. Sequence analysis was performed using Vector NTI software (Invitrogen, Carlsbad, CA).

Supplementary References

- S1. I. F. Davidson, A. Li, J. J. Blow, Deregulated replication licensing causes DNA fragmentation consistent with head-to-tail fork collision. *Mol Cell* 24, 433 (2006).
- S2. B. M. Green, R. J. Morreale, B. Ozaydin, J. L. Derisi, J. J. Li, Genome-wide mapping of DNA synthesis in *Saccharomyces cerevisiae* reveals that mechanisms preventing reinitiation of DNA replication are not redundant. *Mol Biol Cell* 17, 2401 (2006).
- S3. V. Archambault, A. E. Ikui, B. J. Drapkin, F. R. Cross, Disruption of mechanisms that prevent rereplication triggers a DNA damage response. *Mol Cell Biol* 25, 6707 (2005).
- S4. B. M. Green, J. J. Li, Loss of rereplication control in *Saccharomyces cerevisiae* results in extensive DNA damage. *Mol Biol Cell* 16, 421 (2005).

- S5. M. Melixetian *et al.*, Loss of Geminin induces rereplication in the presence of functional p53. *J Cell Biol* 165, 473 (2004).
- S6. C. Vaziri *et al.*, A p53-dependent checkpoint pathway prevents rereplication. *Mol Cell* 11, 997 (2003).
- S7. K. Labib, B. Hodgson, Replication fork barriers: pausing for a break or stalling for time? *EMBO Rep* 8, 346 (2007).
- S8. A. Aguilera, B. Gomez-Gonzalez, Genome instability: a mechanistic view of its causes and consequences. *Nat Rev Genet* 9, 204 (2008).
- S9. R. D. Kolodner, C. D. Putnam, K. Myung, Maintenance of genome stability in *Saccharomyces cerevisiae*. *Science* 297, 552 (2002).
- S10. T. Weinert, S. Kaochar, H. Jones, A. Paek, A. J. Clark, The replication fork's five degrees of freedom, their failure and genome rearrangements. *Curr Opin Cell Biol* 21, 778 (2009).
- S11. F. J. Lemoine, N. P. Degtyareva, K. Lobachev, T. D. Petes, Chromosomal translocations in yeast induced by low levels of DNA polymerase a model for chromosome fragile sites. *Cell* 120, 587 (2005).
- S12. V. Narayanan, P. A. Mieczkowski, H. M. Kim, T. D. Petes, K. S. Lobachev, The pattern of gene amplification is determined by the chromosomal location of hairpin-capped breaks. *Cell* 125, 1283 (2006).
- S13. K. Umez, M. Hiraoka, M. Mori, H. Maki, Structural analysis of aberrant chromosomes that occur spontaneously in diploid *Saccharomyces cerevisiae*: retrotransposon Ty1 plays a crucial role in chromosomal rearrangements. *Genetics* 160, 97 (2002).

- S14. J. J. Blow, X. Q. Ge, A model for DNA replication showing how dormant origins safeguard against replication fork failure. *EMBO Rep* 10, 406 (2009).
- S15. M. Botchan, W. Topp, J. Sambrook, Studies on simian virus 40 excision from cellular chromosomes. *Cold Spring Harb Symp Quant Biol* 43 Pt 2, 709 (1979).
- S16. A. C. Spradling, The organization and amplification of two chromosomal domains containing *Drosophila* chorion genes. *Cell* 27, 193 (1981).
- S17. D. G. Albertson, Gene amplification in cancer. *Trends Genet* 22, 447 (2006).
- S18. P. J. Hahn, Molecular biology of double-minute chromosomes. *Bioessays* 15, 477 (1993).
- S19. E. Wintersberger, DNA amplification: new insights into its mechanism. *Chromosoma* 103, 73 (1994).
- S20. M. Debatisse, B. Malfoy, Gene amplification mechanisms. *Adv Exp Med Biol* 570, 343 (2005).
- S21. J. Herrick *et al.*, Genomic organization of amplified MYC genes suggests distinct mechanisms of amplification in tumorigenesis. *Cancer Res* 65, 1174 (2005).
- S22. Y. Kuwahara *et al.*, Alternative mechanisms of gene amplification in human cancers. *Genes Chromosomes Cancer* 41, 125 (2004).
- S23. J. O'Neil *et al.*, Alu elements mediate MYB gene tandem duplication in human T-ALL. *J Exp Med* 204, 3059 (2007).
- S24. M. P. Strout, G. Marcucci, C. D. Bloomfield, M. A. Caligiuri, The partial tandem duplication of ALL1 (MLL) is consistently generated by Alu-mediated homologous recombination in acute myeloid leukemia. *Proc Natl Acad Sci U S A* 95, 2390 (1998).

- S25. P. J. Stephens *et al.*, Complex landscapes of somatic rearrangement in human breast cancer genomes. *Nature* 462, 1005 (2009).
- S26. J. Kim, H. Feng, E. T. Kipreos, C. elegans CUL-4 prevents rereplication by promoting the nuclear export of CDC-6 via a CKI-1-dependent pathway. *Curr Biol* 17, 966 (2007).
- S27. H. Nishitani, P. Nurse, p53cdc18 plays a major role controlling the initiation of DNA replication in fission yeast. *Cell* 83, 397 (1995).
- S28. M. Thomer, N. R. May, B. D. Aggarwal, G. Kwok, B. R. Calvi, Drosophila double-parked is sufficient to induce re-replication during development and is regulated by cyclin E/CDK2. *Development* 131, 4807 (2004).
- S29. L. A. Loeb, J. H. Bielas, R. A. Beckman, Cancers exhibit a mutator phenotype: clinical implications. *Cancer Res* 68, 3551 (2008).
- S30. E. Arentson *et al.*, Oncogenic potential of the DNA replication licensing protein CDT1. *Oncogene* 21, 1150 (2002).
- S31. M. Liontos *et al.*, Deregulated overexpression of hCdt1 and hCdc6 promotes malignant behavior. *Cancer Res* 67, 10899 (2007).
- S32. J. Seo *et al.*, Cdt1 transgenic mice develop lymphoblastic lymphoma in the absence of p53. *Oncogene* 24, 8176 (2005).
- S33. H. Innan, F. Kondrashov, The evolution of gene duplications: classifying and distinguishing between models. *Nat Rev Genet* 11, 97 (2010).
- S34. F. Zhang, W. Gu, M. E. Hurles, J. R. Lupski, Copy number variation in human health, disease, and evolution. *Annu Rev Genomics Hum Genet* 10, 451 (2009).

- S35. R. T. Schimke, S. W. Sherwood, A. B. Hill, R. N. Johnston, Overreplication and recombination of DNA in higher eukaryotes: potential consequences and biological implications. *Proc Natl Acad Sci U S A* 83, 2157 (1986).
- S36. E. Loh, J. J. Salk, L. A. Loeb, Optimization of DNA polymerase mutation rates during bacterial evolution. *Proc Natl Acad Sci U S A* 107, 1154 (2010).
- S37. M. S. Longtine *et al.*, Additional modules for versatile and economical PCR-based gene deletion and modification in *Saccharomyces cerevisiae*. *Yeast* 14, 953 (1998).
- S38. D. Koshland, J. C. Kent, L. H. Hartwell, Genetic analysis of the mitotic transmission of minichromosomes. *Cell* 40, 393 (1985).
- S39. R. S. Sikorski, P. Hieter, A system of shuttle vectors and yeast host strains designed for efficient manipulation of DNA in *Saccharomyces cerevisiae*. *Genetics* 122, 19 (1989).
- S40. V. Q. Nguyen, C. Co, J. J. Li, Cyclin-dependent kinases prevent DNA re-replication through multiple mechanisms. *Nature* 411, 1068 (2001).
- S41. A. L. Goldstein, J. H. McCusker, Three new dominant drug resistance cassettes for gene disruption in *Saccharomyces cerevisiae*. *Yeast* 15, 1541 (1999).
- S42. V. Q. Nguyen, C. Co, K. Irie, J. J. Li, Clb/Cdc28 kinases promote nuclear export of the replication initiator proteins Mcm2-7. *Curr Biol* 10, 195 (2000).
- S43. V. Berlin, J. A. Brill, J. Trueheart, J. D. Boeke, G. R. Fink, Genetic screens and selections for cell and nuclear fusion mutants. *Methods Enzymol* 194, 774 (1991).

- S44. R. E. Palmer, E. Hogan, D. Koshland, Mitotic transmission of artificial chromosomes in *cdc* mutants of the yeast, *Saccharomyces cerevisiae*. *Genetics* 125, 763 (1990).
- S45. F. Sherman, Getting started with yeast. *Methods Enzymol* 350, 3 (2002).
- S46. S. B. Haase, S. I. Reed, Improved flow cytometric analysis of the budding yeast cell cycle. *Cell Cycle* 1, 132 (2002).
- S47. D. E. Lea, C. A. Coulson, The distribution of the number of mutants in bacterial populations. *J. Genetics* 49, 264 (1949).
- S48. J. A. Pleiss, G. B. Whitworth, M. Bergkessel, C. Guthrie, Transcript specificity in yeast pre-mRNA splicing revealed by mutations in core spliceosomal components. *PLoS Biol* 5, e90 (2007).
- S49. C. S. Hoffman, F. Winston, A ten-minute DNA preparation from yeast efficiently releases autonomous plasmids for transformation of *Escherichia coli*. *Gene* 57, 267 (1987).
- S50. J. M. Cherry *et al.*, Genetic and physical maps of *Saccharomyces cerevisiae*. *Nature* 387, 67 (1997).

Chapter 3

**Single-Stranded Annealing Induced by Re-Initiation of Replication
Origins Provides a Novel and Efficient Mechanism for Generating Copy
Number Expansion via Non-Allelic Homologous Recombination**

Abstract

Copy number expansions such as amplifications and duplications contribute to human phenotypic variation, promote molecular diversification during evolution, and drive the initiation and/or progression of various cancers. The mechanisms underlying these copy number changes are still incompletely understood, however. We recently demonstrated that transient, limited re-replication from a single origin in *Saccharomyces cerevisiae* efficiently induces segmental amplification of the re-replicated region. Structural analyses of such re-replication induced gene amplifications (RRIGA) suggested that RRIGA could provide a new mechanism for generating copy number variation by non-allelic homologous recombination (NAHR). Here we elucidate this new mechanism and provide insight into why it is so efficient. We establish that sequence homology is both necessary and sufficient for repetitive elements to participate in RRIGA and show that their recombination occurs by a single strand annealing (SSA) mechanism. We also find that re-replication forks are prone to breakage, accounting for the widespread DNA damage associated with deregulation of replication proteins. These breaks appear to stimulate NAHR between re-replicated repeat sequences flanking a re-initiating replication origin. Our results support a RRIGA model where the expansion of a re-replication bubble beyond flanking homologous sequences followed by breakage at both forks in *trans* provides an ideal structural context for SSA-mediated NAHR to form a head-to-tail duplication. Given the remarkable efficiency of RRIGA, we suggest it may be an unappreciated contributor to copy number expansions in both disease and evolution.

Author Summary

Duplications and amplifications of chromosomal segments are frequently observed in eukaryotic genomes, including both normal and cancerous human genomes. These copy number variations contribute to the phenotypic variation upon which natural selection acts. For example, the amplification of genes whose excessive copy number facilitates uncontrolled cell division is often selected for during tumor development. Copy number variations can often arise when repetitive sequence elements, which are dispersed throughout eukaryotic genomes, undergo a rearrangement called non-allelic homologous recombination. Exactly how these rearrangements occur is poorly understood. Here, using budding yeast to model this class of copy number variation, we uncover a new and highly efficient mechanism by which these variations can be generated. The precipitating event is the aberrant re-initiation of DNA replication at a replication origin. Normally the hundreds to thousands of origins scattered throughout a eukaryotic genome are tightly controlled such that each is permitted to initiate only once per cell cycle. However, disruptions in these controls can allow origins to re-initiate and we show how the resulting DNA re-replication structure can be readily converted to a tandem duplication via non-allelic homologous recombination. Hence, the re-initiation of DNA replication is a potential source of copy number variation both in disease and during evolution.

Introduction

Duplication or amplification of chromosomal segments is important for evolution, phenotypic variation, human genetic disorders, and cancer [1–5]. Many of these duplications or amplifications are arranged in direct tandem repeat and have homologous sequence elements at their boundary, suggesting they were formed through recombination between non-allelic homologous sequences. Evidence for such non-allelic homologous recombination (NAHR) events is found in the genomes of nearly all species, including humans, where almost half of the human genome is comprised of low or high copy number repeat sequences [6–8].

The mechanisms responsible for these duplications or amplifications have been difficult to discern because these events are usually too rare to characterize their molecular intermediates. Nonetheless, studies primarily in microorganisms have led to a number of models for how these duplications/amplifications might arise. The most established model assumes that these NAHR events occur through the same fundamental mechanism as allelic homologous recombination [9–11]. In this model NAHR is initiated by a simple DNA double-strand break (DSB) in a repeat sequence, which normally provokes a homology search for the intact allelic counterpart as a repair template. An imperfect search arising from misalignment of sister chromatids or homologs, however, would lead to establishment of a double Holliday junction structure between non-allelic homologous sequences that can resolve into an unequal crossover. Evidence of the reciprocal copy number expansions and contractions expected to arise from such unequal crossing over is limited, having only been observed in the context of large tandem arrays of rDNA [12,13] or CUP1 repeats [14], at subtelomeric repeats [15], and in some human genetic disorders [16]. A recent variation on this model suggests that NAHR-mediated tandem duplications/amplifications may be generated by break-induced replication (BIR) [17]. In this model a broken chromosomal end initiates strand invasion and replication fork assembly at a non-allelic homologous sequence. The fork then duplicates the

chromosomal segment between the homologous sequences before proceeding to the end of the chromosome. Again, direct support for this model is minimal.

Recently, we demonstrated that re-replication of a chromosomal segment due to dysregulation of replication controls can efficiently induce NAHR-mediated tandem duplication/amplification of that segment in the budding yeast *Saccharomyces cerevisiae* [18]. Importantly, introduction of simple DSBs failed to induce duplication/amplification with similar efficiency. Our findings raise the possibility that an alternative mechanism initiated by the loss of replication control might be responsible for some NAHR-mediated tandem duplications/amplifications. We have thus been eager to elucidate the mechanism of re-replication induced gene amplification (RRIGA).

The initiation of eukaryotic DNA replication is controlled by a battery of overlapping mechanisms that prevent re-initiation of DNA replication from the hundreds to thousands of replication origins in eukaryotic genomes. Replication initiation normally occurs at these origins in a two-stage process [19,20]. In G1 phase, origins are licensed for initiation by loading the Mcm2-7 core replicative helicase onto them, a process that requires the origin recognition complex (ORC), Cdc6, Cdt1, and Mcm2-7. During S-phase, licensed origins are triggered to initiate DNA replication. To ensure that none of these origins re-initiate, multiple mechanisms inhibit ORC, Cdc6, Cdt1, and Mcm2-7 to minimize the chance that origins will be relicensed after they have initiated [19–21]. Consistent with the non-redundant nature of these controls, experimentally inactivating increasing numbers of these mechanisms leads to progressively increasing amounts of re-initiation and re-replication in budding yeast [22,23].

These replication controls are critical for cell viability and genome stability. When sufficient controls are disrupted to cause overt re-replication (i.e. an increase in genomic DNA content detectable by flow cytometry), extensive DNA damage and a major DNA damage response is observed [24–31]. While the source of damage is not well understood, the amount of damage apparently overwhelms the DNA damage

response and leads to massive cell death. In budding yeast, we developed the ability to induce and detect much lower levels of re-replication compatible with cell viability [23]. Retention of viability allowed us to examine the effect of re-replication on genome stability [18]. We found that limited, transient re-replication of a chromosomal segment induced tandem duplication and occasionally higher order amplification of that segment at a rate approximating 10^{-2} per cell division, about five orders of magnitude higher than spontaneous duplication rates [17]. The tandem duplications were bounded by Ty retrotransposon elements, a class of repetitive elements scattered throughout the yeast genome [32].

Here we uncover the mechanism of this re-replication induced gene amplification. These studies show that re-replication induces DNA damage because re-replication forks are highly susceptible to breakage. Our data support a model for RRIGA in which the two forks of a re-replication bubble both proceed beyond repetitive sequence elements flanking the re-initiating origin and then break. Should these breaks occur in *trans* with respect to the chromosome axis, normal 5' to 3' strand resection at each break will expose complementary strands of the non-allelic repetitive elements, providing a ready substrate for recombination by a single strand annealing (SSA) mechanism. Such repair of these broken re-replication bubbles will result in a tandem duplication arranged in direct repeat. In this model both the susceptibility of re-replication forks to breakage and the special structural context provided by the re-replication bubble contribute to the extraordinary efficiency of RRIGA. Importantly, the critical event triggering the formation of these tandem direct duplications is re-initiation of DNA replication within the duplicated segment. The remarkably efficient channeling of these re-initiation events into tandem direct duplications raises the possibility that even rare spontaneous re-initiation events may be a potent source of copy number variation in evolution and disease.

Results

Homology at amplicon boundaries is necessary and sufficient for RRIGA

RRIGA generates gene duplications and amplifications arrayed in head-to-tail orientation at the original chromosomal locus with boundaries corresponding to Ty retrotransposable elements [18]. We previously reported that the inter-amplicon junctions generated by RRIGA had hybrid sequences consistent with a non-allelic homologous recombination event between Ty retrotransposable elements that flank the re-initiating origin (Figure 1A(i)). The two Ty elements most frequently involved in our RRIGA experiments share a 1.3 kb region of 99% sequence identity where the recombination events occurred (Figure S1A).

What we did not know was whether the homology between Ty elements is sufficient to promote RRIGA or whether other Ty-associated elements or biology are also important. Most Ty elements, including those involved in our RRIGA studies, are surrounded by tRNA genes and long terminal repeats (LTRs) in inverted orientation. These associated elements are known to cause replication forks to pause and possibly to break [33,34], disruptions that could stimulate recombination. Hence, if such associated elements are important for RRIGA, it might constrain RRIGA to specific repetitive elements in budding yeast. On the other hand, if homology is sufficient for sequences to serve as RRIGA boundary elements, RRIGA could offer a potential mechanism for a broad range of NAHR-mediated copy number variations.

To address this question we used our previously described RRIGA assay, which exploits colony sectoring [35] to screen for amplification events [18]. In this assay, an origin particularly prone to re-initiate (*ARS317*) when Cdc6, Orc6, and the MCM complex are deregulated is integrated at 567 kb on Chromosome IV, along with a color based copy number reporter gene (*ade3-2p*). Cells with a single copy of *ade3-2p* are pink, while those with two or more copies are red. After transiently inducing re-initiation at *ARS317* during a nocodazole arrest (G2/M), cells are plated for single colonies

and possible amplification events are identified from pink colonies with red sectors that comprise 1/2-1/8 of the colony. We then verify and characterize amplifications in the red sectors by array Comparative Genomic Hybridization (aCGH). The vast majority of amplifications identified using this assay span the region from 515-650 kb on Chromosome IV, with *YDRCTy2-1* and *YDRCTy1-1* at the left and right boundaries, respectively. These are the closest Ty elements flanking the re-initiating *ARS317* origin at 567 kb, and both are surrounded by tRNA genes and LTRs (Figure S1A).

To determine whether homology is sufficient to support RRIGA, we constructed strains in which: (1) *YDRCTy2-1* was replaced by a 3' portion of the *URA3* gene; (2) *YDRCTy1-1* was replaced by a 5' portion of the *URA3* gene; or (3) both Ty elements were replaced by their respective *URA3* gene fragments (Figure S1). Two versions of these strains were generated. In version 1 some of the adjacent LTRs were replaced along with each Ty element, but tRNA genes and inverted LTR repeats were preserved (Figure S1B). In version 2, all of the adjacent tRNA genes and LTRs were replaced along with each Ty element (Figure S1C). Importantly, the *URA3* fragments share a 390 bp overlapping region of 100% sequence identity. Thus, sequence homology was present at positions 515 kb and 650 kb on Chromosome IV in the strains in which both endogenous Ty elements were intact, as well as the strains in which both Ty elements were replaced by *URA3* fragments. In contrast, no significant homology was present at these loci in strains in which only one Ty element was replaced by a *URA3* fragment, and we refer to these as non-homologous boundary strains.

The non-homologous boundary strains showed a 5- to 10-fold decrease in sector frequency (Figure 1B(i), Figure S2A, Table S1). Subsequent aCGH analysis of a dozen residual sectors induced in version 2 of each of these non-homologous boundary strains failed to detect any amplifications with endpoints at 515 kb and 650 kb on Chromosome IV (Figure S3, Table S2). Thus, when RRIGA frequencies for the 515-650 kb segment were estimated by multiplying sector frequencies by the percent of sectors that amplified

this segment, there was at least a 50- to 100-fold reduction in frequency (Figure 1B(ii)). We note that many red sectors derived from the strain without the right hand Ty element at 650 kb (*YDRCTy1-1*) did have an extra copy of the *ade3-2p* reporter, but achieved this either by using Ty elements further to the right as the right hand RRIGA boundary element, or through translocation or aneuploidy. In contrast, most red sectors derived from the strain without the left hand Ty element at 515 kb (*YDRCTy2-1*) did not have an extra copy of the *ade3-2p* reporter, presumably because there are no other Ty elements on Chromosome IV to serve as left-hand RRIGA boundaries (these red sectors presumably arose from other genomic changes that altered the rate of red pigment accumulation in *ade3-2p* cells). These findings confirmed that homology at the boundaries of amplicons is necessary for efficient RRIGA in budding yeast.

More importantly, when sequence homology was restored by replacing the remaining Ty element with the appropriate *URA3* fragment, RRIGA frequencies were also restored. In strains with Ty elements at both 515 kb and 650 kb replaced by either version 1 or version 2 of the overlapping *URA3* fragments, sectoring occurred at a frequency comparable to the strain with endogenous Ty elements intact (Figure 1B(i), Figure S2A, Table S1). Furthermore, most (14/16) of the red-sectors that were examined by aCGH bore an amplification of the 515 kb to 650 kb region of Chromosome IV (Figure S3, Table S2). Importantly, RRIGA frequency in the context of overlapping *URA3* fragments was unaffected by the presence or absence of the tRNA genes or LTRs (compare Figure 1B and Figure S2A, Figure S2B). Thus, sequence homology at the boundaries of amplicons is sufficient to support RRIGA. Given the prevalence of homologous repetitive elements in eukaryotic genomes [36], this finding implies that these genomes are a potentially rich source of substrates for re-replication induced gene amplification.

Development of a Selection Assay for RRIGA

The fact that RRIGA in budding yeast results in NAHR between homologous sequences flanking a re-initiating origin allowed us to develop a more rapid and sensitive selection-based assay for quantifying RRIGA. We designed the *URA3* fragments replacing the Ty elements at 515 kb and 650 kb such that NAHR between the fragments during RRIGA reconstitutes a full length, functional *URA3* gene at the inter-amplicon junction (Figure 1A(ii)). Thus, in addition to scoring RRIGA between these two endpoints by colony sectoring, we could select for these events on media lacking uracil (Figure 2A, Table S1, Table S3). We note that the selection assay consistently gave a higher frequency than the sectoring assay, most likely because our visual criterion restricted the sectoring assay to capturing amplification events that occurred within 2-3 generations of cell plating (see Text S1).

We characterized the genetic alterations in the *URA3* prototrophs recovered from our selection assay to ensure that they structurally resembled the RRIGA amplifications previously recovered from the sectoring assay. aCGH demonstrated that all prototrophs did indeed bear an amplification that spans the region from 515-650 kb on Chromosome IV (Figure 2B, Table S4). PCR across potential amplicon junctions confirmed that the original amplicon boundaries were intact and that the regenerated *URA3* gene was created from a new head-to-tail amplicon junction (Figure 2C). Such a junction could arise from tandem intrachromosomal amplicons in head-to-tail orientation, as previously observed for RRIGA, but could also arise from circularization of an extrachromosomal amplicon via NAHR between the two *URA3* fragments. These two possibilities can be distinguished by the spontaneous loss rate of the regenerated *URA3* gene, because the latter will be lost at a much higher rate than the former. This loss rate can be estimated by the frequency of cells lacking *URA3* (and thus resistant to the drug 5-fluoroorotic acid (5-FOA)) that accumulate in a population when selection for the gene is removed. As shown in Figure 2D, all the *URA3* prototrophs obtained from our selection assay accumulated

5-FOA resistance at a frequency expected for an intrachromosomal amplification. Thus, the amplifications detected using the *URA3* selection assay were structurally identical to those observed using the sectoring screen.

RRIGA Occurs Through a Single-Strand Annealing Mechanism

Three major forms of homologous recombination have been characterized in budding yeast and shown to have distinct genetic dependencies (Figure 3A): gene conversion (GC), break induced replication (BIR), and single-strand annealing (SSA) [37]. BIR can be further subdivided into a form that requires the RecA homolog Rad51 and one that is independent of Rad51 [38]. We could thus narrow down the form of homologous recombination responsible for RRIGA by using the *URA3* selection assay to quantify the dependence of RRIGA on various recombination genes. Because the frequency of RRIGA is dependent on the amount of induced re-replication, we normalized the measured frequency against the height of the induced re-replication peak (Figure S4A)

The genetic dependencies for RRIGA most closely resembled those for SSA (Figure 3B, Table S3). First, RRIGA was independent of Rad51, which is required for strand invasion in GC and Rad51-dependent BIR but is not required for SSA [39–44]. Second RRIGA was dependent on Rad1 and Msh3. The former functions as part of the Rad1-Rad10 structure specific endonuclease, which removes non-homologous 3' tails during SSA. The latter functions as part of the Msh2-Msh3 complex to stabilize the SSA structure that is recognized by Rad1-Rad10 [45–47]. Finally, RRIGA was independent of Pol32, a non-essential subunit of DNA Polymerase δ that is important for BIR [48]. Similar results for *RAD51* and *RAD1* were observed using the colony sectoring assay, although a partial dependence on Rad51 suggests that a subset of these RRIGA events may require this protein (Figure S4B,C, Table S1). Taken together, these results indicate that most of the NAHR observed in RRIGA is mediated by SSA.

Such a central role for SSA both restricts the possible mechanisms for RRIGA and expands the genetic alterations associated with SSA. SSA is almost always associated with deletion of chromosomal segments that lie between flanking homologous sequences [37]. A break between those sequences followed by 5' end resection past both sequences allows them to anneal and initiate repair through NAHR, but at the cost of deleting the intervening segment. In the context of a re-replication bubble, however, SSA could generate a tandem duplication if both forks of the bubble travel beyond flanking homologous sequences and break in *trans* relative to the chromosome axis. The dual fork breaks would cleave the re-replicated sister chromatid in two, leaving a copy of its re-replicated portion at each broken end. Subsequent 5' end resection back toward the re-replicated homologous sequences closest to each end would then expose complementary strands of these non-allelic sequences for annealing and SSA repair, resulting in a head-to-tail tandem duplication *in loco* (Figure 3C). Such a model provides the most straightforward explanation for how SSA can be responsible for RRIGA. Moreover, in this model, the special context provided by the re-replication bubble to exploit SSA for tandem duplications suggests one reason why re-replication is such a potent inducer of gene amplification.

Re-replication Generates DSBs Distal to Both Flanking Repetitive Elements

A key requirement in our SSA model for RRIGA is that each re-replication fork must break origin-distal to the homologous sequence element that will undergo NAHR (Figure 3C). Although re-replication is known to induce double-strand breaks (DSBs), or at least a robust DNA damage response, in most cases the source of those breaks is unknown and actual breakage of re-replication forks has not been directly implicated [24–31]. We therefore asked whether there is a correspondence between the position of DSBs and re-replication forks and whether DSB do in fact arise distal to both flanking repetitive elements.

To map the location of DSBs that arise during re-replication from *ARS317*, we sized chromosomal fragments generated by these breaks using pulsed field gel electrophoresis (PFGE) (Figure 4, Figure S5). By preparing genomic DNA from cells embedded within agar plugs, this technique minimizes breakage from *in vitro* manipulations. Cells were harvested for PFGE after inducing re-replication for 0, 3, or 6 hr; as a control we harvested cells from a congenic non-rereplicating strain at the same time points. Prior to PFGE, chromosomal DNA was digested with the I-SceI endonuclease, which cuts a single unique I-SceI recognition site engineered very close to *ARS317*. This digest divides Chromosome IV into two fragments containing sequences to the left and right of *ARS317*, respectively. For those molecules that re-initiated from *ARS317*, the digestion will convert the resulting bubble intermediates into left and right Y-shaped chromosome fragments with *ARS317* near the arm tips, telomere at the stem base, and re-replication fork at the branch point. Hence, a DSB in the re-replicated segment will cleave off an arm of the Y, generating a truncated chromosomal fragment whose length defines the position of the break relative to *ARS317* (Figure 4A). After size separation by PFGE, these fragments were detected by southern analysis using probes just to the left or right of the I-SceI cut site (Figure 4B, Figure S5).

Using this approach, we found that re-replication dependent DSBs did indeed arise with significant frequency on both sides of *ARS317* (Figure 4B, Figure S5). Full-length right and left fragments from I-SceI-digested Chromosome IV were detected as discrete bands. Truncated fragments arising from DSBs migrated as a smear representing a range of sizes below the full-length fragments. These truncated fragments were specific to the re-replicating strain and became more abundant with longer induction of re-replication. Quantifying the amount of each fragment length relative to the starting amount of G2/M chromosomes before re-replication (0 hr) allowed us to estimate the percent of these chromosomes that acquired a DSB at each chromosomal position as a consequence of re-replication (see Text S1). Figure 4C shows a plot of this DSB

percentage as a function of distance from *ARS317*. The distribution formed a broad peak centered about the origin similar to the distribution of re-replication forks around *ARS317* (Figure S4A: WT). The similarity of these distributions is consistent with the notion that the DSBs arise from breakage of re-replication forks.

Importantly, many of the DSBs we mapped arose origin-distal to the two flanking repetitive Ty elements that are closest to *ARS317* and that participate most frequently in RRIGA. We suspect our analysis under counts DSB formation because some re-replication forks may not break until after the re-replication induction period, and some forks that break early in this period may already have been repaired. Nonetheless, the data provide a ballpark estimate of the percent of G2 chromosomes that acquire a double strand break beyond the most proximal Ty element as a consequence of re-replication. After 3 hr of re-replication this estimate is roughly 10-15% for either side of *ARS317* (see Text S1). After 6 hr of re-replication the estimate is roughly 30-45%. Thus, these breaks are not rare, and there is a reasonable probability that a re-replication bubble will break at both forks at the positions needed to stimulate the use of homologous sequences in our model for SSA-mediated RRIGA.

Re-replication Forks Must Proceed Beyond Flanking Repetitive Elements for RRIGA

Our model predicts that the further away a homologous sequence is from the origin, the lower the frequency of RRIGA involving that sequence, as fewer re-replication forks will be able to reach that sequence and break beyond it. The fact that RRIGA amplicons preferentially arise from NAHR between the two closest Ty elements flanking the re-initiating origin as endpoints is consistent with this prediction. However, to test this prediction directly we used the *URA3* selection assay to quantify the frequency of RRIGA in a series of strains where the flanking *URA3* fragments were placed at increasing distance from *ARS317* (Figure 5A).

The overall trend supports the prediction. As the flanking *URA3* fragments are

moved further away from *ARS317*, RRIGA frequencies drop (Figure 5B, Table S3). RRIGA isolates from each starting strain were examined by aCGH to confirm that their amplicons did indeed extend from one *URA3* fragment to the other (Figure S6A, Table S4). Importantly, despite the large range of amplicon sizes (11kb to 585 kb) there was no detectable difference in the growth rates of these isolates (Figure S6B). Hence, the decrease in RRIGA frequencies cannot be explained by a decrease in fitness of those RRIGA isolates with larger amplicons. Instead these results support the requirement for forks to replicate and break beyond flanking homologous sequences.

RRIGA Proceeds Most Efficiently With the Re-Initiating Origin Within the Amplicon

In the SSA model of RRIGA, after a re-replication fork breaks origin-distal to a homologous sequence element, 5' end resection from the break must proceed back to the homologous sequence to make it available for SSA. With resection rates in *S. cerevisiae* estimated at 4 kb per hour [49], breaks that arise tens of kilobases past the homologous sequence will require many hours of resection before they can facilitate RRIGA, increasing the likelihood that the break will be repaired by an alternative mechanism or fail to occur before chromosomes finally segregate. Hence, one might expect some constraint on how far a fork break can occur beyond a homologous sequence and still stimulate the use of that sequence for RRIGA.

Such a constraint would influence the optimum position of a re-initiating origin relative to homologous boundaries of a potential amplicon. One would predict that RRIGA should be more efficient when the origin is within the amplicon than when it is outside (see Figure 6A). In the latter case, any distance traveled by the re-replication fork that initially moves away from the amplicon will have to be completely retraced during resection followed by further resection from the origin to the closest boundary.

To test this prediction, we generated a series of re-replicating strains in which the right amplicon boundary was held fixed while the left amplicon boundary lay either to

the left of *ARS317* (positioning the origin within the amplicon) or at two sites to the right of *ARS317* (positioning the origin outside of the amplicon) (Figure 6B). In this series, the rightward re-replication fork has to travel the longest distance to reach the right homologous sequence boundary, and this distance is unchanged. In contrast, the leftward re-replication fork has little or no distance to travel to get past the left homologous sequence boundaries, but wherever it might break the resection distance back to those boundaries increases. In accordance with the prediction, the RRIGA frequency tracks inversely with the anticipated resection distance. The frequency is highest for the strain with the origin contained within the amplicon and becomes progressively lower as the left amplicon boundary is positioned further to the right of the origin (Figure 6C, Table S3).

Because the size of the amplicons varied in this series of strains, we also compared strains with relatively constant amplicon size in which the re-initiating origin was effectively repositioned outside of the amplicon (Figure S7A). In one set of strains, amplicon boundaries approximately 140 kb apart were moved to the right of *ARS317*, causing a precipitous drop in RRIGA (Figure S7B, Table S3). Although part of this drop can be attributed to the increased distance re-replication forks have to travel to the right-most boundary (see Figure 5B, strains YJL9118/9119 versus strains YJL9121/9122), the remainder is likely due to the repositioning of the origin outside of the amplicon (compare Figure S7B strains YJL9145/9146 versus Figure 5B strains YJL9121/9122). Similarly, in strains where the amplicon size is maintained at ~100 kb there is a dramatic decrease in RRIGA frequency when the origin is positioned outside of the amplicon (see Figure S7B, strains YJL9115/9116 versus YJL9147/9148). Thus, as expected from the SSA model for RRIGA, a re-initiating origin is most efficient at inducing amplification if the origin lies between the homologous sequences that define the amplicon boundaries.

Discussion

A model for re-replication induced gene amplification

We have previously shown that re-replication in budding yeast is remarkably efficient at inducing NAHR events that result in tandem gene amplifications oriented in direct repeat [18]. A transient, localized, limited pulse of re-replication from a single origin induced segmental amplifications on the order of 10^{-2} per cell per generation. This efficient amplification appeared to be specific to re-replication, as disruption of S-phase replication with mutant replication proteins or hydroxyurea did not induce equivalent amplification frequencies. In this paper, we propose a model for re-replication induced gene amplification (RRIGA) that helps explain why this amplification is so efficient and provides a new mechanism for NAHR-mediated copy number variation. Such efficiency makes it conceivable that rare or sporadic re-replication events might contribute to DNA copy number changes observed during oncogenesis or evolution.

In our model for RRIGA (Figure 3C), bidirectional re-replication forks proceeding outward from a re-initiating origin can stimulate an efficient NAHR event between flanking homologous sequence elements by replicating beyond them and generating DSBs. Normal processing of these breaks will involve 5' to 3' single-strand resection back toward the homologous sequences. In those cases where the two forks break in *trans*, this resection can expose complementary sequences in non-allelic homologous sequences, resulting in annealing and repair of the break by an SSA mechanism. The result is a head-to-tail tandem duplication at the endogenous chromosomal locus. Such tandem duplications can provide a stepping stone for higher order amplifications [50]. Expansion of the duplication might occur readily without further re-replication, as the initially duplicated segments provide a much larger NAHR substrate. On the other hand, if re-replication were to recur in subsequent generations, it could stimulate a series of stepwise expansions that would lead to multi-copy amplification.

Re-replication fork breakage drives RRIGA

An important premise for our RRIGA model is the ability of re-replication to induce frequent chromosomal breaks. There are many reports associating the deregulation of replication initiation proteins with the generation of chromosomal breaks or the induction of a DNA damage response [24–31]. However, in most cases, this deregulation has been imposed constitutively throughout the cell cycle, making it hard to distinguish whether these breaks are due to re-replication per se or arise from possible disruption of S-phase replication. Because we induced re-replication after completion of an intact S-phase, the chromosomal breaks we observed and mapped can be specifically attributed to re-replication. Importantly, the correspondence between the distribution of breaks and the distribution of re-replication forks along the chromosome suggests that these forks are the source of these DSBs.

Formally, it is possible that the DSBs we mapped were actually the free ends of newly synthesized DNA fragments extruded by head-to-tail fork collisions during multiple rounds of re-replication, as has been proposed to explain induction of a DNA damage response during re-replication in *Xenopus* extracts [51]. However, this scenario is unlikely in our gene amplification studies, where we induced on average only half a round of re-replication near *ARS317* (i.e. copy number increase from 2C to 3C). Hence, it appears that the re-replication forks themselves are breaking, leading to chromosome fragmentation.

The distribution of re-replication-induced breaks did not reveal any striking hotspots, indicating that these breaks do not depend on special DNA elements or structures *that are suspected of potentiating DSB formation by promoting fork stalling and/or collapse* [52–54]. The independence of these breaks from the inverted LTR repeats and multiple tRNA genes that often surround Ty elements is consistent with our ability to replace entire clusters of these elements with simple homologous sequences and still observe high frequency RRIGA.

Our results therefore raise the possibility that re-replication forks are particularly susceptible to breakage. Supporting this notion is our previous observation that the induction of re-replication can lead to a rapid and massive Rad9-dependent DNA damage response, a response that is not seen during unperturbed S-phase [24]. In fact, even when S-phase was subjected to prolonged disruption from hydroxyurea, it did not generate the type of chromosome fragmentation that was readily detected during re-replication [24]. Hence, unlike S-phase, where breakage among thousands of replication forks is a rare accident, during re-replication, fork breakage may be the rule rather than the exception.

Clearly, an important future question will be why forks are so susceptible to breakage during re-replication. Nonetheless, the fact that they are increases the likelihood that re-initiation will lead to a bubble with a break at both forks. Our rough order of magnitude estimate of chromosome breakage frequencies on a single side of *ARS317* (10-15% after 3 hr of re-replication and 30-45% after 6 hr) suggests that such dual fork breaks occur with significant frequency. Thus, even the slightest amount of re-replication may be a potent source of copy number variation.

The structural context provided by the re-replication bubble also facilitates RRIGA

Another key feature of our model that contributes to the efficiency of RRIGA is the structural context provided by the re-replication bubble. First, this structure provides an extra, non-essential chromosomal segment in close proximity to the endogenous segment. Second, when both forks happen to break in *trans* relative to the chromosome axis, this structure channels recombinational repair of the broken ends toward the formation of tandem duplications. Consistent with the importance of this structural context, simply inducing DSBs alone is insufficient to induce amplifications in our assay [18]. DSBs have been implicated in promoting NAHR events that result in the formation of deletions, translocations, and isochromosome formation, but they rarely lead to the type of intrachromosomal amplifications so efficiently induced by re-replication [10,55].

DSBs are also capable of initiating a mechanism of gene amplification referred to as breakage-fusion-bridge (BFB), but the resulting amplification structure is very different from RRIGA, with amplicons oriented in inverted repeat and a terminal deletion beyond the amplified locus [56–59]. Thus, without the context of the re-replication bubble, DSBs do not show the same propensity for forming tandem duplications as observed during RRIGA.

The broader context in which re-replication bubbles appear may also contribute to the efficiency of RRIGA. The multiple overlapping layers of replication controls used by eukaryotic cells [18–20] ensure that only a limited number of origins will re-initiate when some of these controls are disrupted. The isolation of the resulting re-replication bubbles increases the likelihood that both forks of a bubble will eventually stall as they run into problems or simply reach the limits of their processivity. Without converging forks from nearby re-replication bubbles to rescue them, these stalled forks will be even more susceptible to breakage. Thus, we anticipate that a large proportion of re-initiation events will form the broken bubble intermediate that can be channeled into tandem direct amplifications.

In contrast, although S-phase replication bubbles are structurally identical to re-replication bubbles, the redundancy of active and backup origins in S-phase [60,61] ensures that replication bubbles rarely arise in isolation and any fork that happens to stall is readily rescued by a converging fork from a neighboring replication bubble. This may explain why, despite the proposed link between S-phase accidents and various genomic rearrangements [62–64], inhibiting origin function or stressing S-phase forks throughout the genome with mutant replication proteins or DNA synthesis inhibitors does not generate RRIGA-like amplification frequencies [18]. To generate isolated replication bubbles, the origin failure or fork stress would have to be so severe that replication would be catastrophically and lethally disrupted. Examples of more tolerated localized replication fork stress have been identified through the discovery of common fragile

sites (CFS) [65,66]. However, individual CFSs can only affect one of the two forks from an expanding replication bubble and, hence, would not generate the broken bubble intermediate central to our RRIGA model. Consistent with this expectation, although some CFSs have been associated with amplifications, the amplifications are not arranged in tandem direct repeat like RRIGA. Instead they are arranged as inverted repeats and are thought to arise through a BFB mechanism initiated by a CFS break [67–69].

There is one example of a mutation that disrupts S-phase replication and induces segmental duplications structurally similar to RRIGA amplifications. Deletion of *CLB5*, one of the S-phase cyclins that triggers origin firing in budding yeast, reduces or delays origin activity primarily in the later replicating regions of the genome [70]. This deletion significantly stimulates tandem direct duplications involving NAHR at one chromosomal locus [17]. The mechanism by which *clb5Δ* stimulates these duplications is unknown, but whether or not it occurs through a RRIGA-like mechanism, the duplication rate is still more than one hundred fold lower (7.3×10^{-5} per cell division [17]) than the rate of RRIGA induced by *ARS317* re-initiation. Altogether, these observations suggest that origin re-initiation may be particularly efficient at inducing amplifications in direct repeat because it is particularly efficient at generating isolated re-replication bubbles broken at both forks.

A wider set of amplification structures from re-replication?

In principle, once re-replication has generated re-replication bubbles broken at both forks in *trans*, subsequent formation of tandem direct duplications can occur by a variety of available repair mechanisms. In budding yeast, where homologous recombination predominates, we have shown that this repair occurs primarily through SSA-mediated NAHR. However, in other organisms, repair could conceivably proceed through alternative mechanisms that don't require extensive sequence homology, such as non-homologous end-joining (NHEJ) or microhomology mediated end-joining (MMEJ).

Interestingly, numerous tandem duplications with little or no sequence homology at their interamplicon junctions have been observed in both normal and cancerous human genomes [16,71,72]. Hence, we are currently investigating whether re-replication can induce these types of duplications as well.

One can also imagine that if both forks of a re-replication bubble break, they may often break in *cis*, releasing one arm of the re-replication bubble and a full length chromosome. In that event, re-circularization of the arm, whether by SSA-mediated NAHR or some other repair mechanism, would generate a circular extrachromosomal amplicon, such as those frequently seen in human tumors [73]. We did not see evidence of extrachromosomal amplification in our system (Figure 2D), but our amplicons lacked centromeres, and in budding yeast, such amplicons would both be very unstable and preferentially accumulate to high, potentially toxic, copy number in mother cells [74]. It will thus be interesting to see if re-replication can also efficiently stimulate extrachromosomal amplification of centromere containing segments, such as the amplifications reported by Libuda and Winston [75].

Implications for Disease and Evolution

Our work provides a basis for understanding why re-replication arising from the loss of replication controls can generate duplications and amplifications with such remarkable efficiency. A much harder question to address is *does* re-replication contribute to gene amplifications and tandem duplications, such as those observed in cancers? Three observations suggest that this question is worth pursuing. First, dysregulation of replication initiation proteins has been observed in human cancer cells [4,76–81]. Second, overexpression of replication initiation proteins in certain murine models can promote oncogenesis [81–83]. Third, a number of oncogene amplifications display amplicon structures with some or all of the features of yeast RRIGA structures: direct repeat, at the endogenous chromosomal locus, bounded by homologous sequence

elements [84–87]. More recently, cancer genome sequencing efforts have detected the appearance of numerous tandem duplications in certain cancers [72]. Despite the lack of significant sequence homology at many of their boundaries, these duplications could still conceivably arise by some form of RRIGA, as discussed above. Importantly, the most popular model for gene amplification, the breakage-fusion-bridge mechanism [56,57], cannot explain these amplifications/duplications in direct repeat, creating a need for alternative mechanisms.

Recently, it has been suggested that the deregulation of replication initiation might promote oncogenesis more directly through the induction of replication stress, resulting in extensive fork stalling, fork collapse, and DSBs [88–91]. Although the exact nature or source of this replication stress is not clear, our work documenting the extensive DNA damage and DSBs arising from re-replication forks makes re-replication a possible candidate.

Finally, we note that rare spontaneous tandem duplications and/or amplifications involving NAHR have been observed arising in yeast containing intact replication controls [17] (KJ Finn, unpublished results). These observations invite speculation that, despite intact controls, sporadic re-replication might still occur and cause gene copy number expansions that could promote evolution directly by generating phenotypic variation [11] or indirectly by removing constraints on molecular diversification [1]. It thus will be of interest to see whether these spontaneous copy number gains share some of the genetic dependencies of RRIGA established in this work.

Materials and Methods

Strains

All strains used in this study are listed in Table S5 are derived from YJL6974 and YJL6558 [18] using standard methods. Details of their construction, along with the plasmids (Table S6) and oligonucleotides (Table S7) used in their derivation, can be found in the Supplemental Material.

Strain Growth and Induction of Re-Replication

Yeast cells were grown as previously described [18]. Induction of re-replication was performed as previously described [18]. Full details are available in the Supplemental Material.

Colony Sectoring Assay

The colony sectoring assay was performed as previously described [18]. Full details are available in the Supplemental Material.

Uracil Prototrophy Assay

Following induction of re-replication ~5,000 cfu were plated onto each SDC-Ura plate (to isolate uracil prototrophs) and ~250 cfu onto each SDC plate (to determine an accurate cfu plated onto the SDC-Ura plates). Plates were incubated at 30°C for 3-5 days, then colonies were counted. The frequency of uracil prototrophs was determined by dividing the total number of colonies on the SDC-Ura plates by the number of cfus plated on the SDC-Ura plates. This frequency was measured in at least two independent experiments and the mean and standard error of the mean (when 3 or more trials were conducted), or the mean and the standard deviation (when only 2 trials were conducted) are reported.

Pulsed-Field Gel Electrophoresis and Southern Blotting

Cells were fixed and embedded in agarose for PFGE essentially as described [24], except that a proteinase K inactivation step with PMSF was included at the end of plug preparation. 1/3 of each plug was then treated with I-SceI to digest the embedded chromosomal DNA. Plugs were then loaded on a 1% SeaKem LE agarose (wt/vol) gel in 0.5x TBE. The gel was electrophoresed in 14°C 0.5x TBE on a CHEF DR-III system (Bio-Rad) with initial switch time of 50 sec, final switch time of 95 sec, run time of 26 hr, voltage of 6 V/cm, and angle of 120°. The DNA was transferred essentially as described [24], except UV-nicking was used instead of acid hydrolysis. The membrane was probed with a *MAK21* probe generated by PCR from yeast genomic DNA with oligonucleotides OJL2449 and OJL2450, and a *YOS9* probe generated by PCR from yeast genomic DNA with oligonucleotides OJL2231 and OJL2232. A Lambda probe was used to detect a sizing ladder. Images were collected using a Typhoon 9400 (GE Healthcare). Data analysis was carried out using Image J (NIH) and Excel (Microsoft Corp.) software. Full details are available in the Text S1.

aCGH

DNA used for aCGH was prepared as essentially described [18,92]. Labeling, hybridization, data acquisition, and data analysis were performed as described [18]. Full details are available in the Supplemental Material.

Junction PCR

Primers used for junction PCR to determine amplicon orientation and preservation of parental junctions are listed in Table S7. PCR was performed using Phusion DNA polymerase (Finnzymes) according to the manufacturer's instructions. DNA used for junction PCR was prepared using a spheroplasting mini-prep method. Full details are available in the Supplemental Material.

Accession Numbers

All arrayCGH data from this study have been deposited in the Gene Expression Omnibus (GEO) (<http://www.ncbi.nlm.nih.gov/geo>) database (Series Accession Number GSE41259).

Acknowledgements

We thank May Szeto and Stephane Ricoult for conducting some of the sectoring assay experiments. We thank Alexander Johnson for use of his CHEF DR-III pulsed field gel electrophoresis system and for his Nikon microscope and camera. We thank Roland Bainton for the use of his Leica dissection microscope for colony sectoring analysis. We thank David Toczyski, J. Lucas Argueso, Lorraine Symington, Alexander Johnson, and members of the Li lab for helpful discussions and comments on the manuscript.

Author Contributions

Conceived and designed the experiments: KJF JJL. Performed the experiments: KJF. Analyzed the data: KJF. Wrote the paper: KJF JJL.

References

1. Ohno S (1970) Evolution by gene duplication. Springer-Verlag. 184 p.
2. Simmons AD, Carvalho CMB, Lupski JR (2012) What have studies of genomic disorders taught us about our genome? *Methods Mol Biol* 838: 1–27. doi:10.1007/978-1-61779-507-7_1.
3. Beroukhi R, Mermel CH, Porter D, Wei G, Raychaudhuri S, et al. (2010) The landscape of somatic copy-number alteration across human cancers. *Nature* 463: 899–905. doi:10.1038/nature08822.

4. Santarius T, Shipley J, Brewer D, Stratton MR, Cooper CS (2010) A census of amplified and overexpressed human cancer genes. *Nat Rev Cancer* 10: 59–64. doi:10.1038/nrc2771.
5. Girirajan S, Campbell CD, Eichler EE (2011) Human copy number variation and complex genetic disease. *Annu Rev Genet* 45: 203–226. doi:10.1146/annurev-genet-102209-163544.
6. Venter JC, Adams MD, Myers EW, Li PW, Mural RJ, et al. (2001) The sequence of the human genome. *Science* 291: 1304–1351. doi:10.1126/science.1058040.
7. Lander ES, Linton LM, Birren B, Nusbaum C, Zody MC, et al. (2001) Initial sequencing and analysis of the human genome. *Nature* 409: 860–921. doi:10.1038/35057062.
8. Levy S, Sutton G, Ng PC, Feuk L, Halpern AL, et al. (2007) The diploid genome sequence of an individual human. *PLoS Biol* 5: e254. doi:10.1371/journal.pbio.0050254.
9. Chen J-M, Cooper DN, Férec C, Kehrer-Sawatzki H, Patrinos GP (2010) Genomic rearrangements in inherited disease and cancer. *Semin Cancer Biol* 20: 222–233. doi:10.1016/j.semcancer.2010.05.007.
10. Hoang ML, Tan FJ, Lai DC, Celniker SE, Hoskins RA, et al. (2010) Competitive repair by naturally dispersed repetitive DNA during non-allelic homologous recombination. *PLoS Genet* 6: e1001228. doi:10.1371/journal.pgen.1001228.
11. Hastings PJ, Lupski JR, Rosenberg SM, Ira G (2009) Mechanisms of change in gene copy number. *Nat Rev Genet* 10: 551–564. doi:10.1038/nrg2593.
12. Szostak JW, Wu R (1980) Unequal crossing over in the ribosomal DNA of *Saccharomyces cerevisiae*. *Nature* 284: 426–430.
13. Petes TD (1980) Unequal meiotic recombination within tandem arrays of yeast ribosomal DNA genes. *Cell* 19: 765–774.

14. Welch JW, Maloney DH, Fogel S (1990) Unequal crossing-over and gene conversion at the amplified CUP1 locus of yeast. *Mol Gen Genet* 222: 304–310.
15. Louis EJ, Haber JE (1990) Mitotic recombination among subtelomeric Y' repeats in *Saccharomyces cerevisiae*. *Genetics* 124: 547–559.
16. Liu P, Carvalho CM, Hastings P, Lupski JR (2012) Mechanisms for recurrent and complex human genomic rearrangements. *Current Opinion in Genetics & Development* 22: 211–220. doi:10.1016/j.gde.2012.02.012.
17. Payen C, Koszul R, Dujon B, Fischer G (2008) Segmental duplications arise from Pol32-dependent repair of broken forks through two alternative replication-based mechanisms. *PLoS Genet* 4: e1000175. doi:10.1371/journal.pgen.1000175.
18. Green BM, Finn KJ, Li JJ (2010) Loss of DNA replication control is a potent inducer of gene amplification. *Science* 329: 943–946. doi:10.1126/science.1190966.
19. Arias EE, Walter JC (2007) Strength in numbers: preventing rereplication via multiple mechanisms in eukaryotic cells. *Genes Dev* 21: 497–518. doi:10.1101/gad.1508907.
20. Diffley JFX (2011) Quality control in the initiation of eukaryotic DNA replication. *Philos Trans R Soc Lond, B, Biol Sci* 366: 3545–3553. doi:10.1098/rstb.2011.0073.
21. Nguyen VQ, Co C, Li JJ (2001) Cyclin-dependent kinases prevent DNA re-replication through multiple mechanisms. *Nature* 411: 1068–1073. doi:10.1038/35082600.
22. Wilmes GM, Archambault V, Austin RJ, Jacobson MD, Bell SP, et al. (2004) Interaction of the S-phase cyclin Clb5 with an “RXL” docking sequence in the initiator protein Orc6 provides an origin-localized replication control switch. *Genes Dev* 18: 981–991. doi:10.1101/gad.1202304.

23. Green BM, Morreale RJ, Ozaydin B, Derisi JL, Li JJ (2006) Genome-wide mapping of DNA synthesis in *Saccharomyces cerevisiae* reveals that mechanisms preventing reinitiation of DNA replication are not redundant. *Mol Biol Cell* 17: 2401–2414. doi:10.1091/mbc.E05-11-1043.
24. Green BM, Li JJ (2005) Loss of rereplication control in *Saccharomyces cerevisiae* results in extensive DNA damage. *Mol Biol Cell* 16: 421–432. doi:10.1091/mbc.E04-09-0833.
25. Melixetian M, Ballabeni A, Masiero L, Gasparini P, Zamponi R, et al. (2004) Loss of Geminin induces rereplication in the presence of functional p53. *J Cell Biol* 165: 473–482. doi:10.1083/jcb.200403106.
26. Archambault V, Ikui AE, Drapkin BJ, Cross FR (2005) Disruption of mechanisms that prevent rereplication triggers a DNA damage response. *Mol Cell Biol* 25: 6707–6721. doi:10.1128/MCB.25.15.6707-6721.2005.
27. Vaziri C, Saxena S, Jeon Y, Lee C, Murata K, et al. (2003) A p53-dependent checkpoint pathway prevents rereplication. *Mol Cell* 11: 997–1008.
28. Lovejoy CA, Lock K, Yenamandra A, Cortez D (2006) DDB1 maintains genome integrity through regulation of Cdt1. *Mol Cell Biol* 26: 7977–7990. doi:10.1128/MCB.00819-06.
29. Jin J, Arias EE, Chen J, Harper JW, Walter JC (2006) A family of diverse Cul4-Ddb1-interacting proteins includes Cdt2, which is required for S phase destruction of the replication factor Cdt1. *Mol Cell* 23: 709–721. doi:10.1016/j.molcel.2006.08.010.
30. Zhu W, Dutta A (2006) An ATR- and BRCA1-mediated Fanconi anemia pathway is required for activating the G2/M checkpoint and DNA damage repair upon rereplication. *Mol Cell Biol* 26: 4601–4611. doi:10.1128/MCB.02141-05.

31. Zhu W, Chen Y, Dutta A (2004) Rereplication by depletion of geminin is seen regardless of p53 status and activates a G2/M checkpoint. *Mol Cell Biol* 24: 7140–7150. doi:10.1128/MCB.24.16.7140-7150.2004.
32. Mieczkowski PA, Lemoine FJ, Petes TD (2006) Recombination between retrotransposons as a source of chromosome rearrangements in the yeast *Saccharomyces cerevisiae*. *DNA Repair (Amst)* 5: 1010–1020. doi:10.1016/j.dnarep.2006.05.027.
33. Deshpande AM, Newlon CS (1996) DNA replication fork pause sites dependent on transcription. *Science* 272: 1030–1033.
34. Voineagu I, Narayanan V, Lobachev KS, Mirkin SM (2008) Replication stalling at unstable inverted repeats: interplay between DNA hairpins and fork stabilizing proteins. *Proc Natl Acad Sci USA* 105: 9936–9941. doi:10.1073/pnas.0804510105.
35. Koshland D, Kent JC, Hartwell LH (1985) Genetic analysis of the mitotic transmission of minichromosomes. *Cell* 40: 393–403.
36. Richard G-F, Kerrest A, Dujon B (2008) Comparative genomics and molecular dynamics of DNA repeats in eukaryotes. *Microbiol Mol Biol Rev* 72: 686–727. doi:10.1128/MMBR.00011-08.
37. Pâques F, Haber JE (1999) Multiple pathways of recombination induced by double-strand breaks in *Saccharomyces cerevisiae*. *Microbiol Mol Biol Rev* 63: 349–404.
38. McEachern MJ, Haber JE (2006) Break-induced replication and recombinational telomere elongation in yeast. *Annu Rev Biochem* 75: 111–135. doi:10.1146/annurev.biochem.74.082803.133234.
39. Ira G, Haber JE (2002) Characterization of RAD51-independent break-induced replication that acts preferentially with short homologous sequences. *Mol Cell Biol* 22: 6384–6392.

40. Symington LS (2002) Role of RAD52 epistasis group genes in homologous recombination and double-strand break repair. *Microbiol Mol Biol Rev* 66: 630–670, table of contents.
41. Le S, Moore JK, Haber JE, Greider CW (1999) RAD50 and RAD51 define two pathways that collaborate to maintain telomeres in the absence of telomerase. *Genetics* 152: 143–152.
42. Davis AP, Symington LS (2004) RAD51-dependent break-induced replication in yeast. *Mol Cell Biol* 24: 2344–2351.
43. Ivanov EL, Sugawara N, Fishman-Lobell J, Haber JE (1996) Genetic requirements for the single-strand annealing pathway of double-strand break repair in *Saccharomyces cerevisiae*. *Genetics* 142: 693–704.
44. Sugawara N, Ira G, Haber JE (2000) DNA length dependence of the single-strand annealing pathway and the role of *Saccharomyces cerevisiae* RAD59 in double-strand break repair. *Mol Cell Biol* 20: 5300–5309.
45. Sugawara N, Pâques F, Colaiácovo M, Haber JE (1997) Role of *Saccharomyces cerevisiae* Msh2 and Msh3 repair proteins in double-strand break-induced recombination. *Proc Natl Acad Sci USA* 94: 9214–9219.
46. Fishman-Lobell J, Haber JE (1992) Removal of nonhomologous DNA ends in double-strand break recombination: the role of the yeast ultraviolet repair gene RAD1. *Science* 258: 480–484.
47. Lyndaker AM, Alani E (2009) A tale of tails: insights into the coordination of 3' end processing during homologous recombination. *Bioessays* 31: 315–321. doi:10.1002/bies.200800195.
48. Lydeard JR, Jain S, Yamaguchi M, Haber JE (2007) Break-induced replication and telomerase-independent telomere maintenance require Pol32. *Nature* 448: 820–823. doi:10.1038/nature06047.

49. Zhu Z, Chung W-H, Shim EY, Lee SE, Ira G (2008) Sgs1 helicase and two nucleases Dna2 and Exo1 resect DNA double-strand break ends. *Cell* 134: 981–994. doi:10.1016/j.cell.2008.08.037.
50. Romero D, Palacios R (1997) Gene amplification and genomic plasticity in prokaryotes. *Annu Rev Genet* 31: 91–111. doi:10.1146/annurev.genet.31.1.91.
51. Davidson IF, Li A, Blow JJ (2006) Deregulated replication licensing causes DNA fragmentation consistent with head-to-tail fork collision. *Mol Cell* 24: 433–443. doi:10.1016/j.molcel.2006.09.010.
52. Carr AM, Paek AL, Weinert T (2011) DNA replication: failures and inverted fusions. *Semin Cell Dev Biol* 22: 866–874. doi:10.1016/j.semcdb.2011.10.008.
53. Labib K, Hodgson B (2007) Replication fork barriers: pausing for a break or stalling for time? *EMBO Rep* 8: 346–353. doi:10.1038/sj.embor.7400940.
54. Mirkin EV, Mirkin SM (2007) Replication fork stalling at natural impediments. *Microbiol Mol Biol Rev* 71: 13–35. doi:10.1128/MMBR.00030-06.
55. Argueso JL, Westmoreland J, Mieczkowski PA, Gawel M, Petes TD, et al. (2008) Double-strand breaks associated with repetitive DNA can reshape the genome. *Proc Natl Acad Sci USA* 105: 11845–11850. doi:10.1073/pnas.0804529105.
56. Debatisse M, Malfoy B (2005) Gene amplification mechanisms. *Adv Exp Med Biol* 570: 343–361. doi:10.1007/1-4020-3764-3_12.
57. McClintock B (1942) The Fusion of Broken Ends of Chromosomes Following Nuclear Fusion. *Proc Natl Acad Sci USA* 28: 458–463.
58. Narayanan V, Mieczkowski PA, Kim H-M, Petes TD, Lobachev KS (2006) The pattern of gene amplification is determined by the chromosomal location of hairpin-capped breaks. *Cell* 125: 1283–1296. doi:10.1016/j.cell.2006.04.042.

59. VanHulle K, Lemoine FJ, Narayanan V, Downing B, Hull K, et al. (2007) Inverted DNA repeats channel repair of distant double-strand breaks into chromatid fusions and chromosomal rearrangements. *Mol Cell Biol* 27: 2601–2614. doi:10.1128/MCB.01740-06.
60. Dershowitz A, Snyder M, Sbia M, Skurnick JH, Ong LY, et al. (2007) Linear derivatives of *Saccharomyces cerevisiae* chromosome III can be maintained in the absence of autonomously replicating sequence elements. *Mol Cell Biol* 27: 4652–4663. doi:10.1128/MCB.01246-06.
61. Blow JJ, Ge XQ (2009) A model for DNA replication showing how dormant origins safeguard against replication fork failure. *EMBO Rep* 10: 406–412. doi:10.1038/embor.2009.5.
62. Aguilera A, Gómez-González B (2008) Genome instability: a mechanistic view of its causes and consequences. *Nat Rev Genet* 9: 204–217. doi:10.1038/nrg2268.
63. Kolodner RD, Putnam CD, Myung K (2002) Maintenance of genome stability in *Saccharomyces cerevisiae*. *Science* 297: 552–557. doi:10.1126/science.1075277.
64. Weinert T, Kaochar S, Jones H, Paek A, Clark AJ (2009) The replication fork's five degrees of freedom, their failure and genome rearrangements. *Curr Opin Cell Biol* 21: 778–784. doi:10.1016/j.ceb.2009.10.004.
65. Debatisse M, Le Tallec B, Letessier A, Dutrillaux B, Brison O (2012) Common fragile sites: mechanisms of instability revisited. *Trends Genet* 28: 22–32. doi:10.1016/j.tig.2011.10.003.
66. Durkin SG, Glover TW (2007) Chromosome fragile sites. *Annu Rev Genet* 41: 169–192. doi:10.1146/annurev.genet.41.042007.165900.
67. Coquelle A, Pipiras E, Toledo F, Buttin G, Debatisse M (1997) Expression of fragile sites triggers intrachromosomal mammalian gene amplification and sets boundaries to early amplicons. *Cell* 89: 215–225.

68. Hellman A, Zlotorynski E, Scherer SW, Cheung J, Vincent JB, et al. (2002) A role for common fragile site induction in amplification of human oncogenes. *Cancer Cell* 1: 89–97.
69. Ciullo M, Debily M-A, Rozier L, Autiero M, Billault A, et al. (2002) Initiation of the breakage-fusion-bridge mechanism through common fragile site activation in human breast cancer cells: the model of PIP gene duplication from a break at FRA7I. *Hum Mol Genet* 11: 2887–2894.
70. McCune HJ, Danielson LS, Alvino GM, Collingwood D, Delrow JJ, et al. (2008) The temporal program of chromosome replication: genomewide replication in *clb5*Δ *Saccharomyces cerevisiae*. *Genetics* 180: 1833–1847. doi:10.1534/genetics.108.094359.
71. Mills RE, Walter K, Stewart C, Handsaker RE, Chen K, et al. (2011) Mapping copy number variation by population-scale genome sequencing. *Nature* 470: 59–65. doi:10.1038/nature09708.
72. McBride DJ, Etemadmoghadam D, Cooke SL, Alsop K, George J, et al. (2012) Tandem duplication of chromosomal segments is common in ovarian and breast cancer genomes. *The Journal of Pathology*. Available: <http://www.ncbi.nlm.nih.gov/pubmed/22514011>.
73. Hahn PJ (1993) Molecular biology of double-minute chromosomes. *Bioessays* 15: 477–484. doi:10.1002/bies.950150707.
74. Murray AW, Szostak JW (1983) Pedigree analysis of plasmid segregation in yeast. *Cell* 34: 961–970.
75. Libuda DE, Winston F (2006) Amplification of histone genes by circular chromosome formation in *Saccharomyces cerevisiae*. *Nature* 443: 1003–1007. doi:10.1038/nature05205.

76. Bonds L, Baker P, Gup C, Shroyer KR (2002) Immunohistochemical localization of cdc6 in squamous and glandular neoplasia of the uterine cervix. *Arch Pathol Lab Med* 126: 1164–1168.
doi:10.1043/0003-9985(2002)126<1164:ILOCIS>2.0.CO;2.
77. Borlado LR, Méndez J (2008) CDC6: from DNA replication to cell cycle checkpoints and oncogenesis. *Carcinogenesis* 29: 237–243. doi:10.1093/carcin/bgm268.
78. Karakaidos P, Taraviras S, Vassiliou LV, Zacharatos P, Kastrinakis NG, et al. (2004) Overexpression of the replication licensing regulators hCdt1 and hCdc6 characterizes a subset of non-small-cell lung carcinomas: synergistic effect with mutant p53 on tumor growth and chromosomal instability--evidence of E2F-1 transcriptional control over hCdt1. *Am J Pathol* 165: 1351–1365. doi:10.1016/S0002-9440(10)63393-7.
79. Murphy N, Ring M, Heffron CCBB, King B, Killalea AG, et al. (2005) p16INK4A, CDC6, and MCM5: predictive biomarkers in cervical preinvasive neoplasia and cervical cancer. *J Clin Pathol* 58: 525–534.
doi:10.1136/jcp.2004.018895.
80. Ren B, Yu G, Tseng GC, Cieply K, Gavel T, et al. (2006) MCM7 amplification and overexpression are associated with prostate cancer progression. *Oncogene* 25: 1090–1098. doi:10.1038/sj.onc.1209134.
81. Lontos M, Koutsami M, Sideridou M, Evangelou K, Kletsas D, et al. (2007) Deregulated overexpression of hCdt1 and hCdc6 promotes malignant behavior. *Cancer Res* 67: 10899–10909. doi:10.1158/0008-5472.CAN-07-2837.
82. Arentson E, Faloon P, Seo J, Moon E, Studts JM, et al. (2002) Oncogenic potential of the DNA replication licensing protein CDT1. *Oncogene* 21: 1150–1158. doi:10.1038/sj.onc.1205175.

83. Seo J, Chung YS, Sharma GG, Moon E, Burack WR, et al. (2005) Cdt1 transgenic mice develop lymphoblastic lymphoma in the absence of p53. *Oncogene* 24: 8176–8186. doi:10.1038/sj.onc.1208881.
84. Kuwahara Y, Tanabe C, Ikeuchi T, Aoyagi K, Nishigaki M, et al. (2004) Alternative mechanisms of gene amplification in human cancers. *Genes Chromosomes Cancer* 41: 125–132. doi:10.1002/gcc.20075.
85. Herrick J, Conti C, Teissier S, Thierry F, Couturier J, et al. (2005) Genomic organization of amplified MYC genes suggests distinct mechanisms of amplification in tumorigenesis. *Cancer Res* 65: 1174–1179. doi:10.1158/0008-5472.CAN-04-2802.
86. O’Neil J, Tchinda J, Gutierrez A, Moreau L, Maser RS, et al. (2007) Alu elements mediate MYB gene tandem duplication in human T-ALL. *J Exp Med* 204: 3059–3066. doi:10.1084/jem.20071637.
87. Strout MP, Marcucci G, Bloomfield CD, Caligiuri MA (1998) The partial tandem duplication of ALL1 (MLL) is consistently generated by Alu-mediated homologous recombination in acute myeloid leukemia. *Proc Natl Acad Sci USA* 95: 2390–2395.
88. Di Micco R, Fumagalli M, Cicalese A, Piccinin S, Gasparini P, et al. (2006) Oncogene-induced senescence is a DNA damage response triggered by DNA hyper-replication. *Nature* 444: 638–642. doi:10.1038/nature05327.
89. Bartkova J, Rezaei N, Liontos M, Karakaidos P, Kletsas D, et al. (2006) Oncogene-induced senescence is part of the tumorigenesis barrier imposed by DNA damage checkpoints. *Nature* 444: 633–637. doi:10.1038/nature05268.
90. Dominguez-Sola D, Ying CY, Grandori C, Ruggiero L, Chen B, et al. (2007) Non-transcriptional control of DNA replication by c-Myc. *Nature* 448: 445–451. doi:10.1038/nature05953.

91. Halazonetis TD, Gorgoulis VG, Bartek J (2008) An oncogene-induced DNA damage model for cancer development. *Science* 319: 1352–1355.
doi:10.1126/science.1140735.
92. Hoffman CS, Winston F (1987) A ten-minute DNA preparation from yeast efficiently releases autonomous plasmids for transformation of *Escherichia coli*. *Gene* 57: 267–272.

Figure 1

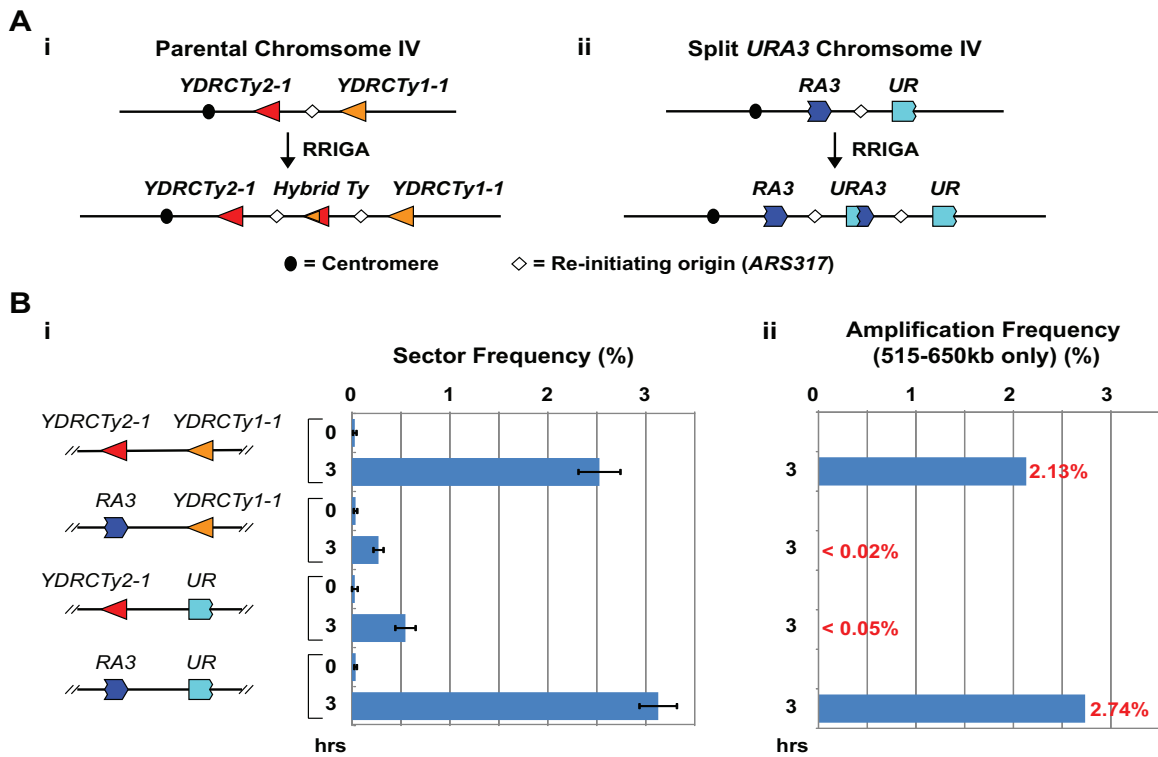


Figure 1. Homologous sequences are necessary and sufficient in *cis* to support RRIGA. A) (i) Schematic of RRIGA arising from NAHR between *YDRCTy2-1* at 515 kb and *YDRCTy1-1* at 650 kb on Chromosome IV; (ii) Schematic of RRIGA arising from NAHR between 3'*URA3* (*RA3*) and 5'*URA3* (*UR*) fragments replacing *YDRCTy2-1* and *YDRCTy1-1*, respectively (see Figure S1). Frequencies shown are for replacement of Ty and all adjacent LTR and tRNA sequences (version 2). B) (i) Sectoring frequencies (mean ± SEM, n = 3 to 5) before (0 hr) and after (3 hr) induction of re-replication in strains with endogenous Ty elements at 515 kb and 650 kb (YJL8100), with *YDRCTy2-1* replaced by *RA3* (YJL8355), with *YDRCTy1-1* replaced by *UR* (YJL8359), or both Ty elements replaced with the respective *URA3* fragments (YJL8363); (ii) Re-replication induced amplification frequency estimated by multiplying 3 hr sector frequency by fraction of sectors containing 515-650 kb amplification (see Figure S3).

Figure 2

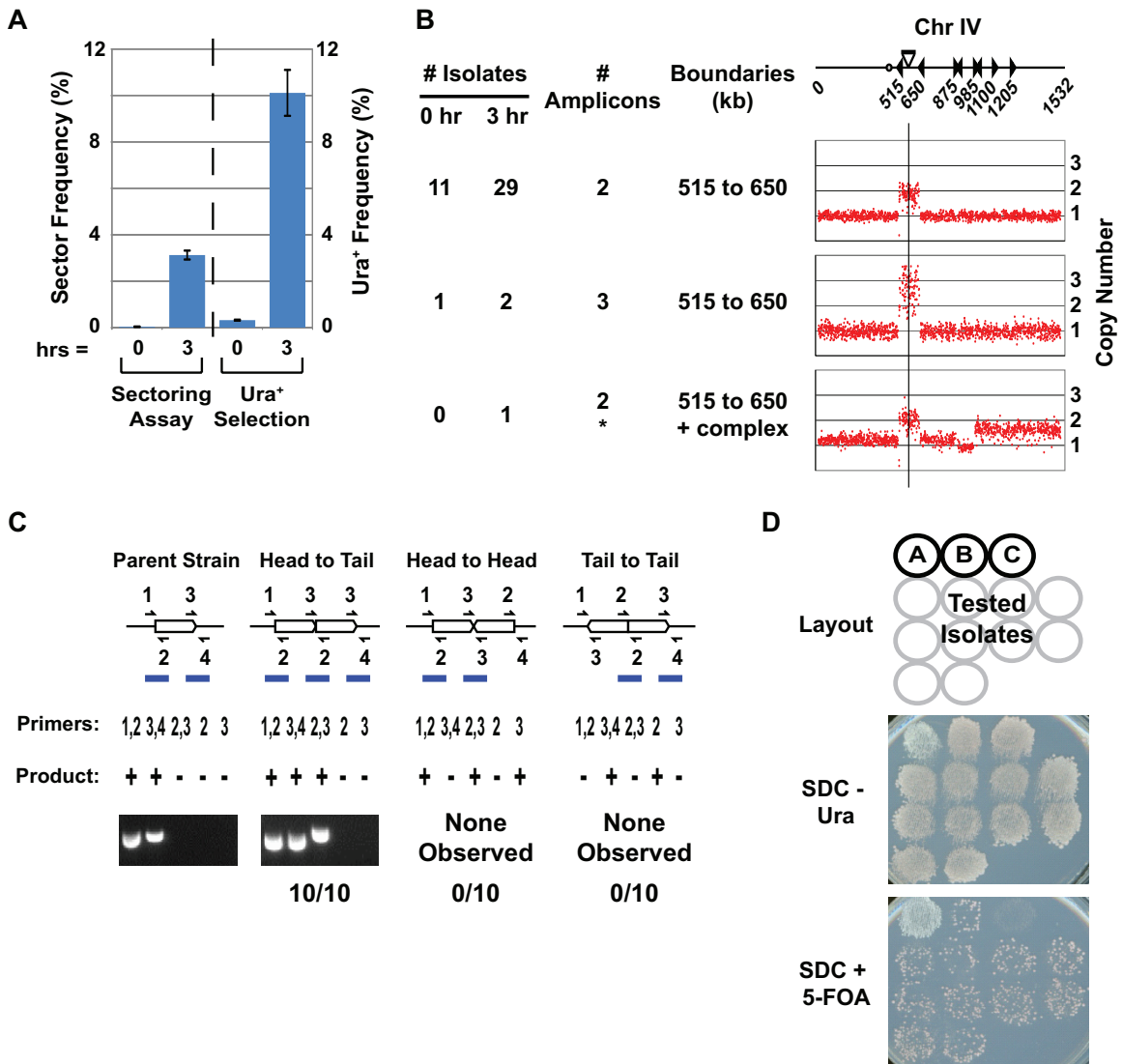


Figure 2. A selection based assay for detecting RRIGA events. A) Comparison of RRIGA frequencies (mean \pm SEM) measured using sectoring assay ($n = 4$) or *URA3* selection assay ($n = 5$) in strains (YJL8363/8364) with *YDRCTy2-1* and *YDRCTy1-1* replaced by *URA3* fragments as described for Figure 1B. B) Isolates from *URA3* selection assay have amplifications spanning the segment between *URA3* fragments (Chromosome IV 515-650 kb). aCGH copy number analysis of Chromosome IV shown for 12 isolates selected before (0 hr) and 32 isolates selected after (3 hr) re-replication from YJL8112/8113 and YJL8363/8364. Chromosome IV schematic shows position and orientation of Ty elements (triangles), centromere (circle), and *ARS317-ade3-2p* re-initiation cassette (bar and vertical line). C) Isolates from *URA3* selection assay have amplifications tandemly arrayed *in loco* in direct repeat. The unamplified parental amplicon and three possible orientations for tandem duplications *in loco* are shown schematically.

Predicted PCR junction fragments are shown for five sets of primers that flank amplicon boundaries (+, PCR product expected; -, no PCR product expected). Representative PCR products are shown for parental strain YJL8363 and 10 re-replication-induced isolates from B. D) Amplicons appear to be chromosomally integrated but excisable. The 10 isolates tested by PCR in C were grown on non-selective media (YEPD), then replica plated to media lacking uracil (SDC-Ura) or media containing 5-FOA (SDC+5-FOA). Patch A, YJL8698 with extrachromosomal copy of *URA3*. Patch B, YJL6974 with integrated but excisable copy of *URA3*. Patch C, YJL8344 with integrated and un-excisable *URA3*.

Figure 3

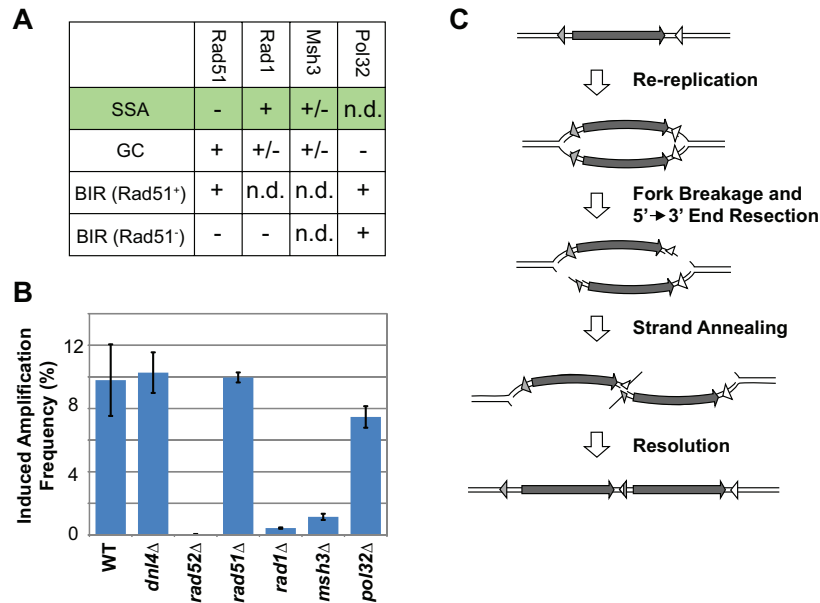


Figure 3. RRIGA is primarily mediated by single-stranded annealing (SSA). A) Summary of genetic requirements for the major sub-types of homologous recombination. SSA = Single Stranded Annealing; GC = Gene Conversion; BIR = Break Induced Replication. “+” = required; “-” = not required; “+/-” = required in some but not all cases; “n.d.” = not determined. B) RRIGA amplification frequencies for WT (YJL8363/8364), *dnl4*Δ (YJL8407/8408), *rad52*Δ (YJL8409/8410); *rad51*Δ (YJL8412/8413), *rad1*Δ (YJL8415/8416), *msh3*Δ (YJL8418/8419), and *pol32*Δ (YJL8421/8422) strains using the *URA3* selection assay. Difference in frequency after 3 hr and 0 hr induction of re-replication was normalized for differences in the amount of re-initiation (see Text S1 and Figure S4). Data are presented as the mean ± combined error (see Text S1). C) Model for RRIGA involving SSA-mediated NAHR. Arrow, amplified segment. Triangles, non-allelic homologous sequences.

Figure 4

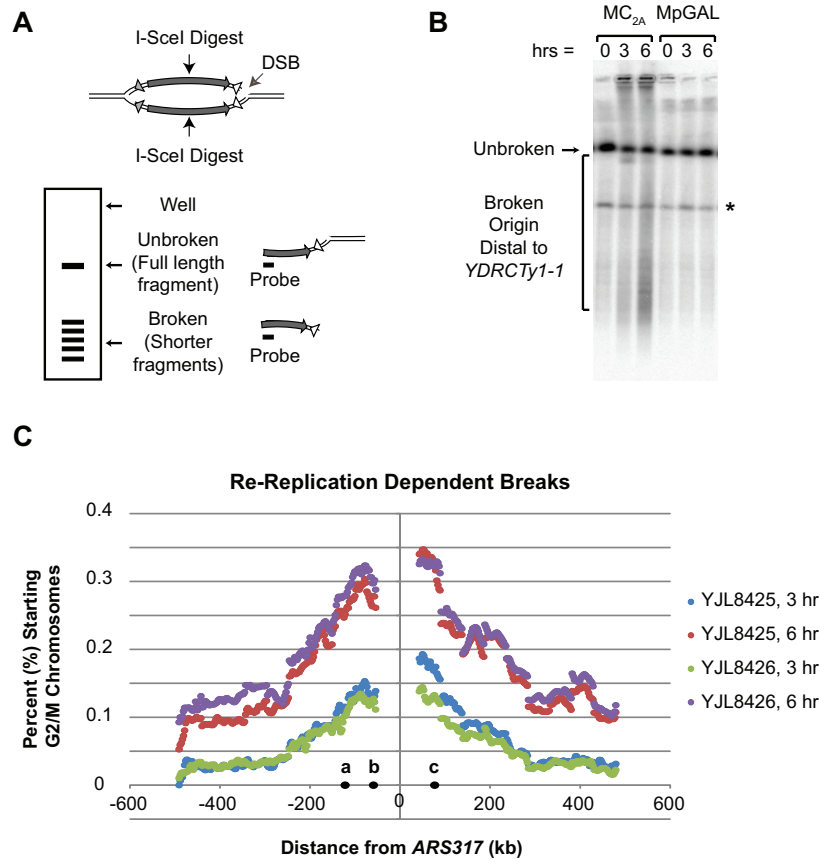


Figure 4. Re-replication induces double stranded DNA breaks distal to flanking repetitive elements.

A) Strategy for mapping DSBs arising during re-replication using an I-SceI site near the re-initiating origin *ARS317* as a physical reference point (see Text S1). The lengths of the small linear fragments generated by DSBs indicate the position of the DSBs relative to the I-SceI cut site. B) Representative Southern blot for DSBs induced by rightward moving re-replication forks. Re-replicating MC_{2A} strains (YJL8425/YJL8426) were induced to re-replicate and at the indicated times chromosomal DNA was prepared, digested with I-SceI, size-separated by PFGE, Southern blotted, and probed for fragments extending rightward from the I-SceI site. Genomic DNA from non-re-replicating Mp_{GAL} control strains (YJL8427/8428) were processed in parallel. Unbroken: full-length Chromosome IV fragment from I-SceI site to right telomere. Bracket: fragments due to DSBs that map origin-distal to *YDRCTy1-1*. * unidentified DNA fragment present independent of re-replication. C) Distribution of DSBs induced by re-replication from *ARS317* (see Text S1 and Figure S5). For each 2425 bp size range, the amount of re-replication induced fragmentation within that size range is displayed as a percent of the total amount of G2/M chromosomes before re-replication was induced. Positions are relative to *ARS317* (at 0 kb) with positions of CEN4 (a), *YDRCTy2-1* (b), and *YDRCTy1-1* (c) indicated.

Figure 5

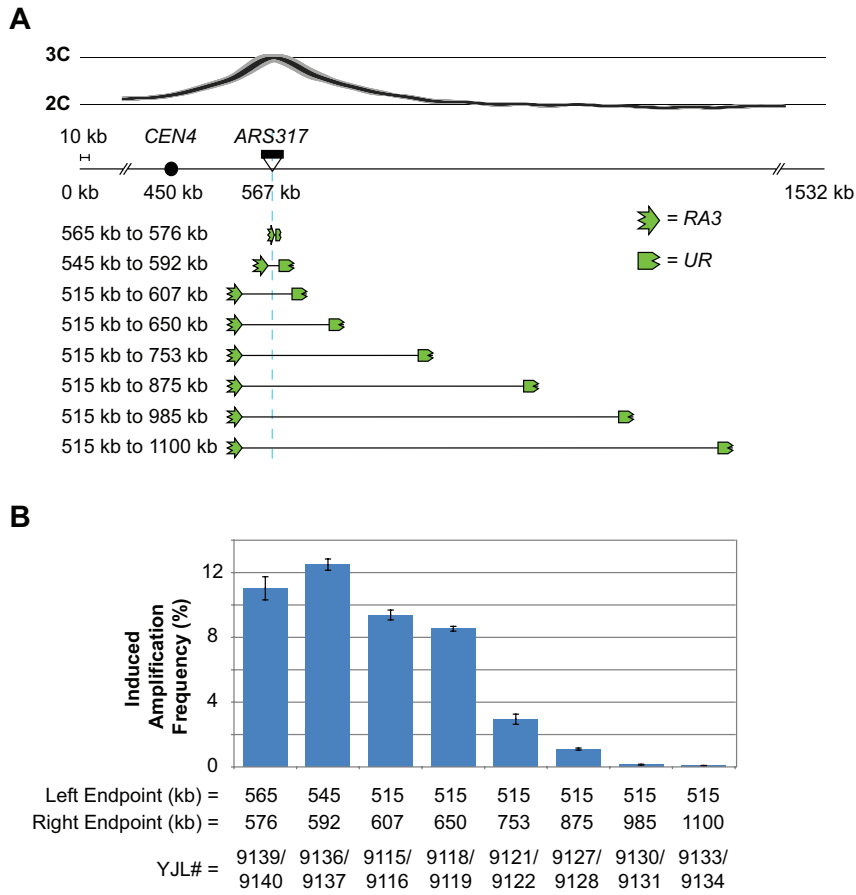


Figure 5. Flanking repetitive elements must be re-replicated in order for RRIGA to occur. A) Schematic showing relocation of the *RA3* and *UR* elements (3' and 5' portions of *URA3*, respectively) used in the *URA3* RRIGA selection assay to change their position relative to the re-initiating origin (*ARS317*, light blue line) and the distribution of re-replication forks (as inferred from the re-replication profile). B) Induced amplification frequencies (mean \pm SEM, n = 3) for strains with the indicated amplicon boundaries as defined by the position of the *URA3* fragments. Induced frequency is frequency after 3 hr re-replication minus frequency after 0 hr re-replication.

Figure 6

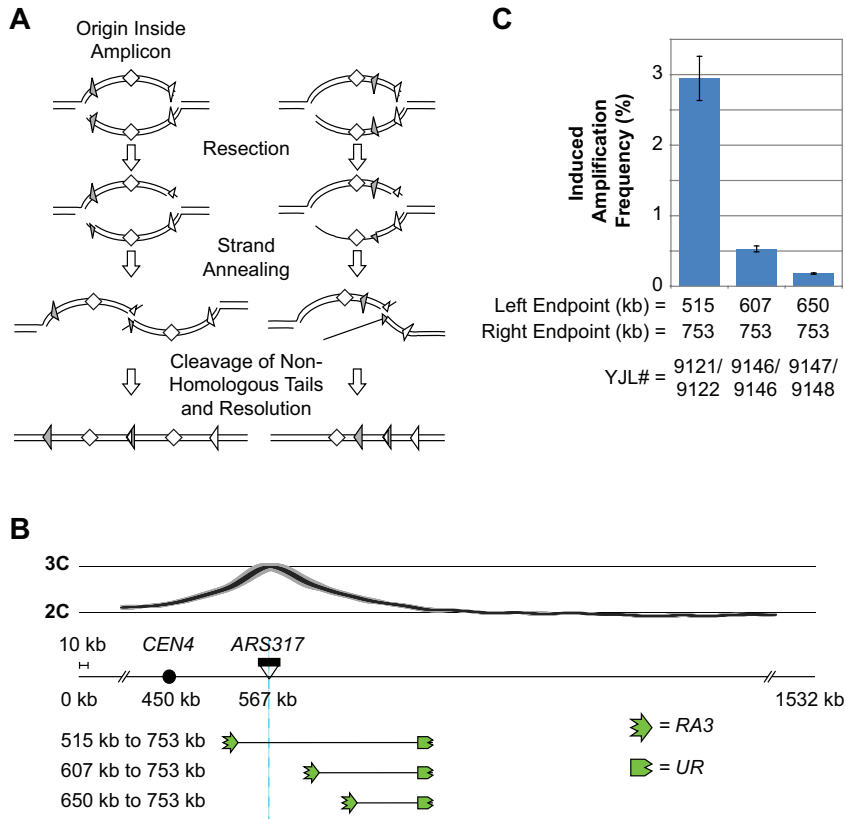


Figure 6. RRIGA proceeds most efficiently when the re-initiating origin lies within the amplicon.

A) Schematic comparing SSA models for RRIGA when the re-initiating origin is within the amplicon versus when the origin is outside. The latter case requires long range strand resection back beyond the re-initiating origin in order to expose homologous sequences for NAHR. B) Schematic showing relocation of the *RA3* element to change its position relative to the re-initiating origin (ARS317, light blue line). The re-replication profile is shown above. C) Induced amplification frequencies (mean \pm SEM, $n = 3$) for strains with the indicated amplicon boundaries. Induced amplification frequency calculated as described for Figure 5B.

Figure S1

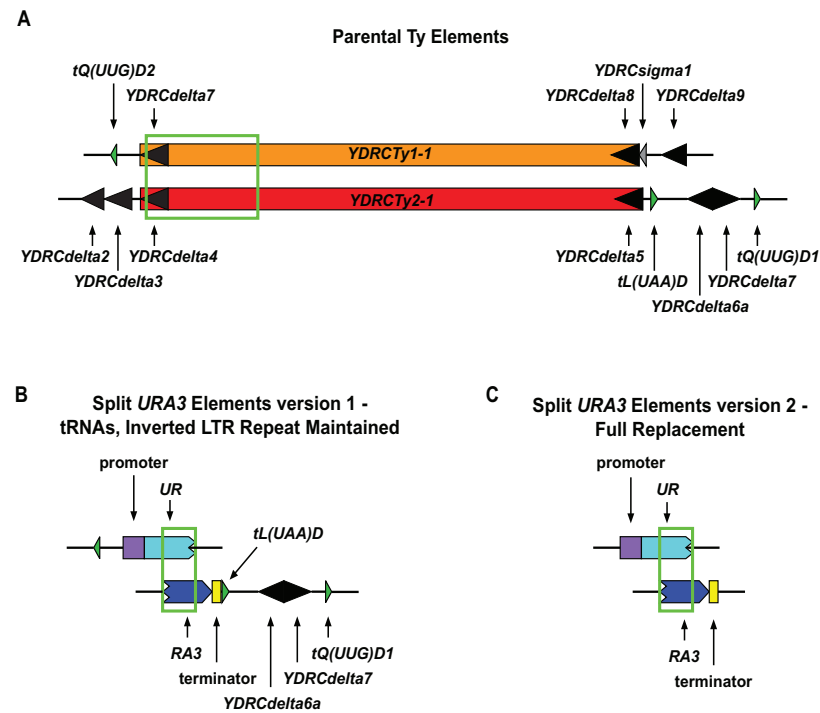


Figure S1. Detailed schematics of *YDRCTy1-1*, *YDRCTy2-1*, and *URA3* gene fragment replacements. Schematic comparing the endogenous Ty elements to two versions of the *URA3* fragment replacements. A) Zoomed in view of *YDRCTy2-1* and *YDRCTy1-1*, along with the nearby LTRs and tRNA genes. The 1.3 kb region of 99% sequence identity shared by the two Ty elements is boxed in green. B) Zoomed in view of Version 1 of the *URA3* fragment replacements. The core Ty elements and some of the LTRs are replaced, but the tRNA genes and an inverted LTR repeat are undisturbed. The 390 bp of overlapping sequence identity is boxed in green. C) Zoomed in view of Version 2 of the *URA3* fragment replacements. All of the tRNA genes and LTRs shown in (A) are deleted by these *URA3* fragment replacements. The 390 bp of overlapping sequence identity is boxed in green.

Figure S2

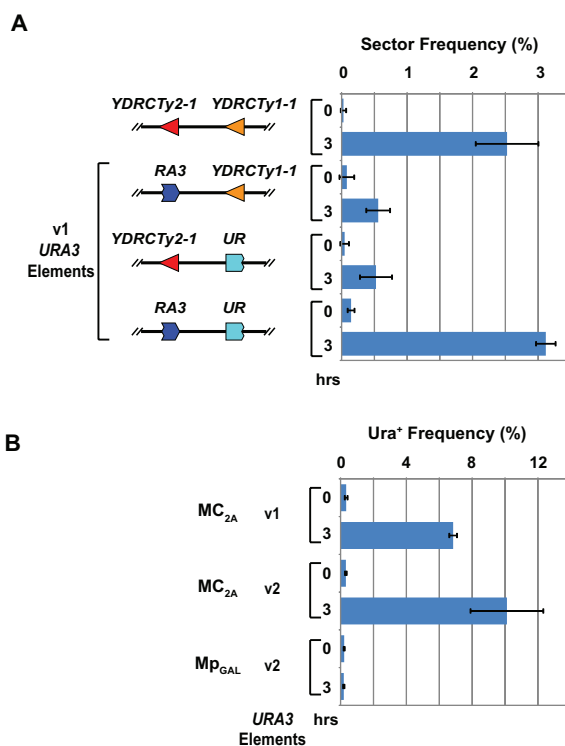


Figure S2. RRIGA requires homology in *cis* and is not enhanced by the presence of inverted LTR repeats or tRNA genes. A) Sectoring frequencies for strains with the endogenous Ty elements at 515 kb and 650 kb (YJL8100), with *YDRCTy2-1* replaced by *RA3* (YJL8104), with *YDRCTy1-1* replaced by *UR* (YJL8108), or both Ty elements replaced (YJL8112). The *URA3* gene fragment replacements used here are Version 1 (see Figure S1). The sectoring frequencies before (0 hr) and after (3 hr) induction of re-replication are shown. Data are presented as the average \pm SD of 2-5 trials for each strain. B) Comparison of amplification frequencies for the Version 1 (YJL8112/8113) and Version 2 (YJL8363/8364) *URA3* fragment replacements using the uracil prototrophy selection assay. A non-re-replicating strain (Mp_{GAL} = YJL9149-9151) is also included as a control. The amplification frequencies before (0 hr) and after (3 hr) induction of re-replication are shown. Data are presented as the average \pm SD of 2-5 trials for each strain.

Figure S3

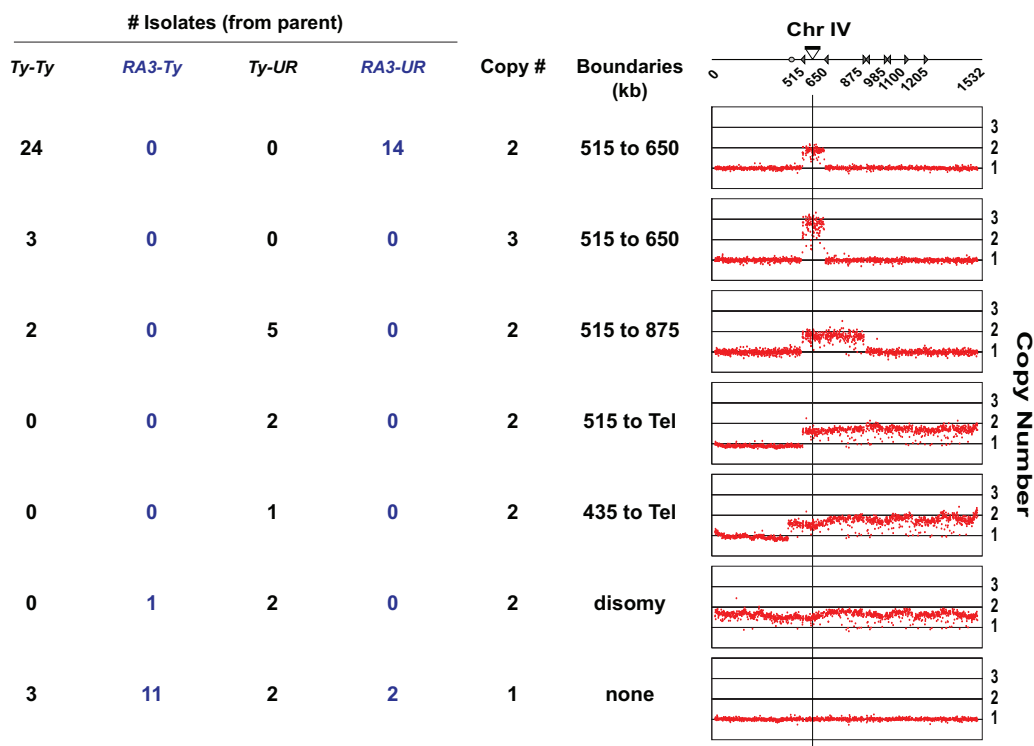


Figure S3. aCGH analysis of selected isolates from the sectoring assay. A subset of the post-induction (3 hr) isolates from the sectoring assay presented in Figure 1 were analyzed using aCGH. Representative aCGH profiles are shown with a tally of how frequently each profile was observed for each strain. *Ty-Ty* = YJL8100; *RA3-Ty* = YJL8355; *Ty-UR* = YJL8359; *RA3-UR* = YJL8363. Chromosome IV schematic shows positions of *Ty* elements (triangles, also showing orientation), centromere (circle), and *ARS317-ade3-2p* re-initiation cassette (bar and vertical line).

Figure S4

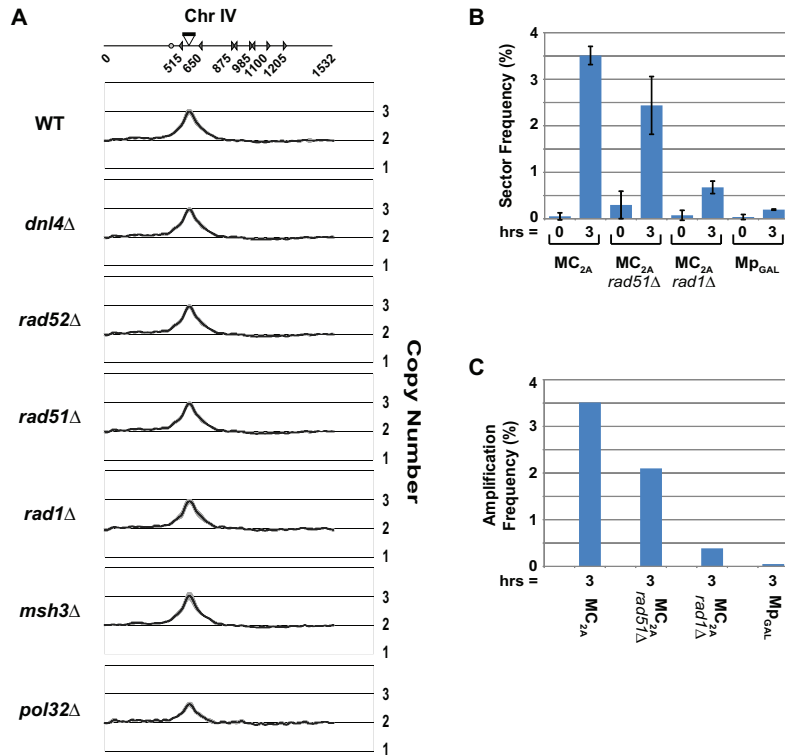


Figure S4. RRIGA is primarily mediated by single-stranded annealing (SSA). A) Re-replication profiles for strains with mutations in recombination factors. WT = YJL8363/8364; *dnl4*Δ = YJL8407/8408; *rad52*Δ = YJL8409/8410; *rad51*Δ = YJL8412/8413; *rad51*Δ = YJL8415/8416; *msh3*Δ = YJL8418/8419; *pol32*Δ = YJL8421/8422. Re-replication from a 3 hour induction was determined using aCGH for each strain. The black line shows the average from 3 independent trials (4 for wild-type). The thick gray band shows ± 1 SD. Chromosome IV schematic shows positions of Ty elements (triangles, also showing orientation), centromere (circle), and *ARS317-ade3-2p* re-initiation cassette (bar). B) Amplification frequencies for various recombination mutants as determined by the sectoring assay. MC_{2A} = YJL6558; MC_{2A} *rad51*Δ = YJL7451; MC_{2A} *rad1*Δ = YJL7445; Mp_{GAL} = YJL6974. The sectoring frequencies before (0 hr) and after (3 hr) induction of re-replication are shown. Data are presented as the average \pm SD of 2 independent trials for each strain. C) Corrected amplification frequencies for the 3 hr timepoint. A subset of sector isolates isolated after induction of re-replication for each strain (10, 36, 28, and 4, respectively) were tested by aCGH to determine whether or not there is an amplification including the reporter cassette. The average sectoring frequency was then multiplied by the fraction of aCGH tested isolates bearing an amplification.

Figure S5

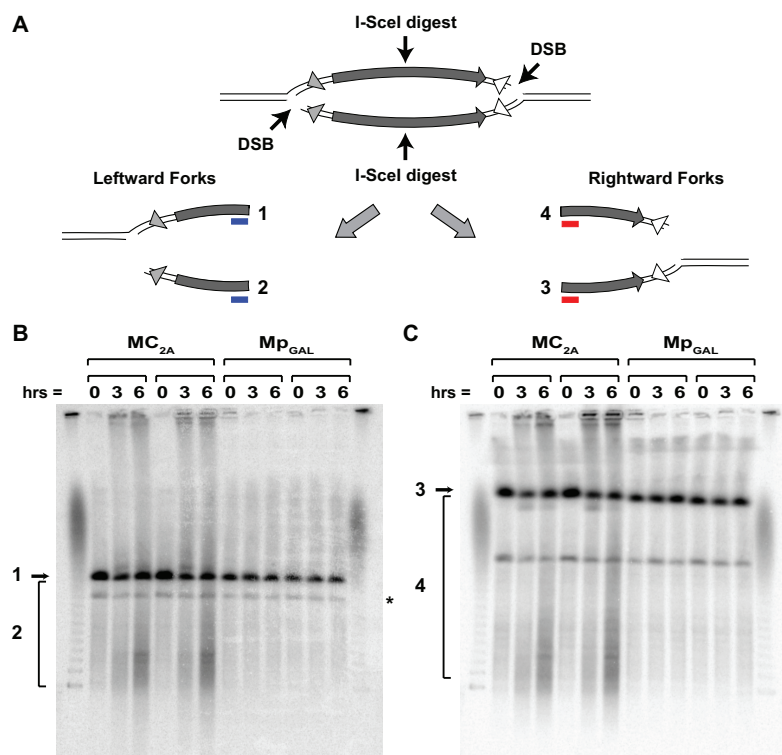


Figure S5. Re-replication induces double stranded DNA breaks distal to flanking repetitive elements on both sides of the origin. A) Following digestion with I-SceI, DSBs at each fork can be mapped by PFGE and Southern blotting using a probe that anneals to sequences to the left of the cleavage site (shown in blue) or to the right of the cleavage site (shown in red). B) Mapping DSBs at the leftward moving fork. Unbroken, full length molecules are indicated at the position labeled “1”. Molecules with DSBs that arose origin distal to *YDRCTy2-1* lie within the bracketed area labeled “2”. C) Mapping DSBs at the rightward moving fork. Unbroken, full length molecules are indicated at the position labeled “3”. Molecules with DSBs that arose origin distal to *YDRCTy1-1* lie within the bracketed area labeled “4”. For (B) and (C), two independent trials using sister isolates are shown (MC_{2A} = YJL8425 and YJL8426; Mp_{GAL} = YJL8427 and YJL8428). Breaks are evident in the re-replicating strains (MC_{2A}) induced to re-replicate, and these increase in number with increased length of induction. These breaks depend upon re-replication, as they are not observed in the non-re-replicating control strains (Mp_{GAL}). The bands indicated with an * are unexplained major species which are not dependent upon re-replication.

Figure S6

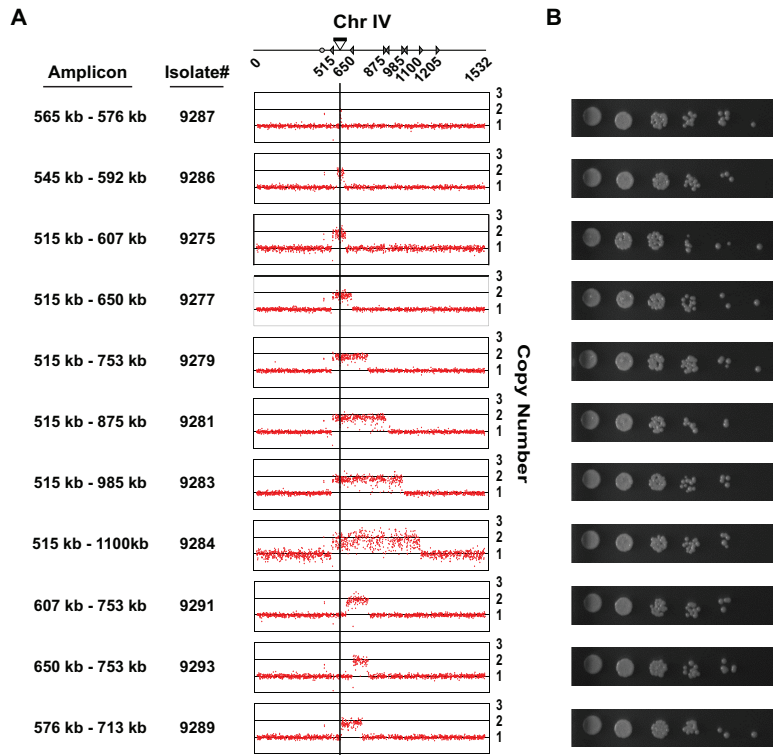


Figure S6. Decreased frequency of amplification observed for relocation of the amplicon boundaries is not caused by fitness defects. A) Uracil prototroph isolates for each combination of amplicon boundaries considered in Figure 5, Figure 6, and Figure S7 were analyzed using aCGH. Each isolate bears the expected amplification for the combination of amplicon boundaries present. B) Each isolate shown in panel (A) was tested for growth defects by a serial dilution spot test on SDC-Ura at 30°C (all on the same plate, 5-fold dilutions). All isolates grow with similar fitness.

Figure S7

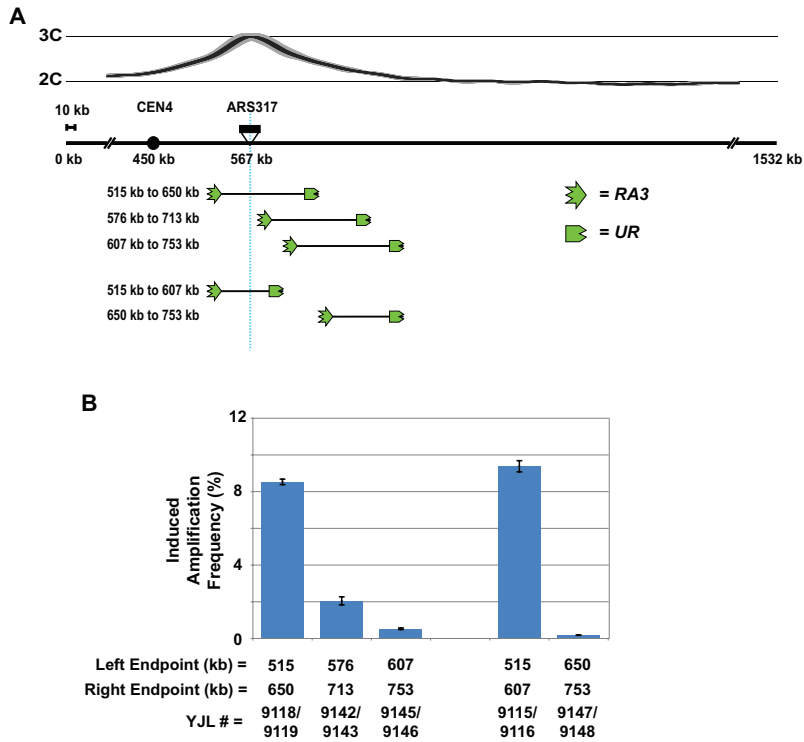


Figure S7. RRIGA proceeds most efficiently when the re-initiating origin lies within the amplicon.

A) Schematic showing relocation of the *RA3* and *UR* elements (3' and 5' portions of *URA3*, respectively) used in the *URA3* RRIGA selection assay to change their position relative to the re-initiating origin (*ARS317*, light blue line) and the distribution of re-replication forks (as inferred from the re-replication profile). The upper group of amplicons are of a similar size, comparing a case where the origin is within the amplicon to a case with the origin just outside of the amplicon to a case with the origin at a great distance from the amplicon. The lower pair of amplicons are of a similar size (slightly smaller than the amplicons in the upper group), comparing a case where the origin is within the amplicon to a case with the origin at a very great distance from the amplicon. B) Induced amplification frequencies (mean \pm SEM, n = 3) for strains with the indicated amplicon boundaries as defined by the position of the *URA3* fragments. Induced frequency is frequency after 3 hr re-replication minus frequency after 0 hr re-replication.

Table S1

Frequency of 1/2, 1/4, and 1/8 red sectored colonies observed in this work

Parent Strain	Genotype	Time	# Trials	Total Colonies Screened	Mean Sector Frequency	Standard Deviation	Standard Error of the Mean
YJL6974	<i>MCM7-2NLS pGAL YDRCTy2-1 YDRCTy1-1</i>	0 hr	2	2881	0.04%	0.05%	0.04%
YJL6974	<i>MCM7-2NLS pGAL YDRCTy2-1 YDRCTy1-1</i>	3 hr	2	7411	0.20%	0.01%	0.01%
YJL6558	<i>MCM7-2NLS pGAL-ΔntCDC6-cdk2A YDRCTy2-1 YDRCTy1-1</i>	0 hr	2	3731	0.05%	0.08%	0.05%
YJL6558	<i>MCM7-2NLS pGAL-ΔntCDC6-cdk2A YDRCTy2-1 YDRCTy1-1</i>	3 hr	2	3608	3.51%	0.20%	0.14%
YJL7445	<i>rad1Δ MCM7-2NLS pGAL-ΔntCDC6-cdk2A YDRCTy2-1 YDRCTy1-1</i>	0 hr	2	3648	0.08%	0.11%	0.08%
YJL7445	<i>rad1Δ MCM7-2NLS pGAL-ΔntCDC6-cdk2A YDRCTy2-1 YDRCTy1-1</i>	3 hr	2	5462	0.68%	0.13%	0.09%
YJL7451	<i>rad51Δ MCM7-2NLS pGAL-ΔntCDC6-cdk2A YDRCTy2-1 YDRCTy1-1</i>	0 hr	2	2888	0.30%	0.30%	0.21%
YJL7451	<i>rad51Δ MCM7-2NLS pGAL-ΔntCDC6-cdk2A YDRCTy2-1 YDRCTy1-1</i>	3 hr	2	5756	2.44%	0.62%	0.44%
YJL8100/8101	<i>MCM7-2NLS pGAL-ΔntCDC6-cdk2A YDRCTy2-1 YDRCTy1-1</i>	0 hr	5	8989	0.03%	0.04%	0.02%
YJL8100/8101	<i>MCM7-2NLS pGAL-ΔntCDC6-cdk2A YDRCTy2-1 YDRCTy1-1</i>	3 hr	5	7373	2.53%	0.48%	0.21%
YJL8104	<i>MCM7-2NLS pGAL-ΔntCDC6-cdk2A ydrcty2-1::RA3(v1) YDRCTy1-1</i>	0 hr	2	2976	0.08%	0.11%	0.08%

Table S1 (continued)

Frequency of 1/2, 1/4, and 1/8 red sectored colonies observed in this work

Parent Strain	Genotype	Time	# Trials	Total Colonies Screened	Mean Sector Frequency	Standard Deviation	Standard Error of the Mean
YJL8104	<i>MCM7-2NLS pGAL-ΔntCDC6-cdk2A ydrcty2-1::RA3(v1) YDRCTy1-1</i>	3 hr	2	6310	0.56%	0.18%	0.13%
YJL8108	<i>MCM7-2NLS pGAL-ΔntCDC6-cdk2A YDRCTy2-1 ydrcty1-1::UR(v1)</i>	0 hr	2	2834	0.05%	0.07%	0.05%
YJL8108	<i>MCM7-2NLS pGAL-ΔntCDC6-cdk2A YDRCTy2-1 ydrcty1-1::UR(v1)</i>	3 hr	2	7269	0.53%	0.24%	0.17%
YJL8112	<i>MCM7-2NLS pGAL-ΔntCDC6-cdk2A ydrcty2-1::RA3(v1) ydrcty1-1::UR(v1)</i>	0 hr	2	2961	0.14%	0.05%	0.04%
YJL8112	<i>MCM7-2NLS pGAL-ΔntCDC6-cdk2A ydrcty2-1::RA3(v1) ydrcty1-1::UR(v1)</i>	3 hr	2	2301	3.12%	0.15%	0.11%
YJL8355/ 8356	<i>MCM7-2NLS pGAL-ΔntCDC6-cdk2A ydrcty2-1::RA3(v2) YDRCTy1-1</i>	0 hr	3	6059	0.04%	0.03%	0.02%
YJL8355/ 8356	<i>MCM7-2NLS pGAL-ΔntCDC6-cdk2A ydrcty2-1::RA3(v2) YDRCTy1-1</i>	3 hr	3	12571	0.27%	0.09%	0.05%
YJL8359/ 8360	<i>MCM7-2NLS pGAL-ΔntCDC6-cdk2A YDRCTy2-1 ydrcty1-1::UR(v2)</i>	0 hr	3	5887	0.03%	0.05%	0.03%
YJL8359/ 8360	<i>MCM7-2NLS pGAL-ΔntCDC6-cdk2A YDRCTy2-1 ydrcty1-1::UR(v2)</i>	3 hr	3	13076	0.55%	0.18%	0.10%
YJL8363/ 8364	<i>MCM7-2NLS pGAL-ΔntCDC6-cdk2A ydrcty2-1::RA3(v2) ydrcty1-1::UR(v2)</i>	0 hr	4	7948	0.04%	0.03%	0.01%
YJL8363/ 8364	<i>MCM7-2NLS pGAL-ΔntCDC6-cdk2A ydrcty2-1::RA3(v2) ydrcty1-1::UR(v2)</i>	3 hr	4	6298	3.13%	0.38%	0.19%

Table S2

aCGH analysis of red-sectored colony isolates.

Parent Strain	Isolate	Timepont	Copy Number	Amplicon Boundaries (kb)	Other CGH Changes
YJL6558	YJL7860	0 hr	2	515 to 650	none
YJL6558	YJL7782	3 hr	2	515 to 650	none
YJL6558	YJL7783	3 hr	2	515 to 875	none
YJL6558	YJL7784	3 hr	2	515 to 650	none
YJL6558	YJL7785	3 hr	2	515 to 650	none
YJL6558	YJL7786	3 hr	2	515 to 650	none
YJL6558	YJL7787	3 hr	2	515 to 650	ChrIII Disomy
YJL6558	YJL7861	3 hr	2	515 to 650	none
YJL6558	YJL7862	3 hr	2	515 to 650	none
YJL6558	YJL7863	3 hr	2	515 to 650	none
YJL6558	YJL7864	3 hr	2	515 to 650	none
YJL6974	YJL7788	3 hr	1	n/a	ChrIV Disomy*
YJL6974	YJL7789	3 hr	1	n/a	none
YJL6974	YJL7900	3 hr	2	515 to 875	none*
YJL6974	YJL7901	3 hr	1	n/a	none
YJL7445	YJL7865	0 hr	1	n/a	ChrV Disomy*
YJL7445	YJL7866	0 hr	1	n/a	none
YJL7445	YJL7867	0 hr	1	n/a	none
YJL7445	YJL7790	3 hr	2	515 to 650	none
YJL7445	YJL7791	3 hr	1	n/a	ChrV Disomy
YJL7445	YJL7792	3 hr	1	n/a	none
YJL7445	YJL7793	3 hr	2	515 to 650	none
YJL7445	YJL7794	3 hr	1	n/a	none
YJL7445	YJL7795	3 hr	2	515 to 650	none
YJL7445	YJL7796	3 hr	2	515 to 650	none
YJL7445	YJL7797	3 hr	1	n/a	Segmental Duplication of ChrIII_TEL-167kb; Segmental Duplication of ChrXII_688kb-TEL

Table S2 (continued)

YJL7445	YJL7798	3 hr	1	n/a	ChrV Disomy
YJL7445	YJL7799	3 hr	2	515 to 650	Segmental Duplication of ChrIII_150-167kb
YJL7445	YJL7800	3 hr	2	515 to 650	none
YJL7445	YJL7801	3 hr	1	n/a	none
YJL7445	YJL7802	3 hr	1	n/a	ChrV Disomy
YJL7445	YJL7803	3 hr	1	n/a	ChrV Disomy
YJL7445	YJL7804	3 hr	2	515 to 650	none
YJL7445	YJL7805	3 hr	2	515 to 650	none
YJL7445	YJL7806	3 hr	2	515 to 650	none
YJL7445	YJL7807	3 hr	2	515 to 650	none
YJL7445	YJL7808	3 hr	2	515 to 650	none
YJL7445	YJL7809	3 hr	2	515 to 650	none
YJL7445	YJL7868	3 hr	2	435 to 650	none*
YJL7445	YJL7869	3 hr	2	515 to 650	none
YJL7445	YJL7870	3 hr	1	n/a	none
YJL7445	YJL7871	3 hr	2	515 to 650	none
YJL7445	YJL7872	3 hr	1	n/a	ChrV Disomy
YJL7445	YJL7873	3 hr	1	n/a	none
YJL7445	YJL7874	3 hr	2	515 to 650	none
YJL7445	YJL7875	3 hr	1	n/a	ChrV Disomy
YJL7451	YJL7876	0 hr	1	n/a	none
YJL7451	YJL7877	0 hr	1	n/a	none
YJL7451	YJL7878	0 hr	1	n/a	none
YJL7451	YJL7879	0 hr	1	n/a	none
YJL7451	YJL7880	0 hr	1	n/a	none
YJL7451	YJL7881	0 hr	1	n/a	none
YJL7451	YJL7882	0 hr	1	n/a	none

Table S2 (continued)

YJL7451	YJL7883	0 hr	1	n/a	none
YJL7451	YJL7810	3 hr	2	515 to 650	ChrIII Disomy
YJL7451	YJL7811	3 hr	2	515 to 650	none
YJL7451	YJL7812	3 hr	2	515 to 650	none
YJL7451	YJL7813	3 hr	2	515 to 650	none
YJL7451	YJL7814	3 hr	2	515 to 650	none
YJL7451	YJL7815	3 hr	1	n/a	none
YJL7451	YJL7816	3 hr	2	515 to 650	none
YJL7451	YJL7817	3 hr	2	515 to 650	none
YJL7451	YJL7818	3 hr	2	515 to 650	none
YJL7451	YJL7819	3 hr	1	n/a	none
YJL7451	YJL7820	3 hr	2	515 to 650	none
YJL7451	YJL7821	3 hr	2	515 to 650	none
YJL7451	YJL7822	3 hr	1	n/a	ChrV Disomy
YJL7451	YJL7823	3 hr	2	515 to 875	none
YJL7451	YJL7824	3 hr	2	515 to 650	none
YJL7451	YJL7825	3 hr	2	515 to 875	none
YJL7451	YJL7826	3 hr	2	515 to 650	none
YJL7451	YJL7827	3 hr	2	515 to 650	none
YJL7451	YJL7828	3 hr	1	n/a	none
YJL7451	YJL7829	3 hr	2	515 to 650	none
YJL7451	YJL7884	3 hr	2	515 to 650	none
YJL7451	YJL7885	3 hr	2	515 to 650	none
YJL7451	YJL7886	3 hr	1	n/a	none
YJL7451	YJL7887	3 hr	2	515 to 650	none
YJL7451	YJL7888	3 hr	1	n/a	none
YJL7451	YJL7889	3 hr	2	515 to 875	none*

Table S2 (continued)

YJL7451	YJL7890	3 hr	2	515 to 650	none
YJL7451	YJL7891	3 hr	2	515 to 650	none
YJL7451	YJL7892	3 hr	2	515 to 650	none*
YJL7451	YJL7893	3 hr	2	515 to 650	none
YJL7451	YJL7894	3 hr	2	515 to 650	none
YJL7451	YJL7895	3 hr	2	515 to 650	Segmental Duplication of ChrIII_150-167kb*
YJL7451	YJL7896	3 hr	2	515 to 650	none
YJL7451	YJL7897	3 hr	2	515 to 875	none
YJL7451	YJL7898	3 hr	2	515 to 650	none
YJL7451	YJL7899	3 hr	2	515 to 650	none
YJL8100	YJL8283	0 hr	1	n/a	ChrV Disomy
YJL8100	YJL9482	0 hr	1	n/a	ChrV Disomy
YJL8100	YJL8128	3 hr	3	515 to 650	none
YJL8100	YJL8129	3 hr	3	515 to 650	none
YJL8100	YJL8130	3 hr	2	515 to 650	none
YJL8100	YJL8131	3 hr	2	515 to 650	none
YJL8100	YJL8132	3 hr	1	n/a	Segmental Duplication of ChrV_289-443kb
YJL8100	YJL8133	3 hr	2	515 to 650	none
YJL8100	YJL8134	3 hr	2	515 to 650	none
YJL8100	YJL8135	3 hr	2	515 to 875	none
YJL8100	YJL8136	3 hr	2	515 to 650	none
YJL8100	YJL8137	3 hr	3	515 to 650	none
YJL8100	YJL8138	3 hr	2	515 to 650	none
YJL8100	YJL8139	3 hr	2	515 to 650	none
YJL8100	YJL8287	3 hr	2	515 to 650	none
YJL8100	YJL8288	3 hr	2	515 to 650	none
YJL8100	YJL8289	3 hr	2	515 to 650	none*

Table S2 (continued)

YJL8100	YJL8290	3 hr	1	n/a	none
YJL8100	YJL8291	3 hr	3	515 to 650	none
YJL8100	YJL8292	3 hr	2	515 to 650	none
YJL8100	YJL8293	3 hr	2	515 to 650	none
YJL8100	YJL8294	3 hr	2	515 to 650	none
YJL8100	YJL9483	3 hr	2	515 to 650	none
YJL8100	YJL9484	3 hr	2	515 to 650	none
YJL8100	YJL9485	3 hr	2	515 to 650	none
YJL8100	YJL9486	3 hr	2	515 to 650	none
YJL8100	YJL9487	3 hr	2	515 to 650	none
YJL8100	YJL9488	3 hr	2	515 to 650	none
YJL8100	YJL9489	3 hr	2	515 to 650	none
YJL8100	YJL9490	3 hr	1	n/a	ChrXIII Disomy
YJL8100	YJL9491	3 hr	2	515 to 875	none
YJL8100	YJL9492	3 hr	2	515 to 650	none
YJL8100	YJL9493	3 hr	2	515 to 650	none
YJL8100	YJL9494	3 hr	2	515 to 650	none
YJL8104	YJL8140	0 hr	1	n/a	ChrXIII Disomy
YJL8104	YJL8141	0 hr	1	n/a	ChrII Disomy
YJL8104	YJL8142	0 hr	1	n/a	ChrII Disomy
YJL8104	YJL8143	3 hr	1	n/a	ChrXIII Disomy
YJL8104	YJL8144	3 hr	1	n/a	ChrIV Disomy
YJL8104	YJL8145	3 hr	2	515 to 875	none
YJL8104	YJL8146	3 hr	1	n/a	Segmental Duplication of ChrXIII_379-838kb
YJL8104	YJL8147	3 hr	1	n/a	ChrV Disomy
YJL8104	YJL8148	3 hr	2	435 to 650	none
YJL8104	YJL8149	3 hr	2	515 to 650	none

Table S2 (continued)

YJL8104	YJL8150	3 hr	2	515 to 875	none
YJL8104	YJL8151	3 hr	1	n/a	ChrXIII Disomy
YJL8104	YJL8152	3 hr	2	515 to 875	none
YJL8104	YJL8153	3 hr	2	567 to 875	none
YJL8104	YJL8154	3 hr	2	515 to 875	none
YJL8104	YJL8155	3 hr	2	515 to 805	none
YJL8104	YJL8156	3 hr	2	515 to 805	none
YJL8104	YJL8295	3 hr	1	n/a	none
YJL8104	YJL8296	3 hr	1	n/a	ChrXIII Disomy
YJL8104	YJL8297	3 hr	3	515 to 805	none
YJL8104	YJL8298	3 hr	1	n/a	ChrI Monosomy*
YJL8104	YJL8299	3 hr	1	n/a	ChrXIII Disomy*
YJL8104	YJL8300	3 hr	1	n/a	Segmental Duplication of ChrIV_650-875kb; Segmental Duplication of ChrXII_688-980kb
YJL8104	YJL8301	3 hr	1	n/a	none
YJL8104	YJL8302	3 hr	2	515 to TEL	Segmental Duplication of ChrX_TEL-537kb
YJL8104	YJL8303	3 hr	2	515 to 805	none
YJL8104	YJL8304	3 hr	1	n/a	ChrV Disomy
YJL8104	YJL8305	3 hr	1	n/a	ChrIII Disomy*
YJL8104	YJL8306	3 hr	1	n/a	Segmental Duplication of ChrII_TEL-260kb; Segmental Duplication of ChrXII_688kb-TEL
YJL8104	YJL8307	3 hr	1	n/a	ChrXIII Disomy
YJL8104	YJL8308	3 hr	3	515 to 985	none
YJL8108	YJL8284	0 hr	1	n/a	none
YJL8108	YJL8157	3 hr	1	n/a	ChrXIII Disomy
YJL8108	YJL8158	3 hr	1	n/a	none
YJL8108	YJL8159	3 hr	1	n/a	ChrXIII Disomy
YJL8108	YJL8160	3 hr	1	n/a	none
YJL8108	YJL8161	3 hr	2	515 to 805	none

Table S2 (continued)

YJL8108	YJL8162	3 hr	1	n/a	Segmental Duplication of ChrXIII_379-838kb
YJL8108	YJL8163	3 hr	2	515 to TEL	Segmental Duplication of ChrVI_144kb-TEL
YJL8108	YJL8164	3 hr	2	515 to 875	none
YJL8108	YJL8165	3 hr	2	515 to 805	none
YJL8108	YJL8166	3 hr	2	515 to 805	none
YJL8108	YJL8167	3 hr	3	515 to 650	none
YJL8108	YJL8168	3 hr	1	n/a	Segmental Duplication of ChrXII_TEL-221kb; Segmental Duplication of ChrXIII_379kb-TEL
YJL8108	YJL8169	3 hr	1	n/a	none
YJL8108	YJL8170	3 hr	2	515 to 875	none
YJL8108	YJL8309	3 hr	2	515 to 875	none
YJL8108	YJL8310	3 hr	2	515 to 805	none
YJL8108	YJL8311	3 hr	1	n/a	ChrIII Trisomy; ChrXVI Disomy
YJL8108	YJL8312	3 hr	2	515 to 875	none
YJL8108	YJL8313	3 hr	1	n/a	ChrI Monosomy*
YJL8108	YJL8314	3 hr	2	515 to 805	none
YJL8108	YJL8315	3 hr	2	515 to 805	none
YJL8108	YJL8316	3 hr	1	n/a	none
YJL8108	YJL8317	3 hr	1	n/a	ChrV Disomy
YJL8108	YJL8318	3 hr	2	515 to 875	none
YJL8108	YJL8319	3 hr	2	515 to 875	none
YJL8108	YJL8320	3 hr	2	515 to 875	none
YJL8108	YJL8321	3 hr	2	515 to 875	none
YJL8108	YJL8322	3 hr	2	515 to 805	none
YJL8112	YJL8171	0 hr	1	n/a	ChrII Disomy
YJL8112	YJL8172	0 hr	1	n/a	ChrIII Disomy
YJL8112	YJL8285	0 hr	1	n/a	ChrII Disomy
YJL8112	YJL8286	0 hr	1	n/a	ChrII Disomy

Table S2 (continued)

YJL8112	YJL8173	3 hr	2	515 to 650	none
YJL8112	YJL8174	3 hr	2	515 to 650	none
YJL8112	YJL8175	3 hr	2	515 to 650	none
YJL8112	YJL8176	3 hr	2	515 to 650	none
YJL8112	YJL8177	3 hr	2	515 to 650	none
YJL8112	YJL8178	3 hr	2	515 to 650	none
YJL8112	YJL8179	3 hr	2	515 to 650	none
YJL8112	YJL8180	3 hr	2	515 to 650	none
YJL8112	YJL8181	3 hr	2	515 to 650	none
YJL8112	YJL8182	3 hr	1	n/a	Segmental Duplication of ChrXIII_769-838kb
YJL8112	YJL8183	3 hr	1	n/a	none
YJL8112	YJL8184	3 hr	2	515 to 650	none
YJL8112	YJL8323	3 hr	2	515 to 650	none
YJL8112	YJL8324	3 hr	2	515 to 650	none
YJL8112	YJL8325	3 hr	1	n/a	none
YJL8112	YJL8326	3 hr	2	515 to 650	none
YJL8112	YJL8327	3 hr	2	515 to 650	none
YJL8112	YJL8328	3 hr	2	515 to 650	none
YJL8112	YJL8329	3 hr	3	515 to 650	none
YJL8112	YJL8330	3 hr	2	515 to 650	none
YJL8355	YJL9495	0 hr	1	n/a	ChrII Disomy
YJL8355	YJL9496	0 hr	1	n/a	none
YJL8355	YJL9497	3 hr	1	n/a	ChrXIV Monosomy*
YJL8355	YJL9498	3 hr	1	n/a	none
YJL8355	YJL9499	3 hr	1	n/a	none
YJL8355	YJL9500	3 hr	1	n/a	ChrV Disomy
YJL8355	YJL9501	3 hr	1	n/a	ChrIII Disomy

Table S2 (continued)

YJL8355	YJL9502	3 hr	1	n/a	Segmental Duplication of ChrIII_TEL-75kb; Segmental Duplication of ChrIX_325kb-TEL
YJL8355	YJL9503	3 hr	1	n/a	none
YJL8355	YJL9504	3 hr	1	n/a	ChrIII Disomy
YJL8355	YJL9505	3 hr	1	n/a	ChrV Disomy
YJL8355	YJL9506	3 hr	1	n/a	none
YJL8355	YJL9507	3 hr	1	n/a	ChrIV Disomy
YJL8355	YJL9508	3 hr	1	n/a	Segmental Triplication of ChrXII_534-656kb; Segmental Duplication of ChrXII_656-688kb
YJL8359	YJL9509	0 hr	1	n/a	none
YJL8359	YJL9518	0 hr	1	n/a	ChrV Disomy
YJL8359	YJL9519	0 hr	1	n/a	none
YJL8359	YJL9510	3 hr	3	515 to 875	none
YJL8359	YJL9511	3 hr	1	n/a	ChrV Disomy
YJL8359	YJL9512	3 hr	2	515 to TEL	Segmental Duplication of ChrIII_TEL-150kb
YJL8359	YJL9513	3 hr	2	515 to 875	none
YJL8359	YJL9514	3 hr	2	515 to 875	none
YJL8359	YJL9515	3 hr	2	515 to 875	none
YJL8359	YJL9516	3 hr	1	n/a	ChrII Disomy
YJL8359	YJL9517	3 hr	2	515 to 875	none
YJL8359	YJL9520	3 hr	2	515 to TEL	Segmental Duplication of ChrX_TEL-540kb
YJL8359	YJL9521	3 hr	1	n/a	ChrIV Disomy
YJL8359	YJL9522	3 hr	1	n/a	ChrIV Disomy
YJL8359	YJL9523	3 hr	2	435 to TEL	Segmental Duplication of ChrVII_TEL-110kb
YJL8363	YJL9524	0 hr	1	n/a	ChrXIII Disomy
YJL8363	YJL9525	0 hr	1	n/a	ChrIV Disomy
YJL8363	YJL9538	0 hr	2	515 to 650	none
YJL8363	YJL9526	3 hr	2	515 to 650	none
YJL8363	YJL9527	3 hr	2	515 to 650	none

Table S2 (continued)

YJL8363	YJL9528	3 hr	2	515 to 650	none
YJL8363	YJL9529	3 hr	2	515 to 650	none
YJL8363	YJL9530	3 hr	2	515 to 650	none
YJL8363	YJL9531	3 hr	2	515 to 650	none
YJL8363	YJL9532	3 hr	2	515 to 650	Chr II Disomy
YJL8363	YJL9533	3 hr	1	n/a	none
YJL8363	YJL9534	3 hr	1	n/a	ChrII Disomy
YJL8363	YJL9535	3 hr	2	515 to 650	none
YJL8363	YJL9536	3 hr	2	515 to 650	none
YJL8363	YJL9537	3 hr	2	515 to 650	none
YJL8363	YJL9539	3 hr	2	515 to 650	none
YJL8363	YJL9540	3 hr	2	515 to 650	none
YJL8363	YJL9541	3 hr	2	515 to 650	none
YJL8363	YJL9542	3 hr	2	515 to 650	none

* - aCGH suggests possible spontaneous diploid or mixed population. This is indicated either by the points in amplified region scattering at a non-quantile value (ie. 1.5) or by the points of an aneuploid chromosome scattering at a non-quantile value. aCGH will not be able to suggest possibly diploidization in cases of amplicons with quantile values or where there are no aneuploidies.

Table S3

Frequency of uracil prototrophs from the selection assay observed in this work.

Parent Strain	Genotype	Time	# Trials	Total cfu Tested	Mean Ura ⁺ Frequency	Standard Deviation	Standard Error of the Mean
YJL8112/8113	MCM7-2NLS pGAL- Δ ntCDC6-cdk2A ydrcty2-1::RA3(v1) ydrcty1-1::UR(v1)	0 hr	2	53750	0.34%	0.08%	0.06%
YJL8112/8113	MCM7-2NLS pGAL- Δ ntCDC6-cdk2A ydrcty2-1::RA3(v1) ydrcty1-1::UR(v1)	3 hr	2	35500	6.85%	0.23%	0.17%
YJL8363/8364	MCM7-2NLS pGAL- Δ ntCDC6-cdk2A ydrcty2-1::RA3(v2) ydrcty1-1::UR(v2)	0 hr	5	109850	0.32%	0.05%	0.02%
YJL8363/8364	MCM7-2NLS pGAL- Δ ntCDC6-cdk2A ydrcty2-1::RA3(v2) ydrcty1-1::UR(v2)	3 hr	5	91000	10.12%	2.21%	0.99%
YJL9149-9151	MCM7-2NLS pGAL ydrcty2-1::RA3(v2) ydrcty1-1::UR(v2)	0 hr	3	48150	0.22%	0.03%	0.02%
YJL9149-9151	MCM7-2NLS pGAL ydrcty2-1::RA3(v2) ydrcty1-1::UR(v2)	3 hr	3	64950	0.20%	0.04%	0.02%
YJL8407/8408	dnl4 Δ MCM7-2NLS pGAL- Δ ntCDC6-cdk2A ydrcty2-1::RA3(v2) ydrcty1-1::UR(v2)	0 hr	2	42650	0.17%	0.01%	0.01%
YJL8407/8408	dnl4 Δ MCM7-2NLS pGAL- Δ ntCDC6-cdk2A ydrcty2-1::RA3(v2) ydrcty1-1::UR(v2)	3 hr	2	25800	10.13%	1.16%	0.82%
YJL8409/8410	rad52 Δ MCM7-2NLS pGAL- Δ ntCDC6-cdk2A ydrcty2-1::RA3(v2) ydrcty1-1::UR(v2)	0 hr	2	34850	0.00%	0.00%	0.00%
YJL8409/8410	rad52 Δ MCM7-2NLS pGAL- Δ ntCDC6-cdk2A ydrcty2-1::RA3(v2) ydrcty1-1::UR(v2)	3 hr	2	12050	0.04%	0.02%	0.02%

Table S3 (continued)

Frequency of uracil prototrophs from the selection assay observed in this work

Parent Strain	Genotype	Time	# Trials	Total cfu Tested	Mean Ura ⁺ Frequency	Standard Deviation	Standard Error of the Mean
YJL8412/ 8413	<i>rad51Δ MCM7-2NLS pGAL-ΔntCDC6-cdk2A ydrcty2-1::RA3(v2) ydrcty1-1::UR(v2)</i>	0 hr	2	35150	0.15%	0.05%	0.04%
YJL8412/ 8413	<i>rad51Δ MCM7-2NLS pGAL-ΔntCDC6-cdk2A ydrcty2-1::RA3(v2) ydrcty1-1::UR(v2)</i>	3 hr	2	25000	8.42%	0.15%	0.11%
YJL8415/ 8416	<i>rad1Δ MCM7-2NLS pGAL-ΔntCDC6-cdk2A ydrcty2-1::RA3(v2) ydrcty1-1::UR(v2)</i>	0 hr	2	29100	0.00%	0.00%	0.00%
YJL8415/ 8416	<i>rad1Δ MCM7-2NLS pGAL-ΔntCDC6-cdk2A ydrcty2-1::RA3(v2) ydrcty1-1::UR(v2)</i>	3 hr	2	11550	0.41%	0.03%	0.02%
YJL8418/ 8419	<i>msh3Δ MCM7-2NLS pGAL-ΔntCDC6-cdk2A ydrcty2-1::RA3(v2) ydrcty1-1::UR(v2)</i>	0 hr	2	30900	0.01%	0.00%	0.00%
YJL8418/ 8419	<i>msh3Δ MCM7-2NLS pGAL-ΔntCDC6-cdk2A ydrcty2-1::RA3(v2) ydrcty1-1::UR(v2)</i>	3 hr	2	12450	1.19%	0.16%	0.11%
YJL8421/ 8422	<i>pol32Δ MCM7-2NLS pGAL-ΔntCDC6-cdk2A ydrcty2-1::RA3(v2) ydrcty1-1::UR(v2)</i>	0 hr	2	20100	0.04%	0.01%	0.01%
YJL8421/ 8422	<i>pol32Δ MCM7-2NLS pGAL-ΔntCDC6-cdk2A ydrcty2-1::RA3(v2) ydrcty1-1::UR(v2)</i>	3 hr	2	8850	4.82%	0.03%	0.02%
YJL9115/ 9116	<i>MCM7-2NLS pGAL-ΔntCDC6-cdk2A ydrcty2-1Δ ydrcty1-1Δ ChrIV_515kb::RA3 ChrIV_607kb::UR</i>	0 hr	3	46950	0.48%	0.10%	0.06%
YJL9115/ 9116	<i>MCM7-2NLS pGAL-ΔntCDC6-cdk2A ydrcty2-1Δ ydrcty1-1Δ ChrIV_515kb::RA3 ChrIV_607kb::UR</i>	3 hr	3	42750	9.86%	0.51%	0.29%

Table S3 (continued)

Frequency of uracil prototrophs from the selection assay observed in this work

Parent Strain	Genotype	Time	# Trials	Total cfu Tested	Mean Ura ⁺ Frequency	Standard Deviation	Standard Error of the Mean
YJL9118/ 9119	MCM7-2NLS pGAL- Δ ntCDC6-cdk2A ydrcty2-1 Δ ydrcty1-1 Δ ChrIV_515kb::RA3 ChrIV_650kb::UR	0 hr	3	49500	0.25%	0.01%	0.00%
YJL9118/ 9119	MCM7-2NLS pGAL- Δ ntCDC6-cdk2A ydrcty2-1 Δ ydrcty1-1 Δ ChrIV_515kb::RA3 ChrIV_650kb::UR	3 hr	3	45300	8.78%	0.26%	0.15%
YJL9121/ 9122	MCM7-2NLS pGAL- Δ ntCDC6-cdk2A ydrcty2-1 Δ ydrcty1-1 Δ ChrIV_515kb::RA3 ChrIV_753kb::UR	0 hr	3	49350	0.12%	0.01%	0.01%
YJL9121/ 9122	MCM7-2NLS pGAL- Δ ntCDC6-cdk2A ydrcty2-1 Δ ydrcty1-1 Δ ChrIV_515kb::RA3 ChrIV_753kb::UR	3 hr	3	42450	3.06%	0.55%	0.32%
YJL9127/ 9128	MCM7-2NLS pGAL- Δ ntCDC6-cdk2A ydrcty2-1 Δ ydrcty1-1 Δ ChrIV_515kb::RA3 ChrIV_875kb::UR	0 hr	3	50100	0.05%	0.02%	0.01%
YJL9127/ 9128	MCM7-2NLS pGAL- Δ ntCDC6-cdk2A ydrcty2-1 Δ ydrcty1-1 Δ ChrIV_515kb::RA3 ChrIV_875kb::UR	3 hr	3	43200	1.15%	0.12%	0.07%
YJL9130/ 9131	MCM7-2NLS pGAL- Δ ntCDC6-cdk2A ydrcty2-1 Δ ydrcty1-1 Δ ChrIV_515kb::RA3 ChrIV_985kb::UR	0 hr	3	50550	0.01%	0.01%	0.01%
YJL9130/ 9131	MCM7-2NLS pGAL- Δ ntCDC6-cdk2A ydrcty2-1 Δ ydrcty1-1 Δ ChrIV_515kb::RA3 ChrIV_985kb::UR	3 hr	3	38400	0.15%	0.05%	0.03%
YJL9133/ 9134	MCM7-2NLS pGAL- Δ ntCDC6-cdk2A ydrcty2-1 Δ ydrcty1-1 Δ ChrIV_515kb::RA3 ChrIV_1100kb::UR	0 hr	3	49500	0.00%	0.01%	0.00%
YJL9133/ 9134	MCM7-2NLS pGAL- Δ ntCDC6-cdk2A ydrcty2-1 Δ ydrcty1-1 Δ ChrIV_515kb::RA3 ChrIV_1100kb::UR	3 hr	3	40650	0.08%	0.03%	0.01%

Table S3 (continued)

Frequency of uracil prototrophs from the selection assay observed in this work

Parent Strain	Genotype	Time	# Trials	Total cfu Tested	Mean Ura ⁺ Frequency	Standard Deviation	Standard Error of the Mean
YJL9136/ 9137	MCM7-2NLS pGAL-ΔntCDC6-cdk2A ydrcty2-1Δ ydrcty1-1Δ ChrIV_545kb::RA3 ChrIV_592kb::UR	0 hr	3	46950	0.79%	0.22%	0.12%
YJL9136/ 9137	MCM7-2NLS pGAL-ΔntCDC6-cdk2A ydrcty2-1Δ ydrcty1-1Δ ChrIV_545kb::RA3 ChrIV_592kb::UR	3 hr	3	44100	13.29%	0.40%	0.23%
YJL9139/ 9140	MCM7-2NLS pGAL-ΔntCDC6-cdk2A ydrcty2-1Δ ydrcty1-1Δ ChrIV_565kb::RA3 ChrIV_576kb::UR	0 hr	3	46800	0.44%	0.10%	0.06%
YJL9139/ 9140	MCM7-2NLS pGAL-ΔntCDC6-cdk2A ydrcty2-1Δ ydrcty1-1Δ ChrIV_565kb::RA3 ChrIV_576kb::UR	3 hr	3	43500	11.47%	1.32%	0.76%
YJL9142/ 9143	MCM7-2NLS pGAL-ΔntCDC6-cdk2A ydrcty2-1Δ ydrcty1-1Δ ChrIV_576kb::RA3 ChrIV_713kb::UR	0 hr	3	50850	0.04%	0.01%	0.00%
YJL9142/ 9143	MCM7-2NLS pGAL-ΔntCDC6-cdk2A ydrcty2-1Δ ydrcty1-1Δ ChrIV_576kb::RA3 ChrIV_713kb::UR	3 hr	3	38850	2.09%	0.37%	0.22%
YJL9145/ 9146	MCM7-2NLS pGAL-ΔntCDC6-cdk2A ydrcty2-1Δ ydrcty1-1Δ ChrIV_607kb::RA3 ChrIV_753kb::UR	0 hr	3	50100	0.02%	0.01%	0.01%
YJL9145/ 9146	MCM7-2NLS pGAL-ΔntCDC6-cdk2A ydrcty2-1Δ ydrcty1-1Δ ChrIV_607kb::RA3 ChrIV_753kb::UR	3 hr	3	42300	0.55%	0.08%	0.05%
YJL9147/ 9148	MCM7-2NLS pGAL-ΔntCDC6-cdk2A ydrcty2-1Δ ydrcty1-1Δ ChrIV_650kb::RA3 ChrIV_753kb::UR	0 hr	3	46050	0.05%	0.04%	0.02%
YJL9147/ 9148	MCM7-2NLS pGAL-ΔntCDC6-cdk2A ydrcty2-1Δ ydrcty1-1Δ ChrIV_650kb::RA3 ChrIV_753kb::UR	3 hr	3	41550	0.23%	0.04%	0.02%

Table S4

aCGH analysis of uracil prototroph isolates.

Parent Strain	Isolate	Timepont	Copy Number	Amplicon Boundaries (kb)	Other CGH Changes
YJL8112	YJL8431	0 hr	2	515 to 650	none
YJL8112	YJL8432	0 hr	2	515 to 650	ChrV Disomy*
YJL8112	YJL8433	0 hr	2	515 to 650	none
YJL8113	YJL8434	0 hr	2	515 to 650	none
YJL8113	YJL8435	0 hr	3	515 to 650	none
YJL8113	YJL8436	0 hr	2	515 to 650	ChrII Disomy; ChrVII Disomy
YJL8363	YJL8437	0 hr	2	515 to 650	none
YJL8363	YJL8438	0 hr	2	515 to 650	none
YJL8363	YJL8439	0 hr	2	515 to 650	none
YJL8364	YJL8440	0 hr	2	515 to 650	none
YJL8364	YJL8441	0 hr	2	515 to 650	none
YJL8364	YJL8442	0 hr	2	515 to 650	none
YJL8112	YJL8443	3 hr	2	515 to 650	none
YJL8112	YJL8444	3 hr	2	515 to 650	none
YJL8112	YJL8445	3 hr	2	515 to 650	ChrX Disomy
YJL8112	YJL8446	3 hr	3	515 to 650	none
YJL8112	YJL8447	3 hr	2	515 to 650	none
YJL8112	YJL8448	3 hr	3	515 to 650	none
YJL8112	YJL8449	3 hr	2	515 to 650	none
YJL8112	YJL8450	3 hr	2	515 to 650	none
YJL8113	YJL8451	3 hr	2	515 to 650	none
YJL8113	YJL8452	3 hr	2	515 to 650	none
YJL8113	YJL8453	3 hr	2	515 to 650	none
YJL8113	YJL8454	3 hr	2‡	515 to 650	ChrI Disomy; ChrIX Disomy; ChrXIII Disomy(?)*
YJL8113	YJL8455	3 hr	2	515 to 650	none
YJL8113	YJL8456	3 hr	2	515 to 650	none

Table S4 (continued)

aCGH analysis of uracil prototroph isolates.

YJL8113	YJL8457	3 hr	2‡	515 to 650	ChrXVI Disomy*
YJL8113	YJL8458	3 hr	2	515 to 650	none
YJL8363	YJL8459	3 hr	2	515 to 650	none
YJL8363	YJL8460	3 hr	2	515 to 650	none
YJL8363	YJL8461	3 hr	1.5†	515 to 650	Segmental Duplication of ChrIII_TEL-167kb; Segmental Duplication of ChrVII_541-820kb*
YJL8363	YJL8462	3 hr	1.5†	515 to 650	ChrXV Disomy*
YJL8363	YJL8463	3 hr	2	515 to 650	none
YJL8363	YJL8464	3 hr	2	515 to 650	none
YJL8363	YJL8465	3 hr	2	515 to 650	none
YJL8363	YJL8466	3 hr	2‡	515 to 650	Segmental Duplication(?) of ChrIV_TEL-515kb; Segmental Duplication(?) of ChrIV_650-875kb; Segmental Duplication(?) of ChrIV_985kb-TEL; Segmental Duplication(?) of ChrXII_947kb-TEL; Segmental Duplication(?) of ChrXIII_TEL-363 kb*
YJL8364	YJL8467	3 hr	2	515 to 650	none
YJL8364	YJL8468	3 hr	2	515 to 650	none
YJL8364	YJL8469	3 hr	1.5†	515 to 650	none*
YJL8364	YJL8470	3 hr	1.5†	515 to 650	ChrIV Disomy; ChrXIII Disomy*
YJL8364	YJL8471	3 hr	2	515 to 650	none
YJL8364	YJL8472	3 hr	2	515 to 650	none
YJL8364	YJL8473	3 hr	2	515 to 650	none
YJL8364	YJL8474	3 hr	2	515 to 650	none
YJL9139	YJL9287	3 hr	2	565 to 576	none
YJL9136	YJL9286	3 hr	2	545 to 592	none
YJL9115	YJL9275	3 hr	2	515 to 607	none
YJL9118	YJL9277	3 hr	2	515 to 650	none
YJL9121	YJL9279	3 hr	2	515 to 753	none
YJL9127	YJL9281	3 hr	2	515 to 875	none
YJL9130	YJL9283	3 hr	2	515 to 985	none

Table S4 (continued)

aCGH analysis of uracil prototroph isolates.

YJL9133	YJL9284	3 hr	2	515 to 1100	none
YJL9145	YJL9291	3 hr	2	607 to 753	none
YJL9147	YJL9293	3 hr	2	650 to 753	none
YJL9142	YJL9289	3 hr	2	576 to 713	none

* - aCGH suggests possible spontaneous diploid or mixed population. This is indicated either by the points in amplified region scattering at a non-quantile value (ie. 1.5) or by the points of an aneuploid chromosome scattering at a non-quantile value. aCGH will not be able to suggest possibly diploidization in cases of amplicons with quantile values or where there are no aneuploidies.

† - We suspect these isolates are diploids in which one copy of Chromosome IV bears an amplification

‡ - We suspect these isolates are diploids in which both copies of Chromosome IV bear an amplification

Table S5

Yeast strains used in this study.

Strain	Genotype	Source
YJL6558	MATa MCM7-2NLS ura3-52::[pGAL- Δ ntCDC6.cdk2A, URA3] ORC2 orc6(S116A) leu2 trp1-289 ade2 ade3 bar1::LEU2 ChrIV _{567kb} ::{kanMX, ade3-2p, ARS317} ars317::natMX	Green et al. ¹
YJL6974	MATa MCM7-2NLS ura3-52::[pGAL, URA3] ORC2 orc6(S116A) leu2 trp1-289 ade2 ade3 bar1::LEU2 ChrIV _{567kb} ::{kanMX, ade3-2p, ARS317} ars317::natMX	Green et al. ¹
YJL7445	MATa rad1::TRP1 MCM7-2NLS ura3-52::[pGAL- Δ ntCDC6.cdk2A, URA3] ORC2 orc6(S116A) leu2 trp1-289 ade2 ade3 bar1::LEU2 ChrIV _{567kb} ::{kanMX, ade3-2p, ARS317} ars317::natMX	This Study
YJL7451	MATa rad51::TRP1 MCM7-2NLS ura3-52::[pGAL- Δ ntCDC6.cdk2A, URA3] ORC2 orc6(S116A) leu2 trp1-289 ade2 ade3 bar1::LEU2 ChrIV _{567kb} ::{kanMX, ade3-2p, ARS317} ars317::natMX	This Study
YJL7607	MATa MCM7-2NLS ura3-52 ORC2 orc6(S116A) leu2 trp1-289 ade2 ade3 bar1::LEU2 ChrIV _{567kb} ::{kanMX, ade3-2p, ARS317} ars317::natMX	This Study
YJL7852	MATa MCM7-2NLS ura3-52::[Upstream URA3, URA3, Downstream URA3] ORC2 orc6(S116A) leu2 trp1-289 ade2 ade3 bar1::LEU2 ChrIV _{567kb} ::{kanMX, ade3-2p, ARS317} ars317::natMX	This Study
YJL7906	MATa MCM7-2NLS ura3- Δ ORF ORC2 orc6(S116A) leu2 trp1-289 ade2 ade3 bar1::LEU2 ChrIV _{567kb} ::{kanMX, ade3-2p, ARS317} ars317::natMX	This Study
YJL7929	MATa MCM7-2NLS ura3- Δ ORF ORC2 orc6(S116A) leu2 trp1-289 ade2 ade3 bar1::LEU2 ChrIV _{567kb} ::{kanMX, ade3-2p, ARS317} ars317::natMX YDRCTy2-1::[YDRCTy2-1 5' homology - RA3 - YDRCTy2-1 3' homology(v1), URA3]	This Study
YJL7931	MATa MCM7-2NLS ura3- Δ ORF ORC2 orc6(S116A) leu2 trp1-289 ade2 ade3 bar1::LEU2 ChrIV _{567kb} ::{kanMX, ade3-2p, ARS317} ars317::natMX YDRCTy1-1::[YDRCTy1-1 5' homology(v1) - UR - YDRCTy1-1 3' homology, URA3]	This Study
YJL7954	MATa MCM7-2NLS ura3- Δ ORF ORC2 orc6(S116A) leu2 trp1-289 ade2 ade3 bar1::LEU2 ChrIV _{567kb} ::{kanMX, ade3-2p, ARS317} ars317::natMX < YDRCDelta2, YDRCDelta3, YDRCDelta4, YDRCTy2-1, YDRCDelta5>::RA3(v1)	This Study

Table S5 (continued)

Yeast strains used in this study.

Y.JL7964	MATa MCM7-2NLS ura3-ΔORF ORC2 orc6(S116A) leu2 trp1-289 ade2 ade3 bar1::LEU2 ChrIV567kb::kanMX, ade3-2p, ARS317::natMX <YDRCCdelta7, YDRCTy1-1, YDRCCdelta8, YDRCSigma1, YDRCCdelta9>Δ::UR(v1)	This Study
Y.JL7986	MATa MCM7-2NLS ura3-ΔORF ORC2 orc6(S116A) leu2 trp1-289 ade2 ade3 bar1::LEU2 ChrIV567kb::kanMX, ade3-2p, ARS317::natMX <YDRCCdelta2, YDRCCdelta3, YDRCCdelta4, YDRCTy2-1, YDRCCdelta5>Δ::RA3(v1) YDRCTy1-1::YDRCTy1-1 5' homology(v1) - UR - YDRCTy1-1 3' homology, URA3	This Study
Y.JL7993	MATa MCM7-2NLS ura3-ΔORF ORC2 orc6(S116A) leu2 trp1-289 ade2 ade3 bar1::LEU2 ChrIV567kb::kanMX, ade3-2p, ARS317::natMX <YDRCCdelta2, YDRCCdelta3, YDRCCdelta4, YDRCTy2-1, YDRCCdelta5>Δ::RA3(v1) YDRCCdelta7, YDRCTy1-1, YDRCCdelta8, YDRCSigma1, YDRCCdelta9>Δ::UR(v1)	This Study
Y.JL8027	MATa MCM7-2NLS ura3-ΔORF::fACT1-pGAL1/10-Δ ntCDC6, cdk2A-tCDC6, URA3} ORC2 orc6(S116A) leu2 trp1-289 ade2 ade3 bar1::LEU2 ChrIV _{567kb} ::kanMX, ade3-2p, ARS317} ars317::natMX	This Study
Y.JL8031	MATa MCM7-2NLS ura3-ΔORF::fACT1-pGAL1/10-ΔntCDC6, cdk2A-tCDC6, URA3} ORC2 orc6(S116A) leu2 trp1-289 ade2 ade3 bar1::LEU2 ChrIV567kb::kanMX, ade3-2p, ARS317} ars317::natMX <YDRCCdelta2, YDRCCdelta3, YDRCCdelta4, YDRCTy2-1, YDRCCdelta5>Δ::RA3(v1)	This Study
Y.JL8035	MATa MCM7-2NLS ura3-ΔORF::fACT1-pGAL1/10-ΔntCDC6, cdk2A-tCDC6, URA3} ORC2 orc6(S116A) leu2 trp1-289 ade2 ade3 bar1::LEU2 ChrIV567kb::kanMX, ade3-2p, ARS317} ars317::natMX <YDRCCdelta7, YDRCTy1-1, YDRCCdelta8, YDRCSigma1, YDRCCdelta9>Δ::UR(v1)	This Study
Y.JL8040	MATa MCM7-2NLS ura3-ΔORF::fACT1-pGAL1/10-ΔntCDC6, cdk2A-tCDC6, URA3} ORC2 orc6(S116A) leu2 trp1-289 ade2 ade3 bar1::LEU2 ChrIV567kb::kanMX, ade3-2p, ARS317} ars317::natMX <YDRCCdelta2, YDRCCdelta3, YDRCCdelta4, YDRCTy2-1, YDRCCdelta5>Δ::RA3(v1) YDRCCdelta7, YDRCTy1-1, YDRCCdelta8, YDRCSigma1, YDRCCdelta9>Δ::UR(v1)	This Study
Y.JL8100/8101	MATa MCM7-2NLS ura3::ACT1-pGAL1/10-Δ ntCDC6, cdk2A-tCDC6 ORC2 orc6(S116A) leu2 trp1-289 ade2 ade3 bar1::LEU2 ChrIV _{567kb} ::kanMX, ade3-2p, ARS317} ars317::natMX	This Study
Y.JL8104	MATa MCM7-2NLS ura3::fACT1-pGAL1/10-ΔntCDC6, cdk2A-tCDC6 ORC2 orc6(S116A) leu2 trp1-289 ade2 ade3 bar1::LEU2 ChrIV567kb::kanMX, ade3-2p, ARS317} ars317::natMX <YDRCCdelta2, YDRCCdelta3, YDRCCdelta4, YDRCTy2-1, YDRCCdelta5>Δ::RA3(v1)	This Study

Table S5 (continued)

Yeast strains used in this study.

YJL8108	MATa MCM7-2NLS <i>ura3::tACT1-pGAL1/10-ΔntCDC6.cdk2A-tCDC6 ORC2 orc6(S116A) leu2 trp1-289 ade2 ade3 bar1::LEU2 ChrIV567kb::fkanMX. ade3-2p, ARS317} ars317::natMX <YDRCCdelta7, YDRCTy1-1, YDRCCdelta8, YDRCSigma1, YDRCCdelta9>Δ::UR(v1)</i>	This Study
YJL8112/8113	MATa MCM7-2NLS <i>ura3::tACT1-pGAL1/10-ΔntCDC6.cdk2A-tCDC6 ORC2 orc6(S116A) leu2 trp1-289 ade2 ade3 bar1::LEU2 ChrIV567kb::fkanMX. ade3-2p, ARS317} ars317::natMX <YDRCCdelta2, YDRCCdelta3, YDRCCdelta4, YDRCTy2-1, YDRCCdelta5>Δ::RA3(v1) YDRCCdelta7, YDRCTy1-1, YDRCCdelta8, YDRCSigma1, YDRCCdelta9>Δ::UR(v1)</i>	This Study
YJL8230	MATa MCM7-2NLS <i>ura3-Δ ORF ORC2 orc6(S116A) leu2 trp1-289 ade2 ade3 bar1::LEU2 ChrIV567kb::fkanMX, ade3-2p, ARS317} ars317::natMX YDRCTy2-1::fYDRCTy2-1 5' homology - RA3 - YDRCTy2-1 3' homology(v2), URA3}</i>	This Study
YJL8259	MATa MCM7-2NLS <i>ura3-Δ ORF ORC2 orc6(S116A) leu2 trp1-289 ade2 ade3 bar1::LEU2 ChrIV567kb::fkanMX, ade3-2p, ARS317} ars317::natMX <YDRCCdelta2, YDRCCdelta3, YDRCCdelta4, YDRCTy2-1, YDRCCdelta5, tL(UAA)D, YDRCCdelta6a, YDRCCdelta7, YDRW034C-A, YDRCCdelta6b, tQ(UUG)D1>Δ::RA3(v2)</i>	This Study
YJL8261	MATa MCM7-2NLS <i>ura3-Δ ORF ORC2 orc6(S116A) leu2 trp1-289 ade2 ade3 bar1::LEU2 ChrIV567kb::fkanMX, ade3-2p, ARS317} ars317::natMX YDRCTy1-1::fYDRCTy1-1 5' homology(v2) - UR - YDRCTy1-1 3' homology, URA3}</i>	This Study
YJL8264	MATa MCM7-2NLS <i>ura3-Δ ORF ORC2 orc6(S116A) leu2 trp1-289 ade2 ade3 bar1::LEU2 ChrIV567kb::fkanMX, ade3-2p, ARS317} ars317::natMX <YDRCCdelta2, YDRCCdelta3, YDRCCdelta4, YDRCTy2-1, YDRCCdelta5, tL(UAA)D, YDRCCdelta6a, YDRCCdelta7, YDRW034C-A, YDRCCdelta6b, tQ(UUG)D1>Δ::RA3(v2) YDRCTy1-1::fYDRCTy1-1 5' homology(v2) - UR - YDRCTy1-1 3' homology, URA3}</i>	This Study
YJL8271	MATa MCM7-2NLS <i>ura3-Δ ORF ORC2 orc6(S116A) leu2 trp1-289 ade2 ade3 bar1::LEU2 ChrIV567kb::fkanMX, ade3-2p, ARS317} ars317::natMX <tQ(UUG)D2, YDRCCdelta7, YDRCTy1-1, YDRCCdelta8, YDRCSigma1, YDRCCdelta9>Δ::UR(v2)</i>	This Study

Table S5 (continued)

Yeast strains used in this study.

YJL8274	MATa MCM7-2NLS ura3-Δ ORF ORC2 orc6(S116A) leu2 trp1-289 ade2 ade3 bar1::LEU2 ChrIV567kb::fkanMX, ade3-2p, ARS317} ars317::natMX <YDRCDelta2, YDRCDelta3, YDRCDelta4, YDRCTy2-1, YDRCDelta5, tL(UAA)D, YDRCDelta6a, YDRCDelta7, YDRW034C-A, YDRCDelta6b, tQ(UUG)D1>Δ::RA3(v2) <tQ(UUG)D2, YDRCDelta7, YDRCTy1-1, YDRCDelta8, YDRCSigma1, YDRCDelta9>Δ::UR(v2)	This Study
YJL8340	MATa MCM7-2NLS URA3 ORC2 orc6(S116A) leu2 trp1-289 ade2 ade3 bar1::LEU2 ChrIV567kb::fkanMX, ade3-2p, ARS317} ars317::natMX <YDRCDelta2, YDRCDelta3, YDRCDelta4, YDRCTy2-1, YDRCDelta5, tL(UAA)D, YDRCDelta6a, YDRCDelta7, YDRW034C-A, YDRCDelta6b, tQ(UUG)D1>Δ::RA3(v2)	This Study
YJL8342	MATa MCM7-2NLS URA3 ORC2 orc6(S116A) leu2 trp1-289 ade2 ade3 bar1::LEU2 ChrIV567kb::fkanMX, ade3-2p, ARS317} ars317::natMX <tQ(UUG)D2, YDRCDelta7, YDRCTy1-1, YDRCDelta8, YDRCSigma1, YDRCDelta9>Δ::UR(v2)	This Study
YJL8344	MATa MCM7-2NLS URA3 ORC2 orc6(S116A) leu2 trp1-289 ade2 ade3 bar1::LEU2 ChrIV567kb::fkanMX, ade3-2p, ARS317} ars317::natMX <YDRCDelta2, YDRCDelta3, YDRCDelta4, YDRCTy2-1, YDRCDelta5, tL(UAA)D, YDRCDelta6a, YDRCDelta7, YDRW034C-A, YDRCDelta6b, tQ(UUG)D1>Δ::RA3(v2) <tQ(UUG)D2, YDRCDelta7, YDRCTy1-1, YDRCDelta8, YDRCSigma1, YDRCDelta9>Δ::UR(v2)	This Study
YJL8355	MATa MCM7-2NLS ura3::tACT1-pGAL1/10-ΔntCDC6, cdk2A-tCDC6 ORC2 orc6(S116A) leu2 trp1-289 ade2 ade3 bar1::LEU2 ChrIV567kb::fkanMX, ade3-2p, ARS317} ars317::natMX <YDRCDelta2, YDRCDelta3, YDRCDelta4, YDRCTy2-1, YDRCDelta5, tL(UAA)D, YDRCDelta6a, YDRCDelta7, YDRW034C-A, YDRCDelta6b, tQ(UUG)D1>Δ::RA3(v2)	This Study
YJL8359	MATa MCM7-2NLS ura3::tACT1-pGAL1/10-ΔntCDC6, cdk2A-tCDC6 ORC2 orc6(S116A) leu2 trp1-289 ade2 ade3 bar1::LEU2 ChrIV567kb::fkanMX, ade3-2p, ARS317} ars317::natMX <tQ(UUG)D2, YDRCDelta7, YDRCTy1-1, YDRCDelta8, YDRCSigma1, YDRCDelta9>Δ::UR(v2)	This Study
YJL8363/8364	MATa MCM7-2NLS ura3::tACT1-pGAL1/10-ΔntCDC6, cdk2A-tCDC6 ORC2 orc6(S116A) leu2 trp1-289 ade2 ade3 bar1::LEU2 ChrIV567kb::fkanMX, ade3-2p, ARS317} ars317::natMX <YDRCDelta2, YDRCDelta3, YDRCDelta4, YDRCTy2-1, YDRCDelta5, tL(UAA)D, YDRCDelta6a, YDRCDelta7, YDRW034C-A, YDRCDelta6b, tQ(UUG)D1>Δ::RA3(v2) <tQ(UUG)D2, YDRCDelta7, YDRCTy1-1, YDRCDelta8, YDRCSigma1, YDRCDelta9>Δ::UR(v2)	This Study

Table S5 (continued)

Yeast strains used in this study.

YJL8407/8 408	MATa <i>dnl4::TRP1 MCM7-2NLS ura3::tACT1-pGAL1/10-ΔntCDC6,cdk2A-tCDC6 ORC2 orc6(S116A) leu2 trp1-289 ade2 ade3 bar1::LEU2 ChrIV567kb::kanMX, ade3-2p, ARS317} ars317::natMX <YDRCCdelta2, YDRCCdelta3, YDRCCdelta4, YDRCTy2-1, YDRCCdelta5, tL(UAA)D, YDRCCdelta6a, YDRCCdelta7, YDRW034C-A, YDRCCdelta6b, tQ(UUG)D1>Δ::RA3(v2) <tQ(UUG)D2, YDRCCdelta7, YDRCTy1-1, YDRCCdelta8, YDRCSigma1, YDRCCdelta9>Δ::UR(v2)</i>	This Study
YJL8409/8 410	MATa <i>rad52::TRP1 MCM7-2NLS ura3::tACT1-pGAL1/10-ΔntCDC6,cdk2A-tCDC6 ORC2 orc6(S116A) leu2 trp1-289 ade2 ade3 bar1::LEU2 ChrIV567kb::kanMX, ade3-2p, ARS317} ars317::natMX <YDRCCdelta2, YDRCCdelta3, YDRCCdelta4, YDRCTy2-1, YDRCCdelta5, tL(UAA)D, YDRCCdelta6a, YDRCCdelta7, YDRW034C-A, YDRCCdelta6b, tQ(UUG)D1>Δ::RA3(v2) <tQ(UUG)D2, YDRCCdelta7, YDRCTy1-1, YDRCCdelta8, YDRCSigma1, YDRCCdelta9>Δ::UR(v2)</i>	This Study
YJL8412/8 413	MATa <i>rad51::TRP1 MCM7-2NLS ura3::tACT1-pGAL1/10-ΔntCDC6,cdk2A-tCDC6 ORC2 orc6(S116A) leu2 trp1-289 ade2 ade3 bar1::LEU2 ChrIV567kb::kanMX, ade3-2p, ARS317} ars317::natMX <YDRCCdelta2, YDRCCdelta3, YDRCCdelta4, YDRCTy2-1, YDRCCdelta5, tL(UAA)D, YDRCCdelta6a, YDRCCdelta7, YDRW034C-A, YDRCCdelta6b, tQ(UUG)D1>Δ::RA3(v2) <tQ(UUG)D2, YDRCCdelta7, YDRCTy1-1, YDRCCdelta8, YDRCSigma1, YDRCCdelta9>Δ::UR(v2)</i>	This Study
YJL8415/8 416	MATa <i>rad1::TRP1 MCM7-2NLS ura3::tACT1-pGAL1/10-ΔntCDC6,cdk2A-tCDC6 ORC2 orc6(S116A) leu2 trp1-289 ade2 ade3 bar1::LEU2 ChrIV567kb::kanMX, ade3-2p, ARS317} ars317::natMX <YDRCCdelta2, YDRCCdelta3, YDRCCdelta4, YDRCTy2-1, YDRCCdelta5, tL(UAA)D, YDRCCdelta6a, YDRCCdelta7, YDRW034C-A, YDRCCdelta6b, tQ(UUG)D1>Δ::RA3(v2) <tQ(UUG)D2, YDRCCdelta7, YDRCTy1-1, YDRCCdelta8, YDRCSigma1, YDRCCdelta9>Δ::UR(v2)</i>	This Study
YJL8418/8 419	MATa <i>msh3::TRP1 MCM7-2NLS ura3::tACT1-pGAL1/10-ΔntCDC6,cdk2A-tCDC6 ORC2 orc6(S116A) leu2 trp1-289 ade2 ade3 bar1::LEU2 ChrIV567kb::kanMX, ade3-2p, ARS317} ars317::natMX <YDRCCdelta2, YDRCCdelta3, YDRCCdelta4, YDRCTy2-1, YDRCCdelta5, tL(UAA)D, YDRCCdelta6a, YDRCCdelta7, YDRW034C-A, YDRCCdelta6b, tQ(UUG)D1>Δ::RA3(v2) <tQ(UUG)D2, YDRCCdelta7, YDRCTy1-1, YDRCCdelta8, YDRCSigma1, YDRCCdelta9>Δ::UR(v2)</i>	This Study
YJL8421/8 422	MATa <i>pol32::TRP1 MCM7-2NLS ura3::tACT1-pGAL1/10-ΔntCDC6,cdk2A-tCDC6 ORC2 orc6(S116A) leu2 trp1-289 ade2 ade3 bar1::LEU2 ChrIV567kb::kanMX, ade3-2p, ARS317} ars317::natMX <YDRCCdelta2, YDRCCdelta3, YDRCCdelta4, YDRCTy2-1, YDRCCdelta5, tL(UAA)D, YDRCCdelta6a, YDRCCdelta7, YDRW034C-A, YDRCCdelta6b, tQ(UUG)D1>Δ::RA3(v2) <tQ(UUG)D2, YDRCCdelta7, YDRCTy1-1, YDRCCdelta8, YDRCSigma1, YDRCCdelta9>Δ::UR(v2)</i>	This Study

Table S5 (continued)

Yeast strains used in this study.

		This Study
YJL842518 426	MATa MCM7-2NLS ura3-52:::pGAL-ΔntCDC6-cdk2A, URA3} ORC2 orc6(S116A) leu2 trp1-289 ade2 ade3 bar1::LEU2 ChrIV _{567kb} :::hphMX, I-SceI cut site, ade3-2p, ARS317} ars317::natMX	This Study
YJL842718 428	MATa MCM7-2NLS ura3-52:::pGAL, URA3} ORC2 orc6(S116A) leu2 trp1-289 ade2 ade3 bar1::LEU2 ChrIV _{567kb} :::hphMX, I-SceI cut site, ade3-2p, ARS317} ars317::natMX	This Study
YJL8799	MATa MCM7-2NLS ura3:::tACT1-pGAL/1/10-ΔntCDC6, cdk2A-tCDC6 ORC2 orc6(S116A) leu2 trp1-289 ade2 ade3 bar1::LEU2 ChrIV _{567kb} :::kanMX, ade3-2p, ARS317} ars317::natMX YDRCTy2-1:::YDRCTy2-1 5' homology-YDRCTy2-1 3' homology(v2), URA3}	This Study
YJL8807	MATa MCM7-2NLS ura3:::tACT1-pGAL/1/10-ΔntCDC6, cdk2A-tCDC6 ORC2 orc6(S116A) leu2 trp1-289 ade2 ade3 bar1::LEU2 ChrIV _{567kb} :::kanMX, ade3-2p, ARS317} ars317::natMX <YDRCDelta2, YDRCDelta3, YDRCDelta4, YDRCTy2-1, YDRCDelta5, tL(UAA)D, YDRCDelta6a, YDRCDelta7, YDRW034C-A, YDRCDelta6b, tQ(UUG)D1> Δ	This Study
YJL8824	MATa MCM7-2NLS ura3:::tACT1-pGAL/1/10-ΔntCDC6, cdk2A-tCDC6 ORC2 orc6(S116A) leu2 trp1-289 ade2 ade3 bar1::LEU2 ChrIV _{567kb} :::kanMX, ade3-2p, ARS317} ars317::natMX <YDRCDelta2, YDRCDelta3, YDRCDelta4, YDRCTy2-1, YDRCDelta5, tL(UAA)D, YDRCDelta6a, YDRCDelta7, YDRW034C-A, YDRCDelta6b, tQ(UUG)D1> Δ YDRCTy1-1:::YDRCTy1-1 5' homology(v2)-YDRCTy1-1 3' homology, URA3}	This Study
YJL8842	MATa MCM7-2NLS ura3:::tACT1-pGAL/1/10-ΔntCDC6, cdk2A-tCDC6 ORC2 orc6(S116A) leu2 trp1-289 ade2 ade3 bar1::LEU2 ChrIV _{567kb} :::kanMX, ade3-2p, ARS317} ars317::natMX <YDRCDelta2, YDRCDelta3, YDRCDelta4, YDRCTy2-1, YDRCDelta5, tL(UAA)D, YDRCDelta6a, YDRCDelta7, YDRW034C-A, YDRCDelta6b, tQ(UUG)D1> Δ <tQ(UUG)D2, YDRCDelta7, YDRCTy1-1, YDRCDelta8, YDRCSigma1, YDRCDelta9> Δ	This Study
YJL9054	MATa MCM7-2NLS ura3:::tACT1-pGAL/1/10-ΔntCDC6, cdk2A-tCDC6 ORC2 orc6(S116A) leu2 trp1-289 ade2 ade3 bar1::LEU2 ChrIV _{567kb} :::kanMX, ade3-2p, ARS317} ars317::natMX <YDRCDelta2, YDRCDelta3, YDRCDelta4, YDRCTy2-1, YDRCDelta5, tL(UAA)D, YDRCDelta6a, YDRCDelta7, YDRW034C-A, YDRCDelta6b, tQ(UUG)D1> Δ <tQ(UUG)D2, YDRCDelta7, YDRCTy1-1, YDRCDelta8, YDRCSigma1, YDRCDelta9> Δ ChrIV515kb:::hphMX, RA3}	This Study

Table S5 (continued)

Yeast strains used in this study.

Y.JL9056	MATa MCM7-2NLS ura3::tACT1-pGAL1/10-ΔntCDC6, cdk2A-tCDC6 ORC2 orc6(S116A) leu2 trp1-289 ade2 ade3 bar1::LEU2 ChrIV567kb::fkanMX, ade3-2p, ARS317} ars317::natMX <YDRCCdelta2, YDRCCdelta3, YDRCCdelta4, YDRCTy2-1, YDRCCdelta5, tL(UAA)D, YDRCCdelta6a, YDRCCdelta7, YDRW034C-A, YDRCCdelta6b, tQ(UUG)D1>Δ <tQ(UUG)D2, YDRCCdelta7, YDRCTy1-1, YDRCCdelta8, YDRCSigma1, YDRCCdelta9>Δ ChrIV545kb::fphMX, RA3}	This Study
Y.JL9057	MATa MCM7-2NLS ura3::tACT1-pGAL1/10-ΔntCDC6, cdk2A-tCDC6 ORC2 orc6(S116A) leu2 trp1-289 ade2 ade3 bar1::LEU2 ChrIV567kb::fkanMX, ade3-2p, ARS317} ars317::natMX <YDRCCdelta2, YDRCCdelta3, YDRCCdelta4, YDRCTy2-1, YDRCCdelta5, tL(UAA)D, YDRCCdelta6a, YDRCCdelta7, YDRW034C-A, YDRCCdelta6b, tQ(UUG)D1>Δ <tQ(UUG)D2, YDRCCdelta7, YDRCTy1-1, YDRCCdelta8, YDRCSigma1, YDRCCdelta9>Δ ChrIV565kb::fphMX, RA3}	This Study
Y.JL9060	MATa MCM7-2NLS ura3::tACT1-pGAL1/10-ΔntCDC6, cdk2A-tCDC6 ORC2 orc6(S116A) leu2 trp1-289 ade2 ade3 bar1::LEU2 ChrIV567kb::fkanMX, ade3-2p, ARS317} ars317::natMX <YDRCCdelta2, YDRCCdelta3, YDRCCdelta4, YDRCTy2-1, YDRCCdelta5, tL(UAA)D, YDRCCdelta6a, YDRCCdelta7, YDRW034C-A, YDRCCdelta6b, tQ(UUG)D1>Δ <tQ(UUG)D2, YDRCCdelta7, YDRCTy1-1, YDRCCdelta8, YDRCSigma1, YDRCCdelta9>Δ ChrIV576kb::fphMX, RA3}	This Study
Y.JL9062	MATa MCM7-2NLS ura3::tACT1-pGAL1/10-ΔntCDC6, cdk2A-tCDC6 ORC2 orc6(S116A) leu2 trp1-289 ade2 ade3 bar1::LEU2 ChrIV567kb::fkanMX, ade3-2p, ARS317} ars317::natMX <YDRCCdelta2, YDRCCdelta3, YDRCCdelta4, YDRCTy2-1, YDRCCdelta5, tL(UAA)D, YDRCCdelta6a, YDRCCdelta7, YDRW034C-A, YDRCCdelta6b, tQ(UUG)D1>Δ <tQ(UUG)D2, YDRCCdelta7, YDRCTy1-1, YDRCCdelta8, YDRCSigma1, YDRCCdelta9>Δ ChrIV607kb::fphMX, RA3}	This Study
Y.JL9067	MATa MCM7-2NLS ura3::tACT1-pGAL1/10-ΔntCDC6, cdk2A-tCDC6 ORC2 orc6(S116A) leu2 trp1-289 ade2 ade3 bar1::LEU2 ChrIV567kb::fkanMX, ade3-2p, ARS317} ars317::natMX <YDRCCdelta2, YDRCCdelta3, YDRCCdelta4, YDRCTy2-1, YDRCCdelta5, tL(UAA)D, YDRCCdelta6a, YDRCCdelta7, YDRW034C-A, YDRCCdelta6b, tQ(UUG)D1>Δ <tQ(UUG)D2, YDRCCdelta7, YDRCTy1-1, YDRCCdelta8, YDRCSigma1, YDRCCdelta9>Δ ChrIV650kb::fphMX, RA3}	This Study
Y.JL9115/9116	MATa MCM7-2NLS ura3::tACT1-pGAL1/10-ΔntCDC6, cdk2A-tCDC6 ORC2 orc6(S116A) leu2 trp1-289 ade2 ade3 bar1::LEU2 ChrIV567kb::fkanMX, ade3-2p, ARS317} ars317::natMX <YDRCCdelta2, YDRCCdelta3, YDRCCdelta4, YDRCTy2-1, YDRCCdelta5, tL(UAA)D, YDRCCdelta6a, YDRCCdelta7, YDRW034C-A, YDRCCdelta6b, tQ(UUG)D1>Δ <tQ(UUG)D2, YDRCCdelta7, YDRCTy1-1, YDRCCdelta8, YDRCSigma1, YDRCCdelta9>Δ ChrIV515kb::fphMX, RA3} ChrIV607kb::fUR, TRP1}	This Study

Table S5 (continued)

Yeast strains used in this study.

YJL9118/9 119	MATa MCM7-2NLS ura3::tACT1-pGAL1/10- Δ ntCDC6, cdk2A-tCDC6 ORC2 orc6(S116A) leu2 trp1-289 ade2 ade3 bar1::LEU2 ChrIV567kb:::{kanMX, ade3-2p, ARS317} ars317::natMX <YDRcdelta2, YDRcdelta3, YDRcdelta4, YDRCTy2-1, YDRcdelta5, tL(UAA)D, YDRcdelta6a, YDRcdelta7, YDRW034C-A, YDRcdelta6b, tQ(UUG)D1> Δ <tQ(UUG)D2, YDRcdelta7, YDRCTy1-1, YDRcdelta8, YDRcdelta9> Δ ChrIV515kb:::{hphMX, RA3} ChrIV650kb:::{UR, TRP1}	This Study
YJL9121/9 122	MATa MCM7-2NLS ura3::tACT1-pGAL1/10- Δ ntCDC6, cdk2A-tCDC6 ORC2 orc6(S116A) leu2 trp1-289 ade2 ade3 bar1::LEU2 ChrIV567kb:::{kanMX, ade3-2p, ARS317} ars317::natMX <YDRcdelta2, YDRcdelta3, YDRcdelta4, YDRCTy2-1, YDRcdelta5, tL(UAA)D, YDRcdelta6a, YDRcdelta7, YDRW034C-A, YDRcdelta6b, tQ(UUG)D1> Δ <tQ(UUG)D2, YDRcdelta7, YDRCTy1-1, YDRcdelta8, YDRcdelta9> Δ ChrIV515kb:::{hphMX, RA3} ChrIV753kb:::{UR, TRP1}	This Study
YJL9127/9 128	MATa MCM7-2NLS ura3::tACT1-pGAL1/10- Δ ntCDC6, cdk2A-tCDC6 ORC2 orc6(S116A) leu2 trp1-289 ade2 ade3 bar1::LEU2 ChrIV567kb:::{kanMX, ade3-2p, ARS317} ars317::natMX <YDRcdelta2, YDRcdelta3, YDRcdelta4, YDRCTy2-1, YDRcdelta5, tL(UAA)D, YDRcdelta6a, YDRcdelta7, YDRW034C-A, YDRcdelta6b, tQ(UUG)D1> Δ <tQ(UUG)D2, YDRcdelta7, YDRCTy1-1, YDRcdelta8, YDRcdelta9> Δ ChrIV515kb:::{hphMX, RA3} ChrIV875kb:::{UR, TRP1}	This Study
YJL9130/9 131	MATa MCM7-2NLS ura3::tACT1-pGAL1/10- Δ ntCDC6, cdk2A-tCDC6 ORC2 orc6(S116A) leu2 trp1-289 ade2 ade3 bar1::LEU2 ChrIV567kb:::{kanMX, ade3-2p, ARS317} ars317::natMX <YDRcdelta2, YDRcdelta3, YDRcdelta4, YDRCTy2-1, YDRcdelta5, tL(UAA)D, YDRcdelta6a, YDRcdelta7, YDRW034C-A, YDRcdelta6b, tQ(UUG)D1> Δ <tQ(UUG)D2, YDRcdelta7, YDRCTy1-1, YDRcdelta8, YDRcdelta9> Δ ChrIV515kb:::{hphMX, RA3} ChrIV985kb:::{UR, TRP1}	This Study
YJL9133/9 134	MATa MCM7-2NLS ura3::tACT1-pGAL1/10- Δ ntCDC6, cdk2A-tCDC6 ORC2 orc6(S116A) leu2 trp1-289 ade2 ade3 bar1::LEU2 ChrIV567kb:::{kanMX, ade3-2p, ARS317} ars317::natMX <YDRcdelta2, YDRcdelta3, YDRcdelta4, YDRCTy2-1, YDRcdelta5, tL(UAA)D, YDRcdelta6a, YDRcdelta7, YDRW034C-A, YDRcdelta6b, tQ(UUG)D1> Δ <tQ(UUG)D2, YDRcdelta7, YDRCTy1-1, YDRcdelta8, YDRcdelta9> Δ ChrIV515kb:::{hphMX, RA3} ChrIV1100kb:::{UR, TRP1}	This Study
YJL9136/9 137	MATa MCM7-2NLS ura3::tACT1-pGAL1/10- Δ ntCDC6, cdk2A-tCDC6 ORC2 orc6(S116A) leu2 trp1-289 ade2 ade3 bar1::LEU2 ChrIV567kb:::{kanMX, ade3-2p, ARS317} ars317::natMX <YDRcdelta2, YDRcdelta3, YDRcdelta4, YDRCTy2-1, YDRcdelta5, tL(UAA)D, YDRcdelta6a, YDRcdelta7, YDRW034C-A, YDRcdelta6b, tQ(UUG)D1> Δ <tQ(UUG)D2, YDRcdelta7, YDRCTy1-1, YDRcdelta8, YDRcdelta9> Δ ChrIV545kb:::{hphMX, RA3} ChrIV592kb:::{UR, TRP1}	This Study

Table S5 (continued)

Yeast strains used in this study.

YJL9139/9 140	MATa MCM7-2NLS <i>ura3::tACT1-pGAL1/10-ΔntCDC6, cdk2A-tCDC6</i> ORC2 <i>orc6(S116A)</i> <i>leu2 trp1-289 ade2 ade3 bar1::LEU2</i> <i>ChrIV567kb::fkanMX, ade3-2p, ARS317</i> <i>ars317::natMX <YDRCdelta2, YDRCdelta3, YDRCdelta4, YDRCTy2-1, YDRCdelta5, tL(UAA)D, YDRCdelta6a, YDRCdelta7, YDRW034C-A, YDRCdelta6b, tQ(UUG)D1>Δ <tQ(UUG)D2, YDRCdelta7, YDRCTy1-1, YDRCdelta8, YDRCSigma1, YDRCdelta9>Δ</i> <i>ChrIV565kb::fphMX, RA3</i> <i>ChrIV576kb::fUR, TRP1}</i>	This Study
YJL9142/9 143	MATa MCM7-2NLS <i>ura3::tACT1-pGAL1/10-ΔntCDC6, cdk2A-tCDC6</i> ORC2 <i>orc6(S116A)</i> <i>leu2 trp1-289 ade2 ade3 bar1::LEU2</i> <i>ChrIV567kb::fkanMX, ade3-2p, ARS317</i> <i>ars317::natMX <YDRCdelta2, YDRCdelta3, YDRCdelta4, YDRCTy2-1, YDRCdelta5, tL(UAA)D, YDRCdelta6a, YDRCdelta7, YDRW034C-A, YDRCdelta6b, tQ(UUG)D1>Δ <tQ(UUG)D2, YDRCdelta7, YDRCTy1-1, YDRCdelta8, YDRCSigma1, YDRCdelta9>Δ</i> <i>ChrIV576kb::fphMX, RA3</i> <i>ChrIV713kb::fUR, TRP1}</i>	This Study
YJL9145/9 146	MATa MCM7-2NLS <i>ura3::tACT1-pGAL1/10-ΔntCDC6, cdk2A-tCDC6</i> ORC2 <i>orc6(S116A)</i> <i>leu2 trp1-289 ade2 ade3 bar1::LEU2</i> <i>ChrIV567kb::fkanMX, ade3-2p, ARS317</i> <i>ars317::natMX <YDRCdelta2, YDRCdelta3, YDRCdelta4, YDRCTy2-1, YDRCdelta5, tL(UAA)D, YDRCdelta6a, YDRCdelta7, YDRW034C-A, YDRCdelta6b, tQ(UUG)D1>Δ <tQ(UUG)D2, YDRCdelta7, YDRCTy1-1, YDRCdelta8, YDRCSigma1, YDRCdelta9>Δ</i> <i>ChrIV607kb::fphMX, RA3</i> <i>ChrIV753kb::fUR, TRP1}</i>	This Study
YJL9147/9 148	MATa MCM7-2NLS <i>ura3::tACT1-pGAL1/10-ΔntCDC6, cdk2A-tCDC6</i> ORC2 <i>orc6(S116A)</i> <i>leu2 trp1-289 ade2 ade3 bar1::LEU2</i> <i>ChrIV567kb::fkanMX, ade3-2p, ARS317</i> <i>ars317::natMX <YDRCdelta2, YDRCdelta3, YDRCdelta4, YDRCTy2-1, YDRCdelta5, tL(UAA)D, YDRCdelta6a, YDRCdelta7, YDRW034C-A, YDRCdelta6b, tQ(UUG)D1>Δ <tQ(UUG)D2, YDRCdelta7, YDRCTy1-1, YDRCdelta8, YDRCSigma1, YDRCdelta9>Δ</i> <i>ChrIV650kb::fphMX, RA3</i> <i>ChrIV753kb::fUR, TRP1}</i>	This Study
YJL9149- 9151	MATa MCM7-2NLS <i>ura3::tACT1-pGAL1/10-tCDC6</i> ORC2 <i>orc6(S116A)</i> <i>leu2 trp1-289 ade2 ade3 bar1::LEU2</i> <i>ChrIV567kb::fkanMX, ade3-2p, ARS317</i> <i>ars317::natMX <YDRCdelta2, YDRCdelta3, YDRCdelta4, YDRCTy2-1, YDRCdelta5, tL(UAA)D, YDRCdelta6a, YDRCdelta7, YDRW034C-A, YDRCdelta6b, tQ(UUG)D1>Δ::RA3(v2) <tQ(UUG)D2, YDRCdelta7, YDRCTy1-1, YDRCdelta8, YDRCSigma1, YDRCdelta9>Δ::UR(v2)</i>	This Study

¹ Green, B.M. et al. *Science* **329**, 943–946 (2010)

Table S6

Plasmids used in this study.

Name	Description	Source
pRS304	TRP1	Sikorski, R.S. et al. <i>Genetics</i> 122 (1), 19-27 (1989)
pRS305	LEU2	Sikorski, R.S. et al. <i>Genetics</i> 122 (1), 19-27 (1989)
pRS306	URA3	Sikorski, R.S. et al. <i>Genetics</i> 122 (1), 19-27 (1989)
pAG26	<i>hphMX4, CEN-ARS, URA3</i>	Goldstein, A.L. et al. <i>Yeast</i> 15 , 1541-1553 (1999)
pSK179	13kb <i>EcoRI</i> fragment containing <i>URA3</i> in pBR322	Natsoulis, G. et al. <i>Genetics</i> 123 (2), 269-279 (1989)
pJL124	<i>URA3</i> in pRS305	This Study
pJL806	pGAL1/10, <i>URA3</i>	Nguyen, V.Q. et al. <i>Nature</i> 411 , 1068-1073 (2001)
pJL1488	pGAL1/10- Δ ntCDC6.cdk2A-tCDC6, <i>URA3</i>	Green, B.M. et al. <i>Mol Biol Cell</i> 17 , 2401-2414 (2005)
pKJF013	<i>YDRCTy2-1</i> replacement with <i>RA3</i> (v1)	This Study
pKJF014	<i>YDRCTy1-1</i> replacement with <i>UR</i> (v1)	This Study
pKJF017	<i>URA3</i> locus deletion (<i>ura3-Δ</i> ORF)	This Study
pKJF019	tACT1-pGAL1/10- Δ ntCDC6.cdk2A-tCDC6 (replace <i>URA3</i> locus)	This Study
pKJF020	tACT1-pGAL1/10-tCDC6 (replace <i>URA3</i> locus)	This Study
pKJF021	<i>YDRCTy2-1</i> replacement with <i>RA3</i> (v2)	This Study
pKJF022	<i>YDRCTy1-1</i> replacement with <i>UR</i> (v2)	This Study
pKJF026	<i>YDRCdelta2</i> to tQ(<i>UUG</i>)D1 deletion	This Study
pKJF027	tQ(<i>UUG</i>)D2 to <i>YDRCdelta9</i> deletion	This Study
pKJF028	<i>UR+TRP1</i> Module	This Study
pKJF029	<i>hphMX+RA3</i> Module	This Study

Table S7

Oligonucleotides used in this study. Listed 5' to 3', left to right. Upper-case letters indicate sequence that anneals to the template during PCR or sequencing. Lowercase letters indicate sequence added by PCR, either to provide homology for genomic integration or to provide restriction sites for cloning. The bold, underlined sequence for OJL2317 is the cleavage site for I-SceI. Subscript numbers are nucleotide coordinates provided by the Saccharomyces Genome Database (version R64-1-1)

Name	Sequence	Purpose
OJL2177	gicacatgcccggAGATGCTAAGAGATAGTGATG	ChrV_115801-116166 for Homology Left in pKJF017
OJL2178	gicacatggaaattcGATTTACTTCGTTTCCTGC	ChrV_115801-116166 for Homology Left in pKJF017
OJL2180	gicacatgggtcgaccTTTACAGTCTGCTCTATTG	ChrV_116871-117211 for Homology Right in pKJF017
OJL2181	gicacatggaaattcAAAACTGATTATAAGTAAATGCATG	ChrV_116871-117211 for Homology Right in pKJF017
OJL2204	gicacatggaccggcAGATGCTAAGAGATAGTGATG	ChrV_115801-116166 for Homology Left in pKJF019 and pKJF020
OJL2205	gicacatggggagctcGATTTTCTTCGTTTCCTGC	ChrV_115801-116166 for Homology Left in pKJF019 and pKJF020
OJL2202	gicacatggggagctcTATGATACAGGGTCCAATGG	ChrV_152988-53259 for for ACT1 terminator in pKJF019 and pKJF020
OJL2203	gicacatggcccggTCTCTGCTTTTGTGCGCG	ChrV_152988-53259 for for ACT1 terminator in pKJF019 and pKJF020
OJL2206	gicacatggctcggAAAACTGATTATAAGTAAATGCATG	ChrV_116871-117211 for Homology Right in pKJF019 and pKJF020
OJL2207	gicacatggggagctcTTTTACAGTCTGCTCTATTG	ChrV_116871-117211 for Homology Right in pKJF019 and pKJF020
OJL2158	gicacatggcccggGGAAAGAAACAGGGAGATAAGG	ChrV_512151-5129128 for Homology Left in pKJF013, pKJF021 and pKJF026
OJL2159	gctcaatgggattccGTAGCCCTTCAAATCTGAGG	ChrV_512151-5129128 for Homology Left in pKJF013, pKJF021 and pKJF026
OJL2167	gicacatggcccggGCATCTGTGCGGTAATTCAC	R43 element in pKJF013, pKJF021, and pKJF029
OJL2170	gicacatgggattccACAGTTAAGCCGCTAAAGGC	R43 element in pKJF013, pKJF021, and pKJF029
OJL2160	cgctaatgggattccgctcaaatgcccggcCAAGTATTTACGGAGGG	ChrV_519721-520163 for Homology Right in pKJF013
OJL2161	gctcaatggctcgaacAAGAATAGGTGGATAATACGG	ChrV_519721-520163 for Homology Right in pKJF013
OJL2265	cgctaatggcccggTTTTCTATTTTTAACCCCTTIG	ChrV_521044-521567 for Homology Right in pKJF021, pKJF026, and pKJF029
OJL2266	gctcaatggctcgaatGTACGCCATAAAATTTGAGAAG	ChrV_521044-521567 for Homology Right in pKJF021, pKJF026, and pKJF029
OJL2162	gicacatggcccggACTGATGGTTCAACAGAGAAGC	ChrV_645119-645467 for Homology Left in pKJF014
OJL2163	cgctaatgggattccgaatgggattccCTCCCTAGCTGAACACTACC	ChrV_645119-645467 for Homology Left in pKJF014
OJL2267	gicacatggcccggCGTCCGCATCAATGGATAAG	ChrV_644738-645152 for Homology Left in pKJF022, pKJF027, and pKJF028
OJL2268	ccatgatgggattccTTTTAACTGTGGCTTCTCTG	ChrV_644738-645152 for Homology Left in pKJF022, pKJF027, and pKJF028
OJL2168	gicacatgggattccGAGCAGATTGACTGAGAGTG	UR element in pKJF014, pKJF024, and pKJF029
OJL2171	gctcaatgggattccGGGTGCATAAATCAACCAATCG	UR element in pKJF014, pKJF024, and pKJF029
OJL2164	gicacatgggattccCAATGAGCGCCCAATTTATCG	ChrV_851962-852532 for Homology Right in pKJF014, pKJF022, and pKJF027
OJL2165	gctcaatggctcgaactCTCTCGTCAACGGGAAGACC	ChrV_851962-852532 for Homology Right in pKJF014, pKJF022, and pKJF027
OJL2543	gicacatgggattccGAGCAGATTGACTGAGAGTG	TRP1 selectable marker in pKJF028
OJL2544	gicacatgggattccCATCTGTGCGGTAATTCAC	TRP1 selectable marker in pKJF028
OJL2097	gaacatgaaggaaatagjaacggattattaggTGAGCAGATTGACTGAGAGTG	<i>dhf4::TRP1</i> , Step 1
OJL2098	caaaaatattagccctcgaacgcacacgcATCTGTCCGGTATTTAC	<i>dhf4::TRP1</i> , Step 1
OJL2099	giggaaaaataaatacaaaaataaaactcaAACTGAAGGAAATAGTAACGG	<i>dhf4::TRP1</i> , Step 2
OJL2100	taacatagtaggattcaataaaactcaAAAAATTAAGCCCTCCCG	<i>dhf4::TRP1</i> , Step 2
OJL2117	gaaggctcgtgcttggctgtaggagcagattgGAGCAGATTGACTGAGAGTG	<i>rad52::TRP1</i> , Step 1
OJL2118	aatgatcaaatatttttttttcgccggaagcggttGCATCTGTCCGGTATTTCAC	<i>rad52::TRP1</i> , Step 1
OJL2119	atgcaacaaggaggcttgcgaagcactgcGAAAGTTCTGTGGCTTTGG	<i>rad52::TRP1</i> , Step 2
OJL2120	aactagaggatttggagtaataaaAATGATGCAAAATTTTTATTTGTTCCGGC	<i>rad52::TRP1</i> , Step 2

Table S7 (continued)

OJL2897	taicatalgccaagtttagcgggaaacgcactcaTGAGAGTGCACCATACCACC	ChrIV_576kb::[UR, TRP1], Step 1
OJL2898	cgtagccaaacigaaglaaacttttagccggtTGAGAGTGCACCATACCACC	ChrIV_592kb::[UR, TRP1], Step 1
OJL2899	caagtgcaattgctggttgcgcaataGCATCTGTGCGGTAATTCAC	ChrIV_592kb::[UR, TRP1], Step 1
OJL2700	gagtaatccactcgggaagggcgcagctgcCGTGGCCAACTGAAGTAATC	ChrIV_592kb::[UR, TRP1], Step 2
OJL2701	alacccctgcacagccgctggggctcCAAGTGCAATGGCGTTTTG	ChrIV_607kb::[UR, TRP1], Step 1
OJL2702	aegtaaaaitaataalcaicacagttccagTTGAGAGTGCACCATACCACC	ChrIV_650kb::[UR, TRP1], Step 1
OJL2703	gatggtcaacagagaagccacagtaaaatGAGAGTGCACCATACCACC	ChrIV_713kb::[UR, TRP1], Step 1
OJL2704	tagagcctatgataagagacgacacgcaatTGAGAGTGCACCATACCACC	ChrIV_713kb::[UR, TRP1], Step 1
OJL2705	ccattglaaaaatgctcacaacgctcaatgGCATCTGTGCGGTAATTCAC	ChrIV_713kb::[UR, TRP1], Step 2
OJL2706	aegtagtattaccgatttttaactcagTAGAGGCAATGATAGAGAGC	ChrIV_713kb::[UR, TRP1], Step 2
OJL2707	ttccacctttattttagtactagCCATTTGTAATAATGGCTCGA	ChrIV_713kb::[UR, TRP1], Step 2
OJL2708	ftaagagaalaaattcttcaaaaatgtagTGAGAGTGCACCATACCACC	ChrIV_753kb::[UR, TRP1], Step 1
OJL2709	aalattctttgattccacataacttgcTGCATCTGTGCGGTAATTCAC	ChrIV_753kb::[UR, TRP1], Step 1
OJL2710	tttagaacaaaatglaaaaagaataTTAAGAGAAATAATCTTTC	ChrIV_753kb::[UR, TRP1], Step 2
OJL2711	alaciatattataatagaaatcaactaaTATCTTTTGGATTTCCAC	ChrIV_753kb::[UR, TRP1], Step 2
OJL2716	aifccattgtacaaaaggatgatattTGAGAGTGCACCATACCACC	ChrIV_875kb::[UR, TRP1], Step 1
OJL2717	atttgggaaaattgctgggataatgtagGATTCATTTGCACAAAGGC	ChrIV_875kb::[UR, TRP1], Step 1
OJL2718	aaatggatgaatlttgagaataatgtagGATTCATTTGCACAAAGGC	ChrIV_875kb::[UR, TRP1], Step 2
OJL2719	aaaaaattgctcttgcgaattcttgaATTTTGGGAAAATTTGTCGGG	ChrIV_875kb::[UR, TRP1], Step 2
OJL2720	acacacatgcaactgttggaaataaatacTGAGAGTGCACCATACCACC	ChrIV_955kb::[UR, TRP1], Step 1
OJL2721	actaaacacttgcctcaaatgttggagGCATCTGTGCGGTAATTCAC	ChrIV_955kb::[UR, TRP1], Step 1
OJL2722	tattatgacacacatcaaacgttaataaaACACACATGCAACTTGTGG	ChrIV_955kb::[UR, TRP1], Step 2
OJL2723	ggcccaacgatggcaactgttattaccACTAAACCACCTTGGCTCAC	ChrIV_955kb::[UR, TRP1], Step 2
OJL2724	aagtggttgattgcattggtaataatccTGAGAGTGCACCATACCACC	ChrIV_1100kb::[UR, TRP1], Step 1
OJL2725	tttaaaegcaactgaacacgcagcttgaatGCATCTGTGCGGTAATTCAC	ChrIV_1100kb::[UR, TRP1], Step 1
OJL2726	atttaataagtagglaaacttggaaatAAGTGTGGGATTCGATTTGG	ChrIV_1100kb::[UR, TRP1], Step 2
OJL2727	tgcataaataagaaatgctgtatcaaaaTTTAAAGCAACTGAAACGC	ChrIV_1100kb::[UR, TRP1], Step 2
OJL2228	GCCAGAAAACAGATCTTATACC	Primer 1 for Junction PCR
OJL2269	CCGATGTGACTAATACTTGAGC	Primer 2 for Junction PCR
OJL2311	CGGAATTGACTGAGTCTTTGC	Primer 3 for Junction PCR
OJL2227	AGTAGAAATGAGGGAAGAAGC	Primer 4 for Junction PCR
OJL2449	GAGGACATACGTGGTGAAGC	MAK21 Probe
OJL2450	AGGCTTCTACTCGTTCAACG	MAK21 Probe
OJL2231	AGGACGACTGGAGTGATAGG	YOS9 Probe
OJL2232	AAACACATGAGTACCAGGC	YOS9 Probe

Text S1

Oligonucleotides

Oligonucleotides used in the plasmid and yeast strain constructions described below are listed in Table S7.

Plasmids

All plasmids used for strain construction are listed in Table S6.

pJL124 contains a BglII-BamHI *URA3* fragment sub-cloned from pSK179 [1] into pRS305 [2]. The BglII end of the fragment is ligated to the BamHI site in pRS305 polylinker, and the BamHI end of the fragment is filled in and blunt-end ligated to a filled in XhoI site in the polylinker.

pKJF017 is used to replace *ura3-52* with *ura3-ΔORF* by loop-in/loop-out replacement. It effectively consists of the following elements: Homology Left (SacII to EcoRI of PCR product from YJL6558 [3] genomic DNA using OJL2177 and OJL2178), Homology Right (EcoRI-SalI of PCR product from YJL6558 genomic DNA using OJL2180 and OJL2181), and vector backbone (SalI to SacII of pRS306 [2]).

pKJF019 is used to replace *ura3-ΔORF* or *URA3* with *tACT1-pGAL1/10-ΔntCDC6,cdk2A-tCDC6* by loop-in/loop-out or direct replacement, respectively. It was generated from pJL1488 [4] by introducing a Homology Left element (NgoMIV to SacI of PCR product from pKJF017 plasmid DNA using OJL2204 and OJL2205) and an *ACT1* terminator element (SacI to SacII of PCR product from YJL6974 [3] genomic DNA using OJL2202 and OJL2203) between the NgoMIV and SacII sites of pJL1488. Then a Homology Right element (XhoI to Asp718I of PCR product from pKJF017 plasmid DNA using OJL2206 and OJL2207) was inserted between the XhoI and Asp718I sites of the resulting plasmid.

pKJF020 is used to replace *ura3-ΔORF* or *URA3* with *tACT1-pGAL1/10-tCDC6* by loop-in/loop-out or direct replacement, respectively. It was generated from pKJF019

by digesting with BamHI and SpeI, filling in the overhangs with Klenow, then ligating the blunted ends together to re-circularize. This removes the $\Delta ntCDC6, cdk2A$ element.

pKJF013 and pKJF021 replace *YDRCTy2-1* with version 1 or version 2 of the 3' *URA3* element (*RA3*), respectively. These effectively consist of the following elements: Homology Left (SacII to BamHI of PCR product from YJL6974 genomic DNA using OJL2158 and OJL2159), *RA3* (BamHI to XmaI of PCR product from pRS306 plasmid DNA using OJL2167 and OJL2170), Homology Right (XmaI to Sall of PCR product from YJL6974 genomic DNA using OJL2160 and OJL2161 for pKJF013, and OJL2265 and OJL2266 for pKJF021), and vector backbone (Sall to SacII of pRS306).

pKJF014 and pKJF022 replace *YDRCTy1-1* with version 1 or version 2 of the 5' *URA3* element (*UR*), respectively. These effectively consist of the following elements: Homology Left (SacII to BamHI of PCR product from YJL6974 genomic DNA using OJL2162 and OJL2163 for pKJF014, and OJL2267 and OJL2268 for pKJF022), *UR* (BamHI to EcoRI of PCR product from pRS306 plasmid DNA using OJL2168 and OJL2171), Homology Right (EcoRI to Sall of PCR product from YJL6974 genomic DNA using OJL2164 and OJL2165), and vector backbone (Sall to SacII of pRS306).

pKJF026 deletes the sequence between sequence from *YDRCDelta2* to *tQ(UUG)D1* through a loop-in/loop-out replacement. It effectively consists of the following elements: Homology Left (SacII to BamHI of PCR product from YJL6974 genomic DNA using OJL2158 and OJL2159), a BamHI-XmaI linker sequence (5'-GGATCCGCTCAAATGCCCGGG-3'), Homology Right (XmaI to Sall of PCR product from YJL6974 genomic DNA using OJL2265 and OJL2266), and vector backbone (Sall to SacII of pRS306).

pKJF027 deletes the sequence between sequence from *tQ(UUG)D2* to *YDRCDelta9* through a loop-in/loop-out replacement. It effectively consists of the following elements: Homology Left (SacII to BamHI of PCR product from YJL6974 genomic DNA using OJL2267 and OJL2268), a BamHI-EcoRI linker sequence

(5'-GGATCCCATTTGAGCGAATTC-3'), Homology Right (EcoRI to Sall of PCR product from YJL6974 genomic DNA using OJL2164 and OJL2165), and vector backbone (Sall to SacII of pRS306).

pKJF028 is used as a PCR template for the *UR* element + *TRP1* selectable marker module for integration at various genomic locations. It effectively consists of the following elements: Homology Left (SacII to BamHI of PCR product from YJL6974 genomic DNA using OJL2267 and OJL2268), *UR* (BamHI to EcoRI of PCR product from pRS306 plasmid DNA using OJL2168 and OJL2171), *TRP1* (EcoRI to Sall of PCR product from pRS304[2] plasmid DNA using OJL2543 and OJL2544), and vector backbone (Sall to SacII of pRS306).

pKJF029 is used as a PCR template for the *RA3* element + *hphMX* selectable marker module for integration at various genomic locations. It effectively consists of the following elements: *hphMX* (SacII to BamHI of pAG26[5]), *RA3* (BamHI to XmaI of PCR product from pRS306 plasmid DNA using OJL2167 and OJL2170), Homology Right (XmaI to Sall of PCR product from YJL6974 genomic DNA using OJL2265 and OJL2266), and vector backbone (Sall to SacII of pRS306).

Strains

All strains used in this study have their genotypes listed in Table S5. All strains used in this study are derived from YJL6558 or YJL6974 (see below for details). As we reported in Green et al. 2010, the *ORC6* gene in these strains has a recently discovered mutation that changes serine 116 to alanine. This *orc6(S116A)* allele is not necessary for the preferential re-initiation of *ARS317* in our “MC_{2A}” strains (i.e. strains with *MCM7-2NLS* and *pGAL-ΔntCDC6,cdk2A*) but enhances the level of initiation 2-3x relative to the wild type *ORC6* allele (data not shown).

Strains used to determine whether or not homology in *cis* is necessary and sufficient for RRIGA (Figure 1, Figure S2, Figure S3) were derived from YJL7906,

which was in turn derived as follows from YJL6974 (*MATa MCM7-2NLS ura3-52::pGAL, URA3*) *ORC2 orc6(S116A) leu2 trp1-289 ade2 ade3 bar1::LEU2 ChrIV_{567kb}::kanMX, ade3-2p, ARS317*) *ars317::natMX*) [3]. YJL7607 was derived from YJL6974 by selection on 5-fluoroorotic acid for loss of pJL806 integrated at *ura3-52*. YJL7906 was derived from YJL7607 by loop-in/loop-out gene replacement of *ura3-52* with *ura3-ΔORF* using *SmaI*-linearized pKJF017.

YJL8100, YJL8104, YJL8108, and YJL8112 were derived from YJL7906, YJL7954, YJL7964, and YJL7993, respectively, by loop-in/loop-out gene replacement of *ura3-ΔORF* with *tACT1-pGAL1/10-ΔntCDC6, cdk2A-tCDC6* using *SmaI*-linearized pKJF019. YJL7954 was derived from YJL7906 by loop-in/loop-out gene replacement of *YDRCTy2-1* with version 1 of *RA3* using *BglIII*-linearized pKJF013. YJL7964 and YJL7993 were derived from YJL7906 and YJL7954, respectively, by loop-in/loop-out gene replacement of *YDRCTy1-1* with version 1 of *UR* using *SpeI*-linearized pKJF014.

YJL8355, YJL8359, and YJL8363/8364 were derived from YJL8259, YJL8271, and YJL8274, respectively, in two steps. An 1162 bp *HindIII* restriction fragment of pJL124 containing the *URA3* gene was used to convert *ura3-ΔORF* to *URA3*. Then a 3350 bp *NgoMIV-Asp781I* restriction fragment of pKJF019 was used to replace *URA3* with *tACT1-pGAL1/10-ΔntCDC6, cdk2A-tCDC6*. YJL8259 was derived from YJL7906 by loop-in/loop-out gene replacement of *YDRCTy2-1* with version 2 of *RA3* using *PacI*-linearized pKJF021. YJL8271 and YJL8274 were derived from YJL7906 and YJL8259, respectively, by loop-in/loop-out gene replacement of *YDRCTy1-1* with version 2 of *UR* using *EagI*-linearized pKJF022.

The non-re-replicating control strain (YJL9149/9150/9151) used in the uracil prototrophy assay (Figure S2) was derived from YJL8274 in 2 steps. An 1162 bp *HindIII* restriction fragment of pJL124 containing the *URA3* gene was used to convert *ura3-ΔORF* to *URA3*. Then a 2113 bp *NgoMIV-Asp781I* restriction fragment of pKJF020 was used to replace *URA3* with *tACT1-pGAL1/10-tCDC6*.

Strains used to determine which recombination factors are involved in RRIGA using the uracil prototrophy assay (Figure 3) are all derived from YJL8363. YJL8407/8408, YJL8409/8410, YJL8412/8413, YJL8415/8416, YJL8418/8419, and YJL8421/8422 were generated by replacing *DNL4*, *RAD52*, *RAD51*, *RAD1*, *MSH3*, or *POL32*, respectively, with *TRP1*. Disruption fragments were generated using PCR in two steps. Step 1 primers (see Table S7) were used to amplify *TRP1* from pRS304 and add short regions of homology flanking the target gene. Step 2 primers extended the region of homology, using the PCR product obtained in Step 1 as a template.

Strains used to determine which recombination factors are involved in RRIGA using the sectoring assay (Figure S4) are all derived from YJL6558 (*MATa MCM7-2NLS ura3-52:: {pGAL-ΔntCDC6-cdk2A, URA3} ORC2 orc6(S116A) leu2 trp1-289 ade2 ade3 bar1::LEU2 ChrIV_{567kb}:: {kanMX, ade3-2p, ARS317} ars317::natMX*) [3]. YJL7445 and YJL7451 were generated by replacing *RAD1* or *RAD51*, respectively, with *TRP1*. Disruption fragments were generated using PCR in two steps. Step 1 primers (see Table S7) were used to amplify *TRP1* from pRS304 and add short regions of homology flanking the target gene. Step 2 primers extended the region of homology, using the PCR product obtained in Step 1 as a template.

Re-replicating strains (YJL8425/8426) for mapping DSBs by PFGE and Southern blotting (Figure 4, Figure S5) and the non-re-replicating controls (YJL8427/8428) were generated by replacing the *kanMX* drug resistance marker with an *hphMX* drug resistance marker along with an I-SceI recognition sequence in YJL6558 and YJL6974, respectively. The replacement fragment was generated using PCR to amplify the *hphMX* marker from pAG26 (see Table S7 for primers). A long tailed primer was used to add the I-SceI site and homology to the *ade3-2p* element in the reporter cassette upstream of *pTEF* in the *hphMX* marker.

All of the strains in which the location of *URA3* gene fragments at the amplicon endpoints were varied (Figure 5, Figure 6, Figure S7) were derived from YJL8842.

YJL8842 was in turn derived from YJL8807 by deleting sequence from *tQ(UUG)D2* to *YDRCdelta9* through a loop-in/loop-out replacement using *EagI*-linearized pKJF027. YJL8807 was in turn derived from YJL8100 by deleting sequence from *YDRCdelta2* to *tQ(UUG)D1* through a loop-in/loop-out replacement using *PacI*-linearized pKJF026.

YJL9115/9116, YJL9118/9119, YJL9121/9122, YJL9127/9128, YJL9130/9131, YJL9133/9134 were all derived from YJL9054 by integrating a PCR product containing the *UR* element and a *TRP1* gene at ChrIV_{607kb}, ChrIV_{650kb}, ChrIV_{753kb}, ChrIV_{875kb}, ChrIV_{985kb}, or ChrIV_{1100kb}, respectively. YJL9136/9137 was derived from YJL9056 by integrating a PCR product containing the *UR* element and a *TRP1* gene at ChrIV_{592kb}. YJL9139/9140 was derived from YJL9057 by integrating a PCR product containing the *UR* element and a *TRP1* gene at ChrIV_{576kb}. YJL9142/9143 was derived from YJL9060 by integrating a PCR product containing the *UR* element and a *TRP1* gene at ChrIV_{713kb}. YJL9145/9146 was derived from YJL9062 by integrating a PCR product containing the *UR* element and a *TRP1* gene at ChrIV_{753kb}. YJL9147/9148 was derived from YJL9067 by integrating a PCR product containing the *UR* element and a *TRP1* gene at ChrIV_{753kb}. Integration constructs were generated using PCR in two steps. Step 1 primers (see Table S7) were used to amplify the *UR* element and *TRP1* from pKJF028 and add short regions of homology flanking the target site. Step 2 primers extended the region of homology, using the PCR product obtained in Step 1 as a template.

YJL9054, YJL9056, YJL9057, YJL9060, YJL9062, and YJL9067 were derived from YJL8842 by integrating a PCR product containing the *RA3* element and an *hphMX* drug resistance marker at ChrIV_{515kb}, ChrIV_{545kb}, ChrIV_{565kb}, ChrIV_{576kb}, ChrIV_{607kb}, or ChrIV_{650kb}, respectively. Integration constructs were generated using PCR in two steps. Step 1 primers (see Table S7) were used to amplify the *RA3* element and *hphMX* from pKJF029 and add short regions of homology flanking the target site. Step 2 primers extended the region of homology, using the PCR product obtained in Step 1 as a template.

Strain Growth and Induction of Re-Replication

For synthetic medium, 1x amino acid concentrations were as described [6], except the amount of leucine was doubled to 60 $\mu\text{g}/\text{mL}$ and the amount of serine was halved to 200 $\mu\text{g}/\text{mL}$. “C” indicates complete medium (all amino acids added). With the exception of plates for red/pink colony color development for the sectoring screen assay, all synthetic medium contained 2x amino acids. Color development plates contained 1x amino acids except 0.5x adenine (10 $\mu\text{g}/\text{mL}$). Synthetic medium contained 2% wt/vol dextrose. For SDC+5-FOA plates 5-fluorouracil was added to a final concentration of 1 mg/mL. All cell growth was performed at 30°C.

To obtain reproducible induction of re-replication, cells were diluted from a fresh unsaturated culture grown in YEPD (YEP + 2% Dextrose) into YEPraf (YEP + 3% wt/vol raffinose + 0.05% wt/vol dextrose) and allowed to grow exponentially for 12–15 hr overnight until they reached an OD_{600} of 0.2–0.8. At this cell density, 15 $\mu\text{g}/\text{mL}$ nocodazole (Sigma M1404 or US Biological N3000) was added for 120–150 min to arrest cells in G2/M phase. The *GALI* promoter (*pGALI*) was then induced by addition of 2–3% galactose for 3 hr (or 6 hours for break mapping experiments). Tight maintenance of the arrest was confirmed by analyzing the distribution of total DNA content by flow cytometry as previously described. For the cultures used for mapping DSBs, alpha-factor was also added to a final concentration of 50 ng/mL in order to prevent cells that escape arrest from entering the next S-phase. Following induction cells were plated onto SDC or SDC-Ura for the uracil prototrophy selection assay, or onto color development plates (described above) for the sectoring screen assay.

Colony Sectoring Assay

To score the frequency of red sectors, ~200 colonies were plated per color development plate (see Strain Growth above). Plates were incubated in the dark at 30°C for 5 days, then in the dark at room temperature for 2–6 days until colony color

development was optimal. Plates were randomized and scored blind. Red sectors were counted if: 1) the sectors were greater than 1/8 of the colony, 2) darker red than the neighboring colonies (ie, not a pink sector in a nearly white colony) and 3) the junctions between the red sector and pink colony were largely straight, to minimize sectors due to poor growth. The frequency of sectored colonies was determined by dividing the total sector counts by the total number of viable colonies. This frequency was measured in at least two independent experiments and the mean and standard error of the mean (when 3 or more trials were conducted), or the mean and the standard deviation (when only 2 trials were conducted) are reported (see Table S1).

Uracil Prototrophy Assay

To score the frequency of uracil prototrophs, following induction of re-replication ~5,000 cfu were plated onto each SDC-Ura plate (to isolate uracil prototrophs) and ~250 cfu onto each SDC plate (to determine an accurate cfu plated onto the SDC-Ura plates). Plates were incubated at 30°C for 3-5 days, then colonies were counted. The frequency of uracil prototrophs was determined by dividing the total number of colonies on the SDC-Ura plates by the number of cfus plated on the SDC-Ura plates. This frequency was measured in at least two independent experiments and the mean and standard error of the mean (when 3 or more trials were conducted), or the mean and the standard deviation (when only 2 trials were conducted) are reported (see Table S3). We note that this assay would score colonies that would not satisfy the criteria of red sector morphology described above, and consequently this assay consistently gave higher frequencies than the sectoring assay.

Pulsed Field Gel Electrophoresis and Southern Blotting

To make plugs for PFGE, 6×10^8 cells were transferred to a 50 mL conical tube and NaN_3 was added to a final concentration of 0.1%. Cells were then pelleted, washed

twice with ice-cold 50 mM EDTA, then resuspended to 500 μ L with 50°C SCE (1 M sorbitol, 0.1 M Na citrate, and 10 mM EDTA). Lyticase (L5263; Sigma) was added to a final concentration of 150 U/mL, and 475 μ L of the sample was mixed with 475 μ L of molten, 50°C 1% InCert agarose (Lonza, Rockland, ME), and then aliquoted into disposal plug molds (170-3713; Bio-Rad). The plug molds were allowed to solidify at 4°C, and then placed in SCEM + lyticase (1 M sorbitol, 0.1 M Na citrate, 10 mM EDTA, 5% β -mercaptoethanol (vol/vol), and 160 U/mL lyticase) for ~40 hr at 37°C. Plugs were then washed three times in $T_{10}E_1$ (10 mM Tris, pH 8.0, and 1 mM EDTA) for 1-2 hr each wash and resuspended in proteinase K solution (1% sarcosyl (wt/vol), 0.5 M EDTA, and 2 mg/ml proteinase K (Roche)) for >48 h at 55°C. Finally, plugs were washed five times in $T_{10}E_1$ for 1-3 hr each wash. The third $T_{10}E_1$ wash contained 1 mM PMSF to inactivate residual proteinase K. Plugs were then stored at 4°C in 0.5 M EDTA until used.

1/3 of each plug was cut off and washed twice with $T_{10}E_1$ for 1-3 hr on ice each wash. Plugs were then soaked in fresh $T_{10}E_1$ at 37°C for 16.5 hr (removes background fluorescence during ethidium bromide visualization of the gel). Plugs were then cooled to 4°C. Plugs were then soaked in 1x I-SceI digest buffer (Roche) on ice for 45 min. Then plugs were placed in 50 μ L of 1x I-SceI digest buffer + 1 μ L of I-SceI Enhancer (20 μ g/mL, Roche) + 4 μ L of I-SceI (10 U/ μ L, Roche) on ice for 1 hr. Digestion was started by adding $MgCl_2$ to a final concentration of 5 mM and placing the plugs at 37°C. Digest proceeded for 1 hr, then plugs were placed in $T_{10}E_1$.

Plugs were loaded on a 1% SeaKem LE agarose (wt/vol) gel in 0.5x TBE (45 mM Tris, 45 mM borate, and 1 mM EDTA). A Lambda concatamer ladder (170-3635, Bio-Rad) was included for sizing purposes. The gel was electrophoresed in 14°C 0.5x TBE on a CHEF DR-III system (Bio-Rad) with initial switch time of 50 s, final switch time of 95 s, run time of 26 h, voltage of 6 V/cm, and angle of 120°. The gel was stained with 1 μ g/mL ethidium bromide in 0.5x TBE for 30 min, then exposed to 130 mJ/cm² UV light using a Stratalinker 2400 (Stratagene, La Jolla, CA) to nick chromosomal DNA.

The gel was then destained in deionized water for 30 min, and quickly imaged with an AlphaImager. The gel was then soaked in two changes of denaturation buffer (0.5 N NaOH, 1.5 M NaCl) at RT for 15 min each. After rinsing with deionized water the gel was soaked in two changes of neutralization buffer (1.0 M Tris-Cl, 1.5 M NaCl, pH 7.5) at RT for 15 min each. The DNA was then transferred to a Roche positively charged nylon membrane using neutral downward capillary transfer (20X SSC, pH 7.0 used as transfer buffer). DNA was cross-linked to the membrane with 120 mJ/cm² of UV light in a Stratalinker 2400. The membrane was probed with a *MAK21* probe generated by PCR from yeast genomic DNA with oligonucleotides OJL2449 and OJL2450, and a *YOS9* probe generated by PCR from yeast genomic DNA with oligonucleotides OJL2231 and OJL2232. A Lambda probe was used to detect the sizing ladder. Images were collected using a Typhoon 9400 (GE Healthcare).

Break Mapping and Quantification

In our system a portion of Chromosome IV molecules at the G2/M boundary were induced to re-replicate *ARS317*, and a portion of these re-replicated chromosomes experienced breaks at various distances from *ARS317*. We wished to estimate the fraction of G2/M Chromosome IV that ended up acquiring a break within each approximately 2.5 kb distance interval from *ARS317*. To do this our analysis of the signal intensity from the southern blot had to correct or normalize for lane to lane differences in sample loading and run distance, for background lane signal from the T=0 hr (pre-induction MC_{2A}) sample, and for nonlinearity of fragment migration versus fragment size. Our starting point was a quantification of intensities obtained with ImageJ software (NIH) using a line trace about half the width of each lane. ImageJ divides each line trace vertically into a stack of thin lane slices each with a height of 0.2 mm along the length of the lane. The software then assigns an intensity value for that slice (an average of the intensity across the width of the slice). This list of intensities versus lane slices was exported to Excel

(Microsoft Corp.) for analysis.

To correct for slight lane to lane variability in electrophoretic migration, we offset all the lists so that a minor re-replication independent band (labeled in Figure S5 with an asterisk) aligned across all the lanes. This only required shifting lanes up or down by at most four slices relative to the adjacent lane(s).

To normalize for sample loading variability we assumed that the total signal in each lane (which comes from hybridization to a probe within 5 kb of *ARS317*) should be proportional to the amount of DNA in the *ARS317* re-replication peak as determined by aCGH. The aCGH peaks at the 3 hr and 6 hr time-points were 1.40625 and 1.84375 times the 2C DNA content at 0 hr (pre-induction) (data not shown). Hence the normalization scalar used for the list of 3 hr signal intensities was $[(\text{Total 0 hr Lane Signal})/(\text{Total 3 hr Lane Signal})]*1.40625$ and that used for the list of 6 hr signal intensities was $[(\text{Total 0 hr Lane Signal})/(\text{Total 6 hr Lane Signal})]*1.84375$. The total signal in each lane included all signal intensity from the well at the top of the lane to the end of the smear of fragmented DNA near the bottom of the lane so that all chromosome structures and fragments contributed to this normalization.

To correct for the background signal (T=0 hr lane) and thereby isolate the re-replication dependent signal at 3 hr and 6 hr, we subtracted the intensity for each lane slice at T=0 hr from the equivalently positioned slice at T=3 hr and T=6 hr. These re-replication induced signal intensities were then divided by the total signal in the T=0hr lane (including molecules trapped in the well) to obtain for each slice an amount of re-replication induced fragmentation as a percent of starting G2 chromosomes.

A Lambda DNA concatamer ladder run in parallel was used to assign the migration positions of fragments that increase in size steps of 48.5 kb. The physical distance separating each concatamer interval only underwent small changes between 97 kb to 485 kb for the southern analysis of breaks to the left of *ARS317* and between 145.5 kb to 485 kb for the southern analysis of breaks to the right of *ARS317*. Thus, within

each concatamer interval in these size ranges, we presumed that the relationship between fragment size and migration distance was almost linear. The number of ImageJ lane slices assigned to each concatamer interval was between 16 and 22 in these size ranges. We separated the physical distance between each concatamer interval (representing a 48.5 kb range of fragment sizes) into 20 equal subintervals (representing a 2.425 kb range of fragment sizes), lined them up against the ImageJ lane slices, and identified the lane slice that overlapped the center of each subinterval. The fragmentation percent of that lane slice was then assigned to the subinterval after normalizing for the difference in physical height. For example, if the subintervals were only 0.18 mm in height (as opposed to the 0.2 mm height of the lane slices) the fragmentation percent was corrected by a factor of 0.18/0.20.

The relationship between fragment size and distance migrated became substantially non-linear for smaller fragments (between 48.5 kb and 97 kb for breaks to the left of *ARS317* and between 48.5 and 145.5 kb for breaks to the right of *ARS317*). Hence a polynomial fit for migration distance versus fragment size was calculated using the three smallest lambda concatamers (48.5kb, 97 kb, and 145.5 kb) and used to determine the center and height of each 2.425 kb subinterval in these regions. With the center and height, a fragmentation percent could be assigned to each subinterval as described above.

Finally, the fragmentation percent for each subinterval was plotted (using the midpoint of each subinterval) as a function of distance in kb from *ARS317*. This required one last adjustment because the fragment sizes from the Southern analysis map the distance of breaks relative to the I-SceI cut site. Those distances were adjusted by 5579 bp to account for the distance between *ARS317* and the I-SceI cut site.

Because our assumptions of linearity between fragment size and migration distance within each concatamer interval only approximated the true relationship between these two parameters, there are discernable discontinuities in the plot, especially at

positions corresponding to the concatamer fragment sizes. Nonetheless the plot provides a good overall representation of the decline in break frequency as a function of distance from *ARS317*.

Our calculations also implicitly assume that every truncated linear chromosomal fragment comes from a separate chromosome; that is, no individual chromosome molecule gives rise to more than one fragment. If both the leading and lagging strands of a given fork were to break, however, this assumption would attribute these fragments to two separate re-replicating chromosomes when only one was actually involved. Nonetheless, in the unlikely case where every fork breaks on both strands, we would overestimate the fraction of chromosomes acquiring a break by at most two-fold. Hence, even if we corrected for such an extreme scenario, our data would still indicate a significant number of DSBs arise as a function of re-replication at positions compatible with our SSA model.

Genomic DNA Preparation for aCGH Analysis

Method 1: Isolates from the sectoring assay were cultured in YEP + 8% Dextrose until they reached saturation (so that most cells were in stationary phase with a 1C DNA content). Isolates from the uracil prototrophy assay were cultured in SDC-Ura media until they reached saturation (so that most cells were in stationary phase with a 1C DNA content), or alpha factor was added to a final concentration of 100 ng/uL (to arrest cells with a 1C DNA content). For all isolates, ~25 OD units of cells were harvested and suspended in 1 mL of sterile water in microfuge tubes. Cells were then vortexed to wash and pelleted. The water was then aspirated off and the cell pellets were snap-frozen in liquid nitrogen. Cell pellets were thawed and resuspended in 200 uL of lysis buffer (2% Triton X-100, 1% SDS, 100 mM NaCl, 10 mM Tris-Cl, 1 mM EDTA (pH 8.0)). To this suspension 200 uL of phenol:chloroform:isoamyl alcohol (25:24:1) and 200 uL of acid washed glass beads (0.5 mm) were added (BioSpec Products, Inc., Bartlesville, OK). Cells were then lysed at room temperature using a Vortex-Genie 2 (Scientific

Industries, NY) at top speed for 10 minutes. To the lysate 450 uL of 10 mM Tris-Cl, 1 mM EDTA (pH 7.5) was added, and the mixture was vortexed for 30 seconds. The mixture was then centrifuged at room temperature for 3 minutes at 20,800 x g. 500 uL of the aqueous phase was transferred to a new microfuge tube, to which 1 uL of 100 mg/mL RNase A (Qiagen, CA) was added. Samples were incubated at 37°C for 1-5 hours to allow digestion of the RNA. 300 uL of phenol:CHCl₃:isoamyl alcohol (25:24:1) was added to each sample, which were then mixed at room temperature for 5 minutes on a multi-mixer (Tomy Tech USA, CA), then centrifuged at room temperature for 3 minutes at 20,800 x g. 400 uL of the aqueous phase was transferred to a new microfuge tube. 300 uL of CHCl₃:isoamyl alcohol (24:1) was added to each sample. Samples were mixed by shaking at room temperature and were then centrifuged at room temperature for 3 minutes at 20,800 x g. 300 uL of the aqueous phase was transferred to a new microfuge tube, to which 750 uL of 100% Ethanol and 3 uL of 10N NH₄OAC (pH 7). Samples were vortexed then centrifuged at room temperature for 7 minutes at 20,800 x g to pellet the DNA. Pellets were washed with 70% Ethanol the air dried. The DNA was suspended in 50 uL of 2 mM Tris-Cl (pH 7.8).

Method 2: To measure re-replication peaks (see Figure S4A) NaN₃ was added to a final concentration of 0.1% to 250 mL cultures (arrested with nocodazole and induced to re-replicate, as described above). To prepare reference DNA for all arrays (copy number as well as re-replication analysis), NaN₃ was added to a final concentration of 0.1% to 250 mL or 450 cultures that were arrested with alpha factor (final concentration = 100 ng/mL) or nocodazole (final concentration = 15 µg/mL). NaN₃ treated cultures were added to 25 mL or 50 mL (for 250 mL or 450 mL cultures, respectively) of frozen, -80°C, 0.2 M EDTA, 0.1% NaN₃. Cells were pelleted, washed with 50 mL of 4°C TE (10 mM Tris-Cl, 1 mM EDTA pH 7.5) and stored frozen at -80°C. Pellets were resuspended in 4 mL lysis buffer (2% Triton X-100, 1% SDS, 100 mM NaCl, 10 mM Tris-Cl, 1 mM EDTA pH

8.0) and mixed with 4 mL of phenol:CHCl₃:isoamyl alcohol (25:24:1) and 8 mL of acid-washed 0.5 mm glass beads (BioSpec Products, Inc., Bartlesville, OK). The suspension was vortexed seven times for 2-3 min separated by 2-3 min intervals at RT to get at least 95% of the cells lysed. The lysate was diluted with 8 mL phenol:CHCl₃:isoamyl alcohol (25:24:1) and 8 mL TE, vortexed once more, and then centrifuged at 18,500 x g for 15 min at RT. After collecting the aqueous phase, the interphase was re-extracted with 8 mL TE, and the second aqueous phase from this re-extraction pooled with the first. The combined aqueous phases were extracted with an equal volume of CHCl₃. The bulk of the RNA in the extract was selectively precipitated by addition of 0.01 volume 5 M NaCl (to a final concentration of 50 mM) and 0.4 volumes isopropanol followed by centrifugation at 9,000 x g for 15 min at RT. The RNA pellet was discarded and an additional 0.4 volumes of isopropanol was added to the supernatant to precipitate the DNA. Following centrifugation at 9,000 x g for 15 min at RT, the pellet was washed with 70% ethanol, dried, and resuspended with 3.5 mL of 10 mM Tris-Cl (pH 8), 1 mM EDTA. RNase A (Qiagen, Valencia, CA) was added to 340 µg/mL and the sample incubated at 37°C for 30-60 min. Then Proteinase K was added to 555 µg/mL followed by another incubation at 55°C for 30-60 min. Finally, 0.5 mL of 10% (w/v) Cetyltrimethylammonium Bromide (CTAB, Sigma H6269), 0.9 M NaCl (prewarmed to 65°C) and 0.9 mL of 5 M NaCl was added. The sample was incubated for 20 min at 65°C before being extracted with 8 mL CHCl₃:isoamyl alcohol (24:1) and centrifuged at 6000 x g for 15-180 min at RT. The DNA in the aqueous phase was precipitated with 0.8 volumes isopropanol at RT, washed with 70% ethanol, dried, and resuspended in 6 mL of 25 mM Tris-Cl (pH 7), 1 mM EDTA. RNase A (Qiagen, Valencia, CA) was added to 33 µg/mL and the sample incubated at 37°C for 15 min. Then the following were added to the sample in the order listed: 1) 1.5 mL of 5 M NaCl; 2) 0.5 mL of 1M MOPS (pH 7); 3) 0.5 mL of Triton X-100 (3% vol/vol); 4) 1.5 mL of isopropanol. The sample was then mixed by vortexing, then purified on a Qiagen Genomic-tip 100/G column as per the

manufacturer's instructions (Qiagen, Valencia, CA). The eluted DNA was precipitated with 0.8 volumes isopropanol at 4°C, washed with 70% ethanol, dried, and resuspended in 275 µL of 2 mM Tris-Cl pH 7.8. Genomic DNA was then sheared by sonication with a Branson Sonifier 450 to an average fragment size of 500 bp.

aCGH Analysis of Gene Amplification

50-100% of each DNA sample (prepared using Method 1 above) was labeled with Cy3 or Cy5 and 1.5-2µg of purified reference DNA from YJL6974 or YJL7695 (prepared using Method 2 above) was labeled with Cy5 or Cy3 (whichever was not used for the test sample) essentially as described. The labeled DNA was isolated using one of two previously described methods (low-throughput [7] or high-throughput [8]). All samples were hybridized and analyzed as described [7]. Detailed results for aCGH of isolates from the sectoring screen assay and the uracil prototrophy assay are listed in Table S2 and Table S4, respectively.

aCGH Analysis of Re-replication

2-2.5µg of each DNA sample (prepared using Method 2 above) was labeled with Cy5 and 1.5-2µg of purified reference DNA from YJL7695 (prepared using Method 2 above) was labeled with Cy3 essentially as described [7], and labeled DNA was isolated as previously described [7]. All samples were hybridized and analyzed as described [7].

Error Calculation for RRIGA in Mutant Strains

RRIGA frequency is dependent upon how much re-replication occurs in a given strain. Since deletion of certain genes impacts the amount of re-replication from *ARS317* in our MC_{2A} strain background, the RRIGA frequencies reported in Figure 3 are normalized against a given strains amount of re-replication.

The amount of re-replication for a given strain for a 3 hr induction was measured

using aCGH for 3 independent cultures for each strain (4 cultures for wild-type). The average peak value over the 2C baseline +/- 1 standard deviation was determined.

The frequency of uracil prototrophs measured is also subject to error, so this error was combined with the error from re-replication measurements to generate a “Combined Error” value as follows:

$$\textit{Combined Error} = (\textit{Relative Combined Error}) \times (\textit{Normalized Mean Amp. Freq.})$$

where
$$\textit{Relative Combined Error} = \sqrt{(a/b)^2 + (c/d)^2}$$

where $a = \textit{Standard Deviation of Re – replication Peak Value}$

$b = \textit{Mean Re – replication Peak Value}$

$c = \textit{Standard Deviation of Amplification Frequency}$

$d = \textit{Mean Amplification Frequency}$

and where

$\textit{Normalized Mean Amp. Freq.}$

$$= (\textit{Mean Amp. Freq.}) / (\textit{Mean Re – replication Peak Value})$$

The data shown in Figure 3B represents the Normalized Mean Amplification Frequency +/- Combined Error. Note that the amplification used in this figure is the “Induced Amplification Frequency”, which is computed as the frequency post induction minus the frequency pre-induction.

Junction PCR

Primers used for junction PCR to determine amplicon orientation and preservation of parental junctions are listed in Table S7. PCR was performed using Phusion DNA polymerase (Finnzymes) according to the manufacturer’s instructions. DNA used for junction PCR was prepared using a spheroplasting mini-prep as follows. $\sim 5 \times 10^8$ cells were suspended in 200 uL of 1 M Sorbitol, 0.1 M Sodium Citrate (pH 7.0), 60 mM

EDTA, 0.8% (vol/vol) β -Mercaptoethanol, 2 mg/mL Zymolyase 20-T (MP Biomedicals) and incubated at 37°C for 70 min. Then 200 μ L of 100 mM Tris-Cl (pH 9.0), 50 mM EDTA, 2% SDS was added to each sample, inverted to mix, then incubated at 65°C for 5 min. Then 200 μ L of 5 M KAc was added to each sample, inverted to mix, then centrifuged at 20,800 x g for 10 min. 350 μ L of the supernatant was transferred to a new microfuge tube with 800 μ L of 100% Ethanol. Samples were inverted to mix, the DNA was pelleted at RT at 3,800 x g for 2 min. Pellets were washed with 70% Ethanol, air dried, the resuspended in 200 μ L of 0.5x TE (pH 8.0). PCR was performed using 0.25 μ L of this DNA as template (in a 25 μ L reaction).

Supplementary References

1. Natsoulis G, Thomas W, Roghmann MC, Winston F, Boeke JD (1989) Ty1 transposition in *Saccharomyces cerevisiae* is nonrandom. *Genetics* 123: 269–279.
2. Sikorski RS, Hieter P (1989) A system of shuttle vectors and yeast host strains designed for efficient manipulation of DNA in *Saccharomyces cerevisiae*. *Genetics* 122: 19–27.
3. Green BM, Finn KJ, Li JJ (2010) Loss of DNA replication control is a potent inducer of gene amplification. *Science* 329: 943–946.
doi:10.1126/ science.1190966.
4. Green BM, Li JJ (2005) Loss of rereplication control in *Saccharomyces cerevisiae* results in extensive DNA damage. *Mol Biol Cell* 16: 421–432.
doi:10.1091/mbc.E04-09-0833.
5. Goldstein AL, McCusker JH (1999) Three new dominant drug resistance cassettes for gene disruption in *Saccharomyces cerevisiae*. *Yeast* 15: 1541–1553.
doi:10.1002/(SICI)1097-0061(199910)15:14<1541::AID-YEA476>3.0.CO;2-K.
6. Sherman F (2002) Getting started with yeast. *Meth Enzymol* 350: 3–41.

7. Green BM, Morreale RJ, Ozaydin B, DeRisi JL, Li JJ (2006) Genome-wide Mapping of DNA Synthesis in *Saccharomyces cerevisiae* Reveals That Mechanisms Preventing Reinitiation of DNA Replication Are Not Redundant. *Mol Biol Cell* 17: 2401–2414. doi:10.1091/mbc.E05-11-1043.
8. Pleiss JA, Whitworth GB, Bergkessel M, Guthrie C (2007) Transcript specificity in yeast pre-mRNA splicing revealed by mutations in core spliceosomal components. *PLoS Biol* 5: e90. doi:10.1371/journal.pbio.0050090.

Chapter 4

Re-Replication Underlies Spontaneous Segmental Amplification in Normal *S. cerevisiae* Cells

Abstract

Duplication and/or amplification of existing genes have long been recognized as major driving forces in the creation of new genes during evolution. Gene amplification also plays a major role in tumor initiation and/or progression, and frequently underlies acquired resistance to chemotherapeutics. Structural analysis of many of the observed amplifications in both evolution and oncogenesis show evidence of non-allelic homologous recombination in their genesis, however the underlying events that cause such ectopic recombination remain largely obscure. The prevailing models forwarded to explain such amplifications posit that simple double stranded breaks or replication stress constitutes the initiating event. These insults then stimulate ectopic recombination via a gene conversion like mechanism, or break-induced replication. We recently reported evidence for an alternative, re-replication driven mechanism wherein the initiating event is instead a pair of breaks, one arising at each fork of a re-replication bubble in a *trans* configuration. Also in contrast to other models, single-stranded annealing is the major recombination pathway involved in resolution of the broken bubble intermediate, not gene conversion or break-induced replication. Here we present evidence suggesting that sporadic, infrequent re-initiation of replication drives spontaneous gene amplification. We report the identification of a recurrent spontaneous segmental amplification in budding yeast with intact replication controls. These amplifications remain at the endogenous chromosomal locus, arranged as head-to-tail repeats, and are bounded by repetitive Ty elements. Strains engineered to be more prone to spontaneous re-initiation have dramatically higher rates of amplification than strains designed to suffer replication stress. Furthermore, genetic analyses reveal that amplification in both a wild-type context as well as in a strain with minor deregulation of re-initiation control depends upon single-stranded annealing, consistent with our model for re-replication induced gene amplification. Taken together, these results indicate that occasional re-replication is a likely driver of spontaneous gene amplification, and hence may underlie duplication/

amplification events during evolution and oncogenesis.

Introduction

Duplication and amplification of genes play an important role in the emergence of new genes with novel functions during evolution by providing a substrate for adaptive innovation [1–3]. Furthermore, the increase in gene product dosage conferred by an increase in gene copy number can itself lead to phenotypic consequences, potentially providing a selective advantage. This latter situation can be well applied to gene amplification in the context of oncogenesis as well. Amplification of oncogenes can drive the initiation and/or progression of human cancers, and gene amplification can also confer resistance to chemotherapeutic agents [4–6]. Copy number expansions also contribute to human copy number variation [7,8]. Despite their importance in an array of biological contexts, the source of many gene duplications/amplifications remains unknown.

The structure of many of the gene duplications and amplifications observed suggests some form of non-allelic homologous recombination (NAHR) in their genesis. This observation has led to the proposal of a number of mechanisms for gene amplification that incorporate some form of NAHR in the resolution of some intermediate state into a final amplification structure. The most popular among these various mechanisms is the so called unequal exchange model, which is essentially a variation on normal allelic recombination, also known as gene conversion (GC) [9–11]. According to this model the precipitating insult is a double stranded break, perhaps resulting from replication stress leading to the collapse of a replication fork. An imperfect search for the proper repair template on a sister chromatid or homolog can result in a misalignment, leading to the use of a homologous, but non-allelic, sequence as a repair template. Resolution of the resultant double Holliday junction intermediate structure as a crossover generates reciprocal expansion and deletion events. Experimental evidence for this model is limited, primarily having been observed in the context of large arrays

of repetitive sequences [12–16]. Similarly, there is little evidence to support a variation of this model which invokes a form of break-induced replication (BIR) instead of a gene conversion-like mechanism [17].

We recently described an alternative mechanism for generating copy number expansions driven by re-replication [18,19]. Re-initiation of replication from a single origin leads to an isolated replication bubble. These forks eventually break, generating a pair of double stranded breaks, one at each fork. This broken bubble intermediate is resolved through single-stranded annealing (SSA) mediated NAHR between repetitive elements that flank the re-initiating origin. Given the remarkable efficiency of Re-Replication Induced Amplification (RRIGA) that we observed when we experimentally caused limited amounts of localized re-replication, we speculated that RRIGA may underlie spontaneous amplification events in an evolutionary context. Here we present evidence supporting this speculation. We identified a recurrent spontaneous amplification, which is structurally consistent with RRIGA, in cells with intact replication controls. While replication stress has a limited ability to stimulate this particular amplification, slight disruption of replication control can boost the rate dramatically. Furthermore, this amplification is dependent on SSA, consistent with RRIGA. Thus, we believe this work strongly supports a role for RRIGA in spontaneous amplifications in evolution, and similarly should be seriously considered as a driving force in copy number expansions in human copy number variation and oncogenesis.

Results

A Recurrent, Spontaneous Amplification Structurally Consistent with RRIGA

Deletion of the *PDS1* gene in budding yeast, which encodes Securin, renders cells temperature sensitive [20]. Cells are unable to proliferate at elevated temperatures (i.e. 31°C), but are able to do so at lower temperatures (i.e. 24°C). However, rare survivors can be isolated from *pds1Δ* populations that are able to grow and divide at

higher temperatures. We examined some such survivors by aCGH during the course of other studies and found that they often bore a segmental amplification of a portion of Chromosome VII, ranging from 145-280 kb in size and including the *ESPI* gene, which encodes Separase (data not shown).

We sought to determine what proportion of the survivors bear such amplifications to assess the importance of gene amplification relative to other means of suppressing temperature sensitivity. Toward this end, we developed a fluorescence activated cell sorting (FACS) assay for identifying amplifications amongst the survivors (Figure 1A). We introduced an *eGFP* fluorescent reporter gene near the *ESPI* gene, as well as a *dTomato* fluorescent reporter gene near the centromere of Chromosome IV. An amplification including the *ESPI* gene will also result in an amplification of the *eGFP* gene, resulting in increased *eGFP* expression and fluorescence. Meanwhile, the *dTomato* gene will remain at a single copy. Thus, amplification of the *ESPI* gene in a given survivor is revealed as increase in the eGFP/dTomato signal intensity ratio as measured by FACS. Using this strategy we found that amplification does indeed make a substantial contribution to the overall pool of survivors, varying from ~1/5 to ~3/4 of the total survivor pool.

A number of survivor isolates determined to have an amplification using the FACS assay were further characterized using aCGH (Figure 1B and data not shown). Intriguingly, the boundaries of the observed segmental amplifications invariably coincided with repetitive Ty elements or LTRs, suggesting that they arose through some form of non-allelic homologous recombination (NAHR). We therefore analyzed the structure of the amplifications further in a few of the isolates using pulsed field gel electrophoresis (PFGE) and Southern blotting to determine if the amplicons remained on the original chromosome and to elucidate the orientation of the amplicons with respect to each other (ie. direct or inverted repeats) (Figure 1C,D). Only isolates that appeared to bear a duplication were selected for this analysis. Southern analyses of intact

chromosomal DNA separated by PFGE using probes that hybridize to *ESPI* (within the amplicon) or *ADH4* (near the left telomere of Chromosome VII) yielded identical results, indicating that all amplicons remained on the original chromosome (Chr VII). Orientation was assessed using an asymmetric digest strategy in conjunction with PFGE and Southern analysis. Chromosomal DNA was digested with a rare cutting restriction enzyme that cuts only once within the amplified sequence, separated by PFGE, then probed for sequences to either side of the cut site within the amplicon. Amplicons arrayed as head-to-tail, head-to-head, or tail-to-tail repeats will yield distinct banding patterns for these two hybridizations owing to the asymmetric position of the cut site within the amplicon. This analysis revealed that all isolate populations examined have amplicons arrayed as direct, head-to-tail repeats.

We note that multiple products are evident in the Southern analyses of both intact and digested chromosomal DNA. Since these isolate populations are unstable and must be expanded at the selective temperature for downstream analysis, secondary events are common, leading to mixed populations. Despite this complication, it remains clear that all amplifications detected reside on Chromosome VII. Furthermore, the amplifications in the majority of each population, and in some cases in the entire population, are arrayed in direct repeat.

Duplication/Amplification of the Chromosome VII Segment is More Potently Stimulated by Disruption of Replication Control than by Replication Stress

The structures of the spontaneous amplifications observed here are consistent with those induced by re-replication that we characterized in our previous studies [18,19]. However, this structure is not a unique signature of RRIGA and is also consistent with other NAHR mechanisms. These alternative mechanisms often invoke replication stress as the precipitating event that leads to NAHR [9–11,17]. Therefore, as a first step toward distinguishing between RRIGA and these alternative models, we asked whether

amplification of this particular segment of the genome is sensitive to slight, constitutive disruption of replication control or to chronic replication stress.

The temperature sensitivity suppression system employed to isolate the original amplifications is extremely sensitive to slight fluctuations in both the selective temperature, as well as the permissive temperature used during the initial outgrowth. Moreover, the isolate populations obtained are highly unstable. Thus, this assay proved unsuitable for the quantitative comparisons we wished to make between different strains. So, we devised an alternative assay for measuring the rate of head-to-tail duplications/amplifications of a segment of Chromosome VII (Figure 2). We integrated fragments of a gene (*natR*) that confers resistance to the drug nourseothricin, which was modified to include the *ACT1* intron, into Chromosome VII (Figure 2A). The 3' portion of this gene was integrated ~570 kb from the end of the left telomere, while the 5' portion was integrated at ~700 kb, corresponding to the most *ESPI* proximal left and right boundaries, respectively, of previously observed amplifications in the *pds1Δ* suppression system. The endogenous repetitive sequence elements (Ty elements and LTRs) were removed by these integrations. Importantly, the two *natR* fragments share 459 bp of overlapping sequence identity, providing a substrate for NAHR. A head-to-tail duplication/amplification formed using the two *natR* gene fragments as the boundaries creates a full length, functional *natR* gene at the inter-amplicon boundary. Thus, cells that acquire such a duplication/amplification will become resistant to nourseothricin.

We devised a variation of the classical P_0 method of fluctuation analysis originally developed by Luria and Delbrück to measure the rate of gene amplification using this split *natR* gene reconstitution system (Figure 2B) [21,22]. We seeded 96 separate cultures in each well of a deep-well microtiter plate with a small initial population of cells. These cultures were expanded without selection prior to addition of nourseothricin to all but 4 wells of the microtiter plate, which were diluted and plated onto non-selective media to determine the final population size at the time drug was added. The microtiter

plate was then incubated further to allow any nourseothricin resistant cells, which bear the segmental amplification of interest, to proliferate. Cultures with one or more resistant cells will eventually grow to saturation, resulting in a 'cloudy' well. On the other hand, the cultures in those wells without any cells bearing the amplification, and hence lacking the ability to proliferate in the presence of drug, remain clear (Figure 2C). The proportion of cultures in which no amplifications (i.e. 'mutants') arose (the P_0) can thus be determined by dividing the number of 'clear' cultures by the total number of cultures (less those used for determining the population size at the time drug was added). The rate of amplification is readily calculated using the P_0 , the initial population size (N_i), and the population size at the time drug was added (N_t).

Re-initiation of replication in budding yeast is normally prevented using a battery of overlapping mechanisms, including CDK phosphorylation of ORC, Cdc6, and Mcm2-7 [23–25]. Disruption of an increasing number of these mechanisms results in progressively more re-replication [26,27]. However, not all regions of the genome are equally susceptible to re-replication. We reasoned that if spontaneous segmental amplification the region of Chromosome VII containing *ESPI* were caused by sporadic re-initiation in cells with intact replication controls, then removal of these control mechanisms might lead to increased re-replication of this region and a corresponding increase in the rate of amplification. So, we assayed the rate of amplification in a series of strains in which we disrupted CDK regulation of ORC, Cdc6, or Mcm2-7 alone, as well as a combination of Cdc6 and Mcm2-7 (Table 1). Hereafter strains with these replication control disruptions will be referred to simply as O, C_{2A} , M, and MC_{2A} , respectively, and will be collectively called 'deregulated strains.' In all cases the rate of amplification was elevated to varying degrees. Removal of CDK regulation of the MCM complex resulted in only a slight increase in the rate of amplification, whereas disruption of Cdc6 or ORC resulted in moderate and dramatic increases in the rates, respectively. The combined disruption of CDK regulation of Cdc6 and Mcm2-7 also caused a massive

increase in the rate of amplification. Thus, amplification of this segment of Chromosome VII can be very efficiently driven through disruption of replication controls, which we presume increases the frequency of spontaneous re-initiation events. Any such re-replication in these strains, however, occurs below the detection limits of existing assays.

It is of course possible that amplification of this region is only caused by re-replication under conditions where control mechanisms are compromised, and that the spontaneous amplifications arise by some other means. Since the competing models for gene amplification involving NAHR often invoke double stranded breaks, or replication stress leading to double stranded breaks, as the initiating event, we also assessed the capacity of replication stress to stimulate amplification by measuring the rate of amplification in strains with hypomorphic, temperature sensitive alleles of replication initiation proteins (Table 2). The presence of these alleles will result in a reduction in the number of origins used during replication. Hence there will be a greater chance of collapsed forks not being rescued by other converging forks from neighboring origins, leading to double stranded breaks. Indeed, strains bearing the temperature sensitive alleles of components of the pre-RC (*orc2-1* or *cdc6-1*) grown at the permissive temperature (23°C) had slightly elevated amplification rates. A strain with a temperature sensitive allele of the catalytic subunit of the Dbf4-dependent kinase (*cdc7-1*), which is required to initiate replication from licensed origins, also had a moderately elevated amplification rate relative to WT. Lastly, a strain carrying a temperature sensitive allele of the catalytic subunit of DNA polymerase alpha (*cdc17-1*), which is required for replication initiation and for priming new Okazaki fragments during replication elongation, grown at a semi-permissive temperature (30°C) displayed a slightly increased rate of amplification relative to wild-type as well. Thus, replication stress is indeed able to stimulate amplification of this segment of Chromosome VII. Hereafter, the strains bearing temperature sensitive alleles of replication proteins will simply be referred to by the relevant allele that they bear (*orc2-1*, *cdc6-1*, *cdc7-1*, or *cdc17-1*), and collectively as

‘replication stress strains.’

Since we cannot directly measure any re-replication that might be occurring in the deregulated strains, and the observation that replication stress can cause some increase in the amplification rate, we wondered whether some portion of the increase in the amplification rate observed in these strains was caused by a defect in normal replication. That is, it is possible that the mutations introduced to prevent CDK regulation of ORC, Cdc6, and Mcm2-7 also compromised their replication activities. To detect evidence of replication stress in these strains we first asked whether there was evidence of an active DNA damage response in exponentially growing cultures of these strains, as measured by phosphorylation of Rad53, a kinase activated in response to DNA damage (Figure 3A) [28]. We examined the replication stress strains in the same manner, each grown at the same temperature used in the fluctuation analyses. As an additional control, each strain was also treated with hydroxyurea (HU) to determine whether or not it is able to fully activate the DNA damage checkpoint, as a previous study with an *orc2-1* strain suggested that replication from too few origins prevents complete activation of the DNA damage response [29]. Indeed, the *orc2-1* strain, as well as the *cdc7-1* strain, shows a somewhat reduced response to the HU treatment compared to the other strains. Only the *cdc17-1* strain, though, showed evidence of a very weak damage response in asynchronous, unperturbed cells using this assay.

Next, we assessed the sensitivity of each strain to the replication inhibitors HU and methyl-methanesulfonate (MMS) using a serial dilution spot growth assay (Figure 3B). We reasoned that strains experiencing replication stress due to defective replication proteins might display increased sensitivity to such inhibitors. In the O and MC_{2A} strains, we did in fact observe a mild sensitivity to the higher concentrations of HU and MMS used, comparable to the degree of sensitivity observed in the *cdc17-1* strain. Disruption of Mcm2-7 or Cdc6 alone, on the other hand, did not confer any increased sensitivity to these agents. The *cdc6-1* and *cdc7-1* strains similarly showed no elevated sensitivity to

these inhibitors. However, the *orc2-1* strain proved exquisitely sensitive to both of these inhibitors.

Lastly we employed a plasmid loss assay to specifically address possible defects in replication initiation (Figure 3C). In this assay, a plasmid will be lost more frequently by strains with defective replication initiation than wild-type cells, due to occasionally failing to replicate the plasmid (see Methods and Materials for details of the assay) [30]. Using this assay, we observed slightly elevated plasmid loss rates for *cdc6-1* and *cdc7-1*, as expected. The *cdc17-1* strain also displayed an increase in plasmid loss. We were unable to isolate stable transformants of the *orc2-1* strain, and hence could not determine a plasmid loss rate here, but a previous study reported a very high loss rate for *orc2-1* [31]. As for the deregulated strains, all have increased plasmid loss rates relative to wild type, comparable to the degree of increase observed in the strains bearing temperature sensitive alleles of replication proteins.

Taking the data from the three ‘replication stress’ assays together, it appears that the deregulated strains may suffer some level of replication stress. However, re-replication itself causes DNA damage and could be responsible for the apparent ‘replication stress’ observed for these strains [19,25,32,33]. But, even if these results are in fact due to defective replication in S-phase, and not due to re-replication, it is clear that the level of stress experience by these strains is at most equal to the levels experienced by the strains with temperature sensitive alleles of replication proteins. Thus, the extremely high rates of amplification observed in some of the deregulated strains cannot be accounted for by replication stress alone, and are likely the result of increased frequencies of spontaneous re-initiation.

When compared to some of the deregulated strains, the amount to which the amplification rate is increased in the replication stress strains is relatively modest. Furthermore, the deregulated strains are quite healthy, with growth rates similar to the wild-type strains. On the other hand, the replication stress strains have severely retarded

growth rates relative to wild-type, even at permissive temperatures. We therefore favor the notion that replication stress is less likely to contribute to spontaneous amplifications than re-replication, as the rate of amplification is increased only modestly even at a level of replication stress that results in a substantial fitness defect. Thus, the very low levels of endogenous replication stress in wild-type cells are likely incapable of accounting for the spontaneous amplifications. Nonetheless, we cannot conclusively rule out a role for replication stress in the genesis of spontaneous amplifications.

Segmental Amplification Depends Upon Single Stranded Annealing

In a previous study we reported that gene amplification caused by experimental induction of re-replication is heavily dependent upon the single-stranded annealing (SSA) subtype of homologous recombination [19]. Other models for gene amplification, on the other hand, invoke either gene conversion (GC) or break-induced replication (BIR) to explain NAHR [9–11,17]. We therefore asked whether the spontaneous amplifications observed here in both the wild-type and O strains require SSA or some other form of homologous recombination for their formation. Toward this end, we generated a series of recombination gene knockouts in both strains then measured the rate of amplification in each using fluctuation analysis as described above (Table 3, Table 4).

Each of the subtypes of homologous recombination has distinct genetic requirements in *S. cerevisiae*. SSA requires Rad1, which functions as part of a structure specific endonuclease that cleaves the non-homologous 3' tails, and Msh3, which acts with Msh2 to stabilize the annealed intermediate [34–36]. These factors do not play a major role in GC or BIR. Consistent with a dominant role for SSA in the formation of the spontaneous amplifications observed here, deletion of either of *RAD1* or *MSH3* results in a dramatic decrease in the rate of amplification in both the wild-type and O contexts. On the other hand, amplification was largely independent of Rad51, which is required for strand invasion in GC and BIR, but is not involved in SSA, again consistent with SSA

being involved in the genesis of the observed spontaneous amplifications in both wild-type cells and cells in which the block to re-initiation is partially compromised [37–41].

Disruption of other recombination factors yielded different results for wild-type and O strains. The most striking difference observed was for disruption of Rad52, which is required for most homologous recombination in budding yeast [42]. While deletion of *RAD52* in the O strain severely reduced the rate of amplification as anticipated, in the wild-type strain the rate actually went up slightly. Since SSA, GC, and BIR all depend upon Rad52 the wild-type result is somewhat puzzling. Rad52 is also involved in the restart of stalled/collapsed replication forks, so we imagine that deletion of *RAD52* may confer some degree of replication stress [43–45]. The rate observed in the *rad52Δ* strain with intact replication controls might therefore be the result of a more complicated situation where the absence of Rad52 compromises SSA-mediated resolution of re-replication driven amplifications, but also stimulates amplification through other pathways. In the O strain the contribution of any replication stress caused by disruption of Rad52 might be dwarfed by the much larger quantitative contribution made by the reduction in SSA-mediated RRIGA. Similarly, disruption of Rad59, which is important for SSA, substantially reduces the rate of amplification in the O strain, yet results in a slight increase in the wild-type strain [46,47]. This might also reflect a complex situation of competing effects that increase or decrease the overall rate of amplification, as suggested for *rad52Δ*.

A previous study of spontaneous amplifications argued that they arise through a form of break induced replication [17]. This conclusion was largely based upon their observation that amplifications detected using an assay based on recovery of normal growth required Pol32, a non-essential subunit of DNA polymerase δ , which is required for BIR, but not GC or SSA [48]. We note, however, that disruption of Pol32 in that study had very little effect on amplifications detected using a different assay based on reconstitution of a split gene, similar to the strategy used here. In our system, Pol32 is

not required for amplifications in the wild-type context, arguing against a role for BIR in their genesis. A decrease was observed in the context of disrupted CDK regulation of ORC, however. Interpretation of this latter result is complicated by the fact that deletion of *pol32Δ* in the O strain resulted in synthetic sickness, which may affect the rate of segmental amplification in an unpredictable manner. No such synthetic interactions were observed with any of the other recombination gene deletions.

The genetic analysis of recombination requirements is most consistent with SSA playing the dominant role in mediating NAHR in spontaneous gene amplifications. Given our previous demonstration that RRIGA depends on SSA, these results are thus also consistent with spontaneous re-initiation of replication driving gene amplification. We note that SSA is typically associated with deletion of sequences between repetitive sequence elements, not amplifications [49]. SSA mediated repair of a simple double stranded break is indeed incompatible with an amplification outcome. However, SSA mediated resolution of the broken bubble intermediate proposed in our RRIGA model, or of a similar structure produced by breakage at both forks of a normal S-phase replication bubble, will generate a head-to-tail amplification. Therefore, taking all of the data presented thus far together, we suggest that sporadic re-replication is very likely a mechanism driving spontaneous amplification in normal cells.

Deletion of Clb5 Drives Gene Amplification Independent of its Effect on Under-Replication

Previous studies on spontaneous amplifications in budding yeast reported that deletion of Clb5, the major S-phase cyclin component of CDK, increases the rate of amplification [17,50]. Both studies suggested that the observed increase in amplification was the result of decreased origin usage in *clb5Δ* strains [51], potentially causing leading to stalled/collapsed replication forks. However, deletion of *CLB5* can also promote re-replication through at least two mechanisms [27,33,52].

To address which role of Clb5, promoting normal replication or blocking re-replication, is important in preventing segmental amplifications and thereby preserving genome integrity we again made use of our split *natR* reconstitution system (Table 5). We first confirmed that deletion of *CLB5* increases the rate of amplification of the segment of Chromosome VII being considered in our assay. Indeed, the *clb5Δ* strain displayed a dramatically higher rate of amplification than the wild-type parent strain. To distinguish between the possibilities of under-replication or failure to prevent re-replication that deletion of *CLB5* might cause, we generated a *clb5Δ clb6Δ* double knockout strain. The late origin firing defect of the *clb5Δ* strain is suppressed by the additional deletion of *CLB6*, resulting in a normal length S-phase, albeit shifted to later time in the cycle. Thus, under-replication should be alleviated in the *clb5Δ clb6Δ*, but the block to re-initiation will still be partially disrupted. Consistent with the primary defect in the *clb5Δ* strain being a failure to oppose re-initiation, the added disruption of *CLB6* failed to suppress the high rate of amplification. This suggests that re-replication, instead of defects in normal replication, might actually underlie the increased rate of amplification observed for *clb5Δ* strains in previous studies.

Discussion

We previously reported that experimental induction of limited, transient re-initiation at a single origin in *S. cerevisiae* causes segmental amplifications to arise at an extraordinary rate [18,19]. This prompted us to hypothesize that even sporadic failure to block re-initiation in cells with intact replication controls might underlie some spontaneous amplification events. Fortunately, we stumbled upon a recurrent, spontaneous amplification event during the course of unrelated studies, providing us with a prime opportunity to critically evaluate that hypothesis. Here we presented evidence that indeed supports a role for re-replication in spontaneous amplification events. These findings in turn suggest that the potential contribution of re-replication to gene

amplification in evolution, oncogenesis, and human copy number variation should be examined.

Multiple Mechanisms for Amplification Involving NAHR

Owing to the rarity of gene amplification events direct molecular observation of the underlying mechanisms has been largely impossible. Therefore, models for gene amplification are primarily based upon the observed final structures of amplifications. Such amplifications adopt a variety of structures, a subset of which are arranged in direct repeat and have homologous sequences at their amplicon boundaries, suggesting that their formation involves NAHR. However, the structure alone cannot reveal the precise mechanism underlying a particular amplification event, as a number of different models are consistent with such a structural outcome. Thus, it is impossible to definitively attribute any amplification event to a particular mechanism retrospectively.

Despite common structural outcomes, different models for amplification involving NAHR predict different initiating events and involve distinct resolution mechanisms. This affords the opportunity to assess the contributions of distinct models for amplification in an experimental setting. The most popular models for generating amplifications in direct repeat involving NAHR propose that the initiating event is a double stranded break, likely caused by replication stress [9–11]. Indeed, from a qualitative perspective we found that increasing replication stress caused an increase in the rate of segmental amplification, supporting the notion that replication stress and double stranded breaks can lead to amplifications. However, from a quantitative perspective replication stress was rather inefficient in stimulating these amplification events. Furthermore, strains engineered to suffer such stress exhibited substantial fitness defects. On the other hand, slight disruption of control mechanisms blocking re-initiation had little to no impact on fitness. These disruptions generally led to dramatically higher rates of amplification, indicating that sporadic re-initiation is extremely efficient

at stimulating amplification. Given the greater efficiency of re-replication at causing segmental amplifications than replication stress, and the difference in apparent fitness costs, we propose that re-replication might play the larger role in promoting spontaneous amplifications.

The shortcoming of the experiments involving deregulation of replication controls and genetically induced replication stress is that they are all loss of function experiments. Strictly speaking, these experiments demonstrate that re-replication and replication stress both have the capacity to stimulate segmental amplifications, but cannot conclusively demonstrate that either mechanism is at work in the case of unperturbed, wild-type cells. It is formally possible that intact replication controls reduce the frequency of spontaneous re-initiation to a negligible level, or that normal S-phase replication is so robust that replication stress occurs below a meaningful level. Ideally, gain of function experiments would be employed to assess the relevant mechanisms in wild-type cells. That is, novel control mechanisms that enhance the block to re-initiation or reduce the probability of replication stress would be introduced and the rate of amplification in those strains measured. If re-replication did in fact underlie amplification in the wild-type setting, then introduction of novel barriers to re-initiation would reduce the rate of amplification. Similarly, if reduction of replication stress relative to wild-type levels yielded a corresponding decrease in the rate of amplification, it would demonstrate that replication stress based mechanisms drive spontaneous amplification. Such experiments are obviously extremely difficult to perform, as they require engineering heretofore non-existent mechanisms. In the case of imposing additional barriers to re-initiation, we have attempted to control the levels of Cdt1 and Orc6 proteins using phosphodegrons derived from Cdc6, as well as a previously published Sic1 destruction box module fused to Cdt1 [53], such that they are degraded as the level of CDK activity rises. In all cases, however, this resulted in the undesirable side effect of compromising the normal S-phase replication functions of these factors, making clear interpretation of any results using

such strains impossible (data not shown). Hopefully more sophisticated strategies can be employed in future studies to further resolve the role of re-replication in spontaneous gene amplifications.

Single-Stranded Annealing Plays a Major Role in Spontaneous Amplifications

While we were unable to employ the ideal gain of function experiments discussed above, we were able to address the contributions of different mechanisms to spontaneous amplifications in an alternative manner. While all of the NAHR-involving mechanisms that might generate amplifications by definition require some form of homologous recombination, the specific sub-type used varies. The major role played by SSA in the spontaneous amplifications studied here is consistent with our published work on the mechanism of RRIGA. Other NAHR models for gene amplification propose a GC-like mechanism or BIR, neither of which appears to make a significant contribution to the spontaneous amplifications examined here. Of course, variations on these models could perhaps account for SSA-mediated resolution. So, an SSA requirement alone cannot conclusively demonstrate the involvement of RRIGA in spontaneous amplifications. However, taken together with the experiments described above comparing the efficiency and fitness costs of replication control disruption to replication stress, the data suggest that sporadic re-initiation is a strong candidate for the driving force behind spontaneous amplifications.

Implications for Disease

In addition to the potential role of RRIGA in driving spontaneous amplifications in wild-type cells with intact replication controls, our data also suggests that RRIGA might make a significant contribution in tumor cells where replication controls are dysregulated. Even if normal replication controls are in fact so robust such that sporadic re-initiation occurs at a negligible frequency and does not significantly contribute to

spontaneous amplifications in wild-type cells, we have clearly shown that even slight disruption of these controls can dramatically boost impact the rate of amplification. So, similar disruptions in the context of human cancer cells could promote RRIGA in those cells, and potentially drive other forms of genomic instability as well. We note that dysregulation of replication initiation proteins has indeed been observed in some human cancer cells, as early as the stage of dysplasia [6,54–59]. Furthermore, overexpression of some replication initiation proteins in particular murine models can promote cancer [59–61]. We therefore think it would be worthwhile to explore the possibility that gene amplification rates are increased in these settings. Of course, a compelling demonstration of RRIGA in the context of oncogenesis, or for spontaneous amplifications for that matter, will require the development of new, extremely sensitive assays for monitoring re-replication.

Contributions of Different Mechanisms to the Block to Re-Initiation

S. cerevisiae, like other eukaryotes, employs a battery of overlapping mechanisms to prevent re-initiation. We disrupted three of these mechanisms, each individually, and observed dramatically different effects on the rate of amplification. While disruption of Mcm2-7 regulation resulted in only a slight elevation in the rate of segmental amplification, disruption of ORC regulation increased the rate dramatically. The simplest interpretation of these findings is that the various mechanisms contributing to the block to re-initiation do not make equal contributions to that barrier. Furthermore, combined disruption of Mcm2-7 and Cdc6 regulation caused an increase in the amplification rate far greater than the product of the increases produced by either single disruption alone. This suggests a level of cooperativity between distinct mechanisms, producing a more robust barrier to re-initiation. Given that different mechanisms preventing re-initiation are used in different organisms, and that the combinations of these mechanisms also vary, it would be unsurprising to find variable levels of susceptibility to re-initiation across

eukaryotes. This in turn could make different evolutionary lineages more or less prone to gene amplifications. With many fully sequenced genomes now available, it would be interesting to examine these for evidence of greater or lesser frequencies of recent gene duplication/amplification events and determine if there is any correlation with what replication control mechanisms are employed in those organisms. Such an observation could provide additional indirect support for RRIGA as a driving force in spontaneous amplifications.

Methods

Oligonucleotides

Oligonucleotides used in the plasmid and yeast strain constructions, as well as in the generation of Southern blot probes, are listed in Table S1.

Plasmids

All plasmids used are listed in Table S2.

pFA6a-natMX6-pTEF2-eGFP (a kind gift from Jonathan Weissman) contains the *eGFP* ORF driven by the promoter of *S. cerevisiae TEF2* inserted between the PmeI and SacII sites of pFA6a-natMX6 [62].

pFA6a-kanMX6-pTEF2-dTomato (a kind gift from Jonathan Weissman) contains the *dTomato* ORF driven by the promoter of *S. cerevisiae TEF2* inserted between the PmeI and SacII sites of pFA6a-kanMX6 [63].

p210-BS-KlacURA3 contains a XhoI-HindIII fragment of *K. lactis* genomic DNA containing the *Kl.URA3* gene inserted between the XhoI and HindIII sites of pBluescript KS(+).

pJL737 is used to replace *orc6-cdk4A* with *ORC6* by loop-in/loop-out replacement. It has been described previously [25].

pJL1033 is used to replace *MCM7-2NLS* with *MCM7* by loop-in/loop-out

replacement. It has been described previously [64].

pUT1549 is used to replace *CDC6* with $\Delta ntCDC6-cdk2A$ by loop-in/loop-out replacement. It effectively consists of an EcoRI-EcoRI fragment of yeast genomic DNA containing the *CDC6* ORF inserted into the EcoRI site of pRS306 [65]. Amino acids 2-46 of *CDC6* were replaced with a NotI site (5'-aGCGGCCGC-3') and serines 354 and 372 were mutated to alanines to disrupt additional CDK sites.

pKJF035 and pKJF036 (described below) are both derived from pKJF034. pKJF034 contains the *natR* gene with the *ACT1* intron inserted between nucleotides +292 and +293 of the *natR* ORF. The 5' portion of the *natR* gene (including the *pTEF* element and nucleotides +1 to +292 of the ORF) was amplified by PCR from pAG36 [66] using oligonucleotides OJL25 and OJL3057. OJL3057 adds sequence corresponding to the 5' end of the *ACT1* intron to the 3' end of the PCR product. The 3' portion of the *natR* gene (including nucleotides +293 to +573 of the ORF and the *tTEF* element) was amplified by PCR from pAG36 using oligonucleotides OJL6 and OJL3058. OJL3058 adds sequence corresponding to the 3' end of the *ACT1* intron to the 5' end of the PCR product. The *ACT1* intron was amplified by PCR from YJL6974 [18] genomic DNA using oligonucleotides OJL3053 and OJL3054. All three PCR products were mixed and used as the template in another PCR reaction using oligonucleotides OJL6 and OJL2374. This reaction results in the *pTEF-natR*₁₋₂₉₂-*ACT1*_{intron}-*natR*₂₉₃₋₅₇₃-*tTEF* fusion product. This product was digested with NotI and inserted into the NotI site of pRS316 [65]

pKJF035 contains *pTEF-natR*₁₋₂₉₂-*ACT1*_{intron}-*natR*₂₉₃₋₃₄₀ (the 5' portion of the split *natR* construct) and an *URA3* selectable marker in pRS314 [65]. The *pTEF-natR*₁₋₂₉₂-*ACT1*_{intron}-*natR*₂₉₃₋₃₄₀ element was amplified by PCR from pKJF034 using oligonucleotides OJL3062 and OJL3063, which add a BamHI site to the 5' end and an EcoRI site to the 3' end of the product, respectively. The *URA3* element was amplified by PCR from pRS316 using oligonucleotides OJL2543 and OJL2544, which add an EcoRI site to the 5' end and a Sall site to the 3' end of the product, respectively. The *pTEF-natR*₁₋₂₉₂-*ACT1*_{intron}-

*natR*₂₉₃₋₃₄₀ product was digested with BamHI and EcoRI, the *URA3* product was digested with EcoRI and Sall, and both products were inserted between the BamHI and Sall sites of pRS314 by a 3-way ligation.

pKJF036 contains *natR*₁₉₁₋₂₉₂-*ACT1*_{intron}-*natR*₂₉₃₋₅₇₃-*tTEF* (the 3' portion of the split *natR* construct) and a *TRP1* selectable marker in pRS316. The *natR*₁₉₁₋₂₉₂-*ACT1*_{intron}-*natR*₂₉₃₋₅₇₃-*tTEF* element was amplified by PCR from pKJF034 using oligonucleotides OJL3064 and OJL3065, which add an EcoRI site to the 5' end and a Sall site to the 3' end of the product, respectively. The *TRP1* element was amplified by PCR from pRS314 using oligonucleotides OJL2543 and OJL3061, which add an EcoRI site to the 5' end and a BamHI site to the 3' end of the product, respectively. The *natR*₁₉₁₋₂₉₂-*ACT1*_{intron}-*natR*₂₉₃₋₅₇₃-*tTEF* product was digested with EcoRI and Sall, the *TRP1* product was digested with EcoRI and BamHI, and both products were inserted between the BamHI and Sall sites of pRS316 by a 3-way ligation.

pJR1267 (a kind gift from Catherine Fox) is used to replace *ORC2* with *orc2-1* by loop-in/loop-out replacement. It is composed of 2.8 kb SacI-SacI fragment containing *orc2-1* inserted into the SacI site of pRS306.

pKJF037 is used to replace *CDC6* with *cdc6-1* by loop-in/loop-out replacement. A 2615 bp fragment containing *cdc6-1* was generated by PCR from yeast genomic DNA from YJL885 (which contains *cdc6-1*) using oligonucleotides OJL3269 and OJL3270. The resultant product was digested with SacII and XhoI (restriction sites added to the ends of the PCR product by the primers) and ligated into pRS306 at the same restriction sites.

pPP117 (a kind gift from Robert Sclafani) is used to replace *CDC7* with *cdc7-1* by loop-in/loop-out replacement. It is composed of a 3.6 kb EcoRI-Sall fragment of pRS285 [67] containing *cdc7-1* inserted into the corresponding sites of pRS306.

pKJF039 is used to replace *CDC17* with *cdc17-1* by loop-in/loop-out replacement. A 5308 bp fragment containing *cdc17-1* was generated by PCR from yeast

genomic DNA from YJL892 (which contains *cdc17-1*) using oligonucleotides OJL3273 and OJL3274. The resultant product was digested with SacII and XmaI (restriction sites added to the ends of the PCR product by the primers) and ligated into pRS306 at the same restriction sites.

pKJF004, used in the plasmid loss assay, contains *ARS1*, *CEN3*, and *ADE3*. It was generated from pDK206 [68] as follows. pRSS56 [65] was digested with BspHI to release a 1008 bp fragment containing the ampicillin resistance gene. The ends of this fragment were filled in with Klenow and the resulting blunt fragment was inserted into the SmaI site of pDK206.

Strains

All strains used in this study have their genotypes listed in Table S3.

YJL9464, used in the *pds1Δ* temperature sensitivity suppression experiments, was constructed as follows from W303-1A. The *pTEF2-dTomato*, *kanMX6* module was amplified by PCR from pFA6a-kanMX6-pTEF2-dTomato using oligonucleotides RFP-F and RFP-R then integrated into W303-1A near *CEN4* (at ~449.5 kb from the end of the left telomere) to create YJL9252. The *pTEF2-eGFP*, *natMX6* module was amplified by PCR from pFA6a-natMX6-pTEF2-eGFP using oligonucleotides GFP-F and GFP-R then integrated into YJL9252 downstream of the *ESP1* gene (between *ESP1* and *ASK10*) to form YJL9272. Finally the *K.lactis URA3* gene was amplified by PCR from p210-BS-KlacURA3 using oligonucleotides *pds1Δ*-F and *pds1Δ*-R then used to replace most of the *PDS1* ORF in YJL9272 to produce YJL9464.

Two versions of a wild-type strain were constructed for use in the split *natR* reconstitution fluctuation analysis experiments. YJL9756 was derived from YJL3151 (*MATa ORC2 orc6-cdk4A leu2 ura3-52 trp1-289 ade2 ade3 MCM7-2NLS bar1::LEU2*) [18] as follows. YJL3158 was derived from YJL3151 by loop-in/loop-out gene replacement of *orc6-cdk4A* with *ORC6* using SphI-linearized pJL737. Note that YJL3158

bears a fully wild-type allele of *ORC6*. This is unlike a sister isolate YJL3155, a strain we used in previous studies and that we reported has serine 116 still mutated to an alanine, disrupting a CDK site [19]. YJL9699 was in turn derived from YJL3158 by loop-in/loop-out gene replacement of *MCM7-2NLS* with *MCM7* using BamHI-linearized pJL1033. YJL9733 was derived from YJL9699 by integrating the 3' *natR* element at ~570kb from the left telomere of Chromosome VII, replacing all of the sequence from YGRCdelta15 through YGRCdelta18. The 3' *natR* element was amplified by PCR from pKJF036 using oligonucleotides OJL3078 and OJL3079, which add sequence homologous to the target integration site to the ends of the PCR product. Additional flanking homologous sequence was added to the each end of this product by fusion PCR. A left-hand homology segment was amplified by PCR from yeast genomic DNA using oligonucleotides OJL2750 and OJL3104. A right-hand homology segment was amplified by PCR from yeast genomic DNA using oligonucleotides OJL2751 and OJL3105. The three PCR products were mixed together and used as the temple for a PCR reaction using oligonucleotides OJL2750 and OJL2751. The resultant fusion product was transformed into YJL9699. YJL9756 was derived from YJL9733 by integrating the 5' *natR* element at ~700kb from the left telomere of Chromosome VII, replacing YGRWdelta19. The 5' *natR* element was amplified by PCR from pKJF035 using oligonucleotides OJL3080 and OJL3081, which add sequence homologous to the target integration site to the ends of the PCR product. Additional flanking homologous sequence was added to the each end of this product by fusion PCR. A left-hand homology segment was amplified by PCR from yeast genomic DNA using oligonucleotides OJL3076 and OJL3108. A right-hand homology segment was amplified by PCR from yeast genomic DNA using oligonucleotides OJL3077 and OJL3112. The three PCR products were mixed together and used as the temple for a PCR reaction using oligonucleotides OJL3076 and OJL3077. The resultant fusion product was transformed into YJL9733.

The second version of a wild-type strain constructed for use in the split *natR*

reconstitution fluctuation analysis experiments, YJL9892, was derived from YJL9756 by removing the *URA3* gene present with the 5' *natR* element. Sequence immediately upstream of the *URA3* ORF was amplified by PCR from YJL9756 genomic DNA using oligonucleotides OJL2625 and OJL2566. Similarly, sequence immediately downstream of the *URA3* ORF was amplified by PCR from YJL9756 genomic DNA using oligonucleotides OJL3247 and OJL3077. OJL3247 adds sequence to the 5' end of the PCR product that is identical to the 3' portion of the upstream product. The two PCR products were then mixed and used as a template for another PCR reaction using oligonucleotides OJL2625 and OJL3077. The resultant fusion product was transformed into YJL9756. Cells were plated onto YEPD plates then replica plated to SDC+5-FOA plates the following day to select cells that had lost the *URA3* gene.

The O strain (*orc2-cdk6A orc6-cdk4A*) used in the split *natR* reconstitution fluctuation analysis experiments, YJL9750, was derived from YJL1737 (*MATa orc2-cdk6A orc6-cdk4A leu2 ura3-52 trp1-289 ade2 ade3 bar1::LEU2*) [25] by integrating the 3' *natR* and 5' *natR* elements as described above for the wild-type strain (YJL9756).

The M strain (*MCM7-2NLS*) used in the split *natR* reconstitution fluctuation analysis experiments, YJL9753, was derived from YJL3158 (described above) by integrating the 3' *natR* and 5' *natR* elements as described above for the wild-type strain (YJL9756).

The C_{2A} strain (Δ *ntCDC6-cdk2A*) used in the split *natR* reconstitution fluctuation analysis experiments, YJL9762, was derived from YJL9699 (described above) as follows. YJL9716 was derived from YJL3158 by loop-in/loop-out gene replacement of *CDC6* with Δ *ntCDC6-cdk2A* using BspEI-linearized pUT1549. YJL9762 was then derived from YJL9716 by integrating the 3' *natR* and 5' *natR* elements as described above for the wild-type strain (YJL9756).

The MC_{2A} strain (*MCM7-2NLS* Δ *ntCDC6-cdk2A*) used in the split *natR* reconstitution fluctuation analysis experiments, YJL9842, was derived from YJL3158

(described above) as follows. YJL9715 was derived from YJL3158 by loop-in/loop-out gene replacement of *CDC6* with $\Delta ntCDC6-cdk2A$ using BspEI-linearized pUT1549. YJL9842 was then derived from YJL9715 by integrating the 3' *natR* and 5' *natR* elements as described above for the wild-type strain (YJL9756).

The *orc2-1* strain used in the split *natR* reconstitution fluctuation analysis experiments, YJL9951, was derived from YJL9892 by loop-in/loop-out gene replacement of *ORC2* with *orc2-1* using EcoNI-linearized pJR1267.

The *cdc6-1* strain used in the split *natR* reconstitution fluctuation analysis experiments, YJL9996, was derived from YJL9892 by loop-in/loop-out gene replacement of *CDC6* with *cdc6-1* using BglII-linearized pKJF037.

The *cdc7-1* strain used in the split *natR* reconstitution fluctuation analysis experiments, YJL9940, was derived from YJL9892 by loop-in/loop-out gene replacement of *CDC7* with *cdc7-1* using ClaI-linearized pPP117.

The *cdc17-1* strain used in the split *natR* reconstitution fluctuation analysis experiments, YJL9945, was derived from YJL9892 by loop-in/loop-out gene replacement of *CDC17* (aka *POL1*) with *cdc17-1* using EagI-linearized pKJF039.

Strains used to assess the recombination requirements in the wild-type setting were all derived from YJL9756. YJL9903/9904, YJL9906, and YJL9909 were generated by replacing *RAD52*, *RAD51*, or *RAD1* respectively, with *hphMX*. Disruption fragments were generated using PCR in two steps. Step 1 primers (see Table S1) were used to amplify *hphMX* from pAG32 [66] and add short regions of homology flanking the target gene. Step 2 primers extended the region of homology, using the PCR product obtained in Step 1 as a template. YJL10143/10144, YJL10146/10147, and YJL10149/10150 were generated by replacing *POL32*, *MSH3*, or *RAD59* respectively, with *hphMX*. Disruption fragments were generated using PCR from pAG32 in one step with very long-tailed oligonucleotides (see Table S1).

Strains used to assess the recombination requirements in the O setting were all

derived from YJL9750. YJL9895, YJL9898, and YJL9901 were generated by replacing *RAD52*, *RAD51*, or *RAD1* respectively, with *hphMX*. Disruption fragments were generated using PCR in two steps. Step 1 primers (see Table S1) were used to amplify *hphMX* from pAG32 and add short regions of homology flanking the target gene. Step 2 primers extended the region of homology, using the PCR product obtained in Step 1 as a template. YJL10133/10134, YJL10136/10137, and YJL10139/10140 were generated by replacing *POL32*, *MSH3*, or *RAD59* respectively, with *hphMX*. Disruption fragments were generated using PCR from pAG32 in one step with very long-tailed oligonucleotides (see Table S1).

The *clb5Δ* strain, YJL10151/10152 was derived from YJL9892 by replacing *CLB5* with *kanMX*. The disruption fragment was generated by PCR from pFA6a-*kanMX6* in a single step using very long-tailed oligonucleotides (see Table S1).

The *clb5Δ clb6Δ* strain, YJL10194/10194 was derived from YJL10151 by replacing *CLB6* with *URA3*. The disruption fragment was generated by PCR from pRS306 in a single step using very long-tailed oligonucleotides (see Table S1).

Media

Cells were grown in or on YEP or synthetic medium containing 2% wt/vol dextrose (making YEPD or SD, respectively). For synthetic medium, 1x amino acid concentrations were as described [69], except the amount of leucine was doubled to 60 μg/mL and the amount of serine was halved to 200 μg/mL. "C" indicates complete medium (all amino acids added; i.e. SDC). For SDC+5-FOA plates 5-fluoroorotic acid was added to a final concentration of 1 mg/mL.

pds1Δ Suppressor Isolation

YJL9464, a strain lacking the *PDS1* gene and bearing fluorescent reporters to facilitate screening for amplifications, was thawed onto YEPD plates at the non-selective

temperature (either 22°C or 24°C) and grown up for 1-2 days. Cells taken from the plate were then used to inoculate liquid YEPD and were grown at the non-selective temperature with orbital shaking for 9-16 hr. Following this outgrowth period, cells were harvested and plated onto fresh YEPD plates, which were placed at the selective temperature (31°C) to isolate suppressors of the *pds1Δ* temperature sensitivity phenotype. After 5 days of growth, survivor isolates from the selective temperature plates were then colony purified (by streaking) on fresh YEPD plates at the selective temperature. After another 5 days of growth, an individual colony from each streak was expanded on a fresh YEPD plate at selective temperature and then stored as a glycerol freezer stock. Depending upon the particular experiment, the non-selective temperature used was either 22°C or 24°C.

Fluorescence Activated Cell Sorting Screen for Amplifications

pds1Δ suppressor isolates were thawed from freezer stocks (see above) onto YEPD plates and grown at 31°C. Cells were transferred from the YEPD plates into phosphate buffer saline (no Ca⁺⁺, no Mg⁺⁺, no EDTA) in a 96-well plate on ice. Control strains were included on each plate. Cells were analyzed using a LSR II flow cytometer (Becton-Dickinson). Fluorescence was measured in the FITC and DsRed channels (for eGFP and dTomato, respectively). The gain for each channel was set using the control strain included within the experiment. 10,000 cells were sampled for each isolate, and the GFP vs. RFP scatter plot for each isolate was plotted on the same axes as the control strain. Amplification was scored as a visible shift of the isolate's scatter plot upward on the GFP axis relative to the control.

*aCGH Analysis of *pds1Δ* Suppressors*

Samples were collected in one of two ways: 1) Cells were cultured on YEPD plates at 31°C. ~10 OD units of cells were harvested and suspended in 1 mL of sterile

water in microfuge tubes. Cells were then vortexed to wash and pelleted. The water was then aspirated off and the cell pellets were snap-frozen in liquid nitrogen. 2) Cells were cultured at 31°C in liquid YEPD and arrested in G2/M with nocodazole (final concentration = 15 µg/mL). ~2.5 x 10⁸ cells were then pelleted by centrifugation, washed with 1 mL of sterile water, then re-pelleted. The water was then aspirated off and the cell pellets were snap-frozen in liquid nitrogen.

Cell pellets were thawed and resuspended in 200 µL of lysis buffer (2% Triton X-100, 1% SDS, 100 mM NaCl, 10 mM Tris-Cl, 1 mM EDTA (pH 8.0)). To this suspension 200 µL of phenol:chloroform:isoamyl alcohol (25:24:1) and 200 µL of acid washed glass beads (0.5 mm) was added. Cells were then lysed at room temperature using a Vortex-Genie 2 (Scientific Industries, NY) at top speed for 10 minutes. To the lysate 450 µL of 10 mM Tris-Cl, 1 mM EDTA (pH 7.5) was added, and the mixture was vortexed for 30 seconds. The mixture was then centrifuged at room temperature for 3 minutes at 20,800 x g. 500 µL of the aqueous phase was transferred to a new microfuge tube, to which 1 µL of 100 mg/mL RNase A (Qiagen, CA) was added. Samples were incubated at 37°C for 3 hours to allow digestion of the RNA. 300 µL of phenol:chloroform:isoamyl alcohol (25:24:1) was added to each sample, which were then mixed at room temperature for 5 minutes on a multi-mixer (Tomy Tech USA, CA), then centrifuged at room temperature for 3 minutes at 20,800 x g. 400 µL of the aqueous phase was transferred to a new microfuge tube. 300 µL of chloroform:isoamyl alcohol (24:1) was added to each sample. Samples were mixed by shaking at room temperature and were then centrifuged at room temperature for 3 minutes at 20,800 x g. 300 µL of the aqueous phase was transferred to a new microfuge tube, to which 750 µL of 100% Ethanol and 3 µL of 10N NH₄OAC (pH 7). Samples were vortexed then centrifuged at room temperature for 7 minutes at 20,800 x g to pellet the DNA. Pellets were washed with 70% Ethanol the air dried. The DNA was suspended in 50 µL of 2 mM Tris-Cl (pH 7.8).

Reference DNA for aCGH was prepared from YJL9272 as previously described (as in Method 2) [19].

40% of each survivor isolate DNA sample was labeled with Cy5 and 2 μg of purified reference DNA was labeled with Cy3 as described [26]. The labeled DNA was isolated as previously described (low-throughput [26] method or high-throughput method [70]). All samples were hybridized and analyzed as described [26].

Pulsed-Field Gel Electrophoresis and Southern Analysis

Cells were cultured in liquid YEPD at 31°C (except for the parent strain which was cultured at 22°C) and then were arrested in G2/M phase with 15 $\mu\text{g}/\text{mL}$ Nocodazole (United States Biologicals, MA). To make plugs for PFGE, 6×10^8 cells were transferred to a 50 mL conical tube then pelleted by centrifugation, washed twice with ice-cold 50 mM EDTA, then resuspended to 500 μL with 50°C SCE (1 M sorbitol, 0.1 M Na citrate, and 10 mM EDTA). Lyticase (L5263; Sigma) was added to a final concentration of 150 U/mL, and 350 μL of the sample was mixed with 350 μL of molten, 50°C 1% InCert agarose (Lonza, Rockland, ME), and then 85 μL of the mixture was aliquoted into each of 5 disposal plug molds (170-3713; Bio-Rad). The plug molds were allowed to solidify at 4°C, and then placed in SCEM + lyticase (1 M sorbitol, 0.1 M Na citrate, 10 mM EDTA, 5% β -mercaptoethanol (vol/vol), and 160 U/mL lyticase) for ~40 hr at 37°C. Plugs were then washed three times in $T_{10}E_1$ (10 mM Tris, pH 8.0, and 1 mM EDTA) for 1-2 hr each wash and resuspended in proteinase K solution (1% sarcosyl (wt/vol), 0.5 M EDTA, and 2 mg/ml proteinase K (Roche)) for >48 hr at 55°C. Finally, plugs were washed six times in $T_{10}E_1$ for 1-3 hr each wash. The third and fourth $T_{10}E_1$ washes contained 1 mM PMSF to inactivate residual proteinase K. Plugs were then stored at 4°C in 0.5 M EDTA until used.

For whole chromosome analysis (undigested), 1/4 of each plug was cut off and soaked in $T_{10}E_1$ at 37°C overnight (removes background fluorescence during ethidium

bromide visualization of the gel). Plugs were then cooled to room temperature. Plugs were loaded on a 1% SeaKem LE agarose (wt/vol) gel in 1x TAE (40 mM Tris, 40 mM acetate, and 1 mM EDTA, pH 8.0). The gel was electrophoresed at 14°C in 1x TAE on a CHEF DR-III system (Bio-Rad) with a switch time of 500 sec, run time of 56 hr, voltage of 3 V/cm, and angle of 106°. The gel was stained with 1 µg/mL ethidium bromide in 1x TAE for 40 min, then exposed to 130 mJ/cm² UV light using a Stratalinker 2400 (Stratagene, La Jolla, CA) to nick chromosomal DNA. The gel was then destained in sterile water for 60 min, and quickly imaged with an AlphaImager. The gel was then soaked in two changes of denaturation buffer (0.5 N NaOH, 1.5 M NaCl) at RT for 15 min each. After rinsing with deionized water the gel was soaked in two changes of neutralization buffer (1.0 M Tris-Cl, 1.5 M NaCl, pH 7.5) at RT for 15 min each. The DNA was then transferred to a Roche positively charged nylon membrane using neutral downward capillary transfer (10X SSC, pH 7.0 used as transfer buffer). DNA was cross-linked to the membrane with 120 mJ/cm² of UV light in a Stratalinker 2400. The membrane was hybridized with radioactive probes recognizing *ESPI* (probe template generated by PCR from yeast genomic DNA with oligonucleotides OJL3035 and OJL3036) and *ADH4* (probe template generated by PCR from yeast genomic DNA with oligonucleotides OJL3039 and OJL3040). Radioactive probes were generated using a Prime-it II Random Primer Labeling kit (Stratagene) with [α -³²P]dATP (Perkin Elmer). Images were collected using a Typhoon 9400 (GE Healthcare).

For determining amplicon orientation, an asymmetric digest approach was employed. The *pTEF2-eGFP*, *natMX* element inserted near *ESPI* in YJL9464 introduced an AscI site. There are no other AscI recognition sites within the amplified region of the strains examined, and the site introduced near *ESPI* is closer to the right end of the amplicon than the left end. There are no AscI recognition sequences to the right of the amplicon, and the nearest site to the left is at ~508.5 kb (close to the centromere). Therefore, chromosomal DNA can be digested with AscI and probed for sequences to

the right or left of the cut site near *ESPI*. Different orientations of amplicons will yield different sized bands detected by Southern blotting.

For this analysis, plugs were cut in half and soaked in $T_{10}E_1$ at 37°C overnight (removes background fluorescence during ethidium bromide visualization of the gel). The plugs were then treated with 200 units of AscI in 50 mM potassium acetate, 20 mM Tris-acetate, 10 mM magnesium acetate, 1 mM DTT, 10 mM spermidine, 0.01% Triton X-100, pH 7.9 at 37°C for 40 hr. Plugs were then equilibrated in running buffer (0.5x TBE) then loaded on a 1% SeaKem LE agarose (wt/vol) gel in 0.5x TBE (45 mM Tris, 45 mM boric acid, and 1 mM EDTA, pH 8.0). Electrophoresis was carried out at 14°C in 1x TBE on a CHEF DR-III system with an initial switch time of 50 sec, a final switch time of 90 sec, a run time of 24 hr, voltage of 6 V/cm, and angle of 120°. The DNA was transferred and fixed to the membrane as described above for the undigested samples. The membrane was hybridized with DIG-labeled probes recognizing *ESPI* (probe template generated by PCR from yeast genomic DNA with oligonucleotides OJL3035 and OJL3036) and *ASK10* (probe template generated by PCR from yeast genomic DNA with oligonucleotides OJL3037 and OJL3038). Probe labeling, hybridization, and detection were carried out using a DIG-High Prime Labeling and Detection Kit (Roche Applied Science, IN). Images were captured using film (Amersham Hyperfilm ECL).

Fluctuation Analysis

Strains were cultured as bulk populations in YEPD at 30°C or 23°C (for temperature sensitive strains) until they reached mid-log phase, at which point they were diluted in YEPD to a density of ~125 cells/mL. 200 µL of this dilution was plated onto each of five YEPD plates to determine the actual initial population size (N_i), and 800 µL of this dilution was aliquoted into each well of a 96-well deep-well microtiter plate, which was then sealed with gas-permeable film. Plates were incubated in a Multitron (Infors-HT) shaker at 900 rpm at 30°C or 23°C, as indicated. After the plates had grown

long enough to allow for a sufficient number of divisions, plates were removed from the incubator. Four wells were withdrawn, diluted in YEPD, and plated onto YEPD plates (two plates per well) to determine the final population size (N_t). Nourseothricin was added to the remaining wells to a final concentration of 100 $\mu\text{g}/\text{mL}$ then the plate was re-sealed and returned to the Multitron incubator. After several additional days of incubation the plate was scanned and scored for cloudy and clear wells to determine the fraction that did not contain nat^R cells (P_0). Only plates for which the P_0 was between 0.1 and 0.7 were used to calculate amplification rates. Amplification rate (μ) was then determined using the equation: $\mu = -\ln(P_0)/(N_t - N_i)$.

SDS-PAGE and Western Blotting

Cells were grown in YEPD at 30°C or 23°C as indicated until they reached mid-log phase, at which point $\sim 4 \times 10^7$ cells were harvested from each culture by centrifugation, washed with sterile water, and then snap frozen in liquid nitrogen. As a positive control for Rad53 activation, hydroxyurea was added to a final concentration of 200 mM to the remaining portion of each culture, which was then incubated for an additional 3 hr (at 30°C or 23°C as indicated). $\sim 4 \times 10^7$ cells were harvested from each treated culture by centrifugation, washed with sterile water, and then snap frozen in liquid nitrogen. Cell pellets were thawed on ice and then lysed with 20% trichloroacetic acid (TCA) and glass beads in a Mini-Beadbeater-96 (BioSpec Products) for 3 minutes. Lysate was collected then beads were washed once with 5% TCA, and the wash was combined with the lysate. Proteins were precipitated then resuspended in high pH reducing, denaturing sample buffer. 10% of the sample was then separated by SDS-PAGE on Tris-HCl 8% acrylamide (37.5:1) gels, which were then electroblotted to PVDF membranes using a tank transfer. Membranes were blocked with 5% non-fat milk in PBST. Rad53 was detected with 1:2000 rabbit-anti-Rad53 (Abcam, ab104232) then 1:10000 goat-anti-rabbit-HRP (Santa Cruz Biotechnology, sc-2004). Tubulin was

detected with 1:100 rat-anti-tubulin YOL1/34 (Seralab, MAS078) then 1:20000 goat-anti-rat-HRP (Santa Cruz Biotechnology, sc-2006). All antibodies were used in 5% milk in PBST. Chemiluminescent detection was performed using SuperSignal West Pico (Thermo Fisher Scientific) and X-ray film (CL-Xposure, Pierce).

Serial Dilution Growth Assay

Strains were diluted in YEPD to a starting concentration of 1×10^6 cells/mL, from which a 5-fold dilution series was prepared. 3 μ L of each dilution was spotted onto each of the following plates: 1) YEPD; 2) YEPD + 100 mM HU; 3) YEPD + 200 mM HU; 4) YEPD + 0.01% MMS; 5) YEPD + 0.03% MMS. Plates were incubated at 30°C or 23°C as indicated in the figure, then photographed at the specified times.

Plasmid Loss Assay

Each strain was transformed with pKJF004, a plasmid bearing a single origin of replication (*ARS1*), a centromere (*CEN3*), and the *ADE3* gene. The *ADE3* gene confers the ability to grow on media lacking histidine and turns cells red. Strains with a replication initiation defect will have elevated plasmid loss rates, owing to sporadic failure to initiate replication at the plasmid's single origin. Three independent transformants for each strain were cultured in liquid SDC-His at 30°C (or 23°C for the temperature sensitive strains) to select for cells bearing the plasmid. These cultures were maintained such that they remained in early log phase. Then a portion of each culture was diluted into YEPD to an initial density of ~ 2000 cells/mL, and a portion of the starting culture was plated onto each of three SDC plates to assess the initial fraction of the population that carried the plasmid as well as the initial population size. The YEPD cultures were then grown for 9-13 generations, during which time cells that have lost the plasmid could accumulate owing to the lack of selection for the plasmid. After this non-selective growth phase, a portion of the culture was plated onto each of three SDC

plates to assess the final fraction of the population that carried the plasmid as well as the final population size. After several days of growth, to allow for full color development, the SDC plates were counted and scored. Colonies that were completely white indicated that the initial cell that formed that colony lacked the plasmid, while any amount of red at all indicated that the initial cell carried the plasmid. Thus, the fraction of cells bearing the plasmid at each time point was determined as the number of colonies with any red at all divided by the total number of colonies. The plasmid loss rate per generation expressed as a percentage was then calculated using the equation $[1-(F/I)]^{1/N} \times 100$, where I is the initial fraction of the population bearing the plasmid, F is the final fraction of the population bearing the plasmid, and N is the number of generations elapsed.

References

1. Ohno S (1970) Evolution by gene duplication. Springer-Verlag. 184 p.
2. Kaessmann H (2010) Origins, evolution, and phenotypic impact of new genes. *Genome Res* 20: 1313–1326. doi:10.1101/gr.101386.109.
3. Zhang J (2003) Evolution by gene duplication: an update. *Trends in Ecology & Evolution* 18: 292–298. doi:10.1016/S0169-5347(03)00033-8.
4. Albertson DG (2006) Gene amplification in cancer. *Trends Genet* 22: 447–455. doi:10.1016/j.tig.2006.06.007.
5. Beroukhi R, Mermel CH, Porter D, Wei G, Raychaudhuri S, et al. (2010) The landscape of somatic copy-number alteration across human cancers. *Nature* 463: 899–905. doi:10.1038/nature08822.
6. Santarius T, Shipley J, Brewer D, Stratton MR, Cooper CS (2010) A census of amplified and overexpressed human cancer genes. *Nat Rev Cancer* 10: 59–64. doi:10.1038/nrc2771.

7. Simmons AD, Carvalho CMB, Lupski JR (2012) What have studies of genomic disorders taught us about our genome? *Methods Mol Biol* 838: 1–27. doi:10.1007/978-1-61779-507-7_1.
8. Girirajan S, Campbell CD, Eichler EE (2011) Human copy number variation and complex genetic disease. *Annu Rev Genet* 45: 203–226. doi:10.1146/annurev-genet-102209-163544.
9. Hoang ML, Tan FJ, Lai DC, Celniker SE, Hoskins RA, et al. (2010) Competitive repair by naturally dispersed repetitive DNA during non-allelic homologous recombination. *PLoS Genet* 6: e1001228. doi:10.1371/journal.pgen.1001228.
10. Hastings PJ, Lupski JR, Rosenberg SM, Ira G (2009) Mechanisms of change in gene copy number. *Nat Rev Genet* 10: 551–564. doi:10.1038/nrg2593.
11. Chen J-M, Cooper DN, Férec C, Kehrer-Sawatzki H, Patrinos GP (2010) Genomic rearrangements in inherited disease and cancer. *Semin Cancer Biol* 20: 222–233. doi:10.1016/j.semcancer.2010.05.007.
12. Szostak JW, Wu R (1980) Unequal crossing over in the ribosomal DNA of *Saccharomyces cerevisiae*. *Nature* 284: 426–430.
13. Petes TD (1980) Unequal meiotic recombination within tandem arrays of yeast ribosomal DNA genes. *Cell* 19: 765–774.
14. Welch JW, Maloney DH, Fogel S (1990) Unequal crossing-over and gene conversion at the amplified CUP1 locus of yeast. *Mol Gen Genet* 222: 304–310.
15. Louis EJ, Haber JE (1990) Mitotic recombination among subtelomeric Y' repeats in *Saccharomyces cerevisiae*. *Genetics* 124: 547–559.

16. Liu P, Carvalho CM, Hastings P, Lupski JR (2012) Mechanisms for recurrent and complex human genomic rearrangements. *Current Opinion in Genetics & Development* 22: 211–220. doi:10.1016/j.gde.2012.02.012.
17. Payen C, Koszul R, Dujon B, Fischer G (2008) Segmental duplications arise from Pol32-dependent repair of broken forks through two alternative replication-based mechanisms. *PLoS Genet* 4: e1000175. doi:10.1371/journal.pgen.1000175.
18. Green BM, Finn KJ, Li JJ (2010) Loss of DNA replication control is a potent inducer of gene amplification. *Science* 329: 943–946. doi:10.1126/science.1190966.
19. Finn KJ, Li JJ (2013) Single-stranded annealing induced by re-initiation of replication origins provides a novel and efficient mechanism for generating copy number expansion via non-allelic homologous recombination. *PLoS Genet* 9: e1003192. doi:10.1371/journal.pgen.1003192.
20. Clarke DJ, Mondesert G, Segal M, Bertolaet BL, Jensen S, et al. (2001) Dosage suppressors of *pds1* implicate ubiquitin-associated domains in checkpoint control. *Mol Cell Biol* 21: 1997–2007. doi:10.1128/MCB.21.6.1997-2007.2001.
21. Luria SE, Delbrück M (1943) Mutations of Bacteria from Virus Sensitivity to Virus Resistance. *Genetics* 28: 491–511.
22. Lea DE, Coulson CA (1949) The distribution of the numbers of mutants in bacterial populations. *Journ of Genetics* 49: 264–285. doi:10.1007/BF02986080.
23. Arias EE, Walter JC (2007) Strength in numbers: preventing rereplication via multiple mechanisms in eukaryotic cells. *Genes Dev* 21: 497–518. doi:10.1101/gad.1508907.

24. Diffley JFX (2011) Quality control in the initiation of eukaryotic DNA replication. *Philos Trans R Soc Lond, B, Biol Sci* 366: 3545–3553. doi:10.1098/rstb.2011.0073.
25. Nguyen VQ, Co C, Li JJ (2001) Cyclin-dependent kinases prevent DNA re-replication through multiple mechanisms. *Nature* 411: 1068–1073. doi:10.1038/35082600.
26. Green BM, Morreale RJ, Ozaydin B, Derisi JL, Li JJ (2006) Genome-wide mapping of DNA synthesis in *Saccharomyces cerevisiae* reveals that mechanisms preventing reinitiation of DNA replication are not redundant. *Mol Biol Cell* 17: 2401–2414. doi:10.1091/mbc.E05-11-1043.
27. Wilmes GM, Archambault V, Austin RJ, Jacobson MD, Bell SP, et al. (2004) Interaction of the S-phase cyclin Clb5 with an “RXL” docking sequence in the initiator protein Orc6 provides an origin-localized replication control switch. *Genes Dev* 18: 981–991. doi:10.1101/gad.1202304.
28. Sun Z, Fay DS, Marini F, Foiani M, Stern DF (1996) Spk1/Rad53 is regulated by Mec1-dependent protein phosphorylation in DNA replication and damage checkpoint pathways. *Genes Dev* 10: 395–406.
29. Shimada K, Pasero P, Gasser SM (2002) ORC and the intra-S-phase checkpoint: a threshold regulates Rad53p activation in S phase. *Genes Dev* 16: 3236–3252. doi:10.1101/gad.239802.
30. Tye BK (1999) Minichromosome maintenance as a genetic assay for defects in DNA replication. *Methods* 18: 329–334. doi:10.1006/meth.1999.0793.
31. Ma L, Zhai Y, Feng D, Chan T, Lu Y, et al. (2010) Identification of novel factors involved in or regulating initiation of DNA replication by a genome-wide phenotypic screen in *Saccharomyces cerevisiae*. *Cell Cycle* 9: 4399–4410.

32. Green BM, Li JJ (2005) Loss of rereplication control in *Saccharomyces cerevisiae* results in extensive DNA damage. *Mol Biol Cell* 16: 421–432. doi:10.1091/mbc.E04-09-0833.
33. Archambault V, Ikui AE, Drapkin BJ, Cross FR (2005) Disruption of mechanisms that prevent rereplication triggers a DNA damage response. *Mol Cell Biol* 25: 6707–6721. doi:10.1128/MCB.25.15.6707-6721.2005.
34. Sugawara N, Pâques F, Colaiácovo M, Haber JE (1997) Role of *Saccharomyces cerevisiae* Msh2 and Msh3 repair proteins in double-strand break-induced recombination. *Proc Natl Acad Sci USA* 94: 9214–9219.
35. Fishman-Lobell J, Haber JE (1992) Removal of nonhomologous DNA ends in double-strand break recombination: the role of the yeast ultraviolet repair gene RAD1. *Science* 258: 480–484.
36. Lyndaker AM, Alani E (2009) A tale of tails: insights into the coordination of 3' end processing during homologous recombination. *Bioessays* 31: 315–321. doi:10.1002/bies.200800195.
37. Ira G, Haber JE (2002) Characterization of RAD51-independent break-induced replication that acts preferentially with short homologous sequences. *Mol Cell Biol* 22: 6384–6392.
38. Symington LS (2002) Role of RAD52 epistasis group genes in homologous recombination and double-strand break repair. *Microbiol Mol Biol Rev* 66: 630–670, table of contents.
39. Le S, Moore JK, Haber JE, Greider CW (1999) RAD50 and RAD51 define two pathways that collaborate to maintain telomeres in the absence of telomerase. *Genetics* 152: 143–152.

40. Davis AP, Symington LS (2004) RAD51-dependent break-induced replication in yeast. *Mol Cell Biol* 24: 2344–2351.
41. Ivanov EL, Sugawara N, Fishman-Lobell J, Haber JE (1996) Genetic requirements for the single-strand annealing pathway of double-strand break repair in *Saccharomyces cerevisiae*. *Genetics* 142: 693–704.
42. Krogh BO, Symington LS (2004) Recombination proteins in yeast. *Annu Rev Genet* 38: 233–271. doi:10.1146/annurev.genet.38.072902.091500.
43. Clemente-Ruiz M, Prado F (2009) Chromatin assembly controls replication fork stability. *EMBO Rep* 10: 790–796. doi:10.1038/embor.2009.67.
44. Irmisch A, Ampatzidou E, Mizuno K, O’Connell MJ, Murray JM (2009) Smc5/6 maintains stalled replication forks in a recombination-competent conformation. *EMBO J* 28: 144–155. doi:10.1038/emboj.2008.273.
45. Lambert S, Mizuno K, Blaisonneau J, Martineau S, Chanet R, et al. (2010) Homologous recombination restarts blocked replication forks at the expense of genome rearrangements by template exchange. *Mol Cell* 39: 346–359. doi:10.1016/j.molcel.2010.07.015.
46. Sugawara N, Ira G, Haber JE (2000) DNA length dependence of the single-strand annealing pathway and the role of *Saccharomyces cerevisiae* RAD59 in double-strand break repair. *Mol Cell Biol* 20: 5300–5309.
47. Davis AP, Symington LS (2001) The yeast recombinational repair protein Rad59 interacts with Rad52 and stimulates single-strand annealing. *Genetics* 159: 515–525.

48. Lydeard JR, Jain S, Yamaguchi M, Haber JE (2007) Break-induced replication and telomerase-independent telomere maintenance require Pol32. *Nature* 448: 820–823. doi:10.1038/nature06047.
49. Pâques F, Haber JE (1999) Multiple pathways of recombination induced by double-strand breaks in *Saccharomyces cerevisiae*. *Microbiol Mol Biol Rev* 63: 349–404.
50. Libuda DE, Winston F (2010) Alterations in DNA replication and histone levels promote histone gene amplification in *Saccharomyces cerevisiae*. *Genetics* 184: 985–997. doi:10.1534/genetics.109.113662.
51. Donaldson AD, Raghuraman MK, Friedman KL, Cross FR, Brewer BJ, et al. (1998) CLB5-dependent activation of late replication origins in *S. cerevisiae*. *Mol Cell* 2: 173–182.
52. Ikui AE, Archambault V, Drapkin BJ, Campbell V, Cross FR (2007) Cyclin and cyclin-dependent kinase substrate requirements for preventing rereplication reveal the need for concomitant activation and inhibition. *Genetics* 175: 1011–1022. doi:10.1534/genetics.106.068213.
53. Drury LS, Diffley JFX (2009) Factors affecting the diversity of DNA replication licensing control in eukaryotes. *Curr Biol* 19: 530–535. doi:10.1016/j.cub.2009.02.034.
54. Bonds L, Baker P, Gup C, Shroyer KR (2002) Immunohistochemical localization of cdc6 in squamous and glandular neoplasia of the uterine cervix. *Arch Pathol Lab Med* 126: 1164–1168. doi:10.1043/0003-9985(2002)126<1164:ILOCIS>2.0.CO;2.
55. Borlado LR, Méndez J (2008) CDC6: from DNA replication to cell cycle checkpoints and oncogenesis. *Carcinogenesis* 29: 237–243. doi:10.1093/carcin/bgm268.

56. Karakaidos P, Taraviras S, Vassiliou LV, Zacharatos P, Kastrinakis NG, et al. (2004) Overexpression of the replication licensing regulators hCdt1 and hCdc6 characterizes a subset of non-small-cell lung carcinomas: synergistic effect with mutant p53 on tumor growth and chromosomal instability--evidence of E2F-1 transcriptional control over hCdt1. *Am J Pathol* 165: 1351–1365. doi:10.1016/S0002-9440(10)63393-7.
57. Murphy N, Ring M, Heffron CCBB, King B, Killalea AG, et al. (2005) p16INK4A, CDC6, and MCM5: predictive biomarkers in cervical preinvasive neoplasia and cervical cancer. *J Clin Pathol* 58: 525–534. doi:10.1136/jcp.2004.018895.
58. Ren B, Yu G, Tseng GC, Cieply K, Gavel T, et al. (2006) MCM7 amplification and overexpression are associated with prostate cancer progression. *Oncogene* 25: 1090–1098. doi:10.1038/sj.onc.1209134.
59. Lontos M, Koutsami M, Sideridou M, Evangelou K, Kletsas D, et al. (2007) Deregulated overexpression of hCdt1 and hCdc6 promotes malignant behavior. *Cancer Res* 67: 10899–10909. doi:10.1158/0008-5472.CAN-07-2837.
60. Arentson E, Faloon P, Seo J, Moon E, Studts JM, et al. (2002) Oncogenic potential of the DNA replication licensing protein CDT1. *Oncogene* 21: 1150–1158. doi:10.1038/sj.onc.1205175.
61. Seo J, Chung YS, Sharma GG, Moon E, Burack WR, et al. (2005) Cdt1 transgenic mice develop lymphoblastic lymphoma in the absence of p53. *Oncogene* 24: 8176–8186. doi:10.1038/sj.onc.1208881.
62. Hentges P, Van Driessche B, Tafforeau L, Vandenhaute J, Carr AM (2005) Three novel antibiotic marker cassettes for gene disruption and marker switching in *Schizosaccharomyces pombe*. *Yeast* 22: 1013–1019. doi:10.1002/yea.1291.

63. Longtine MS, McKenzie A 3rd, Demarini DJ, Shah NG, Wach A, et al. (1998) Additional modules for versatile and economical PCR-based gene deletion and modification in *Saccharomyces cerevisiae*. *Yeast* 14: 953–961. doi:10.1002/(SICI)1097-0061(199807)14:10<953::AID-YEA293>3.0.CO;2-U.
64. Nguyen VQ, Co C, Irie K, Li JJ (2000) Clb/Cdc28 kinases promote nuclear export of the replication initiator proteins Mcm2-7. *Curr Biol* 10: 195–205.
65. Sikorski RS, Hieter P (1989) A system of shuttle vectors and yeast host strains designed for efficient manipulation of DNA in *Saccharomyces cerevisiae*. *Genetics* 122: 19–27.
66. Goldstein AL, McCusker JH (1999) Three new dominant drug resistance cassettes for gene disruption in *Saccharomyces cerevisiae*. *Yeast* 15: 1541–1553. doi:10.1002/(SICI)1097-0061(199910)15:14<1541::AID-YEA476>3.0.CO;2-K.
67. Sclafani RA, Fangman WL (1986) Thymidine utilization by *tut* mutants and facile cloning of mutant alleles by plasmid conversion in *S. cerevisiae*. *Genetics* 114: 753–767.
68. Koshland D, Kent JC, Hartwell LH (1985) Genetic analysis of the mitotic transmission of minichromosomes. *Cell* 40: 393–403.
69. Sherman F (2002) Getting started with yeast. *Meth Enzymol* 350: 3–41.
70. Pleiss JA, Whitworth GB, Bergkessel M, Guthrie C (2007) Transcript specificity in yeast pre-mRNA splicing revealed by mutations in core spliceosomal components. *PLoS Biol* 5: e90. doi:10.1371/journal.pbio.0050090.

Figure 1

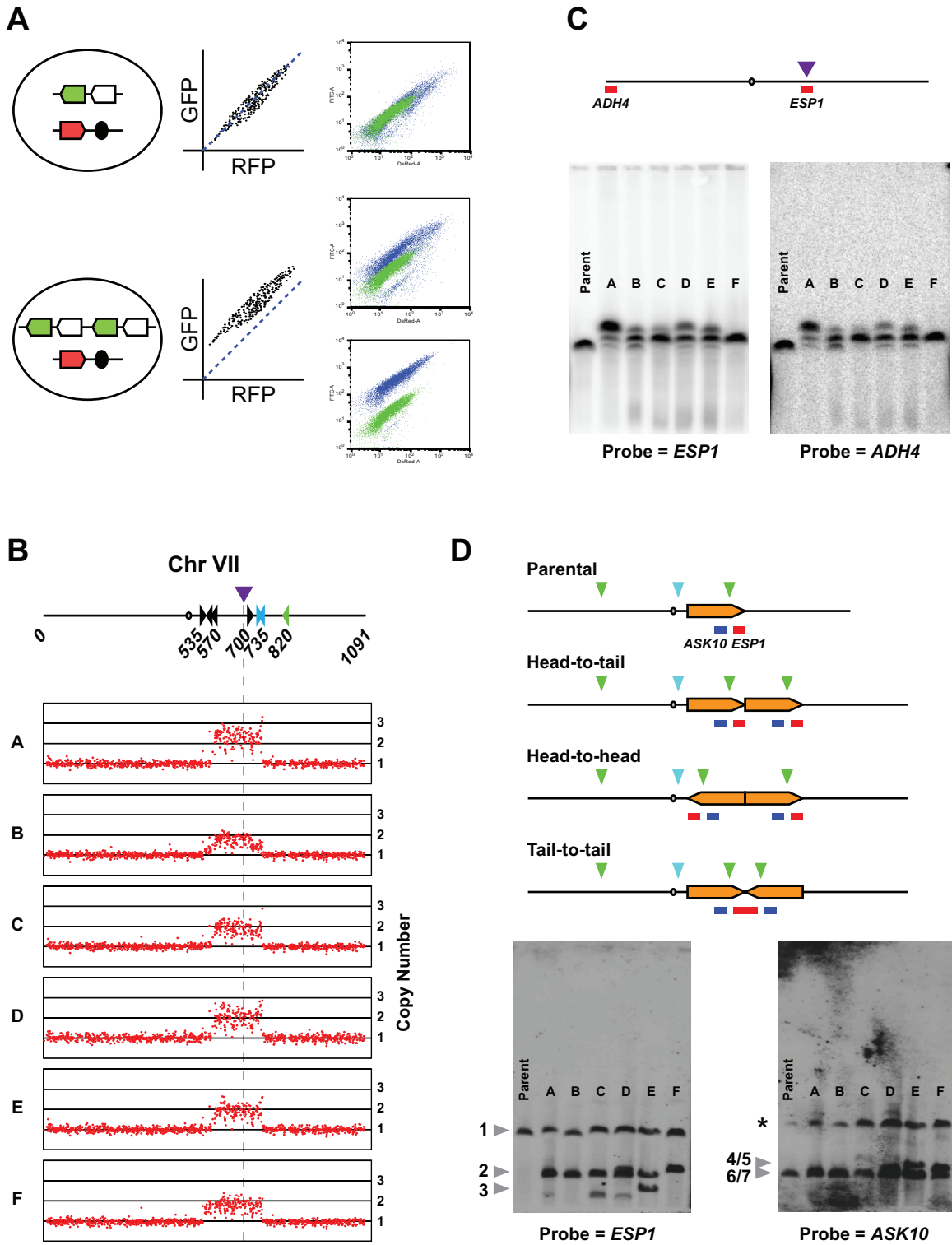


Figure 1. A recurrent spontaneous amplification is structurally consistent with RRIGA. A) Schematic of the FACS assay used to screen for amplifications and example data. Top: The parent strain has a single

copy of the *eGFP* gene (green arrow) integrated near *ESPI* (white arrow) and a single copy of the *dTomato* gene (red arrow) integrated near *CEN4* (black dot). The parent strain is used to set the gain for the GFP and RFP channels such that the intensity distribution of the population falls along a line with a slope ≈ 1 (hypothetical data shown in black). Survivor isolates that lack an amplification of *ESPI* will have a similar distribution to the parent strain (actual data shown with the parent strain in green and a survivor isolate in blue). Bottom: An isolate bearing an amplification that includes *ESPI* will have two copies of the *eGFP* gene, but still will only have a single copy of the *dTomato* gene. This will result in a greater intensity in the GFP channel than the RFP channel during FACS analysis (hypothetical data shown in black). Two examples of survivor isolates that bear an amplification are shown (for both, the parent strain is shown in green and the isolate is shown in blue). One shows a slight upward shift along the GFP axis and the other shows dramatic shift, due to differing degrees of amplification. B) A subset of isolates were analyzed further using aCGH. The aCGH profiles of the six isolates examined using PFGE are shown here. The purple arrowhead and dotted gray line indicates the position of the *ESPI* gene. Ty elements with known orientations are shown as black arrowheads. Blue arrowheads indicate a pair of Ty elements that are likely in an inverted orientation, but it is unclear if they are arranged in a head-to-head or tail-to-tail configuration. The green arrowhead indicates a solo LTR that is frequently used as an amplicon endpoint. *CEN7* is indicated as an open circle. C) Amplicons remain on Chromosome VII. Southern analysis of PFGE separated whole chromosomal DNA for six isolates, as well as the parent strain (YJL9464), with probes recognizing *ESPI*, which lies within the amplified region, and *ADH4*, which lies near the left telomere, yielded indistinguishable banding patterns. Note that all populations are clearly mixed, except for the parent and isolate F. D) Amplicons are arranged as head-to-tail direct repeats. The parental Chromosome VII and three possible amplicon orientations are shown, using an amplicon with endpoints at ~ 540 kb and ~ 735 kb. Arrowhead indicate *AscI* recognition sequences; the site indicated by the blue arrowhead is partially resistant to cutting (data not shown). Probes recognizing *ESPI* and *ASK10* are indicated in red and blue, respectively. The different possible configurations of amplicons will generate distinct banding patterns for the two hybridizations following *AscI* digestion. Bands detected by the *ESPI* probe: (1) the parental telomeric fragment; (2) the amplicon fragment for a head-to-tail amplification; (3) most consistent with the amplicon fragment for a head-to-head amplification. Bands detected by the *ASK10* probe: (4) the amplicon fragment for a head-to-tail amplification (540-735kb); (5) most consistent with the amplicon fragment for a head-to-head amplification; (6) the amplicon fragment for a head-to-tail amplification (570-735kb); (7) the centromere proximal parental fragment; (*) a partial digest product due to incomplete cutting at the *AscI* site indicated by the blue arrowhead (data not shown).

Figure 2

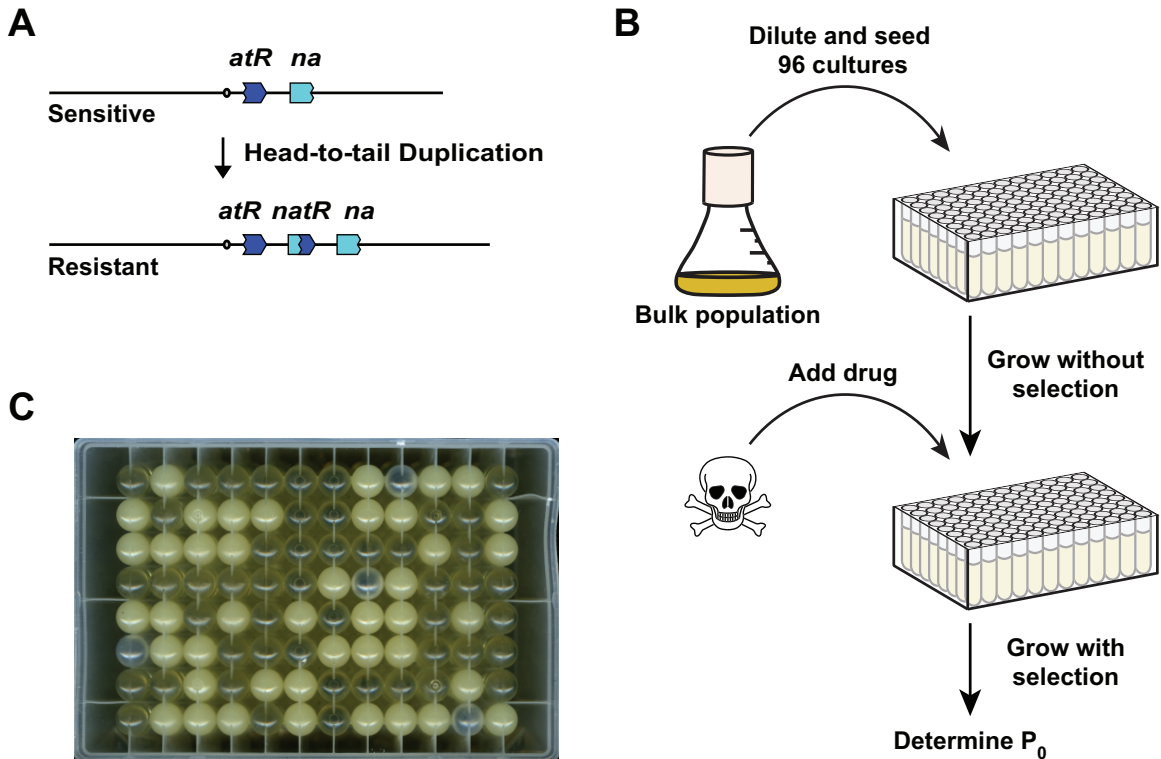


Figure 2. Split *natR* reconstitution fluctuation analysis. A) Fragments of the *natR* gene with overlapping sequence identity were integrated into Chromosome VII (see Methods for details). A head-to-tail duplication involving NAHR between the two gene fragments will generate a full length, functional *natR* gene at the inter-amplicon junction, conferring resistance to nourseothricin. B) Fluctuation analysis workflow. Cells are initially cultured as a single bulk population until they reach mid-log phase. Then cells are diluted in YEPD to seed 96 individual cultures at very low density in a microtiter plate. Samples are also plated onto YEPD at this point to determine the initial population size (N_t). Cultures in the microtiter plate are grown without selection for a number of generations then the cultures from four wells are withdrawn, diluted, and plated to determine the final population size (N_f). At the same time nourseothricin is added to the remaining cultures. The cultures in the microtiter plate are then grown for an additional several days to allow wells containing resistant cells to grow to saturation, at which point the plate is scored to determine the fraction of wells lacking resistant cells (the P_0). The amplification rate (μ) is then calculated using the equation: $\mu = -\ln(P_0)/(N_f - N_t)$. C) An example of a plate at the end of the fluctuation analysis workflow, viewed from the bottom. The four empty wells correspond to those sampled to determine the final population size. Cloudy and clear wells are easily distinguished.

Figure 3

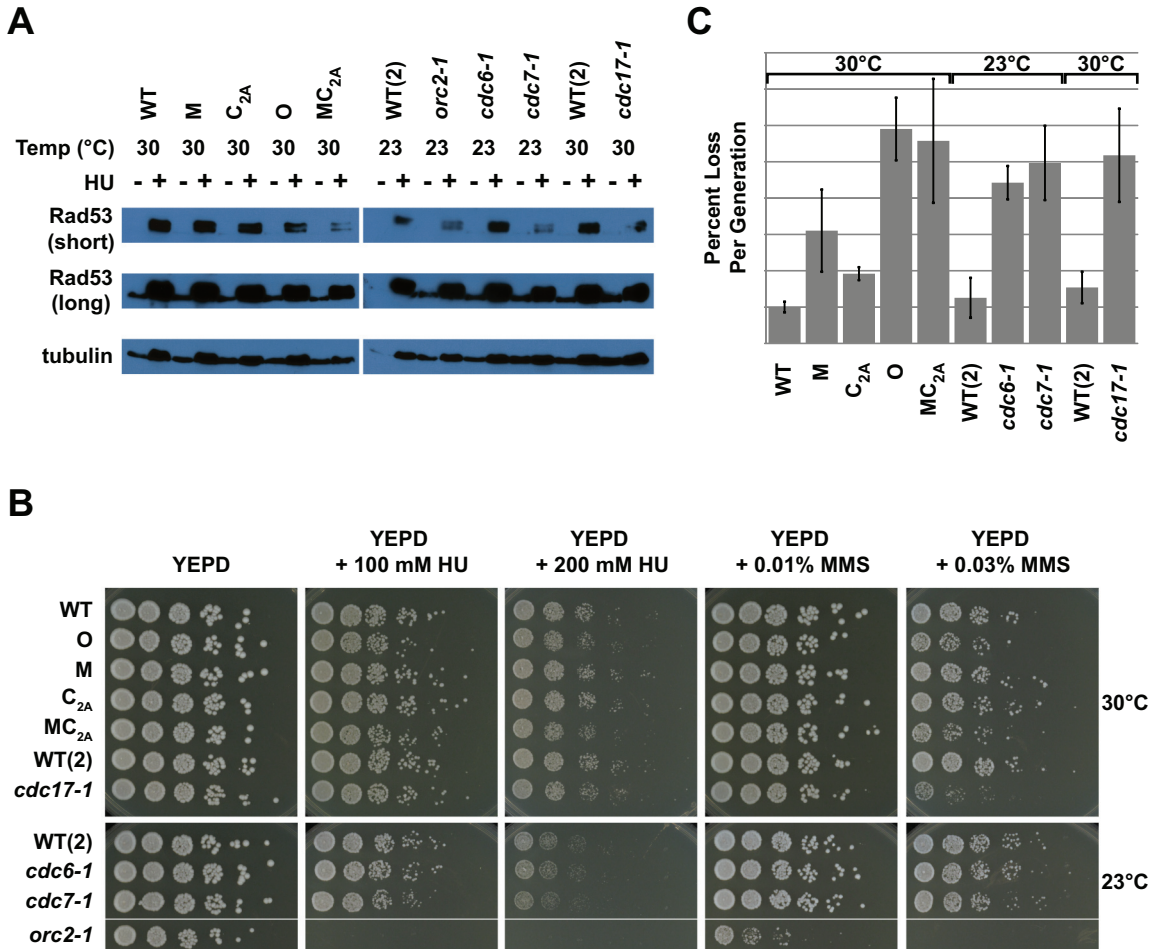


Figure 3. Replication stress levels in deregulated strains are comparable to the levels in the replication stress strains. A) The *cdc17-1* strain displays weak activation of the DNA damage response as measured by Rad53 phosphorylation during unperturbed growth (see long exposure). None of the other strains display such a response. All strains can however activate a DNA damage response as measured by Rad53 hyper-phosphorylation when treated with 200 mM HU for 3 hours. B) 5-fold serial dilutions of each strain were spotted onto the indicated media and grown at the indicated temperature (52.5 hr for the 30°C plates and 94 hr for the 23°C plates). The O, MC_{2A}, and *cdc17-1* strains are mildly sensitive to the higher concentrations of HU and MMS. The *orc2-1* strain is hypersensitive to both inhibitors. C) Plasmid loss rates were measured for three independent transformants for each strain. The non-selective outgrowth phase was performed at the indicated temperatures. The percent loss per generation data are displayed as the mean \pm 1 SD.

Table 1. Amplification rates for deregulated strains.

Strain (YJL#)	Mean Rate (cell ⁻¹ gen ⁻¹)	Standard Deviation	Fold Change/ WT Rate	Trials (n)
WT (YJL9756)	5.26 x 10 ⁻⁸	2.65 x 10 ⁻⁹	1.00	4
M (YJL9753)	1.19 x 10 ⁻⁷	5.05 x 10 ⁻⁸	2.26	3
C _{2A} (YJL9762)	1.98 x 10 ⁻⁶	3.05 x 10 ⁻⁷	37.71	3
O (YJL9750)	4.10 x 10 ⁻⁵	5.98 x 10 ⁻⁶	779.54	4
MC _{2A} (YJL9842)	4.43 x 10 ⁻⁵	8.64 x 10 ⁻⁶	841.88	3

Table 2. Amplification rates for replication stress strains.

Strain (YJL#)	Mean Rate (cell ⁻¹ gen ⁻¹)	Standard Deviation	Fold Change/ WT Rate	Temp (°C)	Trials (n)
WT (YJL9892)	1.18 x 10 ⁻⁷	1.95 x 10 ⁻⁸	1.00	23	4
<i>orc2-1</i> (YJL9951)	3.82 x 10 ⁻⁷	9.65 x 10 ⁻⁸	3.23	23	3
<i>cdc6-1</i> (YJL9996)	4.31 x 10 ⁻⁷	2.57 x 10 ⁻⁸	3.66	23	4
<i>cdc7-1</i> (YJL9940)	3.74 x 10 ⁻⁶	2.10 x 10 ⁻⁶	31.73	23	3
WT (YJL9892)	4.99 x 10 ⁻⁸	5.89 x 10 ⁻⁹	1.00	30	3
<i>cdc17-1</i> (YJL9945)	6.70 x 10 ⁻⁷	4.87 x 10 ⁻⁸	13.41	30	3

Table 3. Amplification rates for recombination mutants in the wild-type context.

Strain (YJL#)	Mean Rate (cell ⁻¹ gen ⁻¹)	Standard Deviation	Fold Change/ WT Rate	Trials (n)
WT (YJL9756)	5.26 x 10 ⁻⁸	2.65 x 10 ⁻⁹	1.00	4
<i>rad1</i> Δ (YJL9909)	1.15 x 10 ⁻⁸	6.64 x 10 ⁻¹⁰	0.22	3
<i>msh3</i> Δ (YJL10146/10147)	9.14 x 10 ⁻⁹	2.45 x 10 ⁻⁹	0.17	3
<i>rad51</i> Δ (YJL9906)	1.18 x 10 ⁻⁷	5.55 x 10 ⁻⁹	2.24	3
<i>rad52</i> Δ (YJL9903/9904)	9.50 x 10 ⁻⁸	1.15 x 10 ⁻⁸	1.81	4
<i>rad59</i> Δ (YJL10149/10150)	8.39 x 10 ⁻⁸	1.60 x 10 ⁻⁸	1.59	3
<i>pol32</i> Δ (YJL10143/10144)	9.21 x 10 ⁻⁸	9.46 x 10 ⁻⁹	1.75	3

Table 4. Amplification rates for recombination mutants in the *orc2-cdk6A orc6-cdk4A* context.

Strain (YJL#)	Mean Rate (cell ⁻¹ gen ⁻¹)	Standard Deviation	Fold Change/ O Rate	Trials (n)
O (YJL9750)	4.10 x 10 ⁻⁵	5.98 x 10 ⁻⁶	1.00	4
O <i>rad1</i> Δ (YJL9901)	9.28 x 10 ⁻⁷	1.73 x 10 ⁻⁷	0.02	3
O <i>msh3</i> Δ (YJL10136/10137)	2.95 x 10 ⁻⁶	2.86 x 10 ⁻⁷	0.07	3
O <i>rad51</i> Δ (YJL9898)	2.85 x 10 ⁻⁵	7.22 x 10 ⁻⁶	0.70	3
O <i>rad52</i> Δ (YJL9895)	8.12 x 10 ⁻⁷	1.46 x 10 ⁻⁷	0.02	4
O <i>rad59</i> Δ (YJL10139/10140)	4.46 x 10 ⁻⁶	1.64 x 10 ⁻⁶	0.11	3
O <i>pol32</i> Δ (YJL10133/10134)	5.22 x 10 ⁻⁶	1.74 x 10 ⁻⁶	0.13	3

Table 5. Amplification rates for *CLB* deletions.

Strain (YJL#)	Mean Rate (cell ⁻¹ gen ⁻¹)	Standard Deviation	Fold Change/ WT Rate	Trials (n)
WT (YJL9892)	4.99 x 10 ⁻⁸	5.89 x 10 ⁻⁹	1.00	3
<i>clb5</i> Δ (YJL10151/10152)	3.07 x 10 ⁻⁵	6.19 x 10 ⁻⁶	614.95	3
<i>clb5</i> Δ <i>clb6</i> Δ (YJL10194/10195)	6.04 x 10 ⁻⁵	5.60 x 10 ⁻⁶	1210.48	3

Table S1

Oligonucleotides used in this study. Listed 5' to 3', left to right. Uppercase letters indicate sequence that anneals to the template during PCR. Lowercase letters indicate sequence added by PCR, either to provide homology for genomic integration or fusion PCR or to provide restriction sites for cloning. Subscript numbers are nucleotide coordinates provided by the Saccharomyces Genome Database (version R64-1-1)

Name	Sequence	Purpose
RFP-F	tgattccggtgtaaaalacalataalacacaatctggcttaataaagtcGGTCGACGGATCCCCGGGTT	Integrate <i>pTEF2-dTomato</i> , <i>kanMX6</i> between nt 449529 and 449530 of <i>ChrIV</i>
RFP-R	aaaafatataagcactagccaaattggcaactcttataagatataattataTCGATGAATTGAGCTCGTT	Integrate <i>pTEF2-dTomato</i> , <i>kanMX6</i> between nt 449529 and 449530 of <i>ChrIV</i>
GFP-F	caittcaattatggccaccctatggcgatacaaaaatatttaagattgcGGTCGACGGATCCCCGGGTT	Integrate <i>pTEF2-eGFP</i> , <i>natMX6</i> between nt 682356 and 682357 of <i>ChrVII</i>
GFP-R	aactgttgtagttggatgigtacgtataaagggttgctgigtatataaaTCGATGAATTCGAGCTCGTT	Integrate <i>pTEF2-eGFP</i> , <i>natMX6</i> between nt 682356 and 682357 of <i>ChrVII</i>
<i>pds1Δ</i> -F	ataaalatcgtalalaacaggaalgaagttccggcaitaactttccacagTAATACGACTCACTATAGGG	Replace nucleotides 79-912 of the <i>PDS1</i> ORF with <i>K1URA3</i>
<i>pds1Δ</i> -R	tcgctcttcaatgittctagtgggagaaatacaactttatctggAAATTAACCCCTCACTAAA GGG	Replace nucleotides 79-912 of the <i>PDS1</i> ORF with <i>K1URA3</i>
OJL25	GCGGATAACAATTTCACACAGG	Amplify 5' <i>natR</i> for pKJF034
OJL3057	gtgcaagcgctagaacalacAGACGACCACGAAGCCCG	Amplify 5' <i>natR</i> for pKJF034
OJL6	GTAATACGACTCACTATAGGGC	Amplify 3' <i>natR</i> for pKJF034; Fusion PCR to make <i>pTEF-natR₁₋₂₉₂-ACT1_{intron}</i>
OJL3058	cttttgtctatataitattgtagCGTACTCCGGCTGGAAC	Amplify 3' <i>natR</i> for pKJF034
OJL3053	GTATGTTTAGCGCTTG	Amplify <i>ACT1</i> intron for pKJF034
OJL3054	CTAAACATATAATATAGCAACA	Amplify <i>ACT1</i> intron for pKJF034
OJL2374	ACTAAAGGGGAACAATAAGCTGG	Fusion PCR to make <i>pTEF-natR₁₋₂₉₂-ACT1_{intron}</i> - <i>natR₂₉₃₋₅₇₃-tTEF</i> for pKJF034
OJL3062	gtcaatagggatccGGCGCCGAGATCTGTTAG	Amplify <i>pTEF-natR₁₋₂₉₂-ACT1_{intron}</i> - <i>natR₂₉₃₋₃₄₀</i> for pKJF035
OJL3063	gtcaicaggggaattcCGACCTCGATGCTCGACG	Amplify <i>pTEF-natR₁₋₂₉₂-ACT1_{intron}</i> - <i>natR₂₉₃₋₃₄₀</i> for pKJF035
OJL2543	gtcaicaggggaattcGAGCAGATTGACTGAGAGTG	Amplify <i>URA3</i> for pKJF035; Amplify <i>TRP1</i> for pKJF036
OJL2544	gtcaicaggggaattcGCATCTGTGGGTAITTCAC	Amplify <i>URA3</i> for pKJF035
OJL3064	gtcaicaggggaattcAATCGGACGACGAATCGGAC	Amplify <i>natR₁₉₁₋₂₉₂-ACT1_{intron}</i> - <i>natR₂₉₃₋₅₇₃-tTEF</i> for pKJF036
OJL3065	gtcaicaggggaattcGGCGGCTTAGTATCG	Amplify <i>natR₁₉₁₋₂₉₂-ACT1_{intron}</i> - <i>natR₂₉₃₋₅₇₃-tTEF</i> for pKJF036
OJL3061	gtcaicaggggaattcGCATCTGTGGGTAITTCAC	Amplify <i>TRP1</i> for pKJF036
OJL3269	gtcaicagggccggACTTGTGCAAAITTAGCTC	Amplify <i>cdc6-1</i> from YJL885 for pKJF037
OJL3270	gtcaicagggccggCGTTTTCCCGTTTTTCTTCCG	Amplify <i>cdc6-1</i> from YJL885 for pKJF037
OJL3273	gtcaicagggccggGCAAAITTTTGAGAAAGTTCCAG	Amplify <i>cdc7-1</i> from YJL892 for pKJF039
OJL3274	gtcaicagggccggTGATGATGTTCTAGGATATTG	Amplify <i>cdc7-1</i> from YJL892 for pKJF039
OJL3078	cglgcaacglaaacaacatctatacaagaiaaaaalggggaaaagaalgctgaaggGCATCTGTGCGGGTATTCCAC	Step 1 PCR core: Integrate <i>natR₁₉₁₋₂₉₂-ACT1_{intron}</i> - <i>natR₂₉₃₋₅₇₃-tTEF</i> , replacing <i>ChrVII₁₅₆₁₈₄₃₋₅₇₄₇₀₀</i>
OJL3079	tcaattgtagatcaccattgcttcaagattatgagaaaagaalgcacaaacataaacGGATGCGCGCTTAGTA TCG	Step 1 PCR core: Integrate <i>natR₁₉₁₋₂₉₂-ACT1_{intron}</i> - <i>natR₂₉₃₋₅₇₃-tTEF</i> , replacing <i>ChrVII₁₅₆₁₈₄₃₋₅₇₄₇₀₀</i>
OJL2750	GCTGTTGTCCCAAAAGTTACC	Step 1 PCR Left Homology: Integrate <i>natR₁₉₁₋₂₉₂-ACT1_{intron}</i> - <i>natR₂₉₃₋₅₇₃-tTEF</i> , replacing <i>ChrVII₁₅₆₁₈₄₃₋₅₇₄₇₀₀</i> . Step 2 Fusion PCR for 3' <i>natR</i> integration fragment
OJL3104	GATTGTTGTTTACGTGCACG	Step 1 PCR Left Homology: Integrate <i>natR₁₉₁₋₂₉₂-ACT1_{intron}</i> - <i>natR₂₉₃₋₅₇₃-tTEF</i> , replacing <i>ChrVII₁₅₆₁₈₄₃₋₅₇₄₇₀₀</i>
OJL2751	CCCCCAAGTAAGTAGCTCAG	Step 1 PCR Right Homology: Integrate <i>natR₁₉₁₋₂₉₂-ACT1_{intron}</i> - <i>natR₂₉₃₋₅₇₃-tTEF</i> , replacing <i>ChrVII₁₅₆₁₈₄₃₋₅₇₄₇₀₀</i> . Step 2 Fusion PCR for 3' <i>natR</i> integration fragment

Table S2

Plasmids used in this study.

Name	Description	Source
pRSS56	<i>Amp^R</i>	Sikorski, R.S. et al. <i>Genetics</i> 122(1) , 19-27 (1989)
pRS306	<i>URA3</i>	Sikorski, R.S. et al. <i>Genetics</i> 122(1) , 19-27 (1989)
pRS314	<i>TRP1, CEN-ARS</i>	Sikorski, R.S. et al. <i>Genetics</i> 122(1) , 19-27 (1989)
pRS316	<i>URA3, CEN-ARS</i>	Sikorski, R.S. et al. <i>Genetics</i> 122(1) , 19-27 (1989)
pFA6a-kanMX6	<i>kanMX6</i>	Longtine, M.S. et al. <i>Yeast</i> 14 , 953-961 (1998)
pAG32	<i>hphMX4</i>	Goldstein, A.L. et al. <i>Yeast</i> 15 , 1541-1553 (1999)
pAG36	<i>natMX4, CEN-ARS, URA3</i>	Goldstein, A.L. et al. <i>Yeast</i> 15 , 1541-1553 (1999)
pDK206	<i>ADE3, LEU2, CEN3, ARS1</i>	Koshland, D. et al. <i>Cell</i> 40 , 393-403 (1985)
pPP117	<i>cdc7-1, URA3</i>	Sclafani, R. Unpublished
pJR1267	<i>orc2-1, URA3</i>	Fox, C.A. Unpublished
pJL737	<i>ORC6, URA3</i>	Nguyen, V.Q. et al. <i>Nature</i> 411 , 1068-1073 (2001)
pJL1033	<i>MCM7, URA3</i>	Nguyen, V.Q. et al. <i>Curr Biol</i> 10 , 195-205 (2000)
pUT1549	Δ <i>ntCDC6-cdk2A, URA3</i>	This Study
pKJF004	<i>ADE3, LEU2, CEN3, ARS1, Amp^R</i>	This Study
pKJF034	<i>pTEF-natR₁₋₂₉₂-ACT1_{intron}-natR₂₉₃₋₅₇₃-tTEF, URA3, CEN-ARS</i>	This Study
pKJF035	<i>pTEF-natR₁₋₂₉₂-ACT1_{intron}-natR₂₉₃₋₃₄₀ + URA3, TRP1, CEN-ARS</i>	This Study
pKJF036	<i>natR₁₉₁₋₂₉₂-ACT1_{intron}-natR₂₉₃₋₅₇₃-tTEF + TRP1, URA3, CEN-ARS</i>	This Study
pKJF037	<i>cdc6-1, URA3</i>	This Study
pKJF039	<i>cdc17-1, URA3</i>	This Study

Table S2 (continued)

Plasmids used in this study.

pFA6a-kanMX6- pTEF2-dTomato	pTEF2-dTomato, kanMX6	This Study
pFA6a-natMX6- pTEF2-eGFP	pTEF2-eGFP, natMX6	This Study
p210-BS- KlacURA3	Kl:URA3	This Study

Table S3

Yeast strains used in this study.

Strain	Genotype	Source
YJL1737	MATa <i>orc2-cdk6A orc6-cdk4A leu2 ura3-52 trp1-289 ade2 ade3 bar1::LEU2</i>	Nguyen et al. ¹
YJL3151	MATa <i>ORC2 orc6-cdk4A MCM7-2NLS leu2 ura3-52 trp1-289 ade2 ade3 bar1::LEU2</i>	Green et al. ²
YJL3158	MATa <i>ORC2 ORC6 MCM7-2NLS leu2 ura3-52 trp1-289 ade2 ade3 bar1::LEU2</i>	This Study
YJL9252	MATa <i>ura3-1 trp1-1 leu2-3,112 his3-11 ade2-1 can1-100 CEN4::[pTEF2-dTomato, kanMX]</i>	This Study
YJL9272	MATa <i>ura3-1 trp1-1 leu2-3,112 his3-11 ade2-1 can1-100 CEN4::[pTEF2-dTomato, kanMX] ESP1::[pTEF2-eGFP, natMX]</i>	This Study
YJL9464	MATa <i>pds1::[KIURA3 ura3-1 trp1-1 leu2-3,112 his3-11 ade2-1 can1-100 CEN4::[pTEF2-dTomato, kanMX] ESP1::[pTEF2-eGFP, natMX]</i>	This Study
YJL9699	MATa <i>ORC2 ORC6 MCM7 leu2 ura3-52 trp1-289 ade2 ade3 bar1::LEU2</i>	This Study
YJL9715	MATa <i>ORC2 ORC6 MCM7-2NLS ΔntCDC6-cdk2A leu2 ura3-52 trp1-289 ade2 ade3 bar1::LEU2</i>	This Study
YJL9716	MATa <i>ORC2 ORC6 MCM7 ΔntCDC6-cdk2A leu2 ura3-52 trp1-289 ade2 ade3 bar1::LEU2</i>	This Study
YJL9727	MATa <i>orc2-cdk6A orc6-cdk4A leu2 ura3-52 trp1-289 ade2 ade3 bar1::LEU2 <ygrcdelta15-ygrcdelta18>::[TRP1, natR₁₉₁₋₂₉₂-ACT1_{intron}, natR₂₉₃₋₅₇₃-tTEF]</i>	This Study
YJL9730	MATa <i>ORC2 ORC6 MCM7-2NLS leu2 ura3-52 trp1-289 ade2 ade3 bar1::LEU2 <ygrcdelta15-ygrcdelta18>::[TRP1, natR₁₉₁₋₂₉₂-ACT1_{intron}, natR₂₉₃₋₅₇₃-tTEF]</i>	This Study
YJL9733	MATa <i>ORC2 ORC6 MCM7 leu2 ura3-52 trp1-289 ade2 ade3 bar1::LEU2 <ygrcdelta15-ygrcdelta18>::[TRP1, natR₁₉₁₋₂₉₂-ACT1_{intron}, natR₂₉₃₋₅₇₃-tTEF]</i>	This Study

Table S3 (continued)

Yeast strains used in this study.

YJL9737	MATa ORC2 ORC6 MCM7-2NLS ΔntCDC6-cdk2A leu2 ura3-52 trp1-289 ade2 ade3 bar1::LEU2 <ygrcdelta15-ygrcdelta18>:::{TRP1, natR ₁₉₁₋₂₉₂ -ACT1 _{intron} , natR ₂₉₃₋₅₇₃ -tTEF}	This Study
YJL9739	MATa ORC2 ORC6 MCM7 ΔntCDC6-cdk2A leu2 ura3-52 trp1-289 ade2 ade3 bar1::LEU2 <ygrcdelta15-ygrcdelta18>:::{TRP1, natR ₁₉₁₋₂₉₂ -ACT1 _{intron} , natR ₂₉₃₋₅₇₃ -tTEF}	This Study
YJL9750	MATa orc2-cdk6A orc6-cdk4A leu2 ura3-52 trp1-289 ade2 ade3 bar1::LEU2 <ygrcdelta15-ygrcdelta18>:::{TRP1, natR ₁₉₁₋₂₉₂ -ACT1 _{intron} , natR ₂₉₃₋₅₇₃ -tTEF} <ygrwdelta19>:::{pTEF-natR ₁₋₂₉₂ -ACT1 _{intron} -natR ₂₉₃₋₃₄₀ , URA3}	This Study
YJL9753	MATa ORC2 ORC6 MCM7-2NLS leu2 ura3-52 trp1-289 ade2 ade3 bar1::LEU2 <ygrcdelta15-ygrcdelta18>:::{TRP1, natR ₁₉₁₋₂₉₂ -ACT1 _{intron} , natR ₂₉₃₋₅₇₃ -tTEF} <ygrwdelta19>:::{pTEF-natR ₁₋₂₉₂ -ACT1 _{intron} -natR ₂₉₃₋₃₄₀ , URA3}	This Study
YJL9756	MATa ORC2 ORC6 MCM7 leu2 ura3-52 trp1-289 ade2 ade3 bar1::LEU2 <ygrcdelta15-ygrcdelta18>:::{TRP1, natR ₁₉₁₋₂₉₂ -ACT1 _{intron} , natR ₂₉₃₋₅₇₃ -tTEF} <ygrwdelta19>:::{pTEF-natR ₁₋₂₉₂ -ACT1 _{intron} -natR ₂₉₃₋₃₄₀ , URA3}	This Study
YJL9762	MATa ORC2 ORC6 MCM7 ΔntCDC6-cdk2A leu2 ura3-52 trp1-289 ade2 ade3 bar1::LEU2 <ygrcdelta15-ygrcdelta18>:::{TRP1, natR ₁₉₁₋₂₉₂ -ACT1 _{intron} , natR ₂₉₃₋₅₇₃ -tTEF} <ygrwdelta19>:::{pTEF-natR ₁₋₂₉₂ -ACT1 _{intron} -natR ₂₉₃₋₃₄₀ , URA3}	This Study
YJL9842	MATa ORC2 ORC6 MCM7-2NLS ΔntCDC6-cdk2A leu2 ura3-52 trp1-289 ade2 ade3 bar1::LEU2 <ygrcdelta15-ygrcdelta18>:::{TRP1, natR ₁₉₁₋₂₉₂ -ACT1 _{intron} , natR ₂₉₃₋₅₇₃ -tTEF} <ygrwdelta19>:::{pTEF-natR ₁₋₂₉₂ -ACT1 _{intron} -natR ₂₉₃₋₃₄₀ , URA3}	This Study
YJL9892	MATa ORC2 ORC6 MCM7 leu2 ura3-52 trp1-289 ade2 ade3 bar1::LEU2 <ygrcdelta15-ygrcdelta18>:::{TRP1, natR ₁₉₁₋₂₉₂ -ACT1 _{intron} , natR ₂₉₃₋₅₇₃ -tTEF} <ygrwdelta19>:::{pTEF-natR ₁₋₂₉₂ -ACT1 _{intron} -natR ₂₉₃₋₃₄₀ }	This Study
YJL9895	MATa orc2-cdk6A orc6-cdk4A leu2 ura3-52 trp1-289 ade2 ade3 bar1::LEU2 <ygrcdelta15-ygrcdelta18>:::{TRP1, natR ₁₉₁₋₂₉₂ -ACT1 _{intron} , natR ₂₉₃₋₅₇₃ -tTEF} <ygrwdelta19>:::{pTEF-natR ₁₋₂₉₂ -ACT1 _{intron} -natR ₂₉₃₋₃₄₀ , URA3} rad52::hphMX	This Study
YJL9898	MATa orc2-cdk6A orc6-cdk4A leu2 ura3-52 trp1-289 ade2 ade3 bar1::LEU2 <ygrcdelta15-ygrcdelta18>:::{TRP1, natR ₁₉₁₋₂₉₂ -ACT1 _{intron} , natR ₂₉₃₋₅₇₃ -tTEF} <ygrwdelta19>:::{pTEF-natR ₁₋₂₉₂ -ACT1 _{intron} -natR ₂₉₃₋₃₄₀ , URA3} rad51::hphMX	This Study

Table S3 (continued)

Yeast strains used in this study.

YJL9901	MATa <i>orc2-cdk6A orc6-cdk4A leu2 ura3-52 trp1-289 ade2 ade3 bar1::LEU2 <ygrcdelta15-ygrcdelta18>::[TRP1, natR₁₉₁₋₂₉₂-ACT1_{intron}. natR₂₉₃₋₅₇₃-tTEF] <ygrwdelta19>::[pTEF-natR₁₋₂₉₂-ACT1_{intron}-natR₂₉₃₋₃₄₀, URA3] rad1::hphMX</i>	This Study
YJL9903/9904	MATa ORC2 ORC6 MCM7 <i>leu2 ura3-52 trp1-289 ade2 ade3 bar1::LEU2 <ygrcdelta15-ygrcdelta18>::[TRP1, natR₁₉₁₋₂₉₂-ACT1_{intron}. natR₂₉₃₋₅₇₃-tTEF] <ygrwdelta19>::[pTEF-natR₁₋₂₉₂-ACT1_{intron}-natR₂₉₃₋₃₄₀, URA3] rad52::hphMX</i>	This Study
YJL9906	MATa ORC2 ORC6 MCM7 <i>leu2 ura3-52 trp1-289 ade2 ade3 bar1::LEU2 <ygrcdelta15-ygrcdelta18>::[TRP1, natR₁₉₁₋₂₉₂-ACT1_{intron}. natR₂₉₃₋₅₇₃-tTEF] <ygrwdelta19>::[pTEF-natR₁₋₂₉₂-ACT1_{intron}-natR₂₉₃₋₃₄₀, URA3] rad51::hphMX</i>	This Study
YJL9909	MATa ORC2 ORC6 MCM7 <i>leu2 ura3-52 trp1-289 ade2 ade3 bar1::LEU2 <ygrcdelta15-ygrcdelta18>::[TRP1, natR₁₉₁₋₂₉₂-ACT1_{intron}. natR₂₉₃₋₅₇₃-tTEF] <ygrwdelta19>::[pTEF-natR₁₋₂₉₂-ACT1_{intron}-natR₂₉₃₋₃₄₀, URA3] rad1::hphMX</i>	This Study
YJL9940	MATa <i>cdc7-1 ORC2 ORC6 MCM7 leu2 ura3-52 trp1-289 ade2 ade3 bar1::LEU2 <ygrcdelta15-ygrcdelta18>::[TRP1, natR₁₉₁₋₂₉₂-ACT1_{intron}. natR₂₉₃₋₅₇₃-tTEF] <ygrwdelta19>::[pTEF-natR₁₋₂₉₂-ACT1_{intron}-natR₂₉₃₋₃₄₀]</i>	This Study
YJL9945	MATa <i>cdc17-1 ORC2 ORC6 MCM7 leu2 ura3-52 trp1-289 ade2 ade3 bar1::LEU2 <ygrcdelta15-ygrcdelta18>::[TRP1, natR₁₉₁₋₂₉₂-ACT1_{intron}. natR₂₉₃₋₅₇₃-tTEF] <ygrwdelta19>::[pTEF-natR₁₋₂₉₂-ACT1_{intron}-natR₂₉₃₋₃₄₀]</i>	This Study
YJL9951	MATa <i>orc2-1 ORC6 MCM7 leu2 ura3-52 trp1-289 ade2 ade3 bar1::LEU2 <ygrcdelta15-ygrcdelta18>::[TRP1, natR₁₉₁₋₂₉₂-ACT1_{intron}. natR₂₉₃₋₅₇₃-tTEF] <ygrwdelta19>::[pTEF-natR₁₋₂₉₂-ACT1_{intron}-natR₂₉₃₋₃₄₀]</i>	This Study
YJL9996	MATa <i>cdc6-1 ORC2 ORC6 MCM7 leu2 ura3-52 trp1-289 ade2 ade3 bar1::LEU2 <ygrcdelta15-ygrcdelta18>::[TRP1, natR₁₉₁₋₂₉₂-ACT1_{intron}. natR₂₉₃₋₅₇₃-tTEF] <ygrwdelta19>::[pTEF-natR₁₋₂₉₂-ACT1_{intron}-natR₂₉₃₋₃₄₀]</i>	This Study
YJL10133/10134	MATa <i>orc2-cdk6A orc6-cdk4A leu2 ura3-52 trp1-289 ade2 ade3 bar1::LEU2 <ygrcdelta15-ygrcdelta18>::[TRP1, natR₁₉₁₋₂₉₂-ACT1_{intron}. natR₂₉₃₋₅₇₃-tTEF] <ygrwdelta19>::[pTEF-natR₁₋₂₉₂-ACT1_{intron}-natR₂₉₃₋₃₄₀, URA3] pol32::hphMX</i>	This Study

Table S3 (continued)

Yeast strains used in this study.

YJL10136/ 10137	MATa <i>orc2-cdk6A orc6-cdk4A leu2 ura3-52 trp1-289 ade2 ade3 bar1::LEU2 <ygrcdelta15-ygrcdelta18>::(TRP1, natR</i> ¹⁹¹⁻²⁹² <i>ACT1</i> ^{intron, natR} ²⁹³⁻⁵⁷³ <i>-tTEF</i> <ygrwdelta19>:: <i>(p TEF-natR</i> ¹⁻²⁹² <i>-ACT1</i> ^{intron -natR} ²⁹³⁻³⁴⁰ <i>URA3</i> <i>msh3::hphMX</i>	This Study
YJL10139/ 10140	MATa <i>orc2-cdk6A orc6-cdk4A leu2 ura3-52 trp1-289 ade2 ade3 bar1::LEU2 <ygrcdelta15-ygrcdelta18>::(TRP1, natR</i> ¹⁹¹⁻²⁹² <i>ACT1</i> ^{intron, natR} ²⁹³⁻⁵⁷³ <i>-tTEF</i> <ygrwdelta19>:: <i>(p TEF-natR</i> ¹⁻²⁹² <i>-ACT1</i> ^{intron -natR} ²⁹³⁻³⁴⁰ <i>URA3</i> <i>rad59::hphMX</i>	This Study
YJL10143/ 10144	MATa ORC2 ORC6 MCM7 <i>leu2 ura3-52 trp1-289 ade2 ade3 bar1::LEU2 <ygrcdelta15-ygrcdelta18>::(TRP1, natR</i> ¹⁹¹⁻²⁹² <i>ACT1</i> ^{intron, natR} ²⁹³⁻⁵⁷³ <i>-tTEF</i> <ygrwdelta19>:: <i>(p TEF-natR</i> ¹⁻²⁹² <i>-ACT1</i> ^{intron -natR} ²⁹³⁻³⁴⁰ <i>URA3</i> <i>pol32::hphMX</i>	This Study
YJL10146/ 10147	MATa ORC2 ORC6 MCM7 <i>leu2 ura3-52 trp1-289 ade2 ade3 bar1::LEU2 <ygrcdelta15-ygrcdelta18>::(TRP1, natR</i> ¹⁹¹⁻²⁹² <i>ACT1</i> ^{intron, natR} ²⁹³⁻⁵⁷³ <i>-tTEF</i> <ygrwdelta19>:: <i>(p TEF-natR</i> ¹⁻²⁹² <i>-ACT1</i> ^{intron -natR} ²⁹³⁻³⁴⁰ <i>URA3</i> <i>msh3::hphMX</i>	This Study
YJL10149/ 10150	MATa ORC2 ORC6 MCM7 <i>leu2 ura3-52 trp1-289 ade2 ade3 bar1::LEU2 <ygrcdelta15-ygrcdelta18>::(TRP1, natR</i> ¹⁹¹⁻²⁹² <i>ACT1</i> ^{intron, natR} ²⁹³⁻⁵⁷³ <i>-tTEF</i> <ygrwdelta19>:: <i>(p TEF-natR</i> ¹⁻²⁹² <i>-ACT1</i> ^{intron -natR} ²⁹³⁻³⁴⁰ <i>URA3</i> <i>rad59::hphMX</i>	This Study
YJL10151/ 10152	MATa ORC2 ORC6 MCM7 <i>leu2 ura3-52 trp1-289 ade2 ade3 bar1::LEU2 <ygrcdelta15-ygrcdelta18>::(TRP1, natR</i> ¹⁹¹⁻²⁹² <i>ACT1</i> ^{intron, natR} ²⁹³⁻⁵⁷³ <i>-tTEF</i> <ygrwdelta19>:: <i>(p TEF-natR</i> ¹⁻²⁹² <i>-ACT1</i> ^{intron -natR} ²⁹³⁻³⁴⁰ <i>URA3</i> <i>clb5::kanMX</i>	This Study
YJL10194/ 10195	MATa ORC2 ORC6 MCM7 <i>leu2 ura3-52 trp1-289 ade2 ade3 bar1::LEU2 <ygrcdelta15-ygrcdelta18>::(TRP1, natR</i> ¹⁹¹⁻²⁹² <i>ACT1</i> ^{intron, natR} ²⁹³⁻⁵⁷³ <i>-tTEF</i> <ygrwdelta19>:: <i>(p TEF-natR</i> ¹⁻²⁹² <i>-ACT1</i> ^{intron -natR} ²⁹³⁻³⁴⁰ <i>clb5::kanMX clb6::URA3</i>	This Study

¹ Nguyen, V.Q. et al. *Nature* **411**, 1068-1073 (2001)

² Green, B.M. et al. *Science* **329**, 943-946 (2010)

Chapter 5

Conclusions

Through the work I conducted over the course of my pre-doctoral training and that I have presented here in this thesis I have attempted to critically evaluate a number of long-held assumptions in the replication and genomic instability fields. I believe I have met with some measure of success in these efforts, and I will discuss the general conclusions that can be gleaned from this work. Of course, this has led to the identification of new questions to be addressed, a few of which I will comment upon here.

Re-Replication as Source of Genomic Instability

From the perspective of the replication field, perhaps the most important findings presented in this thesis come from the work presented in Chapter 2. Prior to that study, which was initiated by Brian Green and continued by myself, the only solid evidence that re-replication could be detrimental to the cell came from studies in which replication control was severely crippled. Under those conditions massive DNA damage was readily apparent and cell death was widespread. This was a general phenomenon, observed in a number of different organisms including budding yeast [1,2], cultured human cells[3–8], and *X. laevis* [7,9]. Clearly, death is a bad thing from the perspective of the cell, and it is therefore obvious that prevention of large amounts of re-replication is desirable. However, the conclusion drawn by extension from these studies that the extremely tight block to re-initiation imposed in all eukaryotes examined to date is important because re-replication threatens genome stability was, frankly, unsupported. No experimental systems were then available for addressing the consequences of low, sub-lethal levels of re-replication.

Indeed, it is this low, sub-lethal level of re-replication that is most interesting when considering the possibility of genomic instability. One of the hallmarks of human cancer is genomic instability, which is thought to contribute to tumor initiation and/or progression [10,11]. An obvious prerequisite for a cell to contribute to the formation of a tumor is the capacity to proliferate. So, the high levels of re-replication observed in

studies where replication control was massively compromised, which lead to cell death, are irrelevant in the context of cancer. That is, if re-replication actually contributes to meaningful genomic alterations in the context of cancer, or evolution, for that matter, those alterations must be heritable and hence be the consequence of low levels of re-replication.

A previous study conducted in the Li lab demonstrated that mechanisms preventing re-replication function in an overlapping, rather than redundant, manner [12]. In the course of this study, it was discovered that simultaneous disruption of CDK regulation of the Mcm2-7 complex and Cdc6 led to re-initiation of replication from primarily a single origin, *ARS317*. Importantly, when transplanted to other parts of the genome this origin maintained its preferential ability to re-initiate. This provided us with the first opportunity to critically evaluate the longstanding belief that low levels of re-replication could cause genomic instability.

Genomic instability is actually a rather broad term, encompassing a wide array of different kinds of genomic alterations. These include translocations, deletions, inversions, aneuploidies, and gene amplifications. Evaluating the role of re-replication in each of these would require a unique experimental setup, so as a practical matter we focused on just one form of genomic instability, gene amplification, in our initial investigation. This choice actually enabled us to not only evaluate the hypothesis that the barrier to re-replication was important for the preservation of genome stability, but also afforded us the opportunity to challenge the conclusion reached by the cancer field that re-replication does *not* contribute to gene amplification [13–15]. Indeed, the ‘over-replication’ model, first formalized in 1981, was one of the earliest considered when high rates of gene amplification were observed in cancer cells in the late 1970s and early 1980s [16–20]. However, no evidence of re-replication in cells with amplified genes could be detected, and little was known about replication control at the time, precluding experimental induction of re-replication. This absence of evidence was taken as evidence

of absence, and the field dismissed re-replication as a potential contributor to gene amplification.

As described in detail in Chapter 2, we were in fact able to demonstrate that re-replication can potently induce gene amplification, a phenomenon we unimaginatively termed ‘Re-Replication Induced Gene Amplification’ (RRIGA). This finding simultaneously validated the belief that the barrier to re-replication is necessary to preserve genome integrity and challenged the conclusion re-replication cannot contribute to gene amplification in cancer.

Of course, these studies could not demonstrate whether or not re-replication actually *does* contribute to gene amplification in cancer, or in any other setting. Rather, we can only state that re-replication *can* cause gene amplification. Additional studies are needed to determine whether or not low levels of re-replication occur in cancer cells, and whether such re-replication leads to gene amplification or any other form of genomic instability. Such endeavors are not trivial, and will require the development of new, extremely sensitive assays for monitoring re-replication and detecting rare gene amplification events. Moreover, the advantage we enjoyed in budding yeast of having a specific origin prone to re-initiation will not be available in other systems, since, unlike budding yeast, other organisms typically do not have replication origins defined by specific sequences. I do, however, think that such studies should be undertaken, despite the technical barriers and the inevitable unforeseen difficulties. Understanding the sources of gene amplification in cancer is crucial to improving our ability to combat it. Moreover, there are several lines of evidence suggesting that re-replication might be involved in oncogenesis, including observations of dysregulated replication initiation proteins in actual human tumors [21–27] and experimental evidence that deliberate over-expression of these same factors can drive tumor formation in some murine models [28,29,21]. Hopefully, our work has removed the psychological barrier to considering a role for re-replication in oncogenesis and such studies will be undertaken.

The Mechanism of RRIGA

One question that followed from the work presented in Chapter 2 demonstrating the phenomenon of RRIGA was, “What makes re-replication so efficient at stimulating gene amplification?” Put another way, what is the mechanism of RRIGA?

The prevailing models for gene amplification involving non-allelic homologous recombination (NAHR) invoke double stranded breaks (DSBs) or replication stress as the initiating event in the amplification process [30–32]. Previous studies had shown that re-replication can lead to DSBs and DNA damage, but as described in Chapter 2 neither inducing DSBs directly nor causing DNA damage or replication stress yielded appreciable frequencies of gene amplification. This argued that some other aspect(s) of re-replication contributes to its remarkable efficiency.

As described in Chapter 3, I demonstrated that RRIGA is heavily dependent upon the single-stranded annealing (SSA) sub-type of homologous recombination. This is significant for at least three reasons. First, SSA is typically associated with deletions, not amplifications. So, this finding expands upon the kinds of genomic alterations that this not so error free form of homologous recombination contributes to. Secondly, the other major models for gene amplification predict that resolution is mediated by a gene conversion-like mechanism or some form of break induced replication, not SSA [30–33]. This provides a potentially useful genetic distinction between RRIGA and other mechanisms for discerning which mechanism may or may underlie a particular amplification event. Lastly, a role for SSA in RRIGA leads to the prediction that two DSBs must arise, one at each fork, in order to generate the final head-to-tail duplication structure.

Indeed, I was able to detect such breaks to both sides of the re-initiating origin, distal to the flanking repetitive sequences involved in NAHR. Furthermore, such DSBs occur frequently enough such that it is reasonable to expect two such breaks to occur with a given re-replication bubble, one at each fork. The role of SSA and the occurrence

of these DSBs together help explain why RRIGA is so uniquely efficient. Re-initiation from *ARS317* leads to the formation of a single, isolated re-replication bubble. This differs from the situation in S-phase where replication initiates from many origins. If a fork stalls or encounters problems during S-phase, it will almost certainly be rescued by a converging fork from a neighboring origin. If the forks of a re-replication bubble encounter similar problems, however, they will remain un-rescued, and eventually collapse, forming DSBs. When DSBs arise at both forks in *trans* with respect to the chromatid axis, as would be expected if one strand were more prone to breakage than the other (I favor the notion that the lagging strand breaks, due to the presence of single stranded regions), then homologous recombination between the non-allelic repetitive sequences flanking the origin via SSA will yield a head-to-tail duplication. While this dual break scenario is nearly guaranteed in the context of re-replication, it would be comparatively rare in S-phase.

While it is clear that re-replication forks break at a rather high frequency, it is presently unclear why this is so. What prevents the re-replication forks from simply proceeding to the end of the chromosome, as has been suggested for replication forks during break-induced replication? A few possibilities have been explored. One possibility is that replisomes established during re-initiation are lacking some component normally incorporated into S-phase replisomes. However, we have assessed the levels of most of the constituents of the replisome and all are present at roughly stoichiometric amounts in re-replication replisomes as compared to S-phase replisomes (data not shown). A former graduate student also investigated the possibility that the presence of cohesin during re-replication inhibits fork progression. Removal of cohesin did not, however, measurably improve fork progression (data not shown).

While there are a number of other possible reasons for impaired re-replication fork progression and breakage, an important question to address first is whether or not re-replication forks are actually impaired relative to normal S-phase forks. We have

operated under the assumption that there is in fact some defect in re-replication forks, but no formal evaluation of the processivity of normal S-phase forks has ever been conducted. Normally, S-phase forks only have to traverse a relatively short distance (average inter-origin distance ~35 kb) [34,35]. Perhaps there is a natural limitation to the distance that any replication fork can traverse and no real difference exists between S-phase forks and re-replication forks, other than the fact that no neighboring origins fire in the re-replication setting. This possibility is presently under investigation in the laboratory.

The amplifications we observed strongly depend on SSA and homologous sequences in *cis* flanking the re-initiating origin. It is worth noting that homologous recombination is strongly favored over other repair pathways, such as non-homologous recombination or micro-homology mediated end-joining, in *S. cerevisiae*. In other organisms where alternative pathways dominate re-replication might still contribute to gene amplifications, but the broken bubble intermediate could be resolved in a different manner. Thus, RRIGA might also drive the formation of amplifications that do not bear repetitive sequences at the amplicon boundaries.

Spontaneous Amplifications and Sporadic Re-Initiation

As mentioned above, the work presented in Chapter 2 only provided evidence that re-replication *can* induce gene amplification, but not that it does so in any relevant biological context. The experiments presented in Chapter 4 represent an attempt to address this issue of significance.

A recurrent, spontaneous amplification event was identified in cells with intact replication controls and subsequent characterization of those amplifications showed they were structurally consistent with RRIGA. This in turn justified (boot-strapping, if you will) engineering of a split gene reconstitution assay to specifically measure the rate of such head-to-tail *in loco* duplications. Using this assay I showed that minor disruption of

replication controls increased the rate of amplification, quite dramatically in some cases. On the other hand, genetically introducing replication stress, the supposed precipitating insult according to other models for NAHR mediated gene amplification, led to a comparatively minor rate elevation. Furthermore, the spontaneous amplifications seem to rely upon SSA, not gene conversion of break induced replication, more consistent with RRIGA than alternative mechanisms. Taking this data all together, I favor the notion that sporadic failure to block re-initiation likely underlies at least some spontaneous amplification events.

Additional experiments are needed to corroborate this general conclusion. The primary shortcoming of the study presented in Chapter 4 is the lack of gain of function approaches. The role of re-replication in spontaneous amplifications is inferred largely from the greater apparent capacity of re-replication to stimulate amplification relative to replication stress. A far superior experiment would be to reduce the frequency of failure to block re-initiation below wild-type levels. This, however, would require quite a feat of molecular engineering, if it is possible at all.

Another much more feasible approach that may be able to address the possible role of re-replication in the genesis of the spontaneous amplifications observed on Chromosome VII is to knockout each individual replication origin within that amplicon, and then to determine the rate of amplification in the resultant strains. If one of those origins is prone to re-initiation that drives amplification, then removing that origin should reduce the spontaneous amplification rate. It is of course possible that multiple origins contribute and that pairwise (or n-wise) disruptions will need to be made to uncover an effect. If, however, many origins must be removed, then a potential pitfall emerges. Removing too many origins may generate increased local replication stress due to the origin desert established, which would produce a countervailing increase in amplification rate.

Setting aside the case of spontaneous amplifications in cells with intact controls,

what is quite clear from the work in Chapter 4 is that very slight disruption of replication control can boost the rate of amplification quite dramatically. Whereas the work in Chapters 2 and 3 was based on a situation where multiple regulatory mechanisms were concomitantly disrupted, the data in Chapter 4 indicates that loss of individual controls has a substantial impact. In terms of potential relevance to pathophysiological states, like cancer, this is a significant observation. It suggests that dysregulation of individual pre-RC components could generate an ‘amplificator’ phenotype [13], similar to the ‘mutator’ phenotype observed when mismatch repair is defective, for example. It will therefore be of great interest to see if any correlation can be found between replication control dysregulation and amplification rate in human cancer cells.

References

1. Archambault V, Ikui AE, Drapkin BJ, Cross FR (2005) Disruption of mechanisms that prevent rereplication triggers a DNA damage response. *Mol Cell Biol* 25: 6707–6721. doi:10.1128/MCB.25.15.6707-6721.2005.
2. Green BM, Li JJ (2005) Loss of rereplication control in *Saccharomyces cerevisiae* results in extensive DNA damage. *Mol Biol Cell* 16: 421–432. doi:10.1091/mbc.E04-09-0833.
3. Vaziri C, Saxena S, Jeon Y, Lee C, Murata K, et al. (2003) A p53-dependent checkpoint pathway prevents rereplication. *Mol Cell* 11: 997–1008.
4. Zhu W, Chen Y, Dutta A (2004) Rereplication by depletion of geminin is seen regardless of p53 status and activates a G2/M checkpoint. *Mol Cell Biol* 24: 7140–7150. doi:10.1128/MCB.24.16.7140-7150.2004.

5. Zhu W, Dutta A (2006) An ATR- and BRCA1-mediated Fanconi anemia pathway is required for activating the G2/M checkpoint and DNA damage repair upon rereplication. *Mol Cell Biol* 26: 4601–4611. doi:10.1128/MCB.02141-05.
6. Melixetian M, Ballabeni A, Masiero L, Gasparini P, Zamponi R, et al. (2004) Loss of Geminin induces rereplication in the presence of functional p53. *J Cell Biol* 165: 473–482. doi:10.1083/jcb.200403106.
7. Jin J, Arias EE, Chen J, Harper JW, Walter JC (2006) A family of diverse Cul4-Ddb1-interacting proteins includes Cdt2, which is required for S phase destruction of the replication factor Cdt1. *Mol Cell* 23: 709–721. doi:10.1016/j.molcel.2006.08.010.
8. Lovejoy CA, Lock K, Yenamandra A, Cortez D (2006) DDB1 maintains genome integrity through regulation of Cdt1. *Mol Cell Biol* 26: 7977–7990. doi:10.1128/MCB.00819-06.
9. Davidson IF, Li A, Blow JJ (2006) Deregulated replication licensing causes DNA fragmentation consistent with head-to-tail fork collision. *Mol Cell* 24: 433–443. doi:10.1016/j.molcel.2006.09.010.
10. Nowell PC (1976) The clonal evolution of tumor cell populations. *Science* 194: 23–28.
11. Lengauer C, Kinzler KW, Vogelstein B (1998) Genetic instabilities in human cancers. *Nature* 396: 643–649. doi:10.1038/25292.
12. Green BM, Morreale RJ, Ozaydin B, Derisi JL, Li JJ (2006) Genome-wide mapping of DNA synthesis in *Saccharomyces cerevisiae* reveals that mechanisms preventing reinitiation of DNA replication are not redundant. *Mol Biol Cell* 17: 2401–2414. doi:10.1091/mbc.E05-11-1043.

13. Albertson DG (2006) Gene amplification in cancer. *Trends Genet* 22: 447–455. doi:10.1016/j.tig.2006.06.007.
14. Hahn PJ (1993) Molecular biology of double-minute chromosomes. *Bioessays* 15: 477–484. doi:10.1002/bies.950150707.
15. Wintersberger E (1994) DNA amplification: new insights into its mechanism. *Chromosoma* 103: 73–81.
16. Varshavsky A (1981) On the possibility of metabolic control of replicon “misfiring”: relationship to emergence of malignant phenotypes in mammalian cell lineages. *Proc Natl Acad Sci USA* 78: 3673–3677.
17. Schimke RT, Sherwood SW, Hill AB, Johnston RN (1986) Overreplication and recombination of DNA in higher eukaryotes: potential consequences and biological implications. *Proc Natl Acad Sci USA* 83: 2157–2161.
18. Schimke RT (1984) Gene amplification in cultured animal cells. *Cell* 37: 705–713.
19. Stark GR, Debatisse M, Giulotto E, Wahl GM (1989) Recent progress in understanding mechanisms of mammalian DNA amplification. *Cell* 57: 901–908.
20. Stark GR, Wahl GM (1984) Gene amplification. *Annu Rev Biochem* 53: 447–491. doi:10.1146/annurev.bi.53.070184.002311.
21. Lontos M, Koutsami M, Sideridou M, Evangelou K, Kletsas D, et al. (2007) Deregulated overexpression of hCdt1 and hCdc6 promotes malignant behavior. *Cancer Res* 67: 10899–10909. doi:10.1158/0008-5472.CAN-07-2837.
22. Santarius T, Shipley J, Brewer D, Stratton MR, Cooper CS (2010) A census of amplified and overexpressed human cancer genes. *Nat Rev Cancer* 10: 59–64. doi:10.1038/nrc2771.

23. Bonds L, Baker P, Gup C, Shroyer KR (2002) Immunohistochemical localization of cdc6 in squamous and glandular neoplasia of the uterine cervix. *Arch Pathol Lab Med* 126: 1164–1168. doi:10.1043/0003-9985(2002)126<1164:ILOCIS>2.0.CO;2.
24. Borlado LR, Méndez J (2008) CDC6: from DNA replication to cell cycle checkpoints and oncogenesis. *Carcinogenesis* 29: 237–243. doi:10.1093/carcin/bgm268.
25. Karakaidos P, Taraviras S, Vassiliou LV, Zacharatos P, Kastrinakis NG, et al. (2004) Overexpression of the replication licensing regulators hCdt1 and hCdc6 characterizes a subset of non-small-cell lung carcinomas: synergistic effect with mutant p53 on tumor growth and chromosomal instability--evidence of E2F-1 transcriptional control over hCdt1. *Am J Pathol* 165: 1351–1365. doi:10.1016/S0002-9440(10)63393-7.
26. Murphy N, Ring M, Heffron CCBB, King B, Killalea AG, et al. (2005) p16INK4A, CDC6, and MCM5: predictive biomarkers in cervical preinvasive neoplasia and cervical cancer. *J Clin Pathol* 58: 525–534. doi:10.1136/jcp.2004.018895.
27. Ren B, Yu G, Tseng GC, Cieply K, Gavel T, et al. (2006) MCM7 amplification and overexpression are associated with prostate cancer progression. *Oncogene* 25: 1090–1098. doi:10.1038/sj.onc.1209134.
28. Arentson E, Faloon P, Seo J, Moon E, Studts JM, et al. (2002) Oncogenic potential of the DNA replication licensing protein CDT1. *Oncogene* 21: 1150–1158. doi:10.1038/sj.onc.1205175.
29. Seo J, Chung YS, Sharma GG, Moon E, Burack WR, et al. (2005) Cdt1 transgenic mice develop lymphoblastic lymphoma in the absence of p53. *Oncogene* 24: 8176–8186. doi:10.1038/sj.onc.1208881.

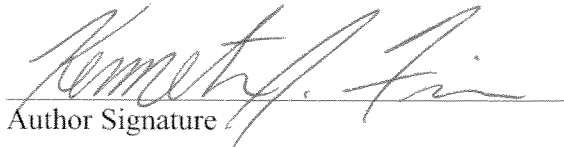
30. Chen J-M, Cooper DN, Férec C, Kehrer-Sawatzki H, Patrinos GP (2010) Genomic rearrangements in inherited disease and cancer. *Semin Cancer Biol* 20: 222–233. doi:10.1016/j.semcancer.2010.05.007.
31. Hastings PJ, Lupski JR, Rosenberg SM, Ira G (2009) Mechanisms of change in gene copy number. *Nat Rev Genet* 10: 551–564. doi:10.1038/nrg2593.
32. Hoang ML, Tan FJ, Lai DC, Celniker SE, Hoskins RA, et al. (2010) Competitive repair by naturally dispersed repetitive DNA during non-allelic homologous recombination. *PLoS Genet* 6: e1001228. doi:10.1371/journal.pgen.1001228.
33. Payen C, Koszul R, Dujon B, Fischer G (2008) Segmental duplications arise from Pol32-dependent repair of broken forks through two alternative replication-based mechanisms. *PLoS Genet* 4: e1000175. doi:10.1371/journal.pgen.1000175.
34. Raghuraman MK, Winzeler EA, Collingwood D, Hunt S, Wodicka L, et al. (2001) Replication dynamics of the yeast genome. *Science* 294: 115–121. doi:10.1126/science.294.5540.115.
35. Newlon CS (1988) Yeast chromosome replication and segregation. *Microbiol Rev* 52: 568–601.

Publishing Agreement

It is the policy of the University to encourage the distribution of all theses, dissertations, and manuscripts. Copies of all UCSF theses, dissertations, and manuscripts will be routed to the library via the Graduate Division. The library will make all theses, dissertations, and manuscripts accessible to the public and will preserve these to the best of their abilities, in perpetuity.

Please sign the following statement:

I hereby grant permission to the Graduate Division of the University of California, San Francisco to release copies of my thesis, dissertation, or manuscript to the Campus Library to provide access and preservation, in whole or in part, in perpetuity.


Author Signature

3/18/2013
Date